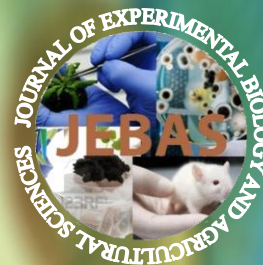


ISSN:2320-8694

# Journal of Experimental Biology And Agricultural Sciences



VOLUME 10 || ISSUE II || APRIL, 2022

Production and Hosting by Horizon Publisher India[HPI]  
(<http://www.horizonpublisherindia.in>)  
All rights reserved.

ISSN No. 2320 - 8694

Peer Reviewed - open access journal

Common Creative License - NC 4.0

Volume No - 10

Issue No - II

April, 2022

Journal of Experimental Biology and Agricultural Sciences (JEBAS) is an online platform for the advancement and rapid dissemination of scientific knowledge generated by the highly motivated researchers in the field of biological agricultural, veterinary and animal sciences. JEBAS publishes high-quality original research and critical up-to-date review articles covering all the aspects of biological sciences. Every year, it publishes six issues.

JEBAS has been accepted by SCOPUS UGC CARE, INDEX COPERNICUS INTERNATIONAL (Poland), AGRICOLA (USA), CAS (ACS, USA), CABI - Full Text (UK), International Committee of Medical Journal Editors (ICMJE), SHERPA - ROMEO; J gate and Indian Science Abstracts (ISA, NISCAIR) like well reputed indexing agencies.

[HORIZON PUBLISHER INDIA [HPI]

<http://www.horizonpublisherindia.in/>]

## Editorial Board

---

### Editor-in-Chief

Prof Y. Norma-Rashid  
(University of Malaya, Kuala Lumpur)  
editor.in.chief.jebas@gmail.com

### Co-Editor-in-Chief

Dr. Kuldeep Dhama, M.V.Sc., Ph.D.  
NAAS Associate, Principal Scientist, IVRI, Izatnagar India - 243 122  
co\_eic@jebas.org

### Managing - Editor

Kamal K Chaudhary, Ph.D. (India)  
jebasonline@gmail.com

### Dr. Anusheel Varshney

University of Salford United Kingdom  
Jebas.managingeditor@gmail.com

## Technical Editors

---

### Dr. Gary Straquadine

Vice Chancellor – USU Eastern Campus, Utah State University Eastern,  
2581 West 5200 South, Rexburg, Idaho, 83440  
Email: gary.straquadine@usu.edu

### Hafiz M. N. Iqbal (Ph.D.)

Research Professor,  
Tecnologico de Monterrey, School of Engineering and Sciences,  
Campus Monterrey, Ave. Eugenio Garza Sada 2501,  
Monterrey, N. L., CP 64849, Mexico  
Tel.: +52 (81) 8358-2000Ext.5561-115  
E-mail: hafiz.iqbal@my.westminster.ac.uk; hafiz.iqbal@itesm.mx

### Prof. Dr. Mirza Barjees Baigis

Professor of Extension (Natural Resource Management),  
Department of Agricultural Extension and Rural Society,  
College of Food and Agriculture Sciences,  
King Saud University, P.O. Box 2460, Riyadh 11451  
Kingdom of Saudi Arabia  
Email: mbaig@ksu.edu.sa

**Dr. Mukesh Kumar Meghvansi**

Scientist, Bioprocess Technology Division, Defence R & D Establishment, Gwalior-474002

Email: mk\_meghvansi@yahoo.co.in

**Dr. B L Yadav**

Head – Botany, MLV Govt. College, Bhilwara, India

E mail: drblyadav@yahoo.com

**Dr. K L Meena**

Associate Professor – Botany, MLV Govt.

College, Bhilwara, India

E mail: kanhaiyameena211@yahoo.com

**Dr. Yashpal S. Malik**

ICAR – National Fellow Indian Veterinary Research Institute (IVRI)

Izatnagar 243 122, Bareilly, Uttar Pradesh, India

**Professor Dr. Muhammad Mukhtar**

Professor of Biotechnology/Biochemistry

American University of Ras Al Khaimah Ras Al Khaimah, United Arab Emirates

**Abdulrasoul M. Alomran**

Prof. of Soil and Water Sciences

Editor in Chief of JSSAS

College of Food and Agricultural Sciences

King Saud University Riyadh, Saudi Arabia

E-mail: alomranrasoul@gmail.com

## Associate Editors

---

**Dr. Sunil K. Joshi**

Laboratory Head, Cellular Immunology

Investigator, Frank Reidy Research Center of Bioelectrics, College of Health Sciences, Old Dominion University, 4211 Monarch Way, IRP-2, Suite # 300, Norfolk, VA 23508 USA Email: skjoshi@odu.edu

**Dr. Vincenzo Tufarelli**

Department of Emergency and Organ Transplantation (DETO),

Section of Veterinary Science and Animal Production,

University of Bari 'Aldo Moro', s.p. Casamassima km 3,

70010 Valenzano, Italy Email: vincenzo.tufarelli@uniba.it

**Dr. Md. Moin Ansari**

Associate Professor-cum-Senior Scientist  
Division of Surgery and Radiology  
Faculty of Veterinary Sciences and Animal Husbandry  
Shuhama, Srinagar-190006, J&K, India

**Prof. Viliانا Vasileva, PhD**

89 "General Vladimir Vazov" Str.  
Institute of Forage Crops  
5800 Pleven, BULGARIA  
E-mail: viliana.vasileva@gmail.com

**Prof. Sanjay-Swami, Ph.D. (Soil Science & Agril. Chemistry),**

School of Natural Resource Management,  
College of Post Graduate Studies in Agricultural Sciences,  
(Central Agricultural University),  
UMIAM (Barapani)-793 103, Meghalaya, INDIA  
Email: sanjay.nrm.cpgsas@cau.ac.in

## Assistant Editors

---

**Mr. Ram Bahadur Khadka (Microbiologist)**

Assistant Professor (Pokhara University)  
Crimson College of Technology (CCT)  
Butwal-13, Rupandehi, Lumbini Province, Nepal  
Email: rambahadurkhadka00@gmail.com

**Prof. A. VIJAYA ANAND**

Professor  
Department of Human Genetics and Molecular Biology  
Bharathiar University  
Coimbatore – 641 046

**Dr. Phetole Mangena**

Department of Biodiversity, School of Molecular and Life Sciences,  
Faculty of Science and Agriculture, University of Limpopo, Republic of South Africa  
Private Bag X1106, Sovenga, 0727  
Email: Phetole.Mangena@ul.ac.za ; mangena.phetole@gmail.com

**Dr Ayman EL Sabagh**

Assistant professor, agronomy department, faculty of agriculture  
[Details]kafresheikh university, Egypt  
E-mail: ayman.elsabagh@agr.kfs.edu.eg

**Dr. Masnat Al Hiary**

Director of the Socio- economic Studies Directorate  
Socio-economic Researcher  
National Center for Agricultural Research and Extension (NCARE)  
P.O.Box 639 Baqa'a 19381 Jordan

**Safar Hussein Abdullah Al-Kahtani (Ph.D.)**

King Saud University-College of Food and Agriculture Sciences,  
Department of the Agricultural Economics  
P.O.Box: 2460 Riyadh 11451, KSA  
email: safark@ksu.edu.sa

**Dr Ruchi Tiwari**

Assistant Professor (Sr Scale)  
Department of Veterinary Microbiology and Immunology,  
College of Veterinary Sciences,  
UP Pandit Deen Dayal Upadhyay Pashu Chikitsa Vigyan Vishwavidyalay Evum Go-Anusandhan Sansthan (DUVASU),  
Mathura, Uttar Pradesh, 281 001, India  
Email: ruchi.vet@gmail.com

**Dr. ANIL KUMAR (Ph.D.)**

Asstt. Professor (Soil Science)  
Farm Science Centre (KVK)  
Booh, Tarn Taran, Punjab (India) – 143 412  
Email: anilkumarhpkv@gmail.com

**Akansha Mishra**

Postdoctoral Associate, Ob/Gyn lab  
Baylor College of Medicine  
1102 Bates Ave, Houston Tx 77030  
Email: akansha.mishra@bcm.edu; aksmisra@gmail.com

**Dr. Muhammad Bilal**

Associate Professor  
School of Life Science and Food Engineering,  
Huaiyin Institute of Technology, Huaian 223003, China  
Email: bilaluaf@hotmail.com

**Dr. Izabela Michalak**

Associate Professor

Faculty of Chemistry, Department of Advanced Material Technologies,  
Wroc?aw University of Science and Technology, Wroc?aw 50-370, Poland

Email: [izabela.michalak@pwr.edu.pl](mailto:izabela.michalak@pwr.edu.pl)

**Dr. Senthilkumar Natesan**

Associate Professor

Department of Infectious Diseases, Indian Institute of Public Health  
Gandhinagar, Opp to Airforce station HQ, Lekawada,

Gandhinagar, Gujarat - 382042, India

Email: [snatesan@iiphg.org](mailto:snatesan@iiphg.org)

**Dr. Jehangeer Rehman Quereishi**

Associate Professor - Botany

Govt. Bangure College, Deedwana.

Email: [quereishi.jrq660@gmail.com](mailto:quereishi.jrq660@gmail.com)

## Table of contents

<b>Bacterial biofilms: role of quorum sensing and quorum quenching</b> <i>10.18006/2022.10(2).278.293</i>	278 — 293
<b>Current and emerging molecular technologies for the diagnosis of plant diseases – An overview</b> <i>10.18006/2022.10(2).294.305</i>	294 — 305
<b>Assessment of Variability and Genetic Diversity Study in an Advanced Segregating Population in Rice with Blast Resistance Genes Introgression</b> <i>10.18006/2022.10(2).306.317</i>	306 — 317
<b>Selection for Upland Rice Varieties Under Different Levels of Light Intensity</b> <i>10.18006/2022.10(2).318.322</i>	318 — 322
<b>An explorative study on the adoption and dis-adoption of improved rice varieties among farmers in the Northern region of Ghana</b> <i>10.18006/2022.10(2).323.334</i>	323 — 334
<b>Characterization of Mature Cladodes of <i>Opuntia ficus-indica</i> L. Using Morphological and Colorimetric Descriptors</b> <i>10.18006/2022.10(2).335.343</i>	335 — 343
<b>Relationship of altitude, individual seed weight, and kernel colonization by <i>Aspergillus flavus</i> with biochemical parameters of various Ethiopian groundnut (<i>Arachis hypogaea</i> L.) accessions</b> <i>10.18006/2022.10(2).344.358</i>	344 — 358
<b>Identification of Genetic Diversity among Mutant Taro (<i>Colocasia esculenta</i> L. cv WANGI) Using Agro-Morphological Trait and Simple Sequence Repeats (SSR) Molecular Markers</b> <i>10.18006/2022.10(2).359.368</i>	359 — 368
<b>Dynamics of land-use Change using Geospatial Techniques From 1986 to 2019: A Case Study of High Oum Er-Rbia Watershed (Middle Atlas Region)</b> <i>10.18006/2022.10(2).369.378</i>	369 — 378
<b>Estimation of nitrogen use efficiency by mango seedlings under nano and convention calcium fertilization using the enriched stable isotope (N-15)</b> <i>10.18006/2022.10(2).379.386</i>	379 — 386
<b>Performance of electrical energy monitoring data acquisition system for plant-based microbial fuel cell</b> <i>10.18006/2022.10(2).387.395</i>	387 — 395
<b>Targeting Omicron (B.1.1.529) SARS CoV-2 spike protein with selected phytochemicals: an in-silico approach for identification of potential drug</b> <i>10.18006/2022.10(2).396.404</i>	396 — 404
<b>Isolation and determination of <i>Vibrio</i> spp. pathogen from <i>Sciaenops ocellatus</i> suffering from hemorrhagic disease under cage culture in Vietnam</b> <i>10.18006/2022.10(2).405.415</i>	405 — 415
<b>Evaluation of Phytochemical and Antibacterial properties of leaf extract of <i>Cinnamomum tamala</i> oil</b> <i>10.18006/2022.10(2).416.422</i>	416 — 422
<b>In silico targeting of osmoporin protein of <i>Salmonella</i> to identify anti-Salmonellosis phyto-compounds</b> <i>10.18006/2022.10(2).423.429</i>	423 — 429
<b>Biodegradation of the Azo Dye Airedale Yellow CHD: Understanding using residuals</b> <i>10.18006/2022.10(2).430.439</i>	430 — 439
<b>Machine learning for the classification of breast cancer tumor: a comparative analysis</b> <i>10.18006/2022.10(2).440.450</i>	440 — 450
<b>Dielectric properties of the tissues with different histological structure: Ex vivo study</b> <i>10.18006/2022.10(2).451.455</i>	451 — 455





## Journal of Experimental Biology and Agricultural Sciences

<http://www.jebas.org>

ISSN No. 2320 – 8694

### Bacterial biofilms: role of quorum sensing and quorum quenching

Dhritishree Ghosh, Madhupa Seth, Priyajit Mondal, Subhra Kanti Mukhopadhyay\*

Department of Microbiology, The University of Burdwan, Burdwan, Purba Bardhaman, West Bengal, India, 713104.

Received – January 24, 2022; Revision – March 24, 2022; Accepted – April 27, 2022

Available Online – April 30, 2022

DOI: [http://dx.doi.org/10.18006/2022.10\(2\).278.293](http://dx.doi.org/10.18006/2022.10(2).278.293)

#### KEYWORDS

Bacterial biofilms

Multi-drug resistance

N-acyl homoserine lactones

Quorum sensing

Quorum quenching

#### ABSTRACT

Bacterial biofilms provide an adjustable strategy to manage themselves in the existing conditions. Biofilms of pathogenic bacteria act as a reservoir for various device and non-device related diseases which are tough to cure. Exposure to a high dose of antibiotics is not an appropriate solution to this problem as high antibiotic concentrations lead to the generation of Multi-drug resistant strains as well as affect the human body. So, it is needed to bypass the use of antibiotics to prevent bacterial biofilms. In this context, Quorum Sensing (QS) may be a potential target since biofilm formation is regulated by QS. N-acyl homoserine lactones (N-AHL) act as predominant QS signal molecules in Gram-negative bacteria. Counteraction of the QS-regulated activities using quorum quenching may be an alternative way to combat biofilm formation in bacteria. Quorum sensing inhibitors (QSIs) and QQ enzymes play a significant role in this regard either by interference with the signal generation, perception, or by degradation, and chemical modification, respectively. Many quorum quenching enzymes have been reported from bacteria. Extremophilic bacteria have also been reported to produce potent quorum quenching enzymes which can effectively break down N-AHLs.

\* Corresponding author

E-mail: [skmmicro@gmail.com](mailto:skmmicro@gmail.com); [skmukhopadhyay@microbio.buruniv.ac.in](mailto:skmukhopadhyay@microbio.buruniv.ac.in);  
(Subhra Kanti Mukhopadhyay)

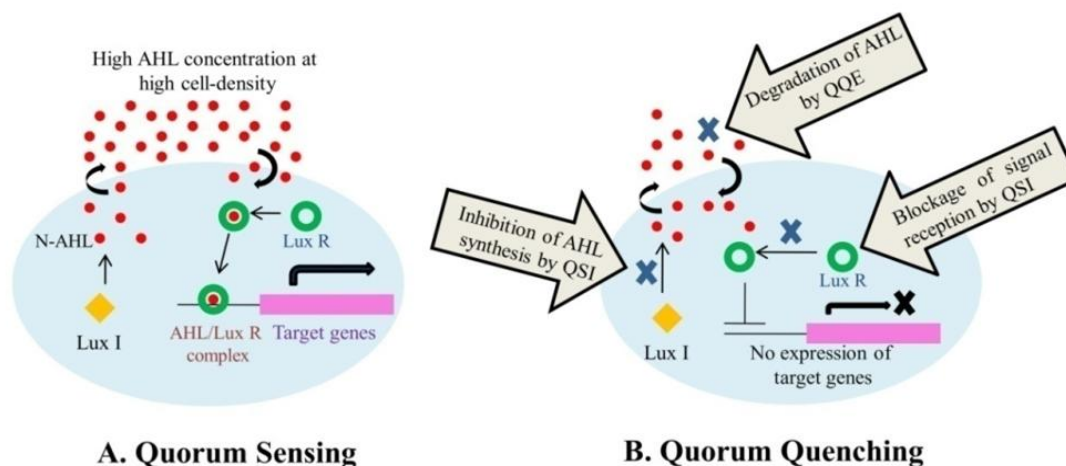
Peer review under responsibility of Journal of Experimental Biology and Agricultural Sciences.

Production and Hosting by Horizon Publisher India [HPI]  
(<http://www.horizonpublisherindia.in/>).  
All rights reserved.

All the articles published by [Journal of Experimental Biology and Agricultural Sciences](#) are licensed under a [Creative Commons Attribution-NonCommercial 4.0 International License](#) Based on a work at [www.jebas.org](http://www.jebas.org).



## GRAPHICAL ABSTRACT



## 1 Introduction

Flexibility in gene expression and adaptability in changing environments allow cosmopolitan distribution of bacteria. Most of them can interchange between planktonic mode of growth to bio-film mode according to the need of life. Bio-films are matrix-enclosed bacterial populations adhered to each other or to the surface. Bio-films contain a complex assembly of polysaccharides, proteins, DNA and loose aggregation of sessile cells embedded in a hydrated matrix made up of extracellular polymeric substances. Most of the pathogenic bacteria such as *Pseudomonas aeruginosa*, *Haemophilus influenzae*, *Staphylococcus aureus*, *Burkholderia cepacia*, *Klebsiella pneumoniae*, *Acinetobacter baumannii* etc. produce biofilms, virulence factors which are associated with pathogenicity. Biofilms also act as a reservoir for pathogenic bacteria in aquaculture (Small and Pagenkopp 2011). Although planktonic bacteria show higher cell growth and reproduction (Rabin et al. 2015), bacterial bio-films represent a strategy of growth either to survive in harsh conditions or to accommodate themselves in a nutrient-rich favorable niche.

## 2 Bacterial Biofilm Associated Human Diseases

It is reported that more or less 65% of all bacterial infections are related to biofilms (Lewis et al. 2011) including both device-related and non-device associated diseases. Biofilms of pathogenic bacteria help them to survive in hosts and make chronic infections resulting in persistent inflammations and tissue damage (Lebeaux et al. 2013). Some examples of non-device associated infections are Cystic Fibrosis, Chronic Obstructive Pulmonary Disease, Urinary Tract Infections, Endocarditis, Chronic Otitis Media, Chronic Rhinosinusitis, Dental Plaque, Dental Caries, Periodontitis, Osteomyelitis (Lebeaux and Ghigo 2012). Bacterial biofilms also inhabit on or within implantable medical devices

such as contact lenses, endotracheal tubes, prosthetic cardiac valves, vascular grafts, pacemakers, vascular central catheters, urinary catheters, breast implants, orthopedic implants, prosthetic joints etc. (Jefferson 2004). Thus biofilms of pathogenic bacteria formed on medical devices, human tissue organs directly affect public health and the economy.

## 3 Insight into conditions, development, and structure of bacterial biofilms

The process of biofilm formation is cyclic and dynamic (Jefferson 2004). Different external cues play important role in biofilm formation. Inside and outside the host body, nutrient deficiency, oxidative stress, osmotic stress, high temperature, pH change, high concentration of drugs, host immune responses etc. trigger the biofilm mode of growth in bacteria from that of planktonic mode. Slow and/or no growth of the biofilm inhabitants during such stresses allows bacterial survivability (Kırmusaoğlu 2016). On the other hand, a surplus of nutrients also promotes biofilm development as high C/N ratio enhances EPS production and biofilm formation in Pseudomonads, *Vibrio cholerae*, *Escherichia coli* and Streptococci (O'Toole et al. 2000; Jefferson et al. 2004). Here EPS acts as a reservoir of carbon sources which may serve as storage during starvation. Thus, biofilms help in the colonization of bacteria in suitable, favorable niches as well as provide support in unfavorable conditions (Jefferson 2004).

Biofilm formation starts with the initial reversible attachment of planktonic cells to biotic/abiotic surface(s). This is achieved by various non-covalent interactions such as van der Waals, electrostatic and hydrophobic interactions between bacterial cells and surface(s). Here flagella and pili assist initial attachment of bacterial cells to the surface. It is reported that rough, hydrophobic surfaces coated with various organic materials are most suitable for

initial reversible attachment (Donlan 2002). Then irreversible attachment is achieved by extracellular polymeric substances (EPS) production (Rabin et al. 2015). During irreversible attachment, several physiological and structural changes take place including non-motility of attached cells (Sauer et al. 2002). The second phase is the multiplication of bacterial cells on surfaces along with the increasing synthesis of EPS matrix. The continuous growth of sessile bacterial cells form microcolonies and achieve mushroom or pillar-shaped structures (Kaplan 2010). The biofilm matrix holds the cell mass together, acts as a structural scaffold and provides physical strength to biofilms (Rabin et al. 2015). Sometimes mature biofilms may be mono-layered consisting of cells in porous EPS or multi-layered with loosely bound microcolonies held together in EPS matrix and intermingled with void spaces, fluid-filled channels and water channels (Chmielewski et al. 2003) which act together as circulatory system in biofilms (Kaplan 2010). eDNA is released from lysed cells as well as actively secreted via the Type IV secretion system (Hamilton et al. 2005). eDNA plays a crucial role in biofilm attachment and adhesion (Rabin et al. 2015). Rhamnolipids help in the microcolony formation and circulatory channel maintenance in biofilms (Pamp and Tolker-Nielsen 2007). Mostly, multi-layered biofilms have heterogeneity in terms of the spatial distribution of metabolically active cells which are resulted from diffusion limitation of nutrients, oxygen, secondary metabolites, signal molecules and antimicrobials (Jefferson 2004). Such local variation also results in the different growth rates of biofilm inhabitants with a difference in gene expression. Metabolically active fast-growing cells reside in the upper surface layer of

biofilm whereas low metabolically active slow-growing cells remain in deeper parts of biofilm. Such metabolically different heterogeneous cells exhibit a wide range of responses to each antimicrobial agent and antibiotic. Some cells become dormant with no growth. These are called persister cells (Kirmusaoglu 2016). Persister cells remain as disease reservoirs in biofilms which can change into infectious particles once antibiotic stresses have been removed (Rabin et al. 2015).

Biofilm dispersal is the last phase of biofilm formation. Nutrient depletion not only triggers the formation of biofilms but also leads to biofilm dispersal where detached cells search for a new source of nutrients and colonize there (O'Toole et al. 2000). Biofilm dispersion is equally important as biofilm formation in bacterial survival and dissemination behind which there are several internal as well as external factors as seen in Figure 1. Active dispersal takes place by bacteria themselves using an enzymatic breakdown of EPS matrix, biofilm substrates, central hollowing followed by seeding dispersal (Kaplan et al. 2003b; Ma et al. 2009), changes in nutrient availability, Oxygen tension, temperature and pH (Karatan and Watnick 2009). Decrease in Cyclic Diguanylate Monophosphate (c-di-GMP) downregulates EPS production and induces biofilm dispersion in several genera viz. *P. aeruginosa*, *P. fluorescense*, *Shewanella oneidensis*, *E. coli* and *Vibrio* sp. (Simm et al. 2004; Thormann et al. 2005; Morgan et al. 2006; Newell et al. 2009; Boehm et al. 2009; Yildiz and Visick 2009). Rhamnolipids are amphipathic, extracellular surfactants that reduce cohesiveness of cell to cell, cell to the matrix, and cell-surface interaction triggering central hollowing,

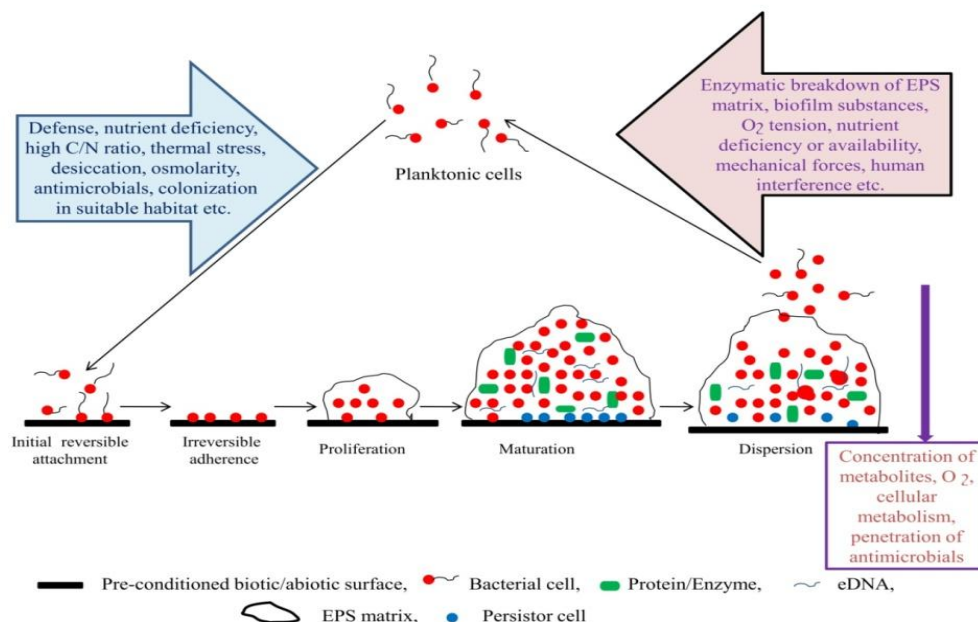


Figure 1 Different stages of biofilm formation showing the effect of various internal and external factors behind biofilm formation and dispersion along with concentration gradients of AHL during the development of biofilm

seeding dispersal and cell detachment followed by biofilm dispersion in a non-specific manner. Rhamnolipids also disrupt matrix components and form central cavities leading to biofilm dispersal (Pamp and Tolker-Nielsen 2007). Exogenous rhamnolipids are also responsible for the dispersion of biofilms in both wild-type and mutant *P. aeruginosa* (Boles et al. 2005; Dong et al. 2008). On the other hand, passive dispersion is achieved by mechanical forces like fluid shear, abrasion (collision between solid particles within biofilm), phagocytosis, increased Nitric Oxide level (due to anaerobic respiration in deeper parts) and human interferences (Kaplan 2010). The process of biofilm formation along with the responsible factors is summarized in figure 1.

#### 4 Molecular Regulation of Bacterial Biofilm Formation

In bacteria, biofilm formation is a complex genetic process in which several genes play different functions at different times. Some genes regulate the initial adherence of bacteria to biotic/abiotic surface(s), Some genes are responsible for the development of proper biofilm architecture while few genes mediate biofilm dispersal. External cues trigger the expression of a subset of genes that initiate biofilm formation. This generates different micro-environment within biofilm that alter further gene expression leading to biofilm maturation and so on. Table 1 shows the involvement of some genes during different stages of biofilm formation.

Table 1 List of various genes and proteins along with their functions responsible for biofilm formation in bacteria

Name of the gene/protein	Function	Reference
operon, <i>csgDEFG</i> and <i>csgBA</i>	Curli synthesis, required for primary adherence to abiotic surfaces and formation of multilayered cell clusters in <i>E. coli</i>	Prigent-Combaret et al. 2000
Catabolite Repression Control protein (Crc)	Type IV pili synthesis in <i>P. aeruginosa</i> , primary adhesion via twitching motility	O'Toole et al. 2000
<i>cupA</i> gene of <i>cup</i> gene cluster	Initial adhesion of cells to inert surfaces by fimbriae in many bacteria	Vallet et al. 2001
<i>degU</i> , <i>flaA</i> , <i>flgL</i> , <i>motB</i>	Flagella synthesis, flagella structure and motility in <i>Listeria monocytogenes</i> ,	Gueriri et al. 2008; Todhanakasem and Young 2008; Lemon et al. 2007
Bap protein	Surface attachment in <i>L. monocytogenes</i> and <i>S. aureus</i>	Cucarella et al. 2001; Jordan et al. 2008
<i>relA</i> and <i>hpt</i>	Exertion of stringent response during starvation after surface attachment in <i>L. monocytogenes</i>	Taylor et al. 2002
<i>pel</i>	Production of glucose-rich exopolysaccharide Pel in <i>P. aeruginosa</i> strain PA14	Friedman and Kolter 2004a
<i>psl</i>	Synthesis of mannose-rich exopolysaccharide Psl in <i>Pseudomonas aeruginosa</i> strains ZK2870	Friedman and Kolter 2004b
<i>algC</i>	Synthesis of alginates, lipopolysaccharides, Pel and Psl exopolysaccharides in <i>P. aeruginosa</i>	Ma et al. 2012
<i>gbp</i>	Biosynthesis of Glucan binding protein (Gbp) which maintain biofilm architecture by tight association of bacteria with EPS in <i>Streptococcus mutans</i>	Lynch et al. 2007
GbpA	Synthesis of glucosyltransferase which mediate synthesis of sucrose-dependent exopolysaccharides during biofilm formation in <i>Streptococcus mutans</i>	Loo 2003
<i>tasA</i>	Formation of strong insoluble fibrous protein that keep sessile cells together and helps biofilms to withstand destructive forces in <i>Bacillus subtilis</i>	Romero et al. 2010
Fap (Amyloid protein)	Induction of cell aggregation and biofilm formation in <i>Pseudomonas</i> spp	Dueholm et al. 2013
Dispersin B (DspB)	Acts as glycoside hydrolase which is EPS matrix-degrading enzyme in <i>Actinobacillus actinomycetemcomitans</i>	Kaplan et al. 2003a
<i>alpP</i>	Encodes Lysine hydrolase enzyme which generates H <sub>2</sub> O <sub>2</sub> leading to cell death in microcolonies followed by dispersal in <i>Marinomonas mediterranea</i> , <i>Chromobacterium violaceum</i> , and <i>Caulobacter crescentus</i> .	Mai-Prochnow et al. 2008
<i>rhaAB</i>	Production of Rhamnolipids which induce central hollowing and seeding dispersal in <i>P. aeruginosa</i>	Boles et al. 2005
RpoN ( $\sigma$ 54)	Induces the expression of <i>rhlI</i> gene which synthesizes rhamnolipids	Heurlier et al. 2003

### 5 Impact of bacterial biofilm on their hosts

Bacterial biofilms have 100 to 1,000 fold higher tolerance toward antibiotics than their free-floating counterparts. Biofilms of pathogenic bacteria lead to the emergence of Multi-Drug Resistance (MDR) property among them which create serious problems in medical treatment. It is observed that the development of MDR strains of biofilm forming pathogen is due to a higher rate of lateral gene transfer in biofilms than in their planktonic counterparts (Madsen et al. 2012). Increased transfer of genes responsible for antibiotic resistance in *S. aureus* and other bacteria is reported in bio-films (Savage et al. 2013). A recent study also showed that many MDR strains of Enterococci, resistant to several conventional antibiotics, have biofilm forming capacity which leads to chronic infections (Haruna et al. 2022). Not only that, biofilms show high resistance to antimicrobial agents by various mechanisms. Some mechanisms of antibiotic resistance are as follows.

- i. Slow growth rate and Stringent Response (Nguyen et al. 2011; Abebe 2020), local variation and heterogeneity inside biofilms (Kirmusaoğlu 2016; Abebe 2020) assist antimicrobial resistance.
- ii. Biofilm-specific efflux pumps (Gills et al. 2005; Zhang and Mah 2008) lead to no penetration or very short retention of antimicrobial agents within the biofilm (Stewart and Costerton 2001; Van Acker et al. 2014).
- iii. The charge of matrix polysaccharides and secreted antibiotic-degrading enzymes cause binding and/or deactivation of antibiotics (Walters et al. 2003; Bagge et al. 2004; Abebe 2020).
- iv. Antibiotic resistance is also exerted by altering target sites as well as hindering the diffusion of antibiotics across the EPS matrix itself (Abebe 2020).
- v. Persister cells in the biofilm also play a significant role in tolerance to a high concentration of antibiotics as persister cells go to a dormant stage so house-keeping processes remain completely shut off (Dufour et al. 2010).

In addition to antimicrobial resistance, bio-films exert resistance to the host immune system (Hall Stoodley and Stoodley 2009). Alginates of biofilm matrix polysaccharides restrict phagocytosis by IFN- $\gamma$ -activated macrophages in *P. aeruginosa* (Leid et al. 2005) while PMN toxin *viz.* Rhamnolipid B in *P. aeruginosa* kills neutrophils (Jensen et al. 2007). Apart from bio-film mediated antimicrobial resistance, intrinsic antibiotic resistance is a well-known phenomenon in bacteria such as in *Burkholderia cepacia*. Treatment with multiple combinations of drugs is reported to kill MDR strains like *B. cepacia* isolated from cystic fibrosis patients.

Although some of the tested isolates raised resistance to such combined antibiotic treatments (Dales et al. 2009). Moreover, long-term use of single or multiple combinations of antibiotics causes harmful effects on the human body. Beneficial microflora of the human body become extremely affected by such treatments. Some other side-effects of antibiotics are failure of multi-organ like liver, kidney; allergy; development of autoimmune diseases, destruction of hemoglobin etc.

### 6 Quorum Sensing and Role in Biofilm Formation

Biofilm formation in bacteria represents a cooperative action where inhabitants of the biofilms are interconnected to each other. It seems that they communicate and mediate structural and physiological changes accordingly. Quorum Sensing (QS) play important role in this context. QS is reported to control various stages of biofilm formation including irreversible attachment, EPS synthesis, formation of pillar-like structures and fluid channels, maturation, dispersal etc. The relationship between QS and biofilm formation in *P. aeruginosa* was studied. They showed that the *lasI/lasR* system is involved in biofilm differentiation and proper development of biofilm architecture in *P. aeruginosa* on abiotic/biotic surfaces (Davies et al. 1998). A *lasI-rhlI* double mutant strain of *P. aeruginosa*, defective in 3-oxo-C<sub>12</sub> HSL and 3-oxo-C<sub>4</sub> HSL synthesis, respectively, showed reduced expression of *pel* gene resulting in defective unstructured biofilms. However, exogenous application of 3-oxo-C<sub>12</sub> HSL restored wild-type phenotype which indicated direct involvement of AHLs in biofilm formation (Sakuragi and Kolter 2007). Another mutant study in *B. cepacia* strain H111 was done to investigate the involvement of AHLs in biofilm formation. Two mutant strains *viz.* H111-I, defective AHL synthase *cepI* (responsible for AHL synthesis) and H111-R, defective *cepR* (receptor of AHL and transcription regulator) show significantly reduced biofilm formation with defective biofilm architecture. Mutant strains H111-I and H111-R restore wild-type phenotype when supplemented with exogenous AHLs. Moreover, this study also reported that AHLs are required in biofilm maturation rather than initial attachment (Huber et al. 2001). Uropathogenic strain of *E. coli* isolated from UTI samples also showed the involvement of N-AHLs in biofilm formation (Taghadosi et al. 2015). The expression and amount of various AHL molecules in *E. coli* increased gradually along with increasing biofilm biomass and weight. AHL concentration was highest during the activation and maturation stage of biofilm development (Hu et al. 2016).

AHLs not only play important role in biofilm formation but they are also required for biofilm dispersion.  $\Delta$ *lasI/rhlI* double mutant strain of *P. aeruginosa* cannot produce C<sub>4</sub>-HSL and does not show central hollowing and seeding dispersal (Purevdorj-Gage et al. 2005). C<sub>4</sub>-HSLs promote rhamnolipid biosynthetic gene *viz.* *rhaA* leading to dispersal in *P. aeruginosa* PAO1 biofilm (Davey et al. 2003).

Rhamnolipids also mediate interspecies signaling pathways. The cooperation of Rhamnolipids and 3-oxo-C<sub>12</sub> HSL of *P. aeruginosa* promote biofilm dispersal in *E. coli* (Bhattacharjee et al. 2016). A recent study also showed that 3-OC12-HSL significantly increased the number of persister cells in *P. aeruginosa* PAO1 during the logarithmic phase (Möker et al. 2010).

From the above-mentioned statements, it is clear that quorum sensing has a significant role in biofilm formation. In some bacteria, AHL is required for initiation of biofilm formation while some others use AHLs for biofilm maturation and/or dispersion. Although biofilm formation is a beneficial feature in bacteria, it creates a serious problem in conventional treatment particularly for biofilm-forming notorious pathogens. Biofilm formation protects them from antibiotics and antimicrobial agents by various mechanisms mentioned above. So scientists are looking for new alternative approaches which can bypass antibiotics and antimicrobials. Quorum quenching may be a trustful alternate strategy in this context. Before discussing quorum quenching, it is important to know about quorum sensing.

Quorum sensing (QS) is a cell-density-dependent synchronized program in bacteria by which bacteria respond accordingly to the changing environment to manage themselves (Fuqua and Greenberg 2002; Whitehead et al. 2001). Bacteria mediate several biological activities via quorum sensing e. g., swarming motility, aggregation, horizontal gene transfer, competence, virulence factor synthesis, antibiotic production, luminescence, biofilm formation, sporulation etc. (Fuqua and Greenberg 2002; Swift et al. 2001; Williams et al. 2007). In pathogenic bacteria, pathogenicity, production of virulence factors, secondary metabolites, exoenzymes, toxins and endospore formation are also under the control of QS. QS Signal molecules are produced and secreted by bacteria constitutively. At high cell density, bacteria sense the extracellular concentration of particular QS signaling molecules. Mostly, Auto-Inducing Peptides (AIPs) and butyryl-lactones are QS signal molecules in Gram-positive bacteria while N-Acyl homoserine lactones (N-AHL) with variable acyl side chains (species specific) in Gram-negative bacteria predominantly (Whitehead et al. 2001). However, *X. campestris*, *S. typhimurium* and *S. pneumoniae* secrete DSF, AI-2 and CSF as QS signal (Hornby et al. 2001; Waters and Bassler 2005). N-acylhomoserine lactone molecules are made up of two parts: an identical homoserine lactone ring and a variable acyl side chain. Different bacteria produce a diverse array of Acyl homoserine lactones, their diversity comes from the length of the acyl side chain which may be saturated or unsaturated with or without C-3 substitution (Fuqua and Greenberg 2002; Swift et al. 2001). AHLs are synthesized by LuxI synthase and AHL receptors belong to the LuxR family of transcription regulators and are secreted by diffusion (LaSaree and Federle 2013).

## 7 Quorum Quenching

Quorum quenching is the counter-acting mechanism to interrupt QS-mediated activities. Interference with quorum sensing may result in the prevention of desired phenotypes without imposing selective pressure on them. As QS-mediated activities are not associated with bacterial house-keeping machinery, so, biofilm formation and pathogenicity can be managed by QQ (Lade et al. 2014). Quorum quenching agents inhibit some particular traits in bacteria that are not house-keeping processes, so bacteria don't need to overcome the inhibitory action of quorum quenching agents. The chance of getting resistance against them is less. However, some reports are also available about resistance against quorum quenching.

### 7.1 Quorum quenching Agents

Quorum quenching agents are broadly categorized into two classes: quorum sensing inhibitors (QSIs) and quorum quenching enzymes (QQEs). QSIs disrupt QS by competitive inhibition, antagonism, mimicry of QS signal molecules or by interfering in QS signal synthesis, secretion and perception (Grandclément et al. 2016). The first reported QSI was halogenated furanone obtained from *Delisea pulchra* (Givskov et al. 1996). QQEs cleave/or modify the QS signal molecules. AiiA (Lactonase) is the first reported quorum quenching enzyme from *Bacillus* sp. 240B (Dong et al. 2000). As quorum quenching enzymes act in the extracellular environment without entering the cell, the tendency of getting resistant is less likely than QSIs which either interact within cells or on the cell surface. Although QQ enzymes are less stable they make their application limited (Lu et al. 2021).

#### 7.1.1 Quorum sensing inhibitors (QSIs)

There are several types of Quorum sensing inhibitors (QSIs) isolated from different bacteria. Halogenated furanone of *Delisea pulchra* inhibits QS-mediated swarming and surface colonization by *Serratia liquefaciens* (Givskov et al. 1996). In *E. coli*, swarming motility and biofilm formation was inhibited by (5Z)-4-bromo-5-(bromomethylene)-3-butyl-2-(5H)-furanone (Ren et al. 2001). Recently 3-methyl-2(5H)-furanone and 2'-hydroxycinnamic acid are reported to inhibit biofilm formation in *K. pneumonia* ATCC 13884 up to 67.38% and 65.06% respectively. Further experiments showed that these compounds irreversibly affect the adhesion phase of the *K. pneumonia* ATCC 1388 (Cadavid and Echeverri 2019). Embeline and piperine inhibited the biofilm formation in *Streptococcus mutans* by interfering with signal perception involved in the QS pathway (Dwivedi and Singh 2016). 2, 6-Di-*tert*-butyl-4-methylphenol (DTBMP) was isolated from marine cyanobacterium *Chroococcus turgidus*. DTBMP effectively inhibited the bioluminescence in *V. harveyi* while biofilm related other

virulence characteristics such as exopolysaccharide production, hydrophobicity index, swimming and swarming motility in three major pathogenic vibrios: *V. harveyi*, *V. parahaemolyticus* and *V. vulnificus* were also inhibited by DTBMP (Santhakumari et al. 2018). Some QSIs which are produced by extremophilic and mesophilic bacteria are represented in Table 2 below.

### 7.1.2 Quorum quenching enzymes

Quorum quenching enzymes include AHL-lactonase, AHL-acylase and oxidoreductase (Fetzner 2015). AHL-lactonase and acylase chemically degrade the ester linkage of lactone ring and amide bond of Acyl homoserine lactone, respectively. However, the

Table 2 Example of some QSIs with their producer organisms

Quencher bacteria	QSIs	Reference
Marine bacterium <i>Halobacillus salinus</i>	N-(2'-phenylethyl)-butyramide 3-methyl-N-(2'-phenylethyl)-butyramide	Teasdale et al. 2009
Hexane, Dichloroethane, and Butanol extracts of <i>Marinobacter</i> sp. SK-3 and <i>Halomonas</i> sp. SK-1	Cyclo-(L-Pro-L-Phe) [DKP] Cyclo-(L-Pro-L-Leu) [DKP] Cyclo-(L-Pro-L-isoLeu) [DKP] Cyclo-(L-Pro-D-Phe) [DKP]	Abed et al. 2013
<i>Staphylococcus delphini</i>	N-(2'-phenylethyl)-urea N-[2-(1H-indol-3-yl)ethyl]-urea	Chu et al. 2013
<i>Rheinheimera aquimaris</i> QSI02	Cyclo(Trp-Ser (diketopiperazine factor))	Sun et al. 2016
<i>Oceanobacillus</i> sp. XC22919	2-methyl-N-(2'-phenylethyl) butyramide 3-methyl-N-(2'-phenylethyl)-butyramide benzyl benzoate	Chen et al. 2019
<i>Vibrio neptunius</i>	3-Methyl-N-(2'-Phenylethyl)-Butyramide	Meschwitz et al. 2019

Table 3 Name of some quorum quenching enzymes reported from mesophilic bacteria

<i>Rhodococcus erythropolis</i> W2	Oxidoreductase and acylase	Both oxidoreductase and amidolytic activity, degradation of short-chain AHLs, reduction of pathogenicity of <i>Pectobacterium carotovorum</i> in potato tubers.	Uroz et al. 2005
<i>Shewanella</i> sp. MIB015	AHL acylase	Degradation of long acyl AHLs, heterologous expression in fish pathogen <i>Vibrio anguillarum</i> reduced biofilm formation.	Morohoshi et al. 2008
<i>P. aeruginosa</i> PAO1	PvdQ (AHL-acylase)	<i>P. aeruginosa</i> virulence in <i>C. elegans</i> , swarming and production of elastase, pyocyanin were significantly reduced by PvdQ	Huang et al. 2003; Papaioannou et al. 2009
<i>Bacillus</i> sp. A196	AiiA <sub>A196</sub> Lactonase (thermostable)	Highest activity at 10 °C-40 °C at pH 8.0, also stable at 70 °C for 1hr, resistance to proteases and carp intestinal juices, oral administration of AiiA <sub>A196</sub> in Zebrafish attenuated infection of <i>Aeromonas hydrophila</i> .	Cao et al. 2012
<i>B. licheniformis</i> DAHB1	AiiA lactonase	Inhibit of severe Gastroenteritis disease and mortality of Indian white shrimps infected by <i>Vibrio parahaemolyticus</i> DAHB1, resistance to acidic intestinal juice, and proteases of the shrimps which make it effective to be used in shrimp aquaculture.	Vinoj et al. 2014
<i>Alteromonas stellipolaris</i> PQQ-42	Ahl lactonase	Prevention of AHL accumulation, production of chitinase, protease, and swarming motility in many <i>Vibrio</i> spp. in a fish hatchery, reduction of the tissue damage of the coral <i>Oculina patagonica</i> infected with aquaculture pathogen <i>V. mediterranei</i> Vibc-Oc-097.	Torres et al. 2016
<i>Kurthia huakui</i> LAM0618 <sup>T</sup>	AiiK lactonase	Heterologous expression of AiiK exhibited variable substrate spectrum, resistance to great resistance to $\alpha$ -chymotrypsin protease K and trypsin. AiiK significantly inhibited biofilm formation and attenuated extracellular proteolytic activity, pyocyanin synthesis of <i>P. aeruginosa</i> PAO1	Dong et al. 2018
<i>Bosea</i> sp. F3-2	AidB lactonase	Thermostability up to 80°C, maximum enzymatic activity at 60°C. Heterologous expression attenuates pyocyanin production and pathogenicity in <i>P. aeruginosa</i> and <i>P. carotovora</i> , respectively	Zhang et al. 2019

enzyme oxidoreductase chemically modifies the AHL without degradation (Liu et al. 2017). These enzymes are very effective against QS-mediated gene expression. Many AHL-lactonase, acylase and oxidoreductase enzymes have been reported from mesophilic as well as extremophilic bacteria. Only a few of them possess both AHL-lactonase and AHL-acylase enzymes as in *Deinococcus radiodurans*, *Photobacterium luminescens*, *Hyphomonas neptunium* and *Rhodococcus erythropolis* W2 (Kalia et al. 2011). Many reported QQ enzymes can effectively degrade AHLs and attenuate the virulence of pathogenic bacteria. Some quorum quenching mesophilic bacteria, their QQ enzyme, and quorum quenching properties are presented in table 3.

Although a lot of Quorum quenching enzymes are reported by various laboratories, the potentiality of enzymes can be limited by

cost, activity level or compatibility with recent biotechnological and industrial plants (Rémy et al. 2016). The exploitation of extremozymes has, therefore, achieved a considerable interest to fulfill the requisites such as tolerance in high temperatures, pH stability, production optimization, wide solvent range etc. (Mayer et al. 2015). There are few reports on the quorum quenching enzymes isolated from halophiles and thermophiles which show high affectivity. Some of these quorum quenching extremozymes are listed below in Table 4.

Actinomycetous bacteria are also reported to possess quorum quenching activity. For example, marine Actinomycete strain A66 extracts were observed to reduce biofilm formation in *V. harveyi* at a concentration of 2.5% (v/v). Strain A66 reduced the number of microcolonies and attenuated biofilm architecture. It was found

Table 4 Name of some quorum quenching enzymes reported from extremophilic microorganisms

<i>Sulfolobus islandicus</i> (Hyperthermophilic archaeon)	sisLac lactonase	Member of Phosphotriesterase like Lactonase (PLL) family, optimum pH and temperature 7 to 10 and 85°C, respectively, preference for medium length (C8, C10) of acyl chain AHLs,	Hiblot et al. 2012
<i>Sulfolobus solfataricus</i> (hyperthermophilic archaeon)	SsoPox lactonase	Member of PLL family, a bifunctional enzyme with organophosphate hydrolase and PLL Lactonase, reduction of virulence factor, elastase pyocyanin production in <i>P. aeruginosa</i> by SsoPox –Lactonase	Ng et al. 2011
<i>Thalassomonas</i> sp. PP2-459 (Marine)	Qqenzyme other than lactonase	Reduction of AHLs with different acyl chains in <i>Halomonas anticariensis</i> FP35 <sup>T</sup> and aquaculture pathogen <i>V. anguillarum</i> ATCC 1926 <sup>T</sup>	Torres et al. 2013
<i>Tenacibaculum</i> sp. Strain 20J	AHL lactonase	Member of phosphotriesterase (PTE) family, a cell-bound soluble AHL-lactonase having the capacity to degrade both short and long-chain Ahls. reduction of pathogenicity of the fish pathogen <i>Edwardsiella tarda</i> ACC 35.1 which otherwise causes Septicaemia Edwardsiellosis.	Romero et al. 2014
<i>Tenacibaculum</i> sp. 20J (marine bacterium)	Aii20J lactonase (thermostable)	Unspecified and broad substrate range, retention of activity at 80 ° C, pH range 3-9, resistance to protease K and alpha-chymotrypsin, reduction of cell viability, and glutamate-dependent acid resistance in <i>E. coli</i> K-12.	Mayer et al. 2015
<i>P. flavipulchra</i> JG1	PfmA acylase	Degradation of AHLs with long side chain, reduction of production virulence facts (protease, pyocyanin) in <i>Vibrio anguillarum</i> VIB72 and <i>P. aeruginosa</i> PAO1. PfmA also increased the survivality of <i>Artemia</i> sp. (model animal) infected with <i>P. aeruginosa</i> .	Liu et al. 2017
<i>Salinicola salaria</i> MCCC1A01339 (halophilic bacterium)	AhIX lactonase	Highly stable, broad substrate specificity, ~100% activity at 60°C after 2 hr incubation, retention of 60% activity at 25% NaCl, dried AhIX powder generated by a spray-dry process at 80-120°C temperature reduced infection of <i>Erwinia carotovora</i> on potato slices and Chinese cabbage.	Liu et al. 2019
<i>Stenotrophomonas maltophilia</i>	QQ enzyme	Inhibition of AHL accumulation, reduction by enzymatic activity in <i>Pectobacterium carotovorum</i> CECT 225 <sup>T</sup> and <i>Vibrio coralliilyticus</i> VibC-Oc-193 in the co-cultivation experiment. Reduction in potato tuber maceration and mortality of <i>Artemia salina</i> by <i>P. carotovorum</i> and <i>V. coralliilyticus</i> , respectively.	Reina et al. 2019
<i>Psychrobacter</i> strain M9-54-1	AhaP Acylase	Wide range of unsubstituted and substituted AHLs (C4-HSL to C14-HSL) at 4°C, 15°C, and 28°C. Reduction of swarming motility and cytotoxic galactophilic lectin synthesis in <i>P. aeruginosa</i> PAO1. Decrease in mortality of brine shrimps infected by <i>Vibrio coralliilyticus</i> VibC-Oc-193	Reina et al. 2021
<i>Reinheimera aquimaris</i> , <i>Acinetobacter junii</i> , <i>Pseudomonas sihuiensis</i> , <i>Ruegeria atlantica</i> and <i>Microbulbifer echini</i>	QQ enzyme other than AHL Lactonase	Degradation of all AHLs in <i>Vibrio coralliilyticus</i> along with a reduction in virulence factors synthesis increased survivality of <i>Artemia salina</i>	Reina et al. 2022



that strain A66 inhibited the *Vibrio* biofilm formation at both the initiation and maturation stages. At a concentration of 2.5% (v/v), the inhibition rate of crude extract was 99.3% while the degradation rate was 75.6% (You et al. 2007). Quorum quenching activity is also reported in Coral Associated Bacteria (CAB). Crude extract of *B. horikoshii* (E6), isolated from the coral *Acropora digitifera* restricted biofilm formation in clinical M serotypes of *S. pyogenes* at very low concentrations [10–50  $\mu\text{g mL}^{-1}$ ] (Thenmozhi et al. 2009). In another study, *Bacillus firmus* and *Vibrio parahemolyticus* which were isolated from *Acropora digitifera*, have shown quorum quenching activity against Methicillin-Resistant *S. aureus* (MRSA) and Methicillin Susceptible *S. aureus* (MSSA). *B. firmus* and *V. parahemolyticus* significantly reduced the synthesis of EPS and hemolysin which resulted in inhibition of biofilms (80–87%) formed by both MRSA and MSSA. Furthermore, CAB extracts strongly decreased Cell Surface Hydrophobicity (CSH) of *S. aureus* which mediates adherence of the bacteria to substrata during biofilm formation (Gowrishankar et al. 2012).

### 7.1.3 Application of QQ Bacteria

Nowadays application of crude QQ enzymes on pathogenic bacteria and medical devices has been reported to attenuate biofilm formation. Immobilization of SsoPox Lactonase enzyme isolated from thermophilic archaeon *Sulfolobus solfataricus* onto the nano alumina membrane showed increased activity up to 25% as compared to control set. Application of Membrane immobilized SsoPox reduced pyocyanin synthesis and elastase activity when added to *P. aeruginosa* PAO1 culture (Ng et al. 2011). Catheter functionalization was investigated using a silicon catheter coated with AHL Acylase of *Aspergillus melleus*. Adhesion of *P. aeruginosa* ATCC 10145 was strongly inhibited in comparison to the control set. Moreover, biofilm formation was also reduced up to 50% in acylase-coated catheters (Ivanova et al. 2015a). The combination of acylase and amylase on multi-layer coatings of urinary catheters reduced biofilm formation in *P. aeruginosa* and *S. aureus*, respectively (Ivanova et al. 2015b). Immobilization of quorum quenching bacteria was done in magnetic nanocomposite beads (IMN) and significant degradation of C6-HSL was achieved (Kaur and Yogalakshmi 2022). Another study showed that QSIs restricted antibiotic-induced resistance mutation in *E. coli* which indicated combination of QSIs and antibiotics may be effective to inhibit bacterial growth (Ning et al. 2021).

## 8 Alternate strategy for inhibition of biofilm formation

### 8.1 Use of Bacteriophages

There are some other regulatory factors regarding biofilm formation in bacteria apart from quorum sensing. Second messengers like c-di-GMP and cAMP mediate different

physiological processes during biofilm formation (Ha and O'Toole 2015; Sutrina et al. 2015; Jenal et al. 2017; Sutrina et al. 2019). Regarding such factors, quorum quenching may not be the sole weapon for controlling biofilm formation. Engineered T7 phage showed a reduction of bacterial count in *E. coli* biofilm when polysaccharide degrading enzyme, Depolymerase gene *dspB* was incorporated within its genome (Lu et al. 2007). Another engineered T7 phage containing AHL Lactonase gene *aiaA* (derived from *B. anthracis*) showed effective degradations of AHLs in many bacteria along with effective cell lysis in the specific host (Pei and Lamas-Samanamud 2014). Sometimes cocktails of phages targeting various cell receptors, have been used to prevent phage resistance (Chan et al. 2013; Pires et al. 2017) as some reports showed re-growth of single phage-treated bacterial biofilms (Pires et al. 2017; Tan et al. 2019). A combination of phage and antibiotics is another way to get rid of phage-resistant host variants (Verma et al. 2009). Although bacteriophages cannot be used in human, animal as well as commercial aspects due to a lack of regulations (Fauconnier 2017) and license (Ferriol-González and Domingo-Calap 2020). Treatment of single Bacteriophages as well as bacteriophage cocktails have been used in medical devices such as urinary catheters and ultra-specific host bacteria (Curtin and Donlan 2006; Goldman et al. 2009; Fu et al. 2010).

### 8.2 Use of EPS matrix-degrading enzymes

Enzymatic breakdown of biofilm matrix is another approach to control bacterial biofilms. Cellulase enzymes obtained from *A. niger* (C1184-Sigma Aldrich) as well as partially purified Cellulase enzyme of *Bacillus* sp. DGV19 (EU053862.1) has significantly reduced biofilm formation in *Burholderia cepacia* on sterile discs made up of polyvinyl chloride (PVC), polystyrene, glass slides and polycarbonate (Rajasekharan and Ramesh 2013). Another experiment showed that an extracellular  $\alpha$ -amylase isolated from marine bacteria *Bacillus subtilis* S8-18 not only inhibited biofilm formation but also degraded pre-formed mature biofilms of Methicillin-Resistant *S. aureus* (MRSA), *P. aeruginosa* and *V. cholerae* (Kalpana et al., 2012). Further 1:1 mixture of commercially purchased cellulase and amylase enzymes reduced EPS biomass of *S. aureus* and *P. aeruginosa* monoculture and co-culture biofilms making the biofilm more susceptible to conventional antimicrobial agents as well as increasing the release of planktonic cells from biofilms both *in vitro* and *in vivo* (Fleming et al. 2017). Alginate lyase, Lysozyme and Dispersin B also showed effective inhibition of biofilms of various pathogenic bacteria when treated alone or in combination with antibiotics (Alkawash et al. 2006; Donelli et al. 2007; Kolkai et al. 2009). DNase and proteases have also capability to break down EPS matrix components as well (Eckhart et al. 2007; Saggiu et al. 2019).

## Conclusion

Biofilm formation, particularly in pathogenic bacteria has appeared as a threatening problem in conventional treatment. Disruption of QS-mediated biofilm formation in pathogenic bacteria, therefore, may show a trustful alternate strategy to control this particular feature instead of the application of excess antibiotics. Many QSIs and QQ enzymes are reported from mesophilic as well as extremophilic microorganisms which can attenuate QS signals, biofilm formation, virulence, pathogenicity etc. of pathogenic bacteria *in vitro* conditions. Recent experiments have been done to control biofilm formation in medical devices which otherwise cause further infection of patients. Apart from quorum quenching, other strategies such as phage therapy, enzymatic breakdown of EPS matrix etc. are also effective to combat the problem of biofilm formation in pathogenic bacteria. The application of these strategies may control biofilms of pathogens actively. A combination of QSIs or QQ enzymes with EPS degrading enzymes may be used in aquaculture to manage QS-mediated bacterial infection. QQ bacteria may also be used as probiotics or as food supplements which may improve disease management and survival of organisms in aquaculture. Though bacteriophages can't be used in humans and animals for their inherent allergenicity; a combination of bacteriophages with EPS degrading enzymes or QQ enzymes may be used in membrane bioreactors during wastewater management to combat bio-fouling. On the other hand, quorum quenching enzymes along with EPS degrading enzymes can be immobilized on medical devices to attenuate medical device-associated diseases in hospitals. Purified QQ enzymes or their heterologous expression in probiotic bacteria can be used in pharmaceutical industries for the production of new medicines as well. Thus, quorum quenching may a suitable tool for the treatment of MDR pathogenic strains as well as biofilm-forming bacteria in various fields where biofilms create serious problems to handle. Exploration of quorum quenching enzymes with a better biotechnological application can lead to novel techniques in wastewater management, aquaculture, agriculture and most importantly conventional chemotherapy in medical science.

## Conflict of interest

The authors declare that there is no conflict of interest.

## Funding information

This work is supported by the Council of Scientific & Industrial Research (CSIR), Government of India.

## Reference

Abebe, G.M. (2020) The Role of Bacterial Biofilm in Antibiotic Resistance and Food Contamination. *International Journal of*

*Microbiology*, Article ID 1705814, <https://doi.org/10.1155/2020/1705814>

Abed, R. M., Dobretsov, S., Al-Fori, M., Gunasekera, S. P., Sudesh, K., & Paul, V. J. (2013). Quorum-sensing inhibitory compounds from extremophilic microorganisms isolated from a hypersaline cyanobacterial mat. *Journal of Industrial Microbiology and Biotechnology*, 40(7), 759-772.

Alkawash, M. A., Soothill, J. S., & Schiller, N. L. (2006). Alginate lyase enhances antibiotic killing of mucoid *Pseudomonas aeruginosa* in biofilms. *Apmis*, 114(2), 131-138

Bagge, N., Hentzer, M., Andersen, J. B., Ciofu, O., Givskov, M., & Høiby, N. (2004). Dynamics and spatial distribution of  $\beta$ -lactamase expression in *Pseudomonas aeruginosa* biofilms. *Antimicrobial Agents and Chemotherapy*, 48(4), 1168-1174

Bhattacharjee, A., Nusca, T. D., & Hochbaum, A. I. (2016). Rhamnolipids mediate an interspecies biofilm dispersal signaling pathway. *ACS Chemical Biology*, 11(11), 3068-3076

Boehm, A., Steiner, S., Zaehring, F., Casanova, A., et al. (2009). Second messenger signalling governs *Escherichia coli* biofilm induction upon ribosomal stress. *Molecular Microbiology*, 72(6), 1500-1516

Boles, B. R., Thoendel, M., & Singh, P. K. (2005). Rhamnolipids mediate detachment of *Pseudomonas aeruginosa* from biofilms. *Molecular Microbiology*, 57(5), 1210-1223

Cadavid, E., & Echeverri, F. (2019). The search for natural inhibitors of biofilm formation and the activity of the autoinductor C6-AHL in *Klebsiella pneumoniae* ATCC 13884. *Biomolecules*, 9(2), 49

Cao, Y., He, S., Zhou, Z., Zhang, M., et al. (2012). Orally administered thermostable N-acyl homoserine lactonase from *Bacillus* sp. strain AI96 attenuates *Aeromonas hydrophila* infection in zebrafish. *Applied and Environmental Microbiology*, 78(6), 1899-1908

Chan, B. K., Abedon, S. T., & Loc-Carrillo, C. (2013). Phage cocktails and the future of phage therapy. *Future Microbiology*, 8(6), 769-783

Chen, X., Chen, J., Yan, Y., Chen, S., et al. (2019). Quorum sensing inhibitors from marine bacteria *Oceanobacillus* sp. XC22919. *Natural Product Research*, 33(12), 1819-1823

Chmielewski, R. A. N., & Frank, J. F. (2003). Biofilm formation and control in food processing facilities. *Comprehensive Reviews in Food Science and Food Safety*, 2(1), 22-32

- Chu, Y. Y., Nega, M., Wölfle, M., Plener, L., et al. (2013) A new class of quorum quenching molecules from *Staphylococcus* species affects communication and growth of gram-negative bacteria. *PLoS Pathogens* 9:e1003654. <https://doi.org/10.1371/journal.ppat.1003654>
- Cucarella, C., Solano, C., Valle, J., Amorena, B., Lasa, I., & Penadés, J. R. (2001). Bap, a *Staphylococcus aureus* surface protein involved in biofilm formation. *Journal of Bacteriology*, 183(9), 2888-2896
- Curtin, J. J., & Donlan, R. M. (2006). Using bacteriophages to reduce formation of catheter-associated biofilms by *Staphylococcus epidermidis*. *Antimicrobial Agents and Chemotherapy*, 50(4), 1268-1275
- Dales, L., Ferris, W., Vandemheen, K., & Aaron, S. D. (2009). Combination antibiotic susceptibility of biofilm-grown *Burkholderia cepacia* and *Pseudomonas aeruginosa* isolated from patients with pulmonary exacerbations of cystic fibrosis. *European Journal of Clinical Microbiology & Infectious Diseases*, 28(10), 1275-1279
- Davey, M. E., Caiazza, N. C., & O'Toole, G. A. (2003). Rhamnolipid surfactant production affects biofilm architecture in *Pseudomonas aeruginosa* PAO1. *Journal of Bacteriology*, 185(3), 1027-1036
- Davies, D. G., Parsek, M.R., Pearson, J.P., Iglewski, B.H., Costerton, J.W., & Greenberg, E.P. (1998). The involvement of cell-to-cell signals in the development of a bacterial biofilm. *Science*, 280, 295-298
- Donelli, G., Francolini, I., Romoli, D., Guaglianone, E., et al. (2007). Synergistic activity of dispersin B and cefamandole nafate in inhibition of staphylococcal biofilm growth on polyurethanes. *Antimicrobial Agents and Chemotherapy*, 51(8), 2733-2740
- Dong, W., Zhu, J., Guo, X., Kong, D., et al. (2018). Characterization of AiiK, an AHL lactonase, from *Kurthia huakui* LAM0618T and its application in quorum quenching on *Pseudomonas aeruginosa* PAO1. *Scientific Reports*, 8(1), 1-11
- Dong, Y. H., Xu, J. L., Li, X. Z., & Zhang, L. H. (2000). AiiA, an enzyme that inactivates the acylhomoserine lactone quorum-sensing signal and attenuates the virulence of *Erwinia carotovora*. *Proceedings of the National Academy of Sciences*, 97(7), 3526-3531
- Dong, Y., Zhang, X. F., An, S. W., Xu, J. L., & Zhang, L. H. (2008). A novel two-component system BqsS-BqsR modulates quorum sensing-dependent biofilm decay in *Pseudomonas aeruginosa*. *Communicative & Integrative Biology*, 1(1), 88-96.
- Donlan, R. M. (2002). Biofilms: microbial life on surfaces. *Emerging infectious diseases*, 8(9), 881
- Dueholm, M. S., Søndergaard, M. T., Nilsson, M., Christiansen, G., et al. (2013). Expression of Fap amyloids in *Pseudomonas aeruginosa*, *P. fluorescens*, and *P. putida* results in aggregation and increased biofilm formation. *Microbiologyopen*, 2(3), 365-382
- Dufour, D., Leung, V., & Lévesque, C. M. (2010). Bacterial biofilm: structure, function, and antimicrobial resistance. *Endodontic Topics*, 22(1), 2-16.
- Dwivedi, D., & Singh, V. (2016). Effects of the natural compounds embelin and piperine on the biofilm-producing property of *Streptococcus mutans*. *Journal of Traditional and Complementary Medicine*, 6(1), 57-61
- Eckhart, L., Fischer, H., Barken, K. B., Tolker-Nielsen, T., & Tschachler, E. (2007). DNase1L2 suppresses biofilm formation by *Pseudomonas aeruginosa* and *Staphylococcus aureus*. *British Journal of Dermatology*, 156(6), 1342-1345
- Fauconner, A. (2017). Regulating phage therapy: the biological master file concept could help to overcome regulatory challenge of personalized medicines. *EMBO Reports*, 18(2), 198-200
- Ferriol-González, C., & Domingo-Calap, P. (2020). Phages for biofilm removal. *Antibiotics*, 9(5), 268
- Fetzner, S. (2015). Quorum quenching enzymes. *Journal of Biotechnology*, 201, 2-14
- Fleming, D., Chahin, L., & Rumbaugh, K. (2017). Glycoside hydrolases degrade polymicrobial bacterial biofilms in wounds. *Antimicrobial Agents and Chemotherapy*, 61(2), e01998-16. <https://doi.org/10.1128/AAC.01998-16>
- Friedman, L., & Kolter, R. (2004a). Genes involved in matrix formation in *Pseudomonas aeruginosa* PA14 biofilms. *Molecular Microbiology*, 51(3), 675-690
- Friedman, L., & Kolter, R. (2004b). Two genetic loci produce distinct carbohydrate-rich structural components of the *Pseudomonas aeruginosa* biofilm matrix. *Journal of Bacteriology*, 186(14):4457-4465
- Fu, W., Forster, T., Mayer, O., Curtin, J. J., Lehman, S. M., & Donlan, R. M. (2010). Bacteriophage cocktail for the prevention of biofilm formation by *Pseudomonas aeruginosa* on catheters in an in vitro model system. *Antimicrobial Agents and Chemotherapy*, 54(1), 397-404

- Fuqua, C., & Greenberg, E. P. (2002). Listening in on bacteria: acyl-homoserine lactone signalling. *Nature Reviews Molecular Cell biology*, 3(9), 685-695
- Gillis, R. J., White, K. G., Choi, K. H., Wagner, V. E., Schweizer, H. P., & Iglewski, B. H. (2005). Molecular basis of azithromycin-resistant *Pseudomonas aeruginosa* biofilms. *Antimicrobial Agents and Chemotherapy*, 49(9), 3858-3867
- Givskov, M., de Nys, R. O. C. K. Y., Manefield, M., Gram, L., et al. (1996). Eukaryotic interference with homoserine lactone-mediated prokaryotic signalling. *Journal of Bacteriology*, 178(22), 6618-6622
- Goldman, G., Starosvetsky, J., & Armon, R. (2009). Inhibition of biofilm formation on UF membrane by use of specific bacteriophages. *Journal of Membrane Science*, 342(1-2), 145-152.
- Gowrishankar, S., Duncun Mosioma, N., & Karutha Pandian, S. (2012). Coral-associated bacteria as a promising antibiofilm agent against methicillin-resistant and-susceptible *Staphylococcus aureus* biofilms. *Evidence-Based Complementary and Alternative Medicine*, 2012. <https://doi.org/10.1155/2012/862374>
- Grandclément, C., Tannières, M., Moréra, S., Dessaux, Y., & Faure, D. (2016). Quorum quenching: role in nature and applied developments. *FEMS Microbiology Reviews*, 40(1), 86-116
- Gueriri, I., Cyncynatus, C., Dubrac, S., Arana, A. T., Dussurget, O., & Msadek, T. (2008). The DegU orphan response regulator of *Listeria monocytogenes* autorepresses its own synthesis and is required for bacterial motility, virulence and biofilm formation. *Microbiology*, 154(8), 2251-2264
- Ha, D. G., & O'Toole, G. A. (2015). c-di-GMP and its effects on biofilm formation and dispersion: a *Pseudomonas aeruginosa* review. *Microbiology Spectrum*, 3(2), 3-2
- Hall-Stoodley, L., & Stoodley, P. (2009). Evolving concepts in biofilm infections. *Cellular Microbiology*, 11(7), 1034-1043
- Hamilton, H. L., Domínguez, N. M., Schwartz, K. J., Hackett, K. T., & Dillard, J. P. (2005). *Neisseria gonorrhoeae* secretes chromosomal DNA via a novel type IV secretion system. *Molecular Microbiology*, 55(6), 1704-1721
- Haruna, Z., Idris, A. H., Muhammad, M. I., Abdulwahab, N. M., Abdullahi, S., & Wada, N. M. (2022). Biofilm forming Enterococci and their Status as Emerging Multidrug Resistant Bacteria. *International Journal of Biological, Physical and Chemical Studies*, 4(1), 01-06
- Heurlier, K., Déneraud, V., Pessi, G., Reimann, C., & Haas, D. (2003). Negative control of quorum sensing by RpoN ( $\sigma_{54}$ ) in *Pseudomonas aeruginosa* PAO1. *Journal of Bacteriology*, 185(7), 2227-2235
- Hiblot, J., Gotthard, G., Chabriere, E., & Elias, M. (2012). Structural and enzymatic characterization of the lactonase *sis lac* from *Sulfolobus islandicus*. <https://doi.org/10.1371/journal.pone.0047028>
- Hornby, J. M., Jensen, E. C., Lisee, A. D., Tasto, J. J., et al. (2001). Quorum sensing in the dimorphic fungus *Candida albicans* is mediated by farnesol. *Applied and Environmental Microbiology*, 67(7), 2982-2992
- Hu, H., He, J., Liu, J., Yu, H., Tang, J., & Zhang, J. (2016). Role of N-acyl-homoserine lactone (AHL) based quorum sensing on biofilm formation on packing media in wastewater treatment process. *Rsc Advances*, 6(14), 11128-11139
- Huang, J. J., Han, J. I., Zhang, L. H., & Leadbetter, J. R. (2003). Utilization of acyl-homoserine lactone quorum signals for growth by a soil *Pseudomonas* and *Pseudomonas aeruginosa* PAO1. *Applied and Environmental Microbiology*, 69(10), 5941-5949
- Huber, B., Riedel, K., Hentzer, M., Heydorn, A., et al. (2001). The cep quorum-sensing system of *Burkholderia cepacia* H111 controls biofilm formation and swarming motility. *Microbiology*, 147(9), 2517-2528
- Ivanova, K., Fernandes, M. M., Francesko, A., Mendoza, E., et al. (2015b). Quorum-quenching and matrix-degrading enzymes in multilayer coatings synergistically prevent bacterial biofilm formation on urinary catheters. *ACS applied materials & interfaces*, 7(49), 27066-27077
- Ivanova, K., Fernandes, M. M., Mendoza, E., & Tzanov, T. (2015a). Enzyme multilayer coatings inhibit *Pseudomonas aeruginosa* biofilm formation on urinary catheters. *Applied Microbiology and Biotechnology*, 99(10), 4373-4385
- Jefferson, K. K. (2004). What drives bacteria to produce a biofilm?. *FEMS Microbiology Letters*, 236(2), 163-173
- Jefferson, K. K., Pier, D. B., Goldmann, D. A., & Pier, G. B. (2004). The teicoplanin-associated locus regulator (TcaR) and the intercellular adhesin locus regulator (IcaR) are transcriptional inhibitors of the *ica* locus in *Staphylococcus aureus*. *Journal of Bacteriology*, 186(8), 2449-2456
- Jenal, U., Reinders, A., & Lori, C. (2017). Cyclic di-GMP: second messenger extraordinaire. *Nature Reviews Microbiology*, 15(5), 271-284
- Jensen, P. Ø., Bjarnsholt, T., Phipps, R., Rasmussen, T. B., et al. (2007). Rapid necrotic killing of polymorphonuclear leukocytes is

- caused by quorum-sensing-controlled production of rhamnolipid by *Pseudomonas aeruginosa*. *Microbiology*, *153*(5), 1329-1338
- Jordan, S. J., Perna, S., Glenn, S., Fernandes, I., et al. (2008). *Listeria monocytogenes* biofilm-associated protein (BapL) may contribute to surface attachment of *L. monocytogenes* but is absent from many field isolates. *Applied and Environmental Microbiology*, *74*(17), 5451-5456
- Kalia, V. C., Raju, S. C., & Purohit, H. J. (2011). Genomic analysis reveals versatile organisms for quorum quenching enzymes: acyl-homoserine lactone-acylase and-lactonase. *The Open Microbiology Journal*, *5*, 1. <https://dx.doi.org/10.2174%2F1874285801105010001>
- Kalpana, B. J., Aarthy, S., & Pandian, S. K. (2012). Antibiofilm activity of  $\alpha$ -amylase from *Bacillus subtilis* S8-18 against biofilm forming human bacterial pathogens. *Applied Biochemistry and Biotechnology*, *167*(6), 1778-1794
- Kaplan, J. Á. (2010). Biofilm dispersal: mechanisms, clinical implications, and potential therapeutic uses. *Journal of Dental Research*, *89*(3), 205-218
- Kaplan, J. B., Meyenhofer, M. F., & Fine, D. H. (2003a). Biofilm growth and detachment of *Actinobacillus actinomycetemcomitans*, *185* (4), <https://doi.org/10.1128/JB.185.4.1399-1404.2003>
- Kaplan, J. B., Raguath, C., Ramasubbu, N., & Fine, D. H. (2003b). Detachment of *Actinobacillus actinomycetemcomitans* biofilm cells by an endogenous  $\beta$ -hexosaminidase activity. *Journal of Bacteriology*, *185*(16), 4693-4698
- Karatan, E., & Watnick, P. (2009). Signals, regulatory networks, and materials that build and break bacterial biofilms. *Microbiology and Molecular Biology Reviews*, *73*(2), 310-347
- Kaur, J., & Yagalakshmi, K. N. (2022). Degradation of n-hexanoyl homoserine lactone with quorum quenching bacteria immobilised magnetic nanocomposite beads. *Environmental Technology*, *43*(6), 885-892
- Kirmusaoğlu, S. (2016). Staphylococcal biofilms: Pathogenicity, mechanism and regulation of biofilm formation by quorum sensing system and antibiotic resistance mechanisms of biofilm embedded microorganisms. *Microbial biofilms: importance and applications. IntechOpen*, 189-209.
- Kokai-Kun, J. F., Chanturiya, T., & Mond, J. J. (2009). Lysostaphin eradicates established *Staphylococcus aureus* biofilms in jugular vein catheterized mice. *Journal of Antimicrobial Chemotherapy*, *64*(1), 94-100
- Lade, H., Paul, D., & Kweon, J. H. (2014). Quorum quenching mediated approaches for control of membrane biofouling. *International Journal of Biological Sciences*, *10*(5), 550.
- LaSarre, B., & Federle, M. J. (2013). Exploiting quorum sensing to confuse bacterial pathogens. *Microbiology and Molecular Biology Reviews*, *77*(1), 73-111
- Lebeaux, D., & Ghigo, J. M. (2012). Infections associées aux biofilms-Quelles perspectives thérapeutiques issues de la recherche fondamentale?. *Médecine/sciences*, *28*(8-9), 727-739
- Lebeaux, D., Chauhan, A., Rendueles, O., & Beloin, C. (2013). From in vitro to in vivo models of bacterial biofilm-related infections. *Pathogens*, *2*(2), 288-356
- Leid, J. G., Willson, C. J., Shirtliff, M. E., Hassett, D. J., Parsek, M. R., & Jeffers, A. K. (2005). The exopolysaccharide alginate protects *Pseudomonas aeruginosa* biofilm bacteria from IFN- $\gamma$ -mediated macrophage killing. *The Journal of Immunology*, *175*(11), 7512-7518
- Lemon, K. P., Higgins, D. E., & Kolter, R. (2007). Flagellar motility is critical for *Listeria monocytogenes* biofilm formation. *Journal of Bacteriology*, *189*(12), 4418-4424
- Lewis, K. (2001). Riddle of biofilm resistance. *Antimicrobial Agents and Chemotherapy*, *45*(4), 999-1007
- Liu, N., Yu, M., Zhao, Y., Cheng, J., An, K., & Zhang, X. H. (2017). PfmA, a novel quorum-quenching N-acylhomoserine lactone acylase from *Pseudoalteromonas flavipulchra*. *Microbiology*, *163*(10), 1389-1398
- Liu, P., Chen, Y., Shao, Z., Chen, J., et al. (2019). AhlX, an N-acylhomoserine lactonase with unique properties. *Marine Drugs*, *17*(7), 387
- Loo, C. Y. (2003). Oral streptococcal genes that encode biofilm formation. *Medical implications of biofilms*, *1*, 212-227.
- Lu, L., Li, M., Yi, G., Liao, L., et al. (2021). Screening strategies for quorum sensing inhibitors in combating bacterial infection. *Journal of Pharmaceutical Analysis*, *12*(1), 1-4. <https://doi.org/10.1016/j.jpha.2021.03.009>
- Lu, T. K., & Collins, J. J. (2007). Dispersing biofilms with engineered enzymatic bacteriophage. *Proceedings of the National Academy of Sciences*, *104*(27), 11197-11202
- Lynch, D. J., Fountain, T. L., Mazurkiewicz, J. E., & Banas, J. A. (2007). Glucan-binding proteins are essential for shaping

- Streptococcus mutans* biofilm architecture. *FEMS Microbiology Letters*, 268(2), 158-165
- Ma, L., Conover, M., Lu, H., Parsek, M. R., Bayles, K., & Wozniak, D. J. (2009). Assembly and development of the *Pseudomonas aeruginosa* biofilm matrix. *PLoS Pathogens*, 5(3), e1000354. <https://doi.org/10.1371/journal.ppat.1000354>
- Ma, L., Wang, J., Wang, S., Anderson, E. M., et al. (2012). Synthesis of multiple *Pseudomonas aeruginosa* biofilm matrix exopolysaccharides is post-transcriptionally regulated. *Environmental Microbiology*, 14(8), 1995-2005
- Madsen, J. S., Burmølle, M., Hansen, L. H., & Sørensen, S. J. (2012). The interconnection between biofilm formation and horizontal gene transfer. *FEMS Immunology & Medical Microbiology*, 65(2), 183-195
- Mai-Prochnow, A., Lucas-Elio, P., Egan, S., Thomas, T., et al. (2008). Hydrogen peroxide linked to lysine oxidase activity facilitates biofilm differentiation and dispersal in several gram-negative bacteria. *Journal of Bacteriology*, 190(15), 5493-5501
- Mayer, C., Romero, M., Muras, A., & Otero, A. (2015). Aii20J, a wide-spectrum thermostable N-acylhomoserine lactonase from the marine bacterium *Tenacibaculum* sp. 20J, can quench AHL-mediated acid resistance in *Escherichia coli*. *Applied Microbiology and Biotechnology*, 99(22), 9523-9539
- Meschwitz, S. M., Teasdale, M. E., Mozzer, A., Martin, N., et al. (2019). Antagonism of quorum sensing phenotypes by analogs of the marine bacterial secondary metabolite 3-methyl-N-(2'-phenylethyl)-butyramide. *Marine Drugs*, 17(7), 389
- Möker, N., Dean, C. R., & Tao, J. (2010). *Pseudomonas aeruginosa* increases formation of multidrug-tolerant persister cells in response to quorum-sensing signaling molecules. *Journal of Bacteriology*, 192(7), 1946-1955
- Morgan, R., Kohn, S., Hwang, S. H., Hassett, D. J., & Sauer, K. (2006). BdlA, a chemotaxis regulator essential for biofilm dispersion in *Pseudomonas aeruginosa*. *Journal of Bacteriology*, 188(21), 7335-7343
- Morohoshi, T., Nakazawa, S., Ebata, A., Kato, N., & Ikeda, T. (2008). Identification and characterization of N-acylhomoserine lactone-acylase from the fish intestinal *Shewanella* sp. strain MIB015. *Bioscience, Biotechnology, and Biochemistry*, 72(7), 1887-1893
- Newell, P. D., Monds, R. D., & O'Toole, G. A. (2009). LapD is a bis-(3', 5')-cyclic dimeric GMP-binding protein that regulates surface attachment by *Pseudomonas fluorescens* Pf0-1. *Proceedings of the National Academy of Sciences*, 106(9), 3461-3466
- Ng, F. S., Wright, D. M., & Seah, S. Y. (2011). Characterization of a phosphotriesterase-like lactonase from *Sulfolobus solfataricus* and its immobilization for disruption of quorum sensing. *Applied and Environmental Microbiology*, 77(4), 1181-1186
- Nguyen, D., Joshi-Datar, A., Lepine, F., Bauerle, E., et al. (2011). Active starvation responses mediate antibiotic tolerance in biofilms and nutrient-limited bacteria. *Science*, 334(6058), 982-986
- Ning, Q., Wang, D., & You, J. (2021). Joint effects of antibiotics and quorum sensing inhibitors on resistance development in bacteria. *Environmental Science: Processes & Impacts*, 23(7), 995-1005
- O'Toole, G., Kaplan, H. B., & Kolter, R. (2000). Biofilm formation as microbial development. *Annual Reviews in Microbiology*, 54(1), 49-79
- Pamp, S. J., & Tolker-Nielsen, T. (2007). Multiple roles of biosurfactants in structural biofilm development by *Pseudomonas aeruginosa*. *Journal of Bacteriology*, 189(6), 2531-2539
- Papaioannou, E., Wahjudi, M., Nadal-Jimenez, P., Koch, G., Setroikromo, R., & Quax, W. J. (2009). Quorum-quenching acylase reduces the virulence of *Pseudomonas aeruginosa* in a *Caenorhabditis elegans* infection model. *Antimicrobial Agents and Chemotherapy*, 53(11), 4891-4897
- Pei, R., & Lamas-Samanamud, G. R. (2014). Inhibition of biofilm formation by T7 bacteriophages producing quorum-quenching enzymes. *Applied and Environmental Microbiology*, 80(17), 5340-5348
- Pires, D. P., Dötsch, A., Anderson, E. M., Hao, Y., et al. (2017). A genotypic analysis of five *P. aeruginosa* strains after biofilm infection by phages targeting different cell surface receptors. *Frontiers in Microbiology*, 8, 1229
- Prigent-Combaret, C., Prensier, G., Le Thi, T. T., Vidal, O., Lejeune, P., & Dorel, C. (2000). Developmental pathway for biofilm formation in curli-producing *Escherichia coli* strains: role of flagella, curli and colanic acid. *Environmental Microbiology*, 2(4), 450-464
- Purevdorj-Gage, B., Costerton, W. J., & Stoodley, P. (2005). Phenotypic differentiation and seeding dispersal in non-mucoid and mucoid *Pseudomonas aeruginosa* biofilms. *Microbiology*, 151(5), 1569-1576
- Rabin, N., Zheng, Y., Opoku-Temeng, C., Du, Y., Bonsu, E., & Sintim, H. O. (2015). Biofilm formation mechanisms and targets

- for developing antibiofilm agents. *Future Medicinal Chemistry*, 7 (4): 493–512
- Rajasekharan, S. K., & Ramesh, S. (2013). Cellulase inhibits Burkholderia cepacia biofilms on diverse prosthetic materials. *Polish Journal of Microbiology*, 62(3), 327-330
- Reina, J. C., Pérez, P., & Llamas, I. (2022). Quorum Quenching Strains Isolated from the Microbiota of Sea Anemones and Holothurians Attenuate *Vibrio coralliilyticus* Virulence Factors and Reduce Mortality in *Artemia salina*. *Microorganisms*, 10(3), 631
- Reina, J. C., Romero, M., Salto, R., Cámara, M., & Llamas, I. (2021). AhaP, A Quorum Quenching Acylase from *Psychrobacter* sp. M9-54-1 That Attenuates *Pseudomonas aeruginosa* and *Vibrio coralliilyticus* Virulence. *Marine drugs*, 19(1), 16
- Reina, J. C., Torres, M., & Llamas, I. (2019). *Stenotrophomonas maltophilia* AHL-degrading strains isolated from marine invertebrate microbiota attenuate the virulence of *Pectobacterium carotovorum* and *Vibrio coralliilyticus*. *Marine Biotechnology*, 21(2), 276-290
- Rémy, B., Plener, L., Poirier, L., Elias, M., Daudé, D., & Chabrière, E. (2016). Harnessing hyperthermostable lactonase from *Sulfolobus solfataricus* for biotechnological applications. *Scientific reports*, 6(1), 1-11
- Ren, D., Sims, J. J., & Wood, T. K. (2001). Inhibition of biofilm formation and swarming of *Escherichia coli* by (5Z)-4-bromo-5-(bromomethylene)-3-butyl-2 (5H)-furanone. *Environmental Microbiology*, 3(11), 731-736
- Romero, D., Aguilar, C., Losick, R., & Kolter, R. (2010). Amyloid fibers provide structural integrity to *Bacillus subtilis* biofilms. *Proceedings of the National Academy of Sciences*, 107(5), 2230-2234
- Romero, M., Muras, A., Mayer, C., Buján, N., Magariños, B., & Otero, A. (2014). In vitro quenching of fish pathogen *Edwardsiella tarda* AHL production using marine bacterium *Tenacibaculum* sp. strain 20J cell extracts. *Diseases of Aquatic Organisms*, 108(3), 217-225
- Saggu, S. K., Jha, G., & Mishra, P. C. (2019). Enzymatic degradation of biofilm by metalloprotease from *Microbacterium* sp. SKS10. *Frontiers in Bioengineering and Biotechnology*, 192. <https://doi.org/10.3389/fbioe.2019.00192>
- Sakuragi, Y., & Kolter, R. (2007). Quorum-sensing regulation of the biofilm matrix genes (pel) of *Pseudomonas aeruginosa*. *Journal of Bacteriology*, 189(14), 5383-5386
- Santhakumari, S., Jayakumar, R., Logalakshmi, R., Prabhu, N. M., et al. (2018). In vitro and in vivo effect of 2, 6-Di-tert-butyl-4-methylphenol as an antibiofilm agent against quorum sensing mediated biofilm formation of *Vibrio* spp. *International Journal of Food Microbiology*, 281, 60-71
- Sauer, K., Camper, A. K., Ehrlich, G. D., Costerton, J. W., & Davies, D. G. (2002). *Pseudomonas aeruginosa* displays multiple phenotypes during development as a biofilm. *Journal of Bacteriology*, 184(4), <https://doi.org/10.1128/jb.184.4.1140-1154.2002>
- Savage, V. J., Chopra, I., & O'Neill, A. J. (2013). *Staphylococcus aureus* biofilms promote horizontal transfer of antibiotic resistance. *Antimicrobial Agents and Chemotherapy*, 57(4), <https://doi.org/10.1128/AAC.02008-12>
- Simm, R., Morr, M., Kader, A., Nimtz, M., & Römling, U. (2004). GGDEF and EAL domains inversely regulate cyclic di-GMP levels and transition from sessility to motility. *Molecular Microbiology*, 53(4), 1123-1134
- Small, H. J., & Pagenkopp, K. M. (2011). Reservoirs and alternate hosts for pathogens of commercially important crustaceans: a review. *Journal of Invertebrate Pathology*, 106(1), 153-164
- Stewart, P. S., & Costerton, J. W. (2001). Antibiotic resistance of bacteria in biofilms. *The Lancet*, 358(9276), 135-138
- Sun, S., Dai, X., Sun, J., Bu, X., et al. (2016). A diketopiperazine factor from *Rheinheimera aquimaris* QSI02 exhibits anti-quorum sensing activity. *Scientific reports*, 6(1), 1-10
- Sutrina, S. L., Callender, S., Grazette, T., Scantlebury, P., et al. (2019). The quantity and distribution of biofilm growth of *Escherichia coli* strain ATCC 9723 depends on the carbon/energy source. *Microbiology*, 165(1), 47-64
- Sutrina, S. L., Daniel, K., Lewis, M., Charles, N. T., Anselm, C. K., & Holder, N. (2015). Biofilm growth of *Escherichia coli* is subject to cAMP-dependent and cAMP-independent inhibition. *Microbial Physiology*, 25(2-3), 209-225
- Swift, S., Downie, A. J., Whitehead, N. A., Barnard, A. M., Salmond, G.P., Williams, Quorum, P. (2001) Sensing as a population-density dependent determinant of bacterial physiology. *Advances in Microbial Physiology*, 45, 199-270
- Taghadosi, R., Shakibaie, M. R., & Masoumi, S. (2015). Biochemical detection of N-Acyl homoserine lactone from biofilm-forming uropathogenic *Escherichia coli* isolated from urinary tract infection samples. *Reports of Biochemistry & Molecular Biology*, 3(2), 56

- Tan, D., Zhang, Y., Cheng, M., Le, S., et al. (2019). Characterization of *Klebsiella pneumoniae* ST11 isolates and their interactions with lytic phages. *Viruses*, *11*(11), 1080
- Taylor, C. M., Beresford, M., Epton, H. A., Sigeo, D. C., et al. (2002). *Listeria monocytogenes* relA and hpt mutants are impaired in surface-attached growth and virulence. *Journal of Bacteriology*, *184*(3), 621-628
- Teasdale, M. E., Liu, J., Wallace, J., Akhlaghi, F., & Rowley, D. C. (2009). Secondary metabolites produced by the marine bacterium *Halobacillus salinus* that inhibit quorum sensing-controlled phenotypes in gram-negative bacteria. *Applied and Environmental Microbiology*, *75*(3), 567-572
- Thenmozhi, R., Nithyanand, P., Rathna, J., & Karutha Pandian, S. (2009). Antibiofilm activity of coral-associated bacteria against different clinical M serotypes of *Streptococcus pyogenes*. *FEMS Immunology & Medical Microbiology*, *57*(3), 284-294
- Thormann, K. M., Saville, R. M., Shukla, S., & Spormann, A. M. (2005). Induction of rapid detachment in *Shewanella oneidensis* MR-1 biofilms. *Journal of Bacteriology*, *187*(3), 1014-1021
- Todhanakasem, T., & Young, G. M. (2008). Loss of flagellum-based motility by *Listeria monocytogenes* results in formation of hyperbiofilms. *Journal of Bacteriology*, *190*(17), 6030-6034
- Torres, M., Romero, M., Prado, S., Dubert, J., Tahrioui, A., Otero, A., & Llamas, I. (2013). N-acylhomoserine lactone-degrading bacteria isolated from hatchery bivalve larval cultures. *Microbiological research*, *168*(9), 547-554
- Torres, M., Rubio-Portillo, E., Antón, J., Ramos-Esplá, A. A., Quesada, E., & Llamas, I. (2016). Selection of the N-acylhomoserine lactone-degrading bacterium *Alteromonas stellipolaris* PQQ-42 and of its potential for biocontrol in aquaculture. *Frontiers in Microbiology*, *7*, 646
- Uroz, S., Chhabra, S. R., Camara, M., Williams, P., Oger, P., & Dessaux, Y. (2005). N-Acylhomoserine lactone quorum-sensing molecules are modified and degraded by *Rhodococcus erythropolis* W2 by both amidolytic and novel oxidoreductase activities. *Microbiology*, *151*(10), 3313-3322
- Vallet, I., Olson, J. W., Lory, S., Lazdunski, A., & Filloux, A. (2001). The chaperone/usher pathways of *Pseudomonas aeruginosa*: identification of fimbrial gene clusters (cup) and their involvement in biofilm formation. *Proceedings of the National Academy of Sciences*, *98*(12), 6911-6916
- Van Acker, H., Van Dijck, P., & Coenye, T. (2014). Molecular mechanisms of antimicrobial tolerance and resistance in bacterial and fungal biofilms. *Trends in Microbiology*, *22*(6), 326-333
- Verma, V., Harjai, K., & Chhibber, S. (2009). Restricting ciprofloxacin-induced resistant variant formation in biofilm of *Klebsiella pneumoniae* B5055 by complementary bacteriophage treatment. *Journal of Antimicrobial Chemotherapy*, *64*(6), 1212-1218
- Vinoj, G., Vaseeharan, B., Thomas, S., Spiers, A. J., & Shanthi, S. (2014). Quorum-quenching activity of the AHL-lactonase from *Bacillus licheniformis* DAHB1 inhibits *Vibrio* biofilm formation in vitro and reduces shrimp intestinal colonisation and mortality. *Marine Biotechnology*, *16*(6), 707-715
- Walters III, M. C., Roe, F., Bugnicourt, A., Franklin, M. J., & Stewart, P. S. (2003). Contributions of antibiotic penetration, oxygen limitation, and low metabolic activity to tolerance of *Pseudomonas aeruginosa* biofilms to ciprofloxacin and tobramycin. *Antimicrobial agents and Chemotherapy*, *47*(1), 317-323
- Waters, C. M., & Bassler, B. L. (2005). Quorum sensing: cell-to-cell communication in bacteria. *Annual Review of Cell and Developmental Biology* *21*, 319-346
- Whitehead, N. A., Barnard, A. M., Slater, H., Simpson, N. J., & Salmond, G. P. (2001). Quorum-sensing in Gram-negative bacteria. *FEMS Microbiology Reviews*, *25*(4), 365-404
- Williams, P., Winzer, K., Chan, W. C., & Camara, M. (2007). Look who's talking: communication and quorum sensing in the bacterial world. *Philosophical Transactions of the Royal Society B: Biological Sciences*, *362*(1483), 1119-1134
- Yildiz, F. H., & Visick, K. L. (2009). *Vibrio* biofilms: so much the same yet so different. *Trends in Microbiology*, *17*(3), 109-118
- You, J., Xue, X., Cao, L., Lu, X., et al. (2007). Inhibition of *Vibrio* biofilm formation by a marine actinomycete strain A66. *Applied Microbiology and Biotechnology*, *76*(5), 1137-1144
- Zhang, J. W., Xuan, C. G., Lu, C. H., Guo, S., et al. (2019). AidB, a novel thermostable N-acylhomoserine lactonase from the bacterium *Bosea* sp. *Applied and Environmental microbiology*, *85*(24), e02065-19
- Zhang, L., & Mah, T. F. (2008). Involvement of a novel efflux system in biofilm-specific resistance to antibiotics. *Journal of Bacteriology*, *190*(13), 4447-4452





## Journal of Experimental Biology and Agricultural Sciences

<http://www.jebas.org>

ISSN No. 2320 – 8694

### Current and emerging molecular technologies for the diagnosis of plant diseases – An overview

Mohammad Malek Faizal Azizi<sup>1</sup>, Noor Hani Mardhiah<sup>2</sup>, Han Yih Lau<sup>1\*</sup>

<sup>1</sup>Biotechnology and Nanotechnology Research Centre, Malaysian Agricultural Research and Development Institute (MARDI), Malaysia.

<sup>2</sup>Department of Bioprocess Technology, Faculty of Biotechnology and Biomolecular Sciences, Universiti Putra Malaysia, 43400, Serdang, Selangor.

Received – January 06, 2022; Revision – March 25, 2022; Accepted – April 17, 2022

Available Online – April 30, 2022

DOI: [http://dx.doi.org/10.18006/2022.10\(2\).294.305](http://dx.doi.org/10.18006/2022.10(2).294.305)

#### KEYWORDS

ELISA

PCR

Real-time PCR

LAMP

Biosensor

NGS

#### ABSTRACT

Plant diseases caused by numerous pathogens such as bacteria, viruses, and fungi are responsible for substantial economic losses in the agricultural industry worldwide. Specific, sensitive, and efficient diagnostic tools have been developed worldwide to mitigate and prevent the pathogenic threat. The diagnostic tools have revolutionized from classical methods to more advanced molecular diagnostic approaches such as enzyme-linked immunosorbent assay (ELISA), conventional polymerase chain reaction (PCR), real-time PCR, loop-mediated isothermal amplification (LAMP), biosensor, and next-generation sequencing (NGS). Hence, this review describes the current and emerging molecular diagnostic tools to distinguish and identify pathogens in crops.

\* Corresponding author

E-mail: [hylau@mardi.gov.my](mailto:hylau@mardi.gov.my) (Han Yih Lau)

Peer review under responsibility of Journal of Experimental Biology and Agricultural Sciences.

Production and Hosting by Horizon Publisher India [HPI]  
(<http://www.horizonpublisherindia.in/>).  
All rights reserved.

All the articles published by [Journal of Experimental Biology and Agricultural Sciences](#) are licensed under a [Creative Commons Attribution-NonCommercial 4.0 International License](#) Based on a work at [www.jebas.org](http://www.jebas.org).



## 1 Introduction

Agricultural production is pivotal to meet the increasing food demand, and it becomes the backbone of industrial and developing countries. As agricultural activity rapidly expands to feed the growing world population, plant diseases and pests significantly affect food production and quality. Diseases and pests may exacerbate yield losses of up to 30% of the world's total annual economy owing to lost food production in the billions of dollars (Savary et al. 2017; Rizzo et al. 2021).

Therefore, it is necessary to define the problem and seek remedies to manage diseases. A vast number of plant pathogens such as fungi, bacteria, viruses, nematodes, oomycetes, and parasitic plants are responsible for a range of serious plant diseases, and they have been categorized as quarantined pathogens globally. Appropriate disease diagnosis and early detection are imperative to overcome disease outbreaks (Fang and Ramasamy 2015). Years of experience coupled with advanced technologies, render the development in various disciplines, including phytopathology, ecology, taxonomy, molecular biology, and immunology. Scientists work on various plant pathogens, pests, invasive species, and organisms associated with species. With the advancement of equipment and laboratory facilities, the reliability of recent techniques can be compared and combined with conventional plant diagnostics. The emergence of accurate diagnostic assays is essential to identify and monitor pests and plant diseases efficiently, where better plant health monitoring can be ensured with the developed diagnostic products. Inaccurate identification and diagnosis could consequently affect disease control and lead to a waste of time and resources. Therefore, specific, rapid disease diagnosis and early detection are paramount in disease management to prevent the establishment and dispersal of pests and pathogens effectively and to minimize the subsequent impact (Myerson and Reaser 2002; Piombo et al. 2021).

Before developing modern and high-tech techniques for plant pathogen detection, traditional methods such as visual symptoms inspection and laboratory tests, including physiological, biochemical, chemical, and pathogenicity tests, were adopted to identify plant pathogens and diseases (Lau and Botella 2017). However, these methods can only be performed once severe damage were observed on the infected plant. Thus, further treatments for the infected plant might not be successful since it has been severely damaged by the disease. Traditional methods are considered irrelevant and insufficient in terms of accuracy, precision, and sensitivity of plant disease diagnosis. Traditional methods are also inexpensive and time-consuming, especially in the analysis process, which requires expertise (Skottrup et al. 2008).

To bridge the gap, scientists begin to develop effective molecular-based techniques such as plant disease diagnostic tools and kits

that could improve decision-making in control management and overcome many shortcomings of the traditional assays. Molecular-based diagnostic tools have emerged rapidly over several decades and have recently moved towards a new era in plant diagnostic technologies. The evolution of diagnostic technologies has enabled effective optional tools with relevance to plant disease diagnosis. Herein, this review summarizes the current and emerging advanced molecular techniques of plant disease detection that could be exceptionally impactful in detecting pathogens and plant diseases.

## 2 Molecular-based Techniques used for early stage plant disease diagnostic

### 2.1 ELISA

ELISA and enzyme immunoassay (EIA) are solid-phase assays that deploy antibodies labeled with enzymes, reacting with a substrate to generate a color change, detecting and quantifying the amount of a specific substance in a sample (Ichiki et al. 2013). This technique has been broadly employed as a diagnostic tool in clinical and plant pathology. Sakudo et al. (2006) found that invasive techniques such as ELISA effectively diagnose viral infections but are not ideal in cost-effectiveness, speed, and accuracy. For instance, a rapid dot-ELISA developed by Wang et al. (2012) to diagnose rice plants infected by the southern rice black-streaked dwarf disease virus (SRBSDV) using anti-SRBSDV rabbit antiserum was found to be highly reliable, sensitive, and specific to the disease. Furthermore, Ichiki et al. (2013) demonstrated that the double antibody sandwich-enzyme-linked immunosorbent assay (DAS-ELISA) method is straightforward to use for routine diagnostic RSV detection in insect vectors. Monitoring the rate of virulent insect vectors in early summer (before rice planting season) is pivotal for predicting rice stripe, a financially devastating disease. This method is simple, as up to 96 insect samples can be processed concurrently using plastic multi sticks. Besides this, in China, the wheat dwarf virus (WDV) was detected accurately in WDV-infected wheat plant tissue crude extracts using ACP-ELISA and dot-ELISA (Zhang et al. 2018). In 2020, Klap et al. (2020) revealed that tomato fruits exhibiting viral-like symptoms of marbled yellow spots in Israel were caused by the tobamovirus ToBRFV and the potyvirus PepMV using the ELISA technique as one of the serological tests.

Though ELISA has many advantages when used for pathogen detection, but this technique also has various drawbacks like the sensitivity of ELISA is not as high as that of many other molecular methods, and the assay takes up to 24 hours to complete (Stackhouse et al. 2020). Further, due to the sophistication of the technique and the high cost of culture cell media required to obtain a specific antibody, ELISA can also be quite expensive and labor-intensive (Sakamoto et al. 2018). Although polyclonal antibodies are effective at detecting pathogens, they are not always

sufficiently specific. Monoclonal antibodies, on the other hand, are more specific but also more costly. While developing antibodies against plant viruses has been extremely successful due to ELISA's high sensitivity for viruses, it is significantly less effective against more complex organisms such as fungal plant pathogens (McCartney et al. 2003). Due to the low sensitivity of this application, it will be ineffective at detecting bacteria (Fang and Ramasamy 2015). As a result, ELISA is considered ineffective for detecting fungal and bacterial pathogens that cause rice diseases. Additionally, due to a lack of specificity, antibodies used in ELISA can react to a variety of strains with clearly distinct symptoms and are unable to distinguish them precisely (Scala et al. 2018).

## 2.2 Conventional PCR

Polymerase chain reaction (PCR), developed by Kary Mullis in the mid-1980s, is one of the greatest molecular biology achievements (Mullis and Faloona 1987). Specific qualification of plant pathogens can be performed by technological advances of PCR to overcome the drawbacks of traditional methods. The PCR technique requires several reagents and components, which include the DNA template, *Taq* polymerase, two primers, deoxynucleotide triphosphates (dNTPs), buffer solution, and bivalent cations ( $Mg^{2+}$  or  $Mn^{2+}$ ), and also monovalent cation ( $K^+$ ) (Figure 1).

It has been also widely used for the detection of a plant pathogen. PCR products can be visualized through gel electrophoresis analysis. However, the PCR sensitivity can be influenced by the nucleic acid extraction method and target DNA variability (Bastien et al. 2008). PCR manages to amplify a small amount of DNA due to its high sensitivity, and it is widely used for detecting pathogens that have a long latent period between infection and the

development of the disease's symptoms. Nevertheless, the limitations of conventional PCR include susceptibility to contamination and the lack of robustness (Boonham et al. 2008). This technique also has very poor resolution, i.e., about 10-fold because agarose gel could not resolve yield variabilities. However, it is more specific and sensitive compared to traditional methods for pathogen detection in plants. To date, conventional PCR remains one of the most commonly used techniques in detecting plant pathogens.

For instance, Azizi et al. (2019a,b) employed a conventional PCR technique for the identification of *Pantoea ananatis* and *P. stewartii* subspecies *indologenes* as the causal agents of bacterial leaf blight (BLB) disease of rice in Malaysia. Likewise, in Southern Karnataka, India, PCR was also deployed to characterize *Ralstonia solanaceum* isolates that cause bacterial wilt in tomatoes (Shweta et al. 2018). Besides that, Murugan et al. (2020) have also successfully identified *Fusarium oxysporum* f.sp. *lycopersici* (*Fol*) isolates from infected tomatoes using PCR technique.

However, there are some limitations to using the PCR technique. One of the most significant disadvantages of this method is the high risk of contamination, which results in a longer time required to obtain the result. Amplicons can be easily dispersed throughout the environment using this method (Hajia 2018). As a result of false-positive results, it is critical to isolate the work environment from the external environment and to establish work disciplines. Although the early theory stated that the PCR's ability to detect target sequences should be less than 10 per sample, researchers have rarely been able to design a test that meets this detection level in different types of protocols. The method's detection level is

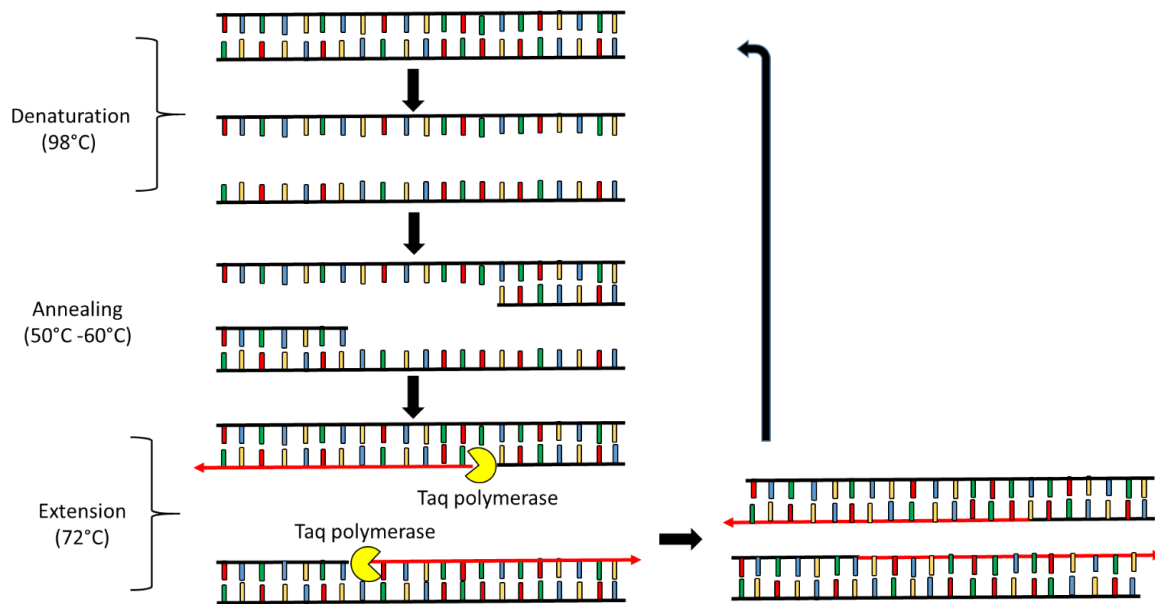


Figure 1 Schematic of conventional PCR

currently much lower than the level mentioned above, and its sensitivity has decreased as a result of interference of various factors. The absence of a standard genomic purification method, the use of low-quality materials, and an inability to optimize the test are all significant influencing factors. However, as working conditions change, test sensitivity decreases. So, continuous quality control of utilized facilities should be considered (Panteghini and Forest 2005; Hajia 2018).

### 2.3 Real-time PCR

Real-time polymerase chain reaction (RT-PCR), also known as quantitative polymerase chain reaction (qPCR), developed by Kary Mullis in the 1980s, is a significant improvement and revolutionary PCR technique (Mullis 1990). The RT-PCR technique has captured the attention of researchers globally and represents a groundbreaking alternative to other molecular techniques. It is one of the most powerful applications among the most rapid and sensitive detection and can reduce cross-contamination risk (Vincelli and Tisserat 2008; White et al. 2011). Furthermore, this technique could detect the minimum amount of DNA pathogens from infected plant tissues and insect vectors (Crosslin et al. 2006). Real-time PCR is performed in a thermal cycler with the capacity to illuminate each sample with a beam of light of at least one specified wavelength and the detection of the amplicon through the use of oligonucleotide probes that emit fluorescence during amplification (Figure 2).

The PCR protocol cycle in which the amount of significant fluorescence emitted during amplification is directly proportional to the amplified DNA/RNA present in the sample. This cycle is termed as quantitation cycle (Cq) or cycle threshold (Ct). To date, real-time PCR has been widely applied by scientists in detecting plant pathogens, including bacteria, oomycetes, fungi, nematodes, and viruses (Lievens et al. 2006).

For example, Carneiro et al. (2017) developed a TaqMan RT-PCR on the *TEF 1- $\alpha$*  gene to detect *Fusarium fujikuroi*, which causes the bakanae disease in different rice tissues. The technique successfully detected and quantified *F. fujikuroi* from rice culms, leaves, roots, and seeds during the analysis. Similarly, He et al. (2020) described a rapid, highly sensitive, and simple DNA-based real-time polymerase chain reaction (RT-PCR) assay for screening resistant tea plant cultivars and identifying differences in pathogen aggressiveness within and among *Colletotrichum* species isolated from infected tea. This technique has replaced lesion size assessment at the infection sites on the leaves that lack sensitivity and accuracy in quantifying pathogen growth (He et al. 2020). Further, *Dickeya fangzhongdat* caused bleeding canker disease in pear in China was detected and identified using TaqMan real-time PCR assay based on an elongation factor G (*fusA*) gene (Tian et al. 2020). This technique was successfully performed as the first detection technique for tomato leaf curl New Delhi virus (ToLCNDV) (Luigi et al. 2020). However, one of the drawbacks of real-time PCR is that it might fail to identify biological

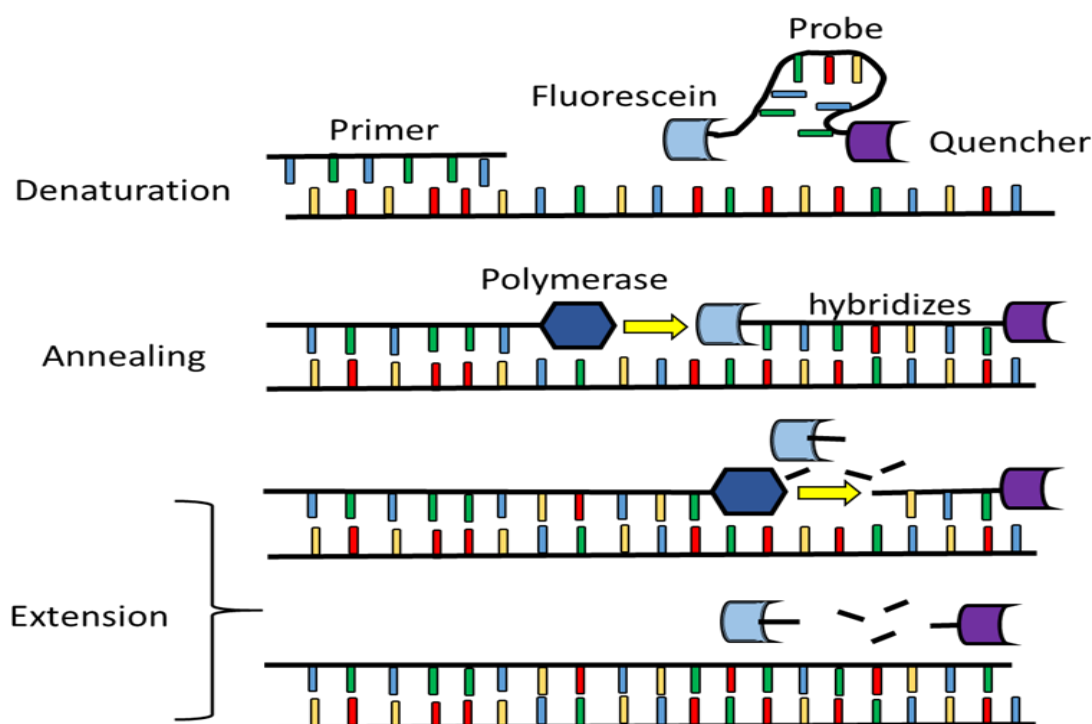


Figure 2 Schematic diagram of Real-time PCR

processes such as alternative splicing since it is performed on small DNA fragments. This method also requires the usage of costly equipment and reagents (Gachon et al. 2004).

A significant disadvantage of qPCR is the requirement for prior sequence data for the desired target gene; consequently, qPCR can be used to target only known genes (Smith and Osborn 2009). However, it will be difficult to target unknown genes because genome or gene fragment sequences from cultured organisms and/or clone libraries are derived via PCR using primers based on current sequence knowledge (Smith and Osborn 2009). As a result, access to the unknown target gene is inevitably limited when compared to analyses of previously characterized sequences.

## 2.4 LAMP

LAMP is one of the successful novel techniques widely employed as an alternative technique to PCR due to its rapidity, simplicity, practicality, and cost-effective equipment. LAMP is a method for amplifying specific DNA sequences initially established by Notomi et al. (2000) to detect hepatitis B virus (HBV) by amplifying a specific DNA region of HBV under isothermal amplification. This technique adopts four different primers (forward and reverse internal and external primers) that recognize the six distinct sequences within the target HBV viral DNA. LAMP consists of four main different primers, including two inner primers (FIP and BIP) and two outer primers (F3 and B3) [a forward outer primer (F3) and a backward outer primer (B3)]. The amplification relies on auto cycling strand and high DNA strand single-stranded displacement activity that contains a loop structure, which is performed under isothermal conditions at 60°C–65°C for

45–60 minutes (Lafar et al. 2020). The amplification process is comprised of three important steps: production of the starting material, cycling amplification, and elongation and recycling (Figure 3) (Hardinge and Murray 2019).

LAMP is considered a more versatile technique due to the detection of the amplicon using three optional methods: turbidimeter, colorimetric detection, and agarose gel electrophoresis or real-time fluorimeter platform (Waliulla et al. 2020). Despite the advantages of this method, the drawbacks of LAMP include the high risk of primer dimer formation and it requires the use of a heat block to maintain the temperature at 65°C (Rani et al. 2019).

The LAMP assay has been established in plant pathology for the detection of various plant pathogens. Recently, Karimi et al. (2020) reported that the genus and species-specific PCR primers can detect and discriminate *Colletotrichum* and *C. Nymphaeae* from other fungal species in pure culture and assays of diseased using the LAMP technique than PCR assay due to its higher sensitivity and specificity. Likewise, the LAMP assay rapidly detected *Pseudomonas syringae* pv. *Tomato* (*Pst*) in artificially and naturally infected tomato leaves and stem tissues in the field without laboratory work (Chen et al. 2020). The sensitivity of the LAMP assay was claimed as similar to qPCR and even 100 times more sensitive compared to RT-PCR in detecting *tomato brown rugose fruit virus* (ToBRFV) (Sarkes et al. 2020).

Additionally, the advancement of the LAMP technique has its own set of constraints. Cross-contamination is the most serious issue,

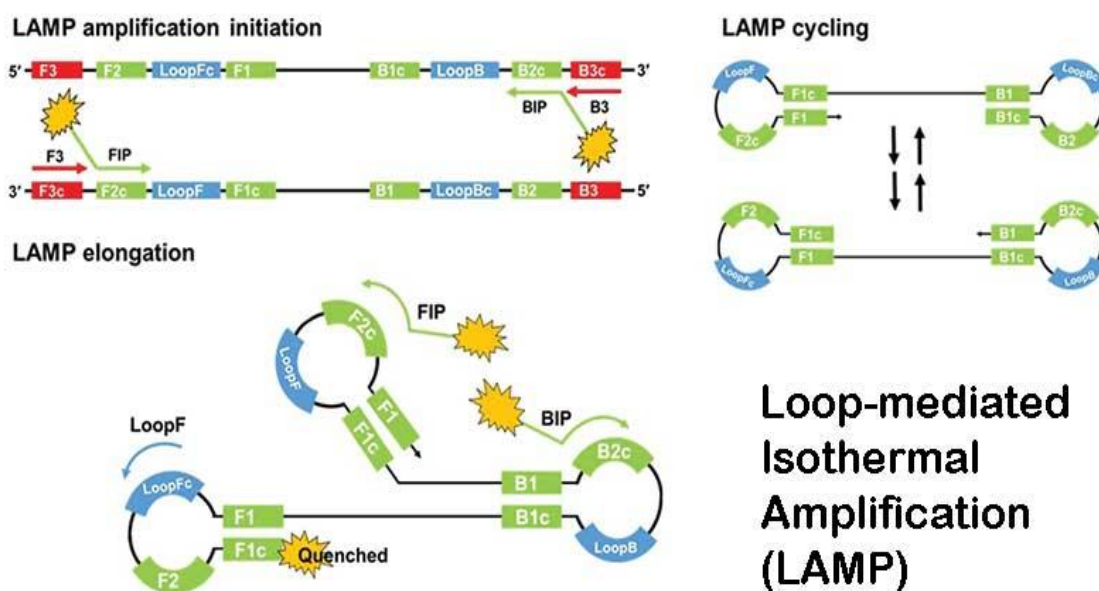


Figure 3 LAMP amplification initiation, cycling and elongation (Hardinge and Murray 2019).

owing to the technique's high sensitivity, particularly following the amplification step and the fact that certain variants require the opening of reaction tubes for amplicon detection (Mori et al. 2006; Tomlinson et al. 2007; Tomlinson and Boonham 2008). Because LAMP amplification products do not degrade readily, the possibility of carry-over contamination exists. As a result, proper handling and practice are necessary to avoid the risk of cross-contamination. The relative complexity of assay design is also a significant hurdle, as each assay requires up to six primers, in comparison to PCR, which only requires two primers (Tomlinson and Boonham 2008). Amplification time affects the duration of the LAMP process. Francois et al. (2011) discovered that the shortest duration for amplification is between 60 and 120 minutes, and a 180-minute negative control reveals amplification (Dhama et al. 2014).

## 2.5 Biosensor

Biosensors are of great importance due to their capability to resolve a potentially wide range of analytical problems and challenges in various fields, including agriculture and food safety, medicine, pharmacology, security, environmental monitoring, etc. The biosensor was first developed by Clark and Lyons (1962) using electrochemical detection of oxygen or hydrogen peroxide to measure glucose in biological samples. Since then, biosensors have been progressively developed with innovative techniques involving electrochemistry, nanotechnology, to bioelectronics (Vigneshvar et al. 2016). According to the International Union of Pure and Applied Chemistry (IUPAC) recommendations (1999), a biosensor is described as a device that deploys the integration of specific biochemical reactions mediated by isolated enzymes, immunosystems, tissues, organelles, or whole cells to detect chemical compounds, commonly by electrical, thermal, or optical

signals. Biosensors are analytical devices comprising a biorecognition element coupled with a transducer and converting the recognition event into some measurable readout/analytical signal (Figure 4).

The development of pathogen biosensor strategies is based on biological recognition using receptors on antibodies, DNA probes, phages, and others. Biosensors play an important role in detecting pathogens as they provide more rapid and specific detection than conventional methods. Antibody-based biosensors offer sensitive and rapid analysis for a wide range of pathogens, including bacterial, fungal, and viral species. For instance, in 2019, a highly sensitive Surface Plasmon Resonance (SPR) immunosensor was successfully developed for early detection of *Pseudocercospora fijiensis*, the causative agent of the banana black Sigatoka disease. It consists of a polyclonal antibody covalently immobilized on a gold-coated chip using the EDC/NHS method via a mixed self-assembled monolayer (SAM) of alkanethiols (Luna-Moreno et al. 2019). The immunosensor technique is also considered an alternative method for fig mosaic virus (FMV) detection due to its advantages such as high sensitivity, simplicity, accuracy, and low cost over conventional methods (Haji-Hashemi et al. 2019). Conversely, the deployment of antibody-based techniques may show cross-reactivity due to limited specificity, which sometimes produces false-negative results (Franken et al. 1992; Lau et al. 2014; Lau and Botella 2017). DNA-based biosensors provide advantages over antibody-based techniques, mostly in terms of sensitivity. Lau et al. (2017) successfully developed a DNA-based biosensor combining recombinase polymerase amplification (RPA) with nanoparticle electrochemistry to detect *P. Syringae* infected with *Arabidopsis thaliana* and infection detection before the appearance of disease symptoms. Nevertheless, the DNA biosensor can be rapidly degraded and needs specific storage and analysis

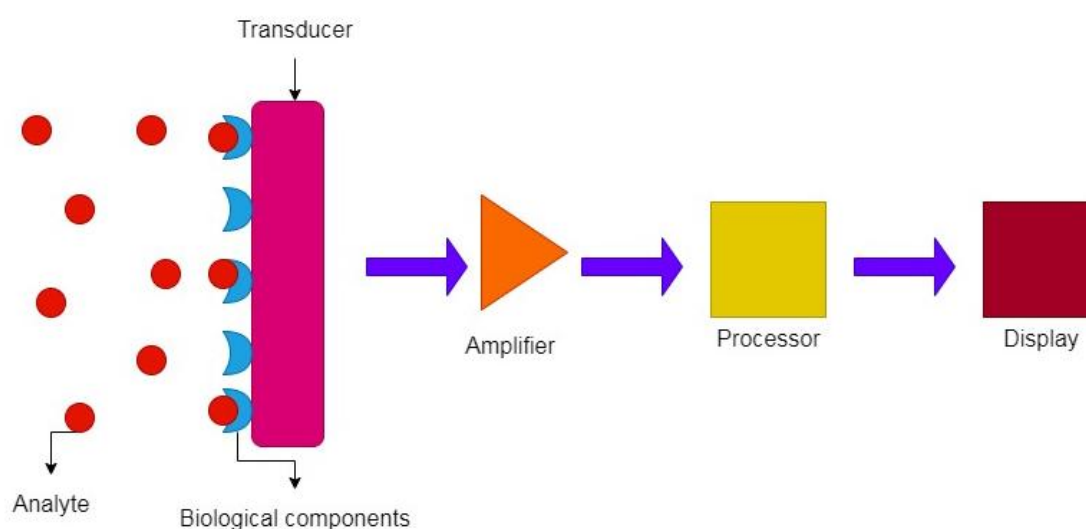


Figure 4 Schematic diagrams of generic components of a biosensor and its processes

conditions to maintain DNA stability and its attachment to the transducer (Peña-Bahamonde et al. 2018). Admittedly, the effectiveness of a DNA biosensor might be significantly impacted by changes in temperature or pH (Koyun et al. 2012). Specifically, in the case of temperature, the sensitivity of DNA biosensors is dependent on experimental temperatures, as this is caused by a hybridization process occurring between the probe and the target molecules that occurs at optimum temperatures, which must be determined before the deployment of the sensor (Kavita 2017; Rahman et al. 2017). In terms of pH conditions, a buffer with potassium or sodium phosphate is required to generate the highest signal at pH 7.0 to improve the sensor's effectiveness (Kavita 2017; Rahman et al. 2017).

The advancements in electrochemical DNA biosensors demonstrated in previous studies for the detection of rice diseases offer many advantages, including simplicity, cost-effectiveness, and enhanced sensitivity and selectivity under optimized conditions. However, because DNA biosensors are prone to degradation, they must be stored and analyzed under conditions that ensure DNA stability. Because DNA is easily degraded, they require special storage and analysis conditions to keep the DNA stable and attached to the transducer (Peña-Bahamonde et al. 2018). Additionally, temperature and pH can affect a DNA biosensor's effectiveness (Koyun et al. 2012). For example, the sensitivity of DNA biosensors is temperature dependent, as the probe hybridizes with target molecules at optimal temperatures that must be determined before sensor deployment.

## 2.6 Next generation sequencing (NGS)

Traditionally, molecular detection techniques greatly relied on the Sanger sequencing technology, which was based on chain termination (Sanger et al. 1977). Due to its high efficiency and low radioactivity, this technique was employed as the primary technology in the "first generation" of laboratory and commercial sequencing (Liu et al. 2012). Though this technology is efficient for sequencing short DNA fragments, it is tedious and ineffective for sequencing large DNA fragments.

The advances in the next generation sequencing (NGS) technology, or also called massively parallel sequencing, between 2004 and 2014 have filled the gap and transformed the sequencing technology in aspects of massively parallel analysis approaches capturing millions of short-read sequences in a much shorter time, high throughput, and dramatically facilitated genome sequencing at a lower cost (Kanzi et al. 2020). The rapid evolution of NGS platforms reduced the cost of sequencing gigabase pairs of nucleic acid from \$1,000 to \$10 (Ronholm 2018). The NGS technology has opened new molecular biology opportunities, including whole-genome sequencing (Walker et al. 2013), transcriptomics (Oono et al. 2013), metagenomics (Qin et al. 2010), epigenomics

(Cruikshanks et al. 2013), proteomics applications such as ProteinSeq (Darmanis et al. 2011), and single-cell sequencing (Navin et al. 2011). The relatively recent NGS development is an invaluable technique for multiple biological disciplines, including plant pathology (Behjati and Tarpey 2013; Díaz-Cruz et al. 2019). The limitations of the approaches above, specifically for helmpathogen diagnosis, can be addressed using this technology (Díaz-Cruz et al. 2019). The combination of this technique with advanced bioinformatics has fuelled innovative ways for a more rapid detection, identification, and elucidation of the causal agents of new and emerging diseases (Chalupowicz et al. 2019). NGS entails numerous DNA-related steps, including DNA isolation and fragmentation, library preparation, massively parallel sequencing, bioinformatics analysis, and variant/mutation annotation and interpretation (Qin 2019).

Advanced sequencing methods in NGS commonly adopt massively parallel signature sequencing, colony sequencing, pyrosequencing, and sequencing by oligonucleotide ligation detection (SOLID) (Rajesh and Jaya 2017). Though NGS can rapidly generate a large amount of data, data analysis is a great challenge. Several free software programs are available for the assembly of NGS data (e.g., SOAP de novo, Abyss, Velvet, and bowtie). Even so, these programs require a proficient and expert researcher in the deployment of command-line driven applications (Kehoe et al. 2014). NGS has been used in the rapid identification of plant pathogens that induce severe diseases. New generation sequencing was adopted to detect *Sarcococca* blight-causing novel fungal pathogen, *Calonectria pseudonaviculata*, in ornamental plants using IlluminaMiSeq. A 51.4 Mb genome of the two host isolates revealed unique single nucleotide polymorphism for the two isolates and identified both as *C. Pseudonaviculata* (Malapi-Wight et al., 2016). RNA-seq based NGS was used to study field pathogenomics and gain insight into the emergence of *Puccinia striiformis* f. sp. *tritici* (PST) populations as the causal agent of wheat yellow (stripe) rust in wheat and triticale (Hubbard et al. 2015).

Next-generation sequencing necessitates the use of sophisticated bioinformatics systems, as well as fast data processing and large data storage capabilities, all of which can be prohibitively expensive (Pabinger et al. 2014; Di Resta et al. 2018). The ability to purchase next-generation sequencing equipment is a common occurrence in academic institutions. However, many institutions lack the computational resources and staffing necessary to analyze and clinically interpret the data (Di Resta et al. 2018).

## 3 Conclusions and future prospects

The occurrence of emerging plant pathogens continues to become a major threat to ecosystems, food security, and the global economy. Furthermore, important factors such as globalization,

increased human mobility, climate change, and vector and pathogen evolution have encouraged the spread of invasive plant pathogens. Thereby, accurate and early diagnoses of the pathogen are critical to providing measure control strategies. The advances of molecular diagnostic tools for plant disease detection have witnessed unprecedented development in the recent decade in combination with modern technology techniques. This review has highlighted the recent and most notable molecular diagnostic tools for plant disease detection. Due to rapid advances in molecular diagnostic approaches in the recent decade, great development in various useful technologies such as biosensors and NGS has continuously emerged for plant disease detection. All techniques mentioned in this review have contributed to the rapid, sensitive, and specific detection of plant pathogens. However, available plant pathogen diagnosis tools remain the major challenges/limitations that should be deliberated in selecting the best tools for detecting plant pathogens.

The continuous development of technological advances in plant disease detection will improve plant diagnostics for the early detection and containment of quarantine pathogens and better-integrated management tools to combat the disease. The detection of plant-pathogen can also be useful in the future for some regulation purposes, e.g., plant import and export screening procedures, where only plants that are free from pathogenic diseases are allowed to be imported from and exported to other countries. Thus, it will help to prevent plant diseases from spreading to other regions or countries. Identifying plant pathogens is also beneficial to plant breeders, helping them to develop disease-resistant varieties. Furthermore, plant pathologists hoped to see more advanced molecular techniques in plant disease detection that provide alternatives to available options and encourage growth in agriculture and the global economy. Although extensive studies have been conducted on developing molecular detection tools for detecting and identifying plant diseases, farmers' involvement is also vital in identifying plant diseases. Farmers may play an active role in identifying diseases affecting their crops in the early stages. Therefore, it is important to develop new user-friendly techniques that are not complex and do not require experts to handle them. Farmer-scientist collaboration is valuable to combat diseases and generate relevant techniques in plant disease detection more efficiently. Efforts and largely tacit knowledge from both farmers and researchers may contribute to remarkable innovations and improvements used in detecting plant diseases.

Human beings live in an era of technological transformation, which is rapidly reshaping lifestyles and erasing distinctions between the physical, digital, and biological realms. Cyberinfrastructure, big data management, and data mining capabilities require painstaking planning and collaboration to amass critical resources for research studies. While these cyber

technologies continue to evolve, the fundamental challenges associated with rice crops will persist. However, since knowledge has become unrestricted, the solutions will be more in-depth and can be solved more quickly. The development of high-throughput sequencing (HTS) technology has transformed research into detecting and identifying plant pathogens in recent years. The development of novel methods for detecting and identifying phytopathogens has been accelerated by the advent of HTS technologies. Due to the ability to sequence multiple organisms concurrently, HTS/NGS methods enable the detection of multiple organisms in a sample. Virus discovery is the most advanced application of HTS/NGS in plant pathology. The technique is rapidly gaining acceptance as a gold standard for determining the aetiology of a novel or uncommon viral symptoms in diagnostic settings. In the short term, HTS/NGS is also an extremely promising technique for screening propagation material for quarantine or certification purposes, particularly for plant viruses, where benefits could be discovered with only minor modifications to existing techniques, but with significant technical and quality control challenges. Simultaneous sequencing is possible with HTS/NGS methods, allowing for the detection of multiple organisms in a sample. The most advanced application of HTS/NGS in plant pathology is virus discovery. The technique is rapidly gaining acceptance as a standard method for determining the aetiology of a novel or uncommon viral symptoms in a diagnostic setting. In the short term, HTS/NGS also represents a highly promising technique for screening propagation material for quarantine or certification purposes, particularly for plant viruses, where benefits could be discovered with only minor modifications to existing techniques, but with technical and quality control challenges. HTS/NGS technologies generate significantly more genomic data than conventional molecular techniques. This can aid researchers in gaining a better understanding of the genomic diversity within a species (or at a lower taxonomic level), resulting in more precise taxonomic assignment for unambiguously identified pathogens, more precise assessment of the impact of a pathogen's genetic diversity, and more targeted molecular test design. HTS/NGS has developed into a technique for sequencing fungal genomes without prior knowledge of the pathogen's sequence. It can be used to identify both novel and emerging infections of rice, as well as previously identified pathogens. The molecular techniques discussed in this study are precise, effective, laboratory-based, and require sophisticated tools for rice pathogen identification.

#### **Author contributions**

MMF and NHM conceived the idea and wrote the manuscript. HYL critically reviewed the manuscript. All others have approved it.



### Acknowledgement

We would like to thank to the Malaysian Agricultural Research and Development Institute (MARDI) for research funding.

### Funding

This review paper received funding from the Malaysian Agricultural Research and Development Institute (MARDI)

### Conflicts of Interest

The authors declare no conflict of interest.

### References

- Azizi, M. M. F., Ismail, S. I., Hata, E. M., Zulperi, D., et al. (2019a). First report of *Pantoea stewartii* subsp. *indologenes* causing leaf blight on rice in Malaysia. *Plant Disease*, *103*, 1407-1407
- Azizi, M. M. F., Zulperi, D., Rahman, M. A. A., Abdul-Basir, B., et al. (2019b). First report of *Pantoea ananatis* causing leaf blight disease of rice in Peninsular Malaysia. *Plant Disease*, *103*, 2122
- Bastien, P., Procop, G.W., & Reischl, U. (2008). Quantitative real-time PCR is not more sensitive than “conventional” PCR. *Journal of Clinical Microbiology*, *46*, 1897–1900
- Behjati, S., & Tarpey, P.S. (2013). What is next generation sequencing?. *Archives of Disease in Childhood-Education and Practice*, *98*, 236-238
- Boonham, N., Glover, R., Tomlinson, J., & Mumford, R. (2008). Exploiting generic platform technologies for the detection and identification of plant pathogens. *European Journal of Plant Pathology*, *121*, 355-363
- Carneiro, G.A., Matić, S., Ortu, G., Garibaldi, A., et al. (2017). Development and validation of a TaqMan real-time PCR assay for the specific detection and quantification of *Fusariumfujikuroi* in rice plants and seeds. *Phytopathology*, *107*, 885-892
- Chalupowicz, L., Dombrowsky, A., Gaba, V., Luria, N., et al. (2019). Diagnosis of plant diseases using the Nanopore sequencing platform. *Plant Pathology*, *68*, 229-238
- Chen, Z.D., Kang, H.J., Chai, A.L., Shi, Y.X., et al. (2020). Development of a loop-mediated isothermal amplification (LAMP) assay for rapid detection of *Pseudomonas syringae*pv. *tomato* in planta. *European Journal of Plant Pathology*, *156*, 739-750
- Clark, L.C., & Lyons, C. (1962). Electrode systems for continuous monitoring in cardiovascular surgery. *Annals of the New York Academy of sciences*, *102*, 29-45
- Crosslin, J.M., Vandemark, G.J., & Munyaneza, J.E. (2006). Development of a real-time, quantitative PCR for detection of the Columbia basin potato purple top phytoplasma in plants and beet leafhoppers. *Plant Disease*, *90*, 663-667
- Cruickshanks, H.A., McBryan, T., Nelson, D.M., et al. (2013). Senescent cells harbour features of the cancer epigenome. *Nature Cell Biology*, *15*, 1495-1506
- Darmanis, S., Nong, R.Y., Vänelid, J., Siegbhan, A., et al. (2011). ProteinSeq: High-performance proteomic analyses by proximity ligation and next generation sequencing. *PLoS One*, *6*, e25583
- Dhama, K., Karthik, K., Chakraborty, S., Tiwari, T., et al. (2014). Loop-mediated isothermal amplification of DNA (LAMP): a new diagnostic tool lights the world of diagnosis of animal and human pathogens: a review. *Pakistan journal of biological sciences*, *17*, 151-166
- Di Resta, C., Galbiati, S., Carrera, P., & Ferrari, M. (2018). Next-generation sequencing approach for the diagnosis of human diseases: open challenges and new opportunities. *Ejifcc*, *29*, 4
- Díaz-Cruz G. A, Smith, C. M, Wiebe, K. F., Villanueva, S.M., et al. (2019). Applications of next-generation sequencing for large-scale pathogen diagnoses in soybean. *Plant Disease*, *103*, 1075-1083
- Fang, Y., & Ramasamy, R .P. (2015). Current and Prospective Methods for Plant Disease Detection. *Biosensors*, *5*, 537-561
- Francois, P., Tangomo, M., Hibbs, J., Bonetti, E.J., et al. (2011). Robustness of a loop-mediated isothermal amplification reaction for diagnostic applications. *FEMS Immunology & Medical Microbiology*, *62*, 41-48
- Franken, A. A. J. M., Zilverentant, J. F., Boonekamp, P. M., & Schots, A. (1992). Specificity of polyclonal and monoclonal-antibodies for the identification of *Xanthomonascampestrispv. campestris*. *Netherlands Journal of Plant Pathology*, *98*, 81-94
- Gachon, C., Mingam, A., & Charrier, B. (2004). Real-time PCR: What relevance to plant studies?. *Journal of Experimental Botany*, *55*, 1445–1454
- Hajia, M. (2018). Limitations of different PCR protocols used in diagnostic laboratories: a short review. *Modern Medical Laboratory Journal*, *1*, 1-6
- Haji-Hashemi, H. Safarnejad, M.R., Norouzi, P., Ebrahimi, M., et al. (2019). Simple and effective label free electrochemical immunosensor for Fig mosaic virus detection. *Analytical Biochemistry*, *566*, 102-106

- Hardinge, P., & Murray, J. A. H. (2019). Reduced false positives and improved reporting of Loop-mediated isothermal amplification using quenched fluorescent primers. *Scientific Reports*, *9*, 1–13
- He, S., Chen, H., Wei, Y., An, T., & Liu, S. (2020). Development of a DNA-based real-time PCR assay for the quantification of *Colletotrichumcamelliae* growth in tea (*Camellia sinensis*). *Plant Methods*, *16*, 1-11
- Hubbard, A., Lewis, C. M., Yoshida, K., Ramirez-Gonzalez, R.H., et al. (2015). Field pathogenomics reveals the emergence of a diverse wheat yellow rust population. *Genome Biology*, *16*, 1-15
- Ichiki, T. U., Shiba, T., Matsukura, K., Ueno, T., et al. (2013). Detection and diagnosis of rice-infecting viruses. *Frontiers in Microbiology*, *4*, 289
- Kanzi, A. M., San, J. E., Chimukangara, B., Ueno, T., et al. (2020). Next Generation Sequencing and Bioinformatics Analysis of Family Genetic Inheritance. *Frontiers in Genetics*, *11*, 1250
- Karimi, K., Arzanlou, M., Pertot, I. (2020). Development of novel species-specific primers for the specific identification of *Colletotrichum nymphaeae* based on conventional PCR and LAMP techniques. *European Journal of Plant Pathology*, *156*, 463-475
- Kavita, V. (2017) DNA biosensors—a review. *Journal Bioengineering and Biomedical Science*, *7*, 222
- Kehoe, M. A., Coutts, B. A., Buirchell, B. J., Jones, R. A. (2014). Plant virology and next generation sequencing: experiences with a Potyvirus. *PLoS One*, *9*, e104580
- Klap, C., Luria, N., Smith, E., Bakelman, E., et al. (2020). The Potential Risk of Plant-Virus Disease Initiation by Infected Tomatoes. *Plants*, *9*, 623
- Koyun, A., Ahlatcolu, E., Koca, Y., & Kara, S. (2012). Biosensors and their principles. A Roadmap of Biomedical Engineers and Milestones. *InTech*, 117-142
- Lafar, S., Zro, K., & Ennaji, M. M. (2020). Capripoxvirus Diseases: Current updates and developed strategies for control. In Ennaji, M.M. (Ed.). *Emerging and Reemerging Viral Pathogens*. United States: Academic Press
- Lau, H. Y., & Botella, J. R. (2017). Advanced DNA-based point-of-care diagnostic methods for plant diseases detection. *Frontiers in Plant Science*, *8*, 2016
- Lau, H. Y., Palanisamy, R., Trau, M., & Botella, J. R. (2014). Molecular inversion probe: a new tool for highly specific detection of plant pathogens. *PLoS One*, *9*, e111182
- Lau, H. Y., Wu, H., & Wee, E. J., (2017). Specific and sensitive isothermal electrochemical biosensor for plant pathogen DNA detection with colloidal gold nanoparticles as probes. *Scientific Reports*, *7*, 1-7
- Lievens, B., Brouwer, M., Vanachter, A. C., Cammue, B. P., & Thomma, B. P. (2006). Real-time PCR for detection and quantification of fungal and oomycete tomato pathogens in plant and soil samples. *Plant Science*, *171*, 155-165
- Liu, L., Li, Y., Li, S., Hu, N., et al. (2012). Comparison of next-generation sequencing systems. *Journal of Biomedicine and Biotechnology*, *251364*. doi: 10.1155/2012/251364
- Luigi, M., Manglli, A., Bertin, S., Donati, L., et al. (2020). Development and validation of a specific real-time PCR protocol for the detection of tomato leaf curl New Delhi virus. *European Journal of Plant Pathology*, *157*, 969-974
- Luna-Moreno, D., Sánchez-Álvarez, A., Islas-Flores, I., Canto-Canche, B., et al. (2019). Early detection of the fungal banana black Sigatoka pathogen *Pseudocercospora fijiensis* by an SPR immunosensor method. *Sensors*, *19*, 465
- Malapi-Wight, M., Salgado-Salazar, C., Demers, J. E., Clement, D.L., et al. (2016). Sarcococca blight: Use of whole-genome sequencing for fungal plant disease diagnosis. *Plant Disease*, *100*, 1093–1100
- McCartney, H. A., Foster, S. J., Fraaije, B. A., & Ward, E. (2003). Molecular diagnostics for fungal plant pathogens. *Pest Management Science: formerly Pesticide Science*, *59*, 129-142
- Mori, Y., Hirano, T., & Notomi, T. (2006). Sequence specific visual detection of LAMP reactions by addition of cationic polymers. *BMC biotechnology*, *6*, 1-10
- Mullis, K. B. (1990). The unusual origin of the polymerase chain reaction. *Scientific American*, *262*, 56-61
- Mullis, K. B., & Faloona, F. A. (1987). Specific synthesis of DNA in vitro via a polymerase-catalyzed chain reaction. *Methods in Enzymology*, *155*, 335–350
- Murugan, L., Krishnan, N., Venkataravanappa, V., Saha, S., et al. (2020). Molecular characterization and race identification of *Fusarium oxysporum* f. sp. *lycopersici* infecting tomato in India. *3 Biotech*, *10*, 1-12
- Myerson, L. A., & Reaser, J. K. (2002). Biosecurity: Moving toward a comprehensive approach. *Bioscience*, *52*, 593-600
- Navin, N., Kendall, J., Troge, J., Rodgers, L., et al. (2011). Tumour evolution inferred by single-cell sequencing. *Nature*, *472*, 90-94

- Notomi, T., Okayama, H., Masubuchi, H., Yonekawa, T., et al. (2000). Loop-mediated isothermal amplification of DNA. *Nucleic Acids Research*, *28*, E63
- Oono, Y., Kobayashi, F., Kawahara, Y., Yazawa, T., et al. (2013). Characterisation of the wheat (*triticumaestivum* L.) transcriptome by de novo assembly for the discovery of phosphate starvation-responsive genes: gene expression in Pi-stressed wheat. *BMC Genomics*, *14*, 1-14
- Pabinger, S., Dander, A., Fischer, M., Snajder, R., et al. (2014). A survey of tools for variant analysis of next-generation genome sequencing data. *Briefings in bioinformatics*, *15*, 256-278
- Panteghini, M., & Forest, J. C. (2005). Standardization in laboratory medicine: new challenges. *Clinica Chimica Acta*, *355*, 1-12
- Peña-Bahamonde, J., Nguyen, H. N., Fanourakis, S. K., & Rodrigues, D. F. (2018). Recent advances in graphene-based biosensor technology with applications in life sciences. *Journal of Nanobiotechnology*, *16*, 75
- Piombo, E., Abdelfattah, A., Droby, S., Wisniewski, M., et al. (2021). Metagenomics approaches for the detection and surveillance of emerging and recurrent plant pathogens. *Microorganisms*, *9*, 188
- Qin, D. (2019). Next-generation sequencing and its clinical application. *Cancer Biology and Medicine*, *16*, 4-10
- Qin, J., Li, R., Raes, J., Arumugam, M., et al. (2010). A human gut microbial gene catalogue established by metagenomic sequencing. *Nature*, *464*, 59-65
- Rahman, M., Heng, L. Y., & Futra, D., (2017). A highly sensitive electrochemical DNA biosensor from acrylic-gold nanocomposite for the determination of arowana fish gender. *Nanoscale Research Letters*, *12*, 484
- Rajesh T, & Jaya M (2017) Next-generation sequencing methods. In Christian, L., Sanroman, D., Du, M. (Eds.), *Current Developments in Biotechnology and Bioengineering*. Amsterdam: Elsevier
- Rani, A., Donovan, N., & Mantri, N. (2019). Review: The future of plant pathogen diagnostics in a nursery production system. *Biosensors and Bioelectronics*, *145*, 111631
- Rizzo, D. M., Lichtveld, M., Mazet, J. A., Togami, E., & Miller, S. A. (2021). Plant health and its effects on food safety and security in a One Health framework: Four case studies. *One Health Outlook*, *3*, 1-9
- Ronholm, J. (2018). Game Changer-Next Generation Sequencing and Its Impact on Food Microbiology. *Frontiers in Microbiology*, *9*, 363
- Sakamoto, S., Putalun, W., Vimolmangkang, S., Phoolcharoen, W., et al. (2018). Enzyme-linked immunosorbent assay for the quantitative/qualitative analysis of plant secondary metabolites. *Journal of Natural Medicines*, *72*, 32-42
- Sakudo, A., Suganuma, Y., Kobayashi, T., Onodera, T., Ikuta, K. (2006). Near-infrared spectroscopy: promising diagnostic tool for viral infections. *Biochemical and Biophysical Research Communications*, *341*, 279-284
- Sanger, F., Nicklen, S., & Coulson, A. R. (1977). DNA sequencing with chain-terminating inhibitors. *Proceedings of the National Academy of Sciences*, *74*, 5463-5467
- Sarkes, A., Fu, H., Feindel, D., Harding, M., & Feng, J. (2020). Development and evaluation of a loop-mediated isothermal amplification (LAMP) assay for the detection of Tomato brown rugose fruit virus (ToBRFV). *PLoS One*, *15*, e0230403
- Savary, S., Bregaglio, S., Willocquet, L., Gustafson, D., et al. (2017). Crop health and its global impacts on the components of food security. *Food Security*, *9*, 311-27
- Scala, V., Pucci, N., & Loreti, S. (2018). The diagnosis of plant pathogenic bacteria: A state of art. *Frontiers in Bioscience*, *10*, 449-460
- Shweta, H. M., Kumar, M. P., Teli, K., Kunduru, B., & Shekar, B. C. (2018). Isolation, identification and molecular characterization of *Ralstonia solanaceum* isolates collected from Southern Karnataka. *Journal of Applied and Natural Science*, *10*, 886-893
- Skottrup, P. D., Nicolaisen, M., & Justesen, A. F. (2008). Towards on-site pathogen detection using antibody-based sensors. *Biosensors and Bioelectronics*, *24*, 339-348
- Smith, C. J., & Osborn, A. M. (2009). Advantages and limitations of quantitative PCR (Q-PCR)-based approaches in microbial ecology. *FEMS microbiology ecology*, *67*, 6-20
- Stackhouse, T., Martinez-Espinoza, A. D., & Ali, M. E. (2020). Turfgrass disease diagnosis: Past, present, and future. *Plants*, *9*, 1544
- Tian, Y. L., Zhao, Y. Q., Chen, B. H., Chen, S., et al. (2020). Real-time PCR assay for detection of *Dickeya fangzhongdai* causing bleeding canker of pear disease in China. *Journal of Integrative Agriculture*, *19*, 898-905

- Tomlinson, J. A., Barker, I., & Boonham, N. (2007). Faster, simpler, more-specific methods for improved molecular detection of *Phytophthora ramorum* in the field. *Applied and Environmental Microbiology*, *73*, 4040-4047
- Tomlinson, J., & Boonham, N. (2008). Potential of LAMP for detection of plant pathogens. *CAB Reviews: Perspectives in Agriculture, Veterinary Science, Nutrition and Natural Resources*, *3*, 1-7
- Vigneshvar, S., Sudhakumari, C. C., Senthikumar, B., & Prakash, H. (2016). Recent advances in biosensor technology for potential applications—an overview. *Frontiers in Bioengineering and Biotechnology*, *4*, 11
- Vincelli, P., Tisserat, N. (2008). Nucleic acid-based pathogen detection in applied plant pathology. *Plant Disease*, *92*, 660-669
- Waliullah, S., Ling, K. S., Cieniewicz, E. J., Oliver, J.E., et al. (2020). Development of loop-mediated isothermal amplification assay for rapid detection of Cucurbit leaf crumple virus. *International Journal of Molecular Sciences*, *21*, 1756
- Walker, T. M., Ip, C. L. C., Harell, R. H., Evans, J.T., et al. (2013). Whole-genome sequencing to delineate *Mycobacterium tuberculosis* outbreaks: a retrospective observational study. *The Lancet Infectious Diseases*, *13*, 137-146
- Wang, Z., Yu, D., Li, X., Zeng, M., et al. (2012). The development and application of a Dot-ELISA assay for diagnosis of southern rice black streaked dwarf disease in the field. *Viruses*, *4*, 167-183
- White, S., Schultz, T., & Enuameh, Y. A. K. (2011). Synthesizing evidence of diagnostic accuracy. Philadelphia: Lippincott Williams & Wilkins
- Zhang, M., Chen, R., Zhou, X., & Wu, J. (2018). Monoclonal antibody-based serological detection methods for wheat dwarf virus. *Virologica Sinica*, *33*, 173-180



## Journal of Experimental Biology and Agricultural Sciences

<http://www.jebas.org>

ISSN No. 2320 – 8694

### Assessment of Variability and Genetic Diversity Study in an Advanced Segregating Population in Rice with Blast Resistance Genes Introgression

N Hasan<sup>1,2,\*</sup>, M Y Rafii<sup>3,4</sup>, A R Harun<sup>5</sup>, N S Ali<sup>6</sup>, N Mazlan<sup>3,4</sup>, S Abdullah<sup>7</sup>

<sup>1</sup>Faculty of Applied Sciences, Universiti Teknologi MARA, Cawangan Negeri Sembilan Kampus Kuala Pilah, Negeri Sembilan, Malaysia

<sup>2</sup>Biotechnology, Microbiology and Environmental Collaborative Science, Universiti Teknologi MARA, Cawangan Negeri Sembilan Kampus Kuala Pilah, 72000, Negeri Sembilan, Malaysia

<sup>3</sup>Institute of Tropical Agriculture and Food Security, Universiti Putra Malaysia, Serdang, Selangor, Malaysia

<sup>4</sup>Department of Crop Science, Universiti Putra Malaysia, Serdang, Selangor, Malaysia

<sup>5</sup>Agrotechnology and Bioscience Division, Malaysian Nuclear Agency, Kajang, Selangor, Malaysia

<sup>6</sup>Department of Agriculture Technology, Universiti Putra Malaysia, Serdang, Selangor, Malaysia

<sup>7</sup>Agricultural Biotechnology Research Group, Faculty of Plantation and Agrotechnology, Universiti Teknologi MA RA Cawangan Melaka, Merlimau, Melaka, Malaysia

Received – February 04, 2022; Revision – March 23, 2022; Accepted – April 24, 2022

Available Online – April 30, 2022

DOI: [http://dx.doi.org/10.18006/2022.10\(2\).306.317](http://dx.doi.org/10.18006/2022.10(2).306.317)

#### KEYWORDS

Genetic diversity

Heritability

Principal component analysis

Rice breeding

UPGMA dendrogram

#### ABSTRACT

Blast disease caused by a pathogenic fungus, *Magnaphorthe oryzae*, is the most destructive disease and has resulted in more than 50% of crop losses worldwide, including in Malaysia. The present study was conducted to investigate genetic variability among 36 advanced lines of MR264 × PS2 rice with blast resistance genes introduced at the Faculty of Applied Sciences, Universiti Teknologi MARA, Malaysia. Traits such as days of maturity, plant height, grain width, and seed setting rate exhibited negative skewness in this study, indicating a doubling of gene effects. Seed setting rate and 1000 grain weight showed positive kurtosis, indicating gene interactions. The phenotypic coefficient of variation (PCV) was slightly higher than the genotypic coefficient of variation (GCV) for all traits, indicating that environmental influences affect the expression of these traits. High heritability associated with high genetic advance as a percentage of the mean was observed for filled grains per panicle. In addition, the second-highest value for high heritability and the high genetic advance was observed for the number of tillers. Cluster and principal component analysis revealed that 36 advanced lines were grouped into four clusters based on ten agromorphological traits. Clusters A and C had higher mean values for most of the traits studied than clusters B and D. Desirable recombinants for higher yields with a broad genetic base can be generated by using cross lines from different clusters.

\* Corresponding author

E-mail: [aishahnh@uitm.edu.my](mailto:aishahnh@uitm.edu.my) (N Hasan)

Peer review under responsibility of Journal of Experimental Biology and Agricultural Sciences.

Production and Hosting by Horizon Publisher India [HPI]  
(<http://www.horizonpublisherindia.in/>).  
All rights reserved.

All the articles published by [Journal of Experimental Biology and Agricultural Sciences](#) are licensed under a [Creative Commons Attribution-NonCommercial 4.0 International License](#) Based on a work at [www.jebas.org](http://www.jebas.org).



## 1 Introduction

Rice (*Oryza sativa* L.) is the most important food crop in the world. Nearly 40% of the world's population consumes rice as a staple food (FAO 2019). Blast disease, also known as rice blight, is the most destructive rice disease caused by the fungus *Magnaporthe oryzae*, resulting in more than 50% of crop losses worldwide (Hasan et al. 2015a; Chukwu et al. 2020). Conventionally, blast disease can be controlled with chemical pesticides and biocontrol agents (Rijal and Devkota 2020; Upadhyay and Bhatta 2020). However, due to environmental and food safety concerns, chemical control is not feasible, practical, and effective (Magar et al. 2015). Therefore, the development and use of resistant cultivars are considered as the most effective, economical, and environmentally friendly method to control the instability of the fungal pathogen *M. oryzae* (Xiao et al. 2019; Shahriar et al. 2020).

The success of a breeding programme always depends on the accessibility of a wide range of genetic resources and germplasm evaluation. A comprehensive study of genetic diversity within accessions would be useful to establish new varieties of breeding material (Govintharaj et al. 2016). Variability in genetic divergence for traits of interest is a major component of the breeding programme to expand the genetic pool of crops and requires an accurate assessment of heritability to prepare for a successful breeding programme (Roy and Shil 2020). A proper understanding of heritability helps plant breeders predicts the type of successful generation to make the appropriate selection and evaluate the extent of genetic improvement through selection. Traits with high genotypic coefficients of variation, as well as high heritability and genetic advance as a percentage of the mean, can be controlled by additive types of gene activity; therefore, traits can be improved by simple breeding methods.

Information on skewness and kurtosis provides information on the type of gene action (Savitha and Kumari 2015) and the number of genes controlling the trait. In addition, the studies on skewness and kurtosis are necessary to evaluate the extent to which the second generation affects the mean of the third generation and whether this parameter can be used for selection. The true genetic potential can only be determined in the performance of the progeny in the individual selection since the mean value of the progeny is a more reliable estimate than the individual values of the selected parents. If the kurtosis value for the traits has a positive sign, it indicates the presence of gene interactions, while a negative sign or a value

close to zero for the kurtosis indicates the absence of gene interactions (Samak et al. 2011). A skewness with a positive sign indicates the presence of complementary gene action, whereas gene action is double (additive  $\times$  additive) when the skewness has a negative sign (Vanitha et al. 2016).

Grain yield is a complex trait that depends on many components and responds poorly to direct selection. Knowledge of the relationship between grain yield and its components is useful for improving grain yield (Lakshmi et al. 2017). Information on the relationship between traits and the direct and indirect effects of each trait on yield is an added advantage in supporting the selection process. Correlation and pathway analyses determine the extent of the relationship between yield and its components and also reveal the relative importance of their direct and indirect effects, providing a clear understanding of their relationship with grain yield (Nikhil et al. 2014). Ultimately, this type of analysis could help growers develop their selection strategies to improve grain yield.

In the light of the above scenario, the present study was conducted to determine the genetic diversity and variability of yield and yield component traits of blast resistance genes introduced into segregating rice populations.

## 2 Material and Methods

### 2.1 Plant materials and Experimental setup

The experiment was conducted from March 2013 to September 2016 at the greenhouse of Agency Nuclear Malaysia Greenhouse in Selangor, Malaysia. The genetic material used in this experiment was MR264 as the recurrent parent (referred to as P1) and Pongsu Seribu 2 as the donor parent (referred to as P2). The parents were differentially resistant to blasts as shown in Table 1.

P1 and P2 were planted as parents in standard plastic pots (28 cm x 25 cm), each containing 5 plants. The F<sub>1</sub> generation was formed by crossing P1/P2, and the F<sub>1</sub> generation was obtained reciprocally. Four of the 32 F<sub>1</sub> plants developed as the female parent were backcrossed to MR264 to develop BC<sub>1</sub>F<sub>1</sub> progeny. Six of 136 BC<sub>1</sub>F<sub>1</sub> were backcrossed to produce BC<sub>2</sub>F<sub>1</sub> plants. Selected BC<sub>2</sub>F<sub>1</sub> plants were then allowed to self-pollinate to produce BC<sub>2</sub>F<sub>2</sub> generation. Foreground and background selection was combined with strict phenotypic selection in each generation after pedigree selection (Figure 1). A total of 36 advanced lines were selected and used for this study (Figure 2). Standard cultivation methods recommended by IRR (2015) were used to grow healthy plants.

Table 1 Panicle characteristics of parents selected for crossing

Parents	Blast resistance level
MR264	Susceptible (score between 7-9)
Pongsu Seribu 2	Resistant (score between 1-3)

\*Scoring was based on IRR standard scoring for blast symptoms (IRRI 2015)

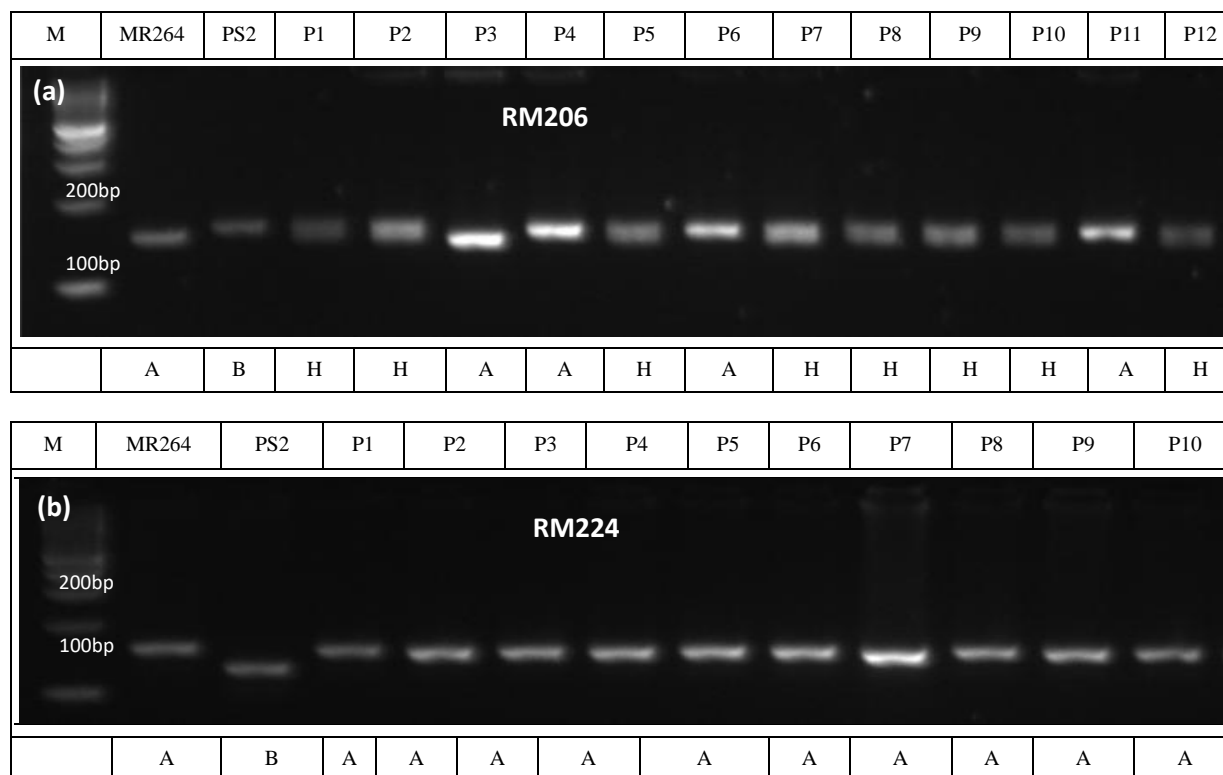


Figure 1 Banding pattern in the  $BC_2F_2$  population using (a) foreground markers; RM206 markers (b) background marker, RM224 (M=100 bp DNA ladder; P= plant no.)

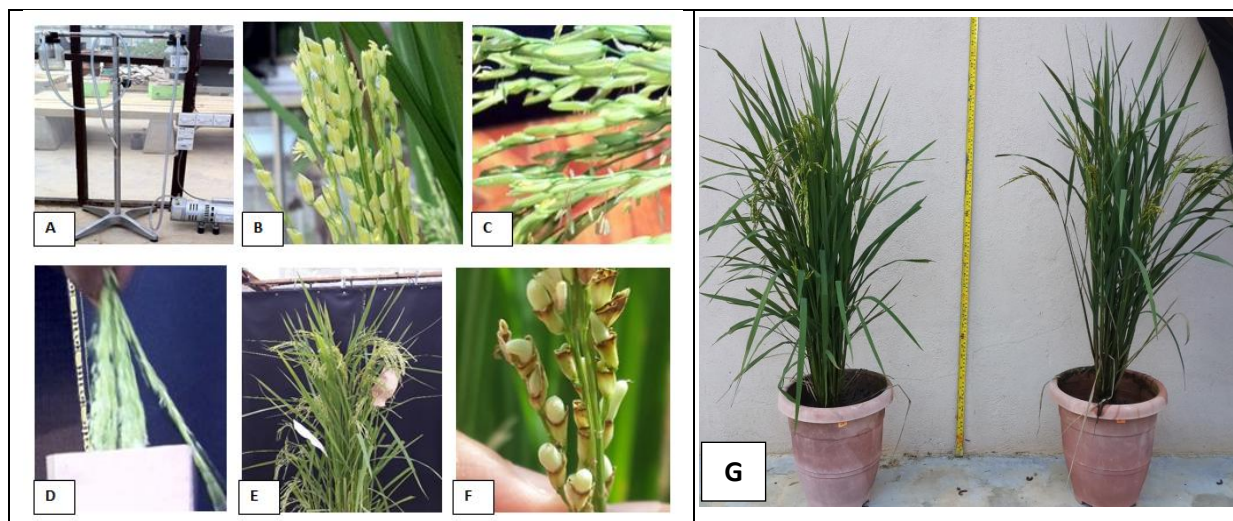


Figure 2 Hybridization process: A) Two selected parents Pongsu Seribu 2 and MR 264, B) Immature spikelets were immersed in hot water at 42.5°C for five minutes, C) end of opened spikelets were snipped off with scissor, D) Pollen from a male parent; E) Fertilized seeds three weeks after pollination. G) Morphological features of plant height of the parental line and blast-resistant improved lines ( $BC_2F_3$ )

## 2.2 Field data collection

At the maturity stage, data were collected and recorded from thirty-six plants of the 234  $BC_2F_3$  populations according to the rice descriptors of IRRI (2015). The traits such as days to maturity

(DOM, days), plant height (PH, cm), number of shoots per hill (NOT, n), panicle length (PL, cm), number of filled grains (FG, n), grain length (GL, cm), grain width (GW, cm), yield per hill (YH, g), 1000-seed weight (SW, g) and seed set rate (SS, %) were collected and recorded.

### 2.3 Statistical analysis

Data were used to estimate variability using simple measures such as mean and range, components of variation such as genotypic coefficient of variation (GCV) and phenotypic coefficient of variation (PCV), genetic parameters such as heritability, and genetic advance as a percentage of mean, and genetic diversity. All parameters in this study were measured on the 36 BC<sub>2</sub>F<sub>3</sub> plants using Microsoft Excel 2007 (Microsoft Corp., Redmond, WA, USA). To analyze the genetic relationships among the rice lines, the UPGMA (Unweighted pair group method with arithmetic means) algorithm and SAHN clustering (Oladosu et al. 2014) were used. The EIGEN and PROJ modules of NTSYS-pc and SAS version 9.2 were used to calculate the PCA of 36 rice lines. The association between the 10 quantitative traits was determined using the Pearson correlation coefficient. The equation for skewness and kurtosis was calculated according to the method presented by Herawati et al. (2021) and calculated as follows:

$$\text{Skewness} = \frac{\sum_{i=1}^N (Y_i - \bar{Y})^3}{(N-1)S^3}$$

$$\text{Kurtosis} = \frac{\sum_{i=1}^N (Y_i - \bar{Y})^4}{(N-1)S^4}$$

## 3 Results and Discussion

### 3.1 Yield and its component traits among 36 BC<sub>2</sub>F<sub>3</sub> lines

Ten quantitative traits of rice yield were calculated for genetic variability (Table 1). Ten traits, including days to maturity, plant height, number of grains on hill<sup>-1</sup>, panicle length, number of filled grains on panicle<sup>-1</sup>, the yield on hill<sup>-1</sup>, 1000-grain weight on hill<sup>-1</sup>, and rate of seed formation, showed highly significant variation ( $P \leq 0.05$ ). The results obtained are in agreement with those of Sumanth et al. (2017) and Girma et al. (2018), which indicated significant differences among genotypes. Therefore, genetic improvement through selection is highly beneficial. High variability in breeding material helps to ensure that the subsequent generation has a better chance of producing superior recombinants.

Plant number 24 (P24) had the highest days to maturity (123), while P13 had the lowest days to maturity (112), which is statistically consistent with parent MR264. The highest plant height was observed in P19 (104 cm), while P4 had the lowest plant height (76 cm). This result is consistent with Mazid et al. (2013) and Hasan et al. (2015b), who found differences in plant height between the progeny of rice and the parent cultivar. The remaining plants showed differences in plant height, but these were not significant, indicating that they were very similar to the height of the parent plant MR264 (Table 1).

Tillering ability is one of the most important yield-determining traits of the rice plant. The number of shoots per hill varied from 28 to 10. The highest number of shoots (28) was found in plant No. 6 (P6), which was statistically similar to P3 and P4. The lowest number of tillers (10) was found in plant number 23, which was statistically similar to MR264. P7 and P8, P26 and P27, P30 and P32, P35 and P36 had a similar number of tillers. Other rice lines had different values but were statistically similar. It can be seen that the number of grains in the new progenies is close to MR264 (Table 1). The number of grains is crucial for high grain yield. The same result was also found in our recent study. Sharif et al. (2013) also found significant differences in the number of grains on hill<sup>-1</sup> in pigmented rice.

In rice, yield is determined by indirect traits such as panicle length. In the present study, the highest panicle length (26 cm) was observed in plant number 4 (P4), followed by P2 (25.67 cm), while the shortest panicle length (21 cm) was observed in P3 and P26, which was statistically similar to P20 and P33. The study was in agreement with the reports of Sabri et al. (2020). Almost all progenies were statistically like MR264 (Table 1).

A significant difference was observed in grains per panicle among all progenies, with values ranging from 210 to 96. The highest number of filled grains (210.67) was obtained from plant number 2 (P2), while the lowest number of filled grains (96) was from P18. The highest yield/ha (44.67 g) was recorded from plant number 6, followed by P4 (43 g), while the lowest value (33.67 g) was observed from P33 (Table 1). The highest amount of total grain weight per hill belonged to P2, while P16 and P33 had the lowest amount of total grain weight per hill. The 1000-grain weight varied significantly among genotypes, ranging from 29.67 to 16.67 g. P1, P20, and P23, and P27, P23, and P30 had similar total grain weight per hill, 22 and 20 g, respectively. The highest percent seeding rate was recorded by P3 (96.33%), which is statically similar to plant numbers 5, 11, and 12. Plant number 36 (P36) had the lowest seeding rate (54.33%). This result is also in agreement with the results of Roy and Shil (2020).

Seed length also varied among progenies, ranging from 11.33 to 7.67 mm. Plant number 34 had the longest (11.33 mm) seeds, while P10 had the shortest (7.67 mm) seeds, similar to P12 and P17. The highest width length (2.07 mm) was found in MR264, while the lowest value (1.83 mm) was observed in P2. The other measured values of progeny length were different but not statistically significant. This indicates that the newly developed lines do not show genetic variation with the parental MR264 lines and are not controlled by environmental factors. This was also noted by Hasan et al. (2015b) and Sabri et al. (2020).



Table 2 Mean performance of 36 BC<sub>2</sub>F<sub>3</sub> rice lines for 10 agronomic traits.

Progeny	Days of maturity	Plant height(cm)	Tiller number/hill	Panicle length (cm)	Filled grain (%)	Grain length	Grain width	Yield /hill (g)	1000 seed wt (g)	Seed setting rate (%)
MR284	112.00 <sup>ab</sup>	83.00 <sup>ac</sup>	24.33 <sup>ab</sup>	21.33 <sup>c</sup>	164.67 <sup>ab</sup>	8.00 <sup>a</sup>	2.07 <sup>a</sup>	40.00 <sup>ac</sup>	23.33 <sup>ab</sup>	91.00 <sup>ac</sup>
P1	113.33 <sup>c</sup>	84.00 <sup>b</sup>	23.67 <sup>c</sup>	23.33 <sup>b</sup>	160.00 <sup>c</sup>	8.33 <sup>a</sup>	2.03 <sup>a</sup>	40.00 <sup>b</sup>	22.00 <sup>c</sup>	90.33 <sup>b</sup>
P2	113.00 <sup>c</sup>	80.33 <sup>b</sup>	24.67 <sup>c</sup>	25.67 <sup>b</sup>	210.67 <sup>c</sup>	10.67 <sup>a</sup>	1.83 <sup>a</sup>	41.80 <sup>b</sup>	29.67 <sup>c</sup>	93.89 <sup>b</sup>
P3	114.33 <sup>c</sup>	77.33 <sup>b</sup>	27.00 <sup>c</sup>	25.00 <sup>b</sup>	193.33 <sup>c</sup>	10.67 <sup>a</sup>	1.97 <sup>a</sup>	42.00 <sup>b</sup>	26.00 <sup>c</sup>	96.33 <sup>b</sup>
P4	118.00 <sup>c</sup>	76.00 <sup>b</sup>	27.00 <sup>c</sup>	26.00 <sup>b</sup>	207.00 <sup>c</sup>	10.00 <sup>a</sup>	2.00 <sup>a</sup>	43.00 <sup>b</sup>	27.33 <sup>c</sup>	92.67 <sup>b</sup>
P5	115.67 <sup>c</sup>	82.33 <sup>b</sup>	21.33 <sup>c</sup>	21.00 <sup>b</sup>	206.33 <sup>c</sup>	8.33 <sup>a</sup>	1.97 <sup>a</sup>	40.00 <sup>b</sup>	24.33 <sup>c</sup>	96.33 <sup>b</sup>
P6	115.67 <sup>c</sup>	76.67 <sup>b</sup>	28.00 <sup>c</sup>	23.33 <sup>b</sup>	177.33 <sup>c</sup>	8.67 <sup>a</sup>	1.93 <sup>a</sup>	44.67 <sup>b</sup>	26.33 <sup>c</sup>	94.33 <sup>b</sup>
P7	117.67 <sup>c</sup>	77.33 <sup>b</sup>	24.00 <sup>c</sup>	25.00 <sup>b</sup>	179.33 <sup>c</sup>	8.33 <sup>a</sup>	1.90 <sup>a</sup>	41.00 <sup>b</sup>	26.67 <sup>c</sup>	91.00 <sup>b</sup>
P8	116.67 <sup>c</sup>	78.67 <sup>b</sup>	24.00 <sup>c</sup>	22.33 <sup>b</sup>	173.67 <sup>c</sup>	10.00 <sup>a</sup>	1.97 <sup>a</sup>	41.07 <sup>b</sup>	25.33 <sup>c</sup>	91.00 <sup>b</sup>
P9	117.00 <sup>c</sup>	105.67 <sup>b</sup>	20.67 <sup>j</sup>	26.67 <sup>b</sup>	105.00 <sup>c</sup>	8.00 <sup>a</sup>	1.90 <sup>a</sup>	40.67 <sup>b</sup>	20.67 <sup>c</sup>	52.00 <sup>b</sup>
P10	116.67 <sup>c</sup>	95.67 <sup>b</sup>	13.33 <sup>c</sup>	23.67 <sup>b</sup>	117.67 <sup>c</sup>	7.67 <sup>a</sup>	2.00 <sup>a</sup>	41.00 <sup>b</sup>	22.00 <sup>c</sup>	76.33 <sup>b</sup>
P11	117.00 <sup>c</sup>	95.00 <sup>b</sup>	21.33 <sup>c</sup>	22.67 <sup>b</sup>	99.33 <sup>c</sup>	8.33 <sup>a</sup>	1.87 <sup>a</sup>	39.67 <sup>b</sup>	19.33 <sup>c</sup>	96.33 <sup>b</sup>
P12	113.67 <sup>c</sup>	98.00 <sup>ac</sup>	19.00 <sup>c</sup>	21.00 <sup>b</sup>	108.0 <sup>c</sup>	7.67 <sup>a</sup>	2.00 <sup>a</sup>	40.33 <sup>b</sup>	18.67 <sup>c</sup>	96.33 <sup>b</sup>
P13	112.00 <sup>c</sup>	92.00 <sup>b</sup>	18.67 <sup>c</sup>	20.00 <sup>b</sup>	100.00 <sup>c</sup>	9.00 <sup>a</sup>	2.03 <sup>a</sup>	37.00 <sup>b</sup>	19.33 <sup>c</sup>	82.33 <sup>b</sup>
P14	116.00 <sup>c</sup>	93.67 <sup>b</sup>	17.33 <sup>c</sup>	22.23 <sup>b</sup>	107.67 <sup>c</sup>	8.67 <sup>a</sup>	1.97 <sup>a</sup>	39.27 <sup>b</sup>	21.00 <sup>c</sup>	81.40 <sup>b</sup>
P15	118.00 <sup>c</sup>	100.33 <sup>b</sup>	16.00 <sup>c</sup>	25.00 <sup>b</sup>	114.33 <sup>c</sup>	8.33 <sup>a</sup>	1.97 <sup>a</sup>	41.00 <sup>b</sup>	20.00 <sup>c</sup>	79.67 <sup>b</sup>
P16	117.67 <sup>c</sup>	99.67 <sup>b</sup>	21.00 <sup>c</sup>	24.67 <sup>b</sup>	98.00 <sup>c</sup>	9.33 <sup>a</sup>	1.97 <sup>a</sup>	35.27 <sup>b</sup>	16.67 <sup>c</sup>	88.00 <sup>b</sup>
P17	113.33 <sup>c</sup>	100.67 <sup>b</sup>	16.67 <sup>c</sup>	21.00 <sup>b</sup>	105.00 <sup>c</sup>	7.67 <sup>a</sup>	1.87 <sup>a</sup>	38.80 <sup>b</sup>	19.67 <sup>c</sup>	90.00 <sup>b</sup>
P18	116.33 <sup>c</sup>	103.67 <sup>b</sup>	14.00 <sup>c</sup>	20.33 <sup>b</sup>	96.00 <sup>c</sup>	8.33 <sup>a</sup>	2.00 <sup>a</sup>	36.47 <sup>b</sup>	19.30 <sup>c</sup>	76.00 <sup>b</sup>
P19	114.00 <sup>c</sup>	104.00 <sup>b</sup>	18.33 <sup>c</sup>	22.00 <sup>b</sup>	97.67 <sup>c</sup>	9.00 <sup>a</sup>	2.00 <sup>a</sup>	36.33 <sup>b</sup>	19.00 <sup>c</sup>	87.67 <sup>b</sup>
P20	118.00 <sup>c</sup>	102.00 <sup>b</sup>	15.00 <sup>c</sup>	20.33 <sup>b</sup>	115.00 <sup>c</sup>	9.67 <sup>a</sup>	1.97 <sup>a</sup>	36.67 <sup>b</sup>	22.00 <sup>c</sup>	81.67 <sup>b</sup>
P21	116.00 <sup>c</sup>	98.00 <sup>a<sup>c</sup></sup>	13.33 <sup>c</sup>	24.67 <sup>b</sup>	179.67 <sup>c</sup>	8.33 <sup>a</sup>	2.00 <sup>a</sup>	41.33 <sup>b</sup>	21.00 <sup>c</sup>	82.00 <sup>b</sup>
P22	115.33 <sup>c</sup>	98.00 <sup>ac</sup>	14.33 <sup>c</sup>	23.67 <sup>b</sup>	185.00 <sup>c</sup>	9.00 <sup>a</sup>	1.97 <sup>a</sup>	41.00 <sup>b</sup>	22.33 <sup>c</sup>	80.33 <sup>b</sup>
P23	121.67 <sup>c</sup>	60.00 <sup>b</sup>	10.33 <sup>c</sup>	25.33 <sup>b</sup>	196.67 <sup>c</sup>	9.00 <sup>a</sup>	2.03 <sup>a</sup>	39.00 <sup>b</sup>	22.00 <sup>c</sup>	90.33 <sup>b</sup>
P24	123.00 <sup>c</sup>	95.33 <sup>b</sup>	10.67 <sup>c</sup>	24.00 <sup>b</sup>	179.33 <sup>c</sup>	10.00 <sup>a</sup>	1.97 <sup>a</sup>	41.00 <sup>b</sup>	21.33 <sup>c</sup>	81.00 <sup>b</sup>
P25	115.00 <sup>c</sup>	92.33 <sup>b</sup>	11.00 <sup>c</sup>	23.67 <sup>b</sup>	173.33 <sup>c</sup>	8.67 <sup>a</sup>	2.10 <sup>a</sup>	44.00 <sup>b</sup>	20.00 <sup>c</sup>	75.67 <sup>b</sup>
P26	121.67 <sup>c</sup>	96.33 <sup>b</sup>	12.33 <sup>c</sup>	20.00 <sup>b</sup>	146.00 <sup>c</sup>	9.67 <sup>a</sup>	2.03 <sup>a</sup>	40.00 <sup>b</sup>	21.00 <sup>c</sup>	81.00 <sup>b</sup>
P27	118.00 <sup>c</sup>	96.00 <sup>b</sup>	12.33 <sup>c</sup>	21.67 <sup>b</sup>	155.33 <sup>c</sup>	11.33 <sup>a</sup>	1.97 <sup>a</sup>	42.33 <sup>b</sup>	20.00 <sup>c</sup>	80.00 <sup>b</sup>
P28	115.67 <sup>c</sup>	95.33 <sup>b</sup>	17.67 <sup>c</sup>	22.00 <sup>b</sup>	162.67 <sup>c</sup>	10.00 <sup>a</sup>	2.03 <sup>a</sup>	36.00 <sup>b</sup>	19.67 <sup>c</sup>	83.67 <sup>b</sup>
P29	116.33 <sup>c</sup>	95.33 <sup>b</sup>	14.33 <sup>c</sup>	22.00 <sup>b</sup>	157.00 <sup>c</sup>	9.67 <sup>a</sup>	2.00 <sup>a</sup>	39.00 <sup>b</sup>	20.33 <sup>c</sup>	90.33 <sup>b</sup>
P30	121.67 <sup>c</sup>	95.33 <sup>b</sup>	15.00 <sup>c</sup>	22.33 <sup>b</sup>	118.33 <sup>c</sup>	10.00 <sup>a</sup>	2.00 <sup>a</sup>	40.33 <sup>b</sup>	20.00 <sup>c</sup>	77.67 <sup>b</sup>
P31	115.00 <sup>c</sup>	102.00 <sup>b</sup>	15.67 <sup>c</sup>	21.33 <sup>b</sup>	109.33 <sup>c</sup>	10.33 <sup>a</sup>	1.97 <sup>a</sup>	37.00 <sup>b</sup>	18.33 <sup>c</sup>	87.67 <sup>b</sup>
P32	114.33 <sup>c</sup>	97.67 <sup>b</sup>	15.00 <sup>c</sup>	22.00 <sup>b</sup>	134.33 <sup>c</sup>	11.00 <sup>a</sup>	1.97 <sup>a</sup>	36.67 <sup>b</sup>	17.33 <sup>c</sup>	79.33 <sup>b</sup>
P33	118.33 <sup>c</sup>	98.67 <sup>b</sup>	13.00 <sup>c</sup>	20.67 <sup>b</sup>	114.67 <sup>c</sup>	11.00 <sup>a</sup>	1.97 <sup>a</sup>	33.67 <sup>b</sup>	16.67 <sup>c</sup>	74.33 <sup>b</sup>
P34	116.67 <sup>c</sup>	98.67 <sup>b</sup>	18.00 <sup>c</sup>	23.00 <sup>b</sup>	124.67 <sup>c</sup>	11.33 <sup>a</sup>	1.97 <sup>a</sup>	36.67 <sup>b</sup>	18.67 <sup>c</sup>	72.33 <sup>b</sup>
P35	119.00 <sup>c</sup>	99.33 <sup>b</sup>	16.33 <sup>c</sup>	21.67 <sup>b</sup>	121.33 <sup>c</sup>	10.67 <sup>a</sup>	1.93 <sup>a</sup>	35.00 <sup>b</sup>	17.33 <sup>c</sup>	65.67 <sup>b</sup>
P36	115.00 <sup>c</sup>	95.00 <sup>b</sup>	16.33 <sup>c</sup>	22.00 <sup>b</sup>	108.00 <sup>c</sup>	10.67 <sup>a</sup>	1.93 <sup>a</sup>	38.33 <sup>b</sup>	18.00 <sup>c</sup>	54.33 <sup>b</sup>
Mean	117.04	93.27	18	22.86	143.65	9.32	1.96	39.11	21.11	83.04
CV%	4.10	4.72	11.78	7.69	5.80	17.20	8.20	4.62	9.34	2.49

Table 3 Variability parameters of different biometrical traits in a BC<sub>2</sub>F<sub>3</sub> population in rice.

Traits	Mean	MSG	MSE	$\sigma^2P$	$\sigma^2G$	PCV (%)	GCV (%)	$h^2B$ (%)	GA (%)	Skewness	Kurtosis
DOM	117.04±2.17	81.24	23.07	42.46	19.39	5.57	3.76	45.66	5.24	-0.191	-0.38
PH	93.27±9.37	388.52	19.37	142.42	123.05	12.79	11.89	86.40	22.77	-0.93	1.16
NOT	18.00±4.73	71.17	4.50	26.72	22.23	28.72	26.19	83.17	49.20	0.25	-0.742
PL	22.86±1.83	10.43	3.09	5.53	2.45	10.29	6.84	44.18	9.37	0.30	-0.71
FG	143.65±36.6	4124.92	69.39	1421.23	1351.84	26.24	25.60	95.12	51.42	0.36	-1.15
GL	9.32±0.50	3.65	2.57	2.93	0.36	18.37	6.42	12.23	4.63	0.37	-0.14
GW	1.96±0.04	0.03	0.03	0.03	0.00	8.24	0.88	1.15	0.20	-0.17	-0.58
Y	39.11±2.18	32.57	3.26	13.03	9.77	9.23	7.99	75.00	14.26	0.02	-0.35
SW	21.11±1.81	28.83	3.89	12.20	8.31	16.55	13.66	68.14	23.23	0.71	0.43
SS	83.04±10.85	331.12	4.29	113.23	108.94	12.81	12.57	96.21	25.40	-1.11	1.51

Data presented as Mean ± SE. Notes: Genetic variance ( $S^2_g$ ), error variance ( $S^2_e$ ), phenotypic variance ( $S^2_P$ ), genotypic coefficient of variation (GCV), phenotypic coefficient of variation (PCV), broad sense heritability ( $h^2_B$ ), and genetic advance (GA), days to maturity (DOM, days), plant height (PH, cm), number of tillers per hill (NOT, n), panicle length (PL, cm), number of filled grains (FG, n), grain length (GL, cm), grain width (GW, cm), yield per hill (YH, g), 1000-seed weight (SW, g) and seed setting rate (SS, %).

### 3.2 Studies on the variability in BC<sub>2</sub>F<sub>3</sub>

The values of the mean, range, genotypic and phenotypic variance, phenotypic and genotypic coefficient of variance, heritability, genetic advance, and genetic advance as a percentage of the mean for ten different traits are shown in Table 3.

Day of maturity, plant height, grain width, and seed setting rate had negative skewness in this study, indicating double gene effects, while all other traits had positive skewness, indicating complementary gene effects. Similar results were previously reported by Raghavendra and Hittalmani (2015). Plant height, 1000-seed weight, and seed setting rate showed positive kurtosis, indicating gene interactions, while other yield and yield-related traits showed no gene interactions. Savitha and Kumari (2015) reported that plant height and 1000-seed weight showed positive kurtosis in rice. Moreover, Nurhidayah et al. (2021) reported the negative kurtosis values in grain width and grain length.

### 3.3 Phenotypic and genotypic variance

The highest phenotypic and genotypic variance was observed in the number of grains per panicle (1351.84% and 1421.23%, respectively), plant height (123.05% and 142.42%, respectively), and seed set rate (108.94% and 113.23%, respectively) while moderate phenotypic and moderate genotypic variance was observed in days to maturity (42.46% and 19.39%, respectively), plant height (142.42% and 123.05%, respectively), and number of shoots (26.72% and 22.23%, respectively). Low phenotypic and genotypic variance was observed in grain length (2.93% and 0.36%, respectively) and grain weight (0.03% and 0.00%, respectively). This study shows that phenotypic variation was

higher than genotypic variation for all studied traits, indicating a significant influence of environment on the expression of these traits. Previous rice studies have found higher phenotypic variation for various agromorphological traits in rice populations, including Bhandari et al. (2015); Adhikari et al. (2018); Herawati et al. (2021); and Mahesh et al. (2022).

### 3.4 Genotypic and phenotypic coefficient of variation

The GCV was lower than the PCV for all traits studied, suggesting that the observed variation was not only controlled by genotype but also influenced by environmental factors on trait expression. High GCV and high PCV were observed for the number of prickers (28.72% and 26.19%, respectively) and the number of grains per panicle (26.24% and 25.60%, respectively). High GCV and PCV levels were also observed in the number of grains filled as reported by Mallimar et al. (2015), Rashid et al. (2017), and Gyawali et al. (2018). In contrast, some researchers observed high GCV and PCV for the number of shoots per hill (Pandey and Anurag 2010; Sabri et al. 2020).

The moderate phenotypic and moderate genotypic variance was observed for 1000-seed weight (16.55% and 13.66%, respectively) and seed set rate (12.81% and 12.57%, respectively), indicating the possibility of improvement in these traits through further selection in segregating generations. The low phenotypic and genotypic variance was observed in days to maturity (5.57% and 3.76%, respectively), grain weight (8.24% and 0.88%, respectively), and yield per hill (9.23% and 7.99%, respectively). The results are in agreement with those of Habib et al. (2005) and Osman et al. (2012) for the same traits. In addition, Anis et al. (2016) and Nishanth et al. (2017) also reported a small difference in GCV and

PCV values for submergence tolerance among 20 rice cultivars and 525 germplasm lines, respectively, for some evaluated traits. In BC<sub>2</sub>F<sub>3</sub> lines, the recorded variability parameters were very low because the strict selection was performed in BC<sub>2</sub>F<sub>2</sub> generation and it was effective (Govintharaj et al. 2016). The current study showed that the variability in the studied traits is very broad.

### 3.5 Heritability and genetic advance

In this study, most of the traits had high heritability except for grain length and grain width, which had the lowest heritability percentage of 12.23% and 1.15%, respectively. High heritability and genetic advance percentage of mean were observed for the number of filled grains per panicle (95.12% and 51.42%, respectively) and seed setting rate (96.21% and 25.40%, respectively), indicating that the presence of additive gene action for trait expression can be improved by simple selection. Previous results of Akhtar et al. (2011) and Sohrabi et al. (2012) also confirmed the results of the present study.

Moderate heritability and moderate genetic advance as a percentage of mean were observed for plant height (86.40% and 22.77%, respectively), 1000-seed weight (68.14% and 23.23%, respectively), and the number of shoots (83.17% and 49.20%, respectively), indicating that simple selection would be effective in

advancing the later generation. These results are consistent with Ghosh and Sharma (2012) for plant height.

On the other hand, moderate heritability and low genetic advance as a percentage of the mean were recorded for yield per hill (75.00% and 14.26%, respectively), indicating that environment influences phenotypic expression. Therefore, direct selection of these traits is less effective. Low heritability and genetic advance as a percentage of the mean were observed for grain width (1.15% and 0.20%, respectively), indicating that non-additive gene action has a large influence. The lowest genetic advance for grain width was also found in the study of Umarani et al. (2017) and Rashid et al. (2017).

### 3.6 Genetic diversity analysis

A total of 36 BC<sub>2</sub>F<sub>3</sub> lines based on ten agromorphological phenotypic traits were classified into four main clusters, with 8 lines in the first cluster (designated C-A), 6 in C- B, 5 in C- C, 17 in C- D (Table 4 and Figure 3). The lines classified in cluster A had higher mean values for the majority of the studied characteristics. The B cluster had lower mean values than the C and D clusters for all characteristics except grain width. This study provides information to select better recombinants for different traits. Thus, this information could be used to generate greater variability in future rice breeding programs.

Table 4 Mean value of 10 quantitative traits for 4 groups constructed by cluster analysis

Groups	Days of maturity	Plant height (cm)	Tiller number/hill	Panicle length(cm)	Filled grain (%)	Grain length	Grain width	Yield /hill (g)	1000 seed wt (g)	Seed setting rate (%)
Cluster A	117.46±3.41	84.33±13.29	18.37±6.62	23.12±1.90	174.79±26.38	8.79±0.68	1.98±0.05	40.46±2.19	23.47±2.13	88.46±5.84
Cluster B	117.11±38.89	95.00±28.46	15.53±4.47	22.73±7.35	146.45±48.55	9.59±3.22	1.99±0.66	40.26±13.20	20.80±6.45	73.59±26.52
Cluster C	115.22±26.10	87.62±21.49	20.77±7.60	23.80±5.86	171.64±53.87	9.87±2.41	1.97±0.44	40.30±9.56	20.93±6.93	83.14±23.54
Cluster D	116.92±2.53	98.88±2.89	15.71±1.74	21.88±0.66	122.17±17.14	10.38±0.75	1.98±0.02	36.83±2.02	19.42±1.26	79.38±8.35

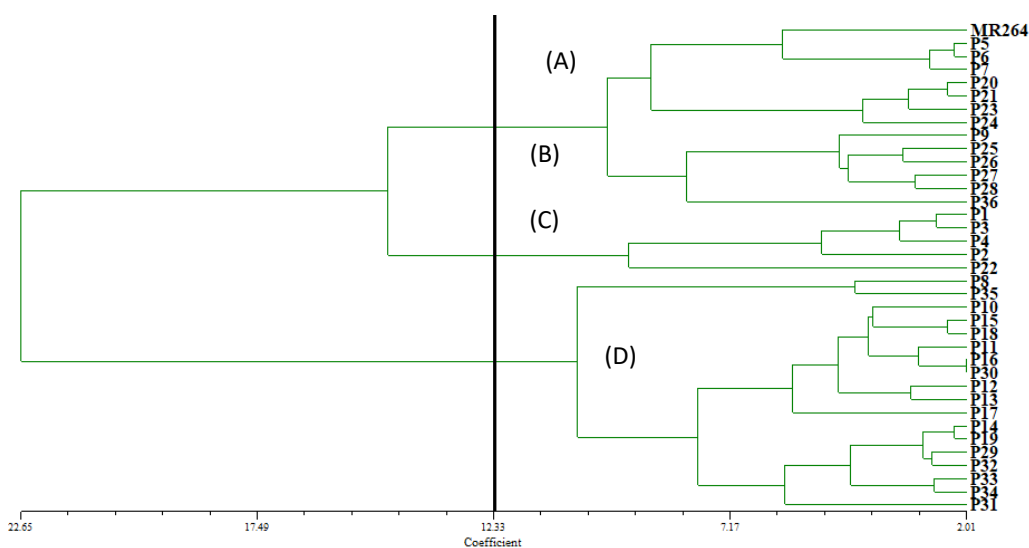


Figure 3 Dendrogram generated by cluster analysis of agro-morphological among 36 BC<sub>2</sub>F<sub>3</sub> rice lines

Table 5 Principal components for rice lines based on ten characters

Variable	PC1	PC2	PC3
Eigenvalue	3.91805724	1.99821384	1.19673420
Variation (%)	39.18	19.98	11.97
Cumulative (%)	39.18	59.16	71.13
Characters	Latent vectors (loading)		
1000 seed wt (g)	0.81010	0.42638	0.00590
Yield /hill (g)	0.79555	-0.34195	0.03248
Filled grain (%)	0.78954	0.23863	0.33615
Seed setting rate (%)	0.58326	0.12315	-0.55082
Tiller number/hill	0.55668	0.29005	-0.14776
Plant height (cm)	-0.87142	0.10121	-0.08219
Days of maturity	-0.47634	0.71528	0.14880
Panicle length (cm)	0.47040	0.49931	0.32276
Grain width	0.37766	-0.84407	0.03253
Grain length	-0.07266	-0.24414	0.78949

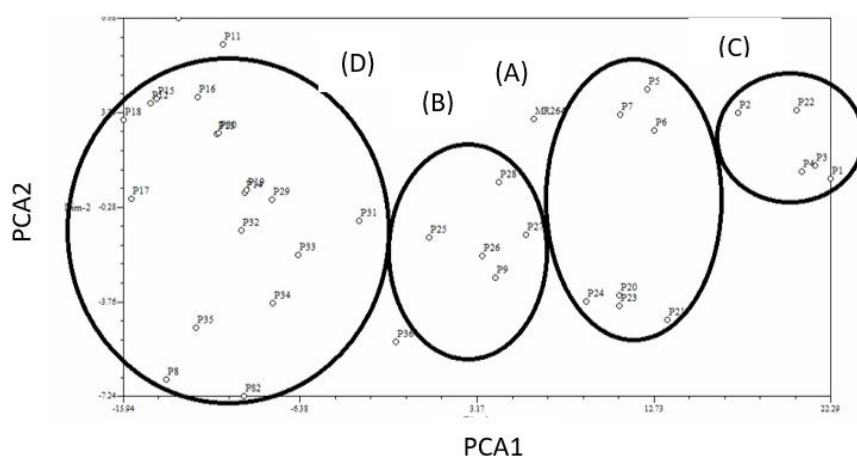


Figure 4 Graphical representation of the PCA analysis among 36 BC<sub>2</sub>F<sub>3</sub> rice lines for identification of the genetic diversity and the traits responsible for the main source of variability.

### 3.7 Principal component analysis (PCA)

Principal component analysis (PCA) is a powerful tool and the most basic statistical technique for multivariate data reduction. The results of PCA showed that all three principal components were significant (eigenvalue > 1) and accounted for 71.23% of the total variation (Table 5 and Figure 4). PC1 accounted for 39.18%, PC 2 for 19.98%, and PC3 for 11.97% of the total variation. PCA revealed the same grouping pattern as in the cluster analysis, indicating that there was significant variation in this study. Partitioning of PC 1, PC 2, and PC 3 showed that 36 lines were scattered in all quarters, indicating a high degree of genotypic variation among lines. Lines 5, 6, 7, 20, 21, 23, 24 and traits such as 1000 seed weight, number of filled grains, and panicle length showed greater variation than any other traits. An almost parallel finding was also made by Manohara et al. (2020) and

Okasa et al. (2022), who found about 68.4% and 83.46% of the total variation, respectively, in all the traits studied and a high correlation among them.

### 3.8 Interrelations among the morphological traits

Knowledge of the correlation between different traits is crucial for developing an implicit breeding strategy for any crop. Yield traits are quantitatively inherited and influenced by genetic effects and genotype-environment interaction. Therefore, direct selection for yield development can be complicated and tedious, and sometimes the key trait is expressed late. For some reason, the indirect selection is much easier and preferable. Accordingly, it is reasonable to determine and use highly correlated traits (Ahmadikhah et al. 2008; Silva et al. 2016).

Traits											
DOM	1										
PH	0.307*	1									
NOT	-0.261*	-0.416*	1								
PL	0.081	-0.228*	0.254*	1							
FG	-0.049	-0.652*	0.241*	0.319*	1						
GL	0.0175	-0.023	-0.048	-0.072	0.055	1					
GW	-0.314*	-0.249*	-0.042	-0.177	0.121	-0.006	1				
Y	-0.445*	-0.542*	0.264*	0.196*	0.481*	0.025	0.290*	1			
SW	-0.132*	-0.566*	0.545*	0.300*	0.682*	-0.039	0.026	0.439*	1		
SS	-0.170	-0.482*	0.385*	-0.042	0.408*	-0.143	0.0557	0.236*	0.428*	1	
Indicator	-1	-0.8	-0.6	-0.4	-0.2	0.2	0.4	0.6	0.8	1	

Figure 5 The phenotypic correlations among the traits.

Note: \*significant at 0.05 probability level. Strength of a particular association between two traits is indicated by the color assigned to a point in the heat map grid. Positive correlation is indicated by red, while negative correlation is indicated by blue

Pearson's correlation coefficient was estimated for 10 morphological traits in 36 BC<sub>2</sub>F<sub>3</sub> lineages (Figure 5). Most of the traits showed a positive correlation. A positive and strong correlation was found between filled grain per panicle and 1000-grain weight ( $r=0.6821$ ), followed by the number of shoots and 1000-grain weight ( $r=0.5456$ ). The results are in agreement with the study of Nor et al. (2013), which demonstrated a positive and strong association between filled grain per panicle and 1000-grain weight in F<sub>1</sub> rice lines from MR264 x PS2. These traits also showed moderate to high heritability and genetic advantage as a percentage of the mean. Therefore, the results suggest that 1000-grain weight and number of grains per panicle are important yield-enhancing traits, and selection based on these traits would be most effective.

Yield hill<sup>-1</sup> was highly significant ( $P \leq 0.05$ ) and positively correlated with the number of filled grains panicle<sup>-1</sup> (0.4819), 1000-grain weight hill<sup>-1</sup> (0.4393), seed set rate (0.2360), and the number of panicles hill<sup>-1</sup> (0.1964). The seeding rate was significantly positively related to the number of tillers, yield hill<sup>-1</sup>, seeding rate, 1000-grain weight, and the number of filled grains. This study was also supported by Kumar & Singh (2018) and Zarbafi et al. (2019). This shows that traits other than filled grains per panicle and 1000-grain weight can be used for direct selection. The significant phenotypic correlation between traits was due to genetic cause, possibly pleiotropic effect rather than linkage between genes affecting different traits (Pandey et al. 2012).

A significant negative correlation was also observed between plant height and yield ( $-r=0.5420$ ), between plant height and 1000-grain weight ( $-r=0.5420$ ), between filled grain and plant height ( $-r=0.6525$ ), and plant height and days to maturity ( $-r=0.4453$ ), which was also reported by Kumar & Singh (2018).

## Conclusion

Marker-assisted backcrossing plays an important role in generating genetic variation and creating lines with superior traits. The significant correlation between the number of grains per panicle, grain weight per panicle, and the number of panicles indicated that simultaneous selection for these traits would be very effective. The multivariate approach used in this study could help growers better select lines that should be recommended for release based on their high yields. The combination potential of the high-yielding line from cluster A could be further investigated. Thus, the observed genotypes can be crossed to produce desirable traits with higher heterotic potential.

## Acknowledgments

The authors would like to thank Universiti Teknologi MARA, Universiti Putra Malaysia, and Agency Nuclear Malaysia for their guidance and support. The author would also like to thank the Ministry of Higher Education (MOHE) for financial support in this research.

## Conflict of Interest

The authors declare that there is no conflict of interest regarding the publication of this manuscript.

## References

Adhikari, B. N., Joshi, B. P., Shrestha, J., & Bhatta, N. R. (2018). Genetic variability, heritability, genetic advance, and correlation among yield and yield components of rice (*Oryza sativa* L.). *Journal of Agriculture and Natural Resources*, 1(1), 149-160.

- Ahmadikhah, A., Nasrollanejad, S., & Alishah, O. (2008). Quantitative studies for investigating variation and its effect on heterosis of rice. *International Journal Plant Production*, 2, 6-11
- Akhtar, N., Nazir, M.F., Rabnawaz, A., Mahmood, T., et al. (2011). Estimation of heritability correlation and path coefficient analysis in fine-grain rice (*Oryza sativa* L). *Journal Animal Plant Sciences*, 21(4), 660-664.
- Anis, G., El-Sabagh, A., Ghareb, A., & El-Rewainy, I. (2016). Evaluation of Promising Lines in Rice (*Oryza sativa* L) to Agronomic and Genetic Performance under Egyptian Conditions. *International Journal Agronomy Agricultural Research*, 8, 52–57.
- Bhandari, N.B., Bhattarai, D., & Aryal, M. (2015). Cost, production and price spread of cereal crops in Nepal: A time series analysis. MoAD, Lalitpur, Nepal, pp. 45-55.
- Chukwu, S.C., Rafii, M.Y., Ramlee, S.I., & Ismail, S.I. (2020). Marker-assisted introgression of multiple resistance genes confers broad spectrum resistance against bacterial leaf blight and blast diseases in Putra-1 rice variety. *Agronomy*, 10, 42.
- FAO. (2019). Sustainable healthy diets. Guiding principles Rome. Retrieved from <http://www.fao.org/3/ca6640en/ca6640en.pdf>. Accessed 29 Dec 2019
- Ghos, S.C., & Sharma, D. (2012). Genetic parameters of agromorpho-physiological traits in rice (*Oryza sativa* L). *Electron Journal Plant Breeding*, 3(1), 711-714.
- Girma, B.T., Kitil, M.A., Banje, D.G., Biru, H.M., & Serbessa, T.B. (2018) Genetic Variability Study of Yield and Yield Related Traits in Rice (*Oryza sativa* L) Genotypes. *Advances Crop Sciences Technology*, 6, 381.
- Govintharaj, P., Shalini, T., Manonmani, S., & Robin, S. (2016). Estimates of genetic variability heritability and genetic advance for blast resistance gene introgressed segregating population in rice. *International Journal Current Microbiology Applied Sciences*, 5, 672–677.
- Gyawali, S., Poudel, A., & Poudel, S. (2018). Genetic variability and association analysis in different rice genotypes in mid hill of western Nepal. *Acta Science Agricultural*, 2(9), 69-76.
- Habib, S.H., Bashar, M.K., Khalequzzaman, M., Ahmed, M.S., & Rashid, E.S.M.H. (2005). Genetic analysis and morpho-physiological selection criteria for traditional Biroin Bangladesh rice germplasms. *Journal Biology Science*, 5, 315–318.
- Hasan, M.M., Yusop, M.R., Ismail, M.R., Mahmood, M., Rahim, H.A., & Latif, M.A. (2015a). Performance of yield and yield contributing characteristics of BC<sub>2</sub>F<sub>3</sub> population with addition of blast resistant gene. *Ciències Agrotecnology*, 39, 463–476.
- Hasan, N., Rafii, M.Y., Abdul Rahim, H., Nusaibah, S.A., Mazlan, N., & Abdullah, S. (2015b). Genetic analysis and identification of SSR markers associated with rice blast disease in a BC<sub>2</sub> F<sub>1</sub> backcross population. *Genetics Molecular Research*, 16 (1), 1-11.
- Herawati, R., Masdar, Alnopri & Widodo (2021). Genetic analysis of panicle architecture traits in F5 from singlecross of local rice varieties for developing high yielding new type of upland rice. *International Journal of Agricultural Technology*, 7(1), 87-102.
- International Rice Research Institute. (2015). *Step to successful rice production*. International Rice Research Institute Philippines ISBN 978-971-22-0313-8.
- Kumar, V., & Singh, D. (2018). Association Studies for Yield and Its Component Traits in Basmati Genotypes of Himachal Pradesh India. *International Journal Current Microbiology Applied Sciences*, 7, 1243–1249.
- Lakshmi, L., Brahmeswara M.V.R., Surender, C.R. & Reddy, S. N. (2017). Variability, Correlation and Path Analysis in Advanced Generation of Aromatic Rice. *International Journal of Current Microbiology and Applied Sciences*, 6(7), 1798-1806
- Magar, P.B., Acharya, B., & Pandey, B. (2015). Use Of Chemical Fungicides for The Management of Rice Blast (*Pyricularia grisea*) Disease at Jyotinagar, Chitwan, Nepal. *International Journal Applied Science Biotechnology*, 3(3), 474-478
- Mahesh, G., Ramesh, T., Narendar, Reddy, S., et al. (2022). Genetic variability, heritability, genetic advance and path coefficients for grain protein content, quality traits and grain yield in rice (*Oryza sativa* L.) germplasm lines. *The Pharma Innovation Journal*, 11(3), 1836-1839
- Mallimar, M., Surendra, P., Hanamaratti, N.G., Jogi, M., Sathisha, T.N., & Hundekar, R. (2015). Genetic variability for yield and yield attributing traits in F3 generation of rice (*Oryza sativa* L). *Journal Environmental Sciences*, 9(1), 24-28.
- Manohara, K. K., Morajkar, S. & Shanbagh, Y. (2020). Genetic analysis of grain yield and its associated traits in diverse salttolerant rice genotypes under coastal salinity condition. *Journal of Cereal Research*, 12(3), 290-296.
- Mazid, M.S., Rafii, M.Y., Hanafi, M.M., & Harun, A.R. (2013). Agro-morphological characterization and assessment of variability heritability genetic advance and divergence in bacterial blight resistant rice genotypes. *South Africa Journal Botany*, 86, 15-23.

- Nikhil, B.S.K., Rangare, N.R., & Saideaiah, P. (2014). Correlation and path analysis in rice (*Oryza sativa*L.). *National Academy of Agricultural Sciences*, 32, 1- 2.
- Nishanth, G.K., Dushyanthakumar, B.M., Gangaprasad, S., Gowda, T.H., Nataraju, S.P., & Shashidhar, H.E. (2017). Screening and Genetic Variability Studies in Submergence Tolerance Rice Germplasm Lines Under Flood Prone Lowlands of Hill Zone of Karnataka India. *International Journal Current Microbiology Applied Sciences*, 6, 1254–1260.
- Nor, A.H., Abdul, R.H., Mohd, R.Y., Norain, M.N., & NurIzzah, J. (2013). Correlation analysis on agronomic Characters in F1 population derived from a cross of Pongsu Seribu 2 and MR 264. *INIS IAEA Org.*
- Nurhidayah, S., Firmansyah, E., Haryanto, D.T.A. & Dewi, P.S. (2021). Genetic analysis on grain physical characteristics and grain color from the crosses of black × white rice genotypes. *Biodiversiti*, 22(5), 2763-2772.
- Okasa, A.M., Sjahril, R., Riadi, M., & Mahendradatta, M. (2022). Multivariate Analysis of Agronomic Traits in M4 Generation of Aromatic Rice Lines. *Pakistan Journal of Biological Sciences*, 25, 182-190.
- Oladosu, Y., Rafii, M.Y., Abdullah, N., Abdul Malek, A., et al. (2014). Genetic variability and selection criteria in rice mutant lines as revealed by quantitative traits. *Science World Journal*, 2014, 190531. doi: 10.1155/2014/190531.
- Osman, K.A., Mustafa, A.M., Ali, F., Yonglain, Z., & Fazhan, Q. (2012) Genetic variability for yield and related attributes of upland rice genotypes in semi-arid zone (Sudan). *African Journal Agricultural Research*, 7, 4613–4619.
- Pandey, P., & Anurag, P.J. (2010). Estimation of genetic parameters in indigenous rice. *AAB Bioflux*, 2(1),79-84.
- Pandey, V.R., Singh, P.K., Verma, O.P., & Pandey, P. (2012). Inter-relationship and Path Coefficient Estimation in Rice under Salt Stress Environment. *International Journal of Agricultural Research*, 7, 169-184.
- Raghavendra, P., & Hittalmani, S. (2015). Genetic Parameters of Two BC<sub>2</sub>F<sub>1</sub> Populations for Development of Superior Male Sterile Lines Pertaining to Morpho-Floral Traits for Aerobic Rice (*Oryza sativa* L.). *SAARC Journal of Agriculture*, 13(2), 198-213.
- Rashid, M.M., Nuruzzaman, M., Hassan, L., & Begum, S.N. (2017). Genetic variability analysis for various yield attributing traits in rice genotypes. *Journal Bangladesh Agricultural University*, 15(1), 15-19.
- Rijal, S., & Devkota, Y. (2020). A review on various management method on rice blast disease. *Malaysian Journal of Sustainable Agriculture*, 4(1), 29-33.
- Roy, S.C., & Shil. P. (2020). Assessment of Genetic Heritability in Rice Breeding Lines Based on Morphological Traits and Caryopsis Ultrastructure. *Science Reproduction*, 10, 7830.
- Sabri, R.S., Rafii, M.Y., Ismail, M.R., Yusuff, O., Chukwu, S.C., & Hasan, N. (2020). Assessment of Agro-Morphologic Performance Genetic Parameters and Clustering Pattern of Newly Developed Blast Resistant Rice Lines Tested in Four Environments. *Agronomy*, 10:1098.
- Samak, N.R.A., Hittalmani, S., Shashidhar, N. & Biradar, H. (2011). Exploratory studies on genetic variability and genetic control for protein and micronutrient content in F4 and F5 generation of rice (*Oryza sativa* L.). *Asian Journal of Plant Science*, 10, 376-379.
- Savitha, P., Kumari, R. U. (2015). Studies on skewness, kurtosis and parent progeny regression for yield and its related traits in segregating generations of rice. *Oryza*, 52(2), 80-86.
- Shahriar, S.A., Imtiaz, A.A., Hossain, M.B., Husna, A., & Eaty, N.K. (2020). Review: Rice Blast Disease. *Annual Research Revision*, 35(1), 50-64.
- Sharif, P., Dehghani, H., Momeni, A., & Moghadam, M. (2013). Study the genetic relations of some of rice agronomic traits with grain yield by using multivariate statistical methods. *Iranian Journal Field Crop Science*, 44(2), 273-82.
- Silva, T.N., Moro, G.V., Moro, F.B., Santos, D.M.M., & Buzinaro, R. (2016). Correlation and path analysis of agronomic and morphological traits in maize. *Revision Ciencias Agronomy*, 47(2), 351-357.
- Sohrabi, M., Rafii, M.Y., Hanafi, M.M., Siti Nor Akmar, A., & Latif, M.A. (2012). Genetic diversity of upland rice germplasm in Malaysia based on quantitative traits. *Science World Journal*, 416291,1-9.
- Sumanth, V., Suresh, B.G., Ram, B.J., & Srujana, G. (2017). Estimation of genetic variability heritability and genetic advance for grain yield components in rice (*Oryza sativa* L). *Journal Pharmacology Phytochemical*, 6, 1437-1439.
- Umarani, E., Radhika, K., Padma, V., & Subbarao, L.V. (2017). Variability Heritability and Genetic Advance for Agro-Morphological and grain Quality Parameters in Landraces of Rice (*Oryza sativa* L). *Journal Environmental Protection Ecology*, 35(3), 1682-1687.

- Upadhyay, K., & Bhatta, B. (2020). Rice Blast (*Magnaporthe oryzae*) Management: A Review. *Journal Agricultural Sciences*, 15(4), 42 – 48.
- Vanitha, J., Amutha, K., Mahendran, R., Srinivasan, J., Robin, S., & Usha, K.R. (2016). Genetic variability studies for Zinc efficiency in aerobic rice. *SABRAO Journal of Breeding and Genetics*, 48(4), 425-433.
- Xiao, W., Yang, Q., Huang, M., Guo, T., et al. (2019). Improvement of rice blast resistance by developing monogenic lines two-gene pyramids and three-gene pyramid through MAS. *Rice*, 12(1),78.
- Zarbaifi, S.S., Rabiei, B., Ebadi, A.A., & Ham, J.H. (2019). Statistical analysis of phenotypic traits of rice (*Oryza sativa* L) related to grain yield under neck blast disease. *Journal Plant Disease Protection*, 126, 293–306.





## Journal of Experimental Biology and Agricultural Sciences

<http://www.jebas.org>

ISSN No. 2320 – 8694

### Selection for Upland Rice Varieties Under Different Levels of Light Intensity

Raumjit Nokkoul<sup>1\*</sup>, Karnchanaporn Unsup<sup>1</sup>, Apichart Krutsuwan<sup>2</sup>, Thirayut Wichitparp<sup>1</sup>

<sup>1</sup>Department of Agricultural Technology, King Mongkut's Institute of Technology Ladkrabang, Prince of Chumphon Campus Chumphon Province, Tambon Chum Kho, Amphur Pathiu, Chumphon Province, 86160, Thailand.

<sup>2</sup>Center of Technology, Agriculture, Food, and Energy, King Mongkut's Institute of Technology Ladkrabang, Prince of Chumphon Campus Chumphon Province, Tambon Chum Kho, Amphur Pathiu, Chumphon Province, 86160.

Received – January 05, 2022; Revision – March 11, 2022; Accepted – April 14, 2022

Available Online – April 30, 2022

DOI: [http://dx.doi.org/10.18006/2022.10\(2\).318.322](http://dx.doi.org/10.18006/2022.10(2).318.322)

#### KEYWORDS

Light intensity

Selection

Shading tolerance

Upland rice

#### ABSTRACT

Upland rice varieties were selected under varying levels of light intensity. This study identified shade-tolerant upland rice varieties with a high yield. From November 2016 to March 2017, the experiment was conducted at King Mongkut's Institute of Technology in Ladkrabang, Prince of Chumphon, Thailand. For this, ten varieties of upland rice i.e. Dawk Pa-yawm, Nangdam, Dokkam, Nangchuan, Lebnoakrai, Samduen, Maepung, Damgatondom, Lebmuengang, Pukaotong were grown at different levels of 0%, 50%, 60%, and 70% shading levels. The experiment was conducted in a randomized complete block design with four replications. The results of qualitative characteristics indicated that shadowing conditions didn't have any significant effect on plant height, 50% flowering age, harvesting age, and panicle length. On the other hand, shaded conditions have a substantial effect on the number of plants per tiller, the number of panicles per tiller, the number of perfect grains per panicle, and the amount of empty grain per panicle since there was a quantitative character. Among the tested varieties, Lebmuengang, Pukaotong, Damgatondom, and Nangchuan varieties are suited for growing under 50% shade conditions while Samduen was only suited for cultivation in 70% shaded conditions, whereas Pukaotong was good for growing in 50% and 60% shade situations. The results of this experiment did not encourage farmers to use the other varieties as cultivars under shaded conditions due to low yields. However, the outcomes of this study can be used as a reference for breeding programs in low-light conditions.

\* Corresponding author

E-mail: [knraumjit@gmail.com](mailto:knraumjit@gmail.com) (Raumjit Nokkoul)

Peer review under responsibility of Journal of Experimental Biology and Agricultural Sciences.

Production and Hosting by Horizon Publisher India [HPI]  
(<http://www.horizonpublisherindia.in/>).  
All rights reserved.

All the articles published by [Journal of Experimental Biology and Agricultural Sciences](#) are licensed under a [Creative Commons Attribution-NonCommercial 4.0 International License](#) Based on a work at [www.jebas.org](http://www.jebas.org).



## 1 Introduction

Farmers in the southern region of Thailand plant upland rice (*Oryza sativa* L.) as an alternative crop for home consumption (Nokkoul and Wichitparp 2013). It is grown in a variety of environments as a monoculture and as an intercropping with other 1-3 years old crops such as palm oil, coconut, rubber, and fruit plantations (Nokkoul 2017). If these crops are more than three years old, they could not allow any crop to grow as an intercrop. Further, environmental factors, particularly under shade conditions also, determine the essential characteristics of rice cultivation (Liu et al. 2014). It is one of the challenges that must be solved in the development of upland rice growing as an intercrop plantation (Jonatan et al. 2015). Low light can disrupt various physiological metabolisms, including photosynthetic characteristics of rice plants, activities of antioxidant enzymes in rice leaves, and key enzymes involved in starch production in grains (Liu et al. 2014). Further, Jonatan et al. (2015) reported that shaded condition reduces the number of tillers and panicles in upland rice varieties, reduced the panicle growth (Wang et al. 2018), decreases the number of productive grains, grain output per hill, and overall sugar content of upland rice plants. The development of highland rice agriculture in the shade of tree stands necessitates the development of early-duration rice varieties with a moderate range of 80 to 120 days and plant heights of 110 - 125 cm (Jonatan et al. 2015).

The purpose of this experiment was to identify upland rice varieties that could provide yield under shade and could be planted as an intercrop for further testing in association with 5 to 10 years old rubber plantations, or with 8 to 25-year-old oil palm plantations, or with 10 to 20-year-old fruit crops. This maximizes the use of space between the primary rows of plants. This will have an effect on household and community food security in Thailand's southern region.

## 2 Materials and Methods

Ten varieties of upland rice including Dawk Pa-yawm, Nangdam, Dokkam, Nangchuan, Lebnokrai, Samduen, Maepeung, Damgatondom, Lebmuengang, and Pukaotong have been selected for this study. All the varieties had passed selection by the mass selection method by King Mongkut's Institute of Technology Ladkrabang Prince of Chumphon Campus, Chumphon province, Thailand (10°43'26.1"N 99°22'28.5"E of 26.00 m. above the sea level). The seeds were planted to select varieties that could produce satisfactory high yields under black-net houses at the King Mongkut's Institute of Technology Ladkrabang Prince of Chumphon Campus Chumphon Province, Thailand from November 2016 to March 2017.

The experiments were performed under 4 shade conditions i.e. no shade treatment (natural light), 50% of the black-net house, 60% of

the black-net house, and 70% of the black-net house. All treatments were applied at the rate of 200 kg/ acre of cow manure, and zeolite was applied at the rate of 20 kg/acre (mixed into the soil before growing). Upland rice seeds were sown per hole at a spacing of 25 cm within rows and 30 cm between rows, with three rows of cultivation of each variety (1.5 m long per row). The plants were thinned to two plants per hole 14 days after germination. The fertilizer (15N-15P-15K) was applied at a rate of 14 kg/acre at the ages of 20 and 40 days after seedling emergence. Weeding was eliminated either by hoe least twice, at the ages of 20 and 40 days after seed germination and watered once per week.

The study used a randomized complete block design (RCB) with four replications and was compared by Duncan's Multiple Range Test (DMRT). Plant height, days to 50% flowering, days to grain harvesting, number of plants per tiller, number of panicles per tiller, panicle length, number of perfect grains per panicle, number of empty grains per panicle, and grain yield (reduced moisture content by hot air oven at 43°C for 48 hours for moisture content of 14%, following the IRRI (2002) standard procedure.

Data were analyzed to find suitable varieties focus on yield per area of each variety (yield is not less than 50% compared to varieties under 0% shading). The environmental data included light intensity and temperatures were taken with a HOBO Pendant Temperature/Light Data Logger (Part # UA-002-XX) at the plant's height, as well as rainfall amount measured with an ordinary rain gage.

## 3 Results

Results presented in figure 1 depict the average rainfall and temperature from November 2016 to March 2017, as well as the amount of light intensity received by rice plants from December 2016 to March 2017. Tables 1–5 indicate the plant height, days to 50% flowering age, days to grain harvesting, number of plants per tiller, number of panicles per tiller, panicle length, number of perfect grains per panicle, number of empty grains per panicle, and grain yield per growing area of ten upland rice varieties. The yield of ten varieties of upland rice grown under varying levels of light intensity in the summer was the focus of the data analysis. The results revealed that the grain yield of ten upland rice varieties with 0% shadowing (natural light) were significantly different among the treatments (Table 5). The Nangchuan variety had the maximum yield of 125.84 kg/acre under these conditions. It is advised that it can be grown in natural light settings (0 % shading). Dawk Pa-yawm, Nangdam, Samduen, Lebmuengang, and Pukaotong varieties had a yield of 88.60, 92.44, 93.47, 88.40, and 85.50 kg/acre, respectively, and these were not significantly different from the Nangchuan variety. Under 50% of shading conditions, Lebmuengang, Pukaotong, Damgatondom, and Nangchuan had yields of 98.80, 98.73, 96.28, and 95.80 kg/acre, respectively and all these four varieties are suitable to grow in dry season under 50% shading conditions. The

cultivation of upland rice at 60% shading, Nangchuan, Damgatondom, and Pukaotong upland rice varieties had a yield of 64.32, 50.43, and 48.78 kg/acre, respectively. All three varieties are suitable to grow in the dry season under 60% shading conditions.

The cultivation of upland rice at 70% shading in Nangchuan, Samduen, and Damgatondom had a yield of 45.08, 42.16, and 39.23 kg/acre, respectively. Among the tested varieties, Samduen was suitable to grow in the dry season under 70% shading conditions.

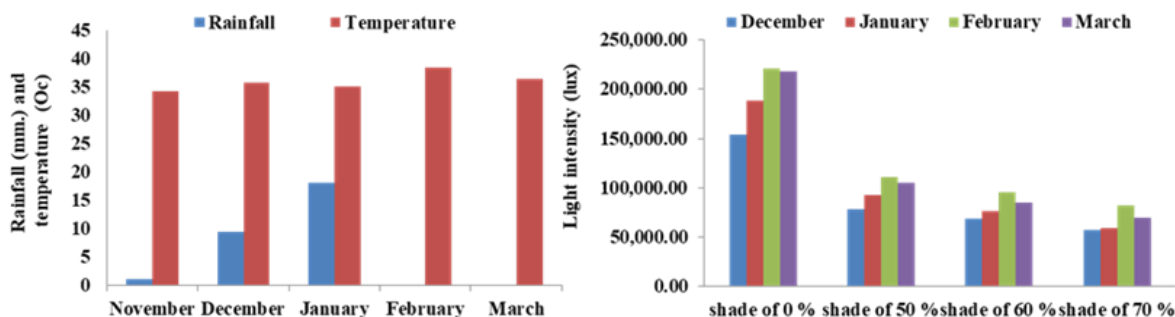


Figure 1 The average rainfall, temperature, and light intensity from November 2016 to March 2017.

Table 1 Plant height and flowering age at 50% of selected varieties

Varieties	Plant height (cm)				Flowering age at 50% days			
	0% shade	50 % shade	60 % shade	70 % shade	0 % shade	50 % shade	60 % shade	70 % shade
Dawk Pa-yawm	101.83	102.43 <sup>abc</sup>	101.54 <sup>cd</sup>	102.08 <sup>b</sup>	95 <sup>bc</sup>	96 <sup>bc</sup>	96 <sup>bc</sup>	96 <sup>cb</sup>
Nangdum	102.39	103.56 <sup>ab</sup>	103.43 <sup>bc</sup>	102.57 <sup>b</sup>	94 <sup>cd</sup>	95 <sup>c</sup>	95 <sup>cd</sup>	95 <sup>cd</sup>
Dokkam	102.43	104.01 <sup>ab</sup>	104.64 <sup>ab</sup>	103.15 <sup>b</sup>	93 <sup>d</sup>	94 <sup>d</sup>	94 <sup>ed</sup>	94 <sup>e</sup>
Nangchuan	100.76	103.37 <sup>ab</sup>	103.93 <sup>abc</sup>	103.79 <sup>a</sup>	96 <sup>b</sup>	97 <sup>b</sup>	96 <sup>bc</sup>	97 <sup>b</sup>
Lebnok	103.80	105.89 <sup>a</sup>	106.34 <sup>a</sup>	106.48 <sup>a</sup>	95 <sup>bc</sup>	96 <sup>bc</sup>	96 <sup>bc</sup>	96 <sup>bc</sup>
Samduen	104.79	99.31 <sup>c</sup>	99.86 <sup>d</sup>	100.75 <sup>bc</sup>	76 <sup>e</sup>	77 <sup>e</sup>	76 <sup>f</sup>	76 <sup>f</sup>
Lebmuenang	102.80	104.36 <sup>ab</sup>	102.11 <sup>bcd</sup>	101.82 <sup>b</sup>	96 <sup>b</sup>	97 <sup>b</sup>	97 <sup>b</sup>	97 <sup>b</sup>
Pukaotong	105.79	103.58 <sup>ab</sup>	102.69 <sup>bc</sup>	101.89 <sup>b</sup>	93 <sup>bc</sup>	94 <sup>d</sup>	94 <sup>e</sup>	94 <sup>e</sup>
Maepung	105.93	101.33 <sup>bc</sup>	97.13 <sup>c</sup>	97.95 <sup>c</sup>	77 <sup>e</sup>	78 <sup>e</sup>	77 <sup>f</sup>	77 <sup>f</sup>
Domgatondom	101.25	104.71 <sup>ab</sup>	103.21 <sup>bc</sup>	104.11 <sup>ab</sup>	99 <sup>a</sup>	100 <sup>a</sup>	100 <sup>a</sup>	100 <sup>a</sup>
F-test	ns	*	*	*	*	*	*	*
C.V.%	3.62	2.08	1.57	1.97	0.89	0.85	0.95	0.84

ns = non – significant, \* means not followed by the same letter are significantly different at the 5% level of probability as determined by DMRT

Table 2 Harvesting age of the grains and number plant per tiller in selected varieties

Varieties	Harvesting age of the grains (days)				No. plant per tiller			
	0 % shade	50 % shade	60 % shade	70 % shade	0 % shade	50 % shade	60 % shade	70 % shade
Dawk Pa-yawm	129 <sup>c</sup>	130 <sup>c</sup>	130 <sup>b</sup>	131 <sup>b</sup>	5 <sup>ab</sup>	4	2	3 <sup>f</sup>
Nangdum	130 <sup>bc</sup>	130 <sup>c</sup>	130 <sup>b</sup>	130 <sup>b</sup>	4 <sup>b</sup>	5	3	2
Dokkam	127 <sup>d</sup>	127 <sup>d</sup>	128 <sup>c</sup>	128 <sup>c</sup>	5 <sup>ab</sup>	4	3	3
Nangchuan	127 <sup>d</sup>	127 <sup>d</sup>	127 <sup>cd</sup>	127 <sup>cd</sup>	6 <sup>a</sup>	4	3	3
Lebnok	127 <sup>d</sup>	127 <sup>d</sup>	127 <sup>cd</sup>	126 <sup>d</sup>	5 <sup>ab</sup>	4	2	2
Samduen	110 <sup>f</sup>	113 <sup>f</sup>	110 <sup>f</sup>	111 <sup>f</sup>	6 <sup>a</sup>	5	3	3
Lebmuenang	131 <sup>b</sup>	131 <sup>b</sup>	130 <sup>b</sup>	131 <sup>b</sup>	5 <sup>ab</sup>	4	3	3
Pukaotong	126 <sup>d</sup>	126 <sup>d</sup>	126 <sup>d</sup>	126 <sup>d</sup>	5 <sup>ab</sup>	4	3	3
Maepung	115 <sup>e</sup>	116 <sup>e</sup>	115 <sup>e</sup>	115 <sup>e</sup>	5 <sup>ab</sup>	3	2	3
Domgatondom	134 <sup>a</sup>	135 <sup>a</sup>	134 <sup>a</sup>	135 <sup>a</sup>	5 <sup>ab</sup>	4	3	3
F-test	*	*	*	*	*	ns	ns	ns
C.V.%	0.81	0.78	0.80	0.77	21.11	20.10	19.90	23.36

ns = non – significant, \* Means not followed by the same letter are significantly different ( $p \leq 0.05$ ) by Duncan's multiple range test

Table 3 Number panicle per tiller and panicle length of selected varieties

Varieties	No. panicle per tiller				Panicle length (cm)			
	0 % shade	50 % shade	60 % shade	70 % shade	0 % shade	50 % shade	60 % shade	70 % shade
Dawk Pa-yawm	3.50 <sup>abc</sup>	3.00 <sup>ab</sup>	1.75 <sup>bc</sup>	1.25	26.17 <sup>c</sup>	28.99 <sup>cd</sup>	25.69 <sup>bc</sup>	25.57 <sup>cd</sup>
Nangdum	3.75 <sup>abc</sup>	2.75 <sup>ab</sup>	2.00 <sup>abc</sup>	1.50	27.92 <sup>b</sup>	30.91 <sup>abc</sup>	27.06 <sup>ab</sup>	26.10 <sup>c</sup>
Dokkam	3.25 <sup>abc</sup>	2.25 <sup>b</sup>	2.00 <sup>abc</sup>	1.25	29.33 <sup>a</sup>	32.95 <sup>a</sup>	28.84 <sup>a</sup>	30.24 <sup>a</sup>
Nangchuan	4.50 <sup>a</sup>	3.25 <sup>ab</sup>	2.50 <sup>ab</sup>	1.75	24.44 <sup>d</sup>	26.16 <sup>e</sup>	24.07 <sup>c</sup>	23.65 <sup>de</sup>
Lebnok	3.00 <sup>bc</sup>	2.75 <sup>ab</sup>	2.00 <sup>abc</sup>	1.50	27.05 <sup>bc</sup>	31.38 <sup>ab</sup>	27.71 <sup>ab</sup>	28.38 <sup>ab</sup>
Samduen	4.25 <sup>ab</sup>	3.75 <sup>a</sup>	3.00 <sup>a</sup>	2.25	27.20 <sup>bc</sup>	26.53 <sup>e</sup>	23.64 <sup>c</sup>	26.48 <sup>bc</sup>
Lebmuenang	3.50 <sup>abc</sup>	3.00 <sup>ab</sup>	2.25 <sup>abc</sup>	1.50	27.70 <sup>b</sup>	32.50 <sup>ab</sup>	26.34 <sup>abc</sup>	27.32 <sup>bc</sup>
Pukaotong	3.50 <sup>abc</sup>	3.50 <sup>ab</sup>	2.25 <sup>ab</sup>	2.00	24.70 <sup>d</sup>	27.24 <sup>de</sup>	23.82 <sup>c</sup>	22.83 <sup>e</sup>
Maepung	2.75 <sup>b</sup>	2.50 <sup>ab</sup>	1.25 <sup>c</sup>	1.50	23.48 <sup>d</sup>	22.72 <sup>f</sup>	19.06 <sup>d</sup>	20.74 <sup>f</sup>
Domgatondom	2.75 <sup>b</sup>	2.75 <sup>ab</sup>	2.50 <sup>ab</sup>	1.75	27.65 <sup>bc</sup>	30.36 <sup>bc</sup>	27.34 <sup>ab</sup>	27.47 <sup>bc</sup>
F-test	*	*	*	ns	*	*	*	*
C.V.%	25.42	27.67	31.37	36.83	0.55	4.72	7.14	5.26

ns = non – significant, \* Means not followed by the same letter are significantly different ( $p \leq 0.05$ ) by Duncan's multiple range test

Table 4 Number perfect grains per panicle and number of empty grains per panicle in selected varieties

Varieties	No. perfect grains per panicle (grains)				No. of empty grain per panicle (grains)			
	0 % shade	50 % shade	60 % shade	70 % shade	0 % shade	50 % shade	60 % shade	70 % shade
Dawk Pa-yawm	161 <sup>a</sup>	202 <sup>a</sup>	125 <sup>a</sup>	162 <sup>ab</sup>	58 <sup>a</sup>	47 <sup>ab</sup>	35 <sup>ab</sup>	63 <sup>ab</sup>
Nangdum	148 <sup>ab</sup>	206 <sup>a</sup>	126 <sup>a</sup>	129 <sup>abcd</sup>	54 <sup>ab</sup>	40 <sup>ab</sup>	54 <sup>ab</sup>	62 <sup>ab</sup>
Dokkam	153 <sup>ab</sup>	203 <sup>a</sup>	146 <sup>a</sup>	177 <sup>a</sup>	51 <sup>ab</sup>	43 <sup>ab</sup>	46 <sup>ab</sup>	62 <sup>ab</sup>
Nangchuan	129 <sup>abc</sup>	206 <sup>a</sup>	155 <sup>a</sup>	169 <sup>ab</sup>	55 <sup>ab</sup>	50 <sup>ab</sup>	46 <sup>ab</sup>	76 <sup>a</sup>
Lebnok	91 <sup>c</sup>	149 <sup>bc</sup>	127 <sup>a</sup>	149 <sup>abc</sup>	59 <sup>a</sup>	47 <sup>ab</sup>	47 <sup>ab</sup>	65 <sup>ab</sup>
Samduen	106 <sup>bc</sup>	110 <sup>c</sup>	66 <sup>bc</sup>	98 <sup>d</sup>	51 <sup>ab</sup>	50 <sup>ab</sup>	35 <sup>ab</sup>	62 <sup>ab</sup>
Lebmuenang	126 <sup>abc</sup>	189 <sup>ab</sup>	114 <sup>ab</sup>	122 <sup>bcd</sup>	52 <sup>ab</sup>	60 <sup>a</sup>	45 <sup>ab</sup>	60 <sup>ab</sup>
Pukaotong	149 <sup>ab</sup>	190 <sup>ab</sup>	101 <sup>ab</sup>	102 <sup>cd</sup>	70 <sup>a</sup>	47 <sup>ab</sup>	64 <sup>a</sup>	42 <sup>ab</sup>
Maepung	30 <sup>d</sup>	47 <sup>d</sup>	32 <sup>c</sup>	23 <sup>e</sup>	37 <sup>b</sup>	30 <sup>b</sup>	23 <sup>b</sup>	36 <sup>b</sup>
Domgatondom	91 <sup>c</sup>	219 <sup>a</sup>	113 <sup>ab</sup>	142 <sup>abcd</sup>	54 <sup>ab</sup>	32 <sup>b</sup>	64 <sup>a</sup>	53 <sup>ab</sup>
F-test	*	*	*	*	*	*	*	*
C.V.%	25.04	17.21	29.81	23.01	20.68	37.91	42.20	37.32

\* Means not followed by the same letter are significantly different ( $p \leq 0.05$ ) by Duncan's multiple range test

Table 5 Final yield of selected varieties

Varieties	Yield per acre			
	0 % shade	50 % shade	60 % shade	70 % shade
Dawk Pa-yawm	88.60 <sup>ab</sup>	87.85 <sup>ab</sup>	34.45 <sup>b</sup>	31.20 <sup>ab</sup>
Nangdum	92.44 <sup>ab</sup>	84.78 <sup>ab</sup>	41.45 <sup>ab</sup>	30.80 <sup>a</sup>
Dokkam	82.57 <sup>b</sup>	68.67 <sup>ab</sup>	44.53 <sup>ab</sup>	36.96 <sup>a</sup>
Nangchuan	125.84 <sup>a</sup>	95.80 <sup>ab</sup>	64.32 <sup>a</sup>	45.08 <sup>a</sup>
Lebnok	52.94 <sup>bc</sup>	63.89 <sup>b</sup>	41.56 <sup>ab</sup>	35.52 <sup>a</sup>
Samduen	93.47 <sup>ab</sup>	69.08 <sup>ab</sup>	37.13 <sup>ab</sup>	42.16 <sup>a</sup>
Lebmuenang	88.40 <sup>ab</sup>	98.80 <sup>a</sup>	47.39 <sup>ab</sup>	28.62 <sup>ab</sup>
Pukaotong	85.50 <sup>ab</sup>	98.73 <sup>a</sup>	48.78 <sup>ab</sup>	31.07 <sup>ab</sup>
Maepung	25.52 <sup>c</sup>	22.88 <sup>c</sup>	8.40 <sup>c</sup>	9.36 <sup>b</sup>
Domgatondom	54.89 <sup>bc</sup>	96.28 <sup>ab</sup>	50.43 <sup>ab</sup>	39.23 <sup>a</sup>
F-test	*	*	*	*
C.V.%	32.11	26.22	10.62	42.03

\* Means not followed by the same letter are significantly different ( $p \leq 0.05$ ) by Duncan's multiple range test

#### 4 Discussion

Results of the current experiment demonstrated that light intensity levels had little effect on plant height, 50% flowering age, harvesting age, and panicle length at 0%, 50%, 60%, and 70% shading level. Upland rice varieties grown under natural light (0% shading) had higher numbers of tillers and panicles than plants grown under 50%, 60%, and 70% shading. Emmanuel and Mary (2014) and Jonatan et al. (2015) reported that shading reduced the number of plants per tiller and the number of panicles per tiller. Tillering is a genetic characteristic that is also influenced by environmental factors such as low light. Upland rice varieties grown under 50% shade conditions had higher numbers of perfect grains per panicle than rice grown at 0% shading, probably because flowering, seed formation, and ripening stages had no rain, with high average monthly temperatures at 35.69 to 38.42° C (Figure 1) that reduced the number of perfect grains per panicle. Shading conditions also reduced soil moisture loss. In addition, it could reduce the soil and plant temperature during the day (Stigter 1984), with increased numbers of perfect grains per panicle at 50% shading. The ten upland rice varieties responded to shade conditions differently. Among the tested varieties, Lebmuenang, Pukaotong, Damgatondom, and Nangchuan varieties showed good growth and yield under 50% shade, while Pukaotong can be grown under 50 to 60% shade and Samduen can only be grown under 70% shade. Plants that were resistant to shade showed high adaptability to the environment (Muhidin et al. 2013). The upland rice varieties gave diverse yields when grown under shade and suitable cultural practices must be followed for the best results.

#### Conclusion

Ten varieties of upland rice were grown under diverse shade levels. Lebmuenang, Pukaotong, Damgatondom, and Nangchuan varieties were suited for growth under 50% shade conditions, while Pukaotong, Labnok and Damgatondom varieties were best suited for growth under 60% shade. Samduen was the only variety suitable for cultivation under 70% shade, while Pukaotong grew well under 50 to 60% shaded conditions. The other varieties gave yield at less than 50% compared to upland rice varieties under natural light.

#### Acknowledgment

This research was supported by a grant from Thailand's Office of the Higher Education Commission. The authors would like to thank the Department of Agricultural Technology, King Mongkut's Institute of Technology, Ladkrabang, Prince of Chumphon

Campus, Pathio, Chumphon, Thailand, for supplying experimental equipment and the field in which the indigenous highland rice was planted. The authors would like to express their gratitude to Assoc. Prof. Dr. Withya Buajareern for her critical revision of the work.

#### Conflict of interest

We all the authors hereby declare that there is no conflict of interest among us.

#### References

- Emmanuel, G.A., & Mary, D.M. (2014). Effect of Light Intensity on Growth and Yield of a Nigerian Local Rice Variety-Ofada. *International Journal of Plant Research*, 4, 89-94
- IRRI. (2002). Standard Evaluation System for Rice. International Rice Research Institute, Manila.
- Jonatan, G.J., Damanik, B.S.J., Sitanggang, J.M., & Muluk C (2015). Effect of Shade, Organic Materials and Varieties On Growth and Production of Upland Rice. *International Journal of Scientific & Technology Research*, 4, 68-74.
- Liu, Q.H., Wu, X., Chen, B.C., Ma, J.Q., & Gao, O.J. (2014). Effects of Low Light on Agronomic and Physiological Characteristics of Rice Including Grain Yield and Quality. *Rice Science China National Rice Research Institute*, 21, 243 – 251.
- Muhidin, Jusoff, K., Elwakib, S., Yunus, M., et al. (2013). The development of upland red rice under shade trees. *World Applied Sciences Journal*, 24, 23-30.
- Nokkoul, R. (2017). Cultivation and upland rice seeds production for the food security of the community. Sahamit Pattana Printing Company Limited, Bangkok, Thailand.
- Nokkoul, R., & Wichitparp, T. (2013). Effects of Rainfall on Yield and Seed Quality of Three Local Upland Rice Varieties Produced Under Organic Farming System. *Research Journal of Environmental and Earth Sciences*, 5, 462-465.
- Strigter, C.J. (1984). Shading: A Traditional Method of Microclimate Manipulation. *Netherlands Journal of Agriculture*, 32, 81-86.
- Wang, Y., Lu, Y., Wang, Z.C.S., Ding, Y., & Ding, C. (2018). Transcriptomic analysis of field-grown rice (*Oryza sativa* L.) reveals responses to shade stress in reproductive stage. *Plant Growth Regulation*, 84, 583–592.



## Journal of Experimental Biology and Agricultural Sciences

<http://www.jebas.org>

ISSN No. 2320 – 8694

### An explorative study on the adoption and dis-adoption of improved rice varieties among farmers in the Northern region of Ghana

S. B. Azumah<sup>1</sup>, C. Y. Lamptey<sup>2</sup>, N. Sulemana<sup>2</sup>, S. Donkoh<sup>3</sup>, A. Zakaria<sup>3</sup>, P. M. I. Maanikuu<sup>4,\*</sup>

<sup>1</sup>DAAD climap Africa Postdoctoral fellow, University for Development Studies, P. O. Box TL 1350, Tamale, Ghana

<sup>2</sup>Department of Agricultural Innovation Communication, Faculty of Agriculture, Food and Consumer Science, University for Development Studies, P. O. Box TL 1350, Tamale, Ghana

<sup>3</sup>School of Applied Economics and Management Sciences, University for Development Studies, P. O. Box TL 1350, Tamale, Ghana

<sup>4</sup>Department of Agricultural Economics, Agribusiness and Extension, School of Agriculture and Technology, University of Energy and Natural Resources, Sunyani, Ghana

Received – September 25, 2021; Revision – December 06, 2021; Accepted – March 30, 2022

Available Online – April 30, 2022

DOI: [http://dx.doi.org/10.18006/2022.10\(2\).323.334](http://dx.doi.org/10.18006/2022.10(2).323.334)

#### KEYWORDS

Adoption

Dis-adoption

Improved Varieties

Rice

Northern Region

Ghana

#### ABSTRACT

Rice consumption in Ghana has increased steadily over the years. To enhance rice productivity to meet demand, several high-performing rice varieties have been disseminated via numerous interventions to smallholders in Northern Ghana. Nevertheless, productivity is still low at farm gate compared to research stations, due to smallholder poor adoption of the varieties. Using primary data collected from 404 farmers, the study examines the adoption levels of the main rice varieties among farmers and investigates the reasons for their adoption and dis-adoption. The empirical results revealed that rice varieties namely, Agra, Sakai, Jasmine 85, and Afife were the most adopted in the study area. Also, the study finds that GR-18, Nerica, Digang, Tox, Mandee, and Faro-15 were the most dis-adopted rice varieties. The main reasons for which farmers adopted the improved rice varieties were availability of a ready market for the produce, crop resistance to pests and diseases, consumer higher demand for rice, advice by extension staff to cultivate, and encouragement from researchers to adopt. The reasons for the dis-adoption of improved rice varieties in the study area were high input requirements, lack of ready market for the varieties, and unfavorable climatic conditions. The findings of the study give direction as to the angle from which the adoption of improved rice varieties can be stepped up while dis-adoption is reduced. Research scientists should research into rice varieties that are more suitable for the soil and climatic conditions of the study area and continue to sensitize and motivate the farmers to adopt them, while government should step up its support for the research scientists as well as the extension officers to deliver on their mandate.

\* Corresponding author

E-mail: [patrick.maanikuu@uenr.edu.gh](mailto:patrick.maanikuu@uenr.edu.gh) (P. M. I. Maanikuu)

Peer review under responsibility of Journal of Experimental Biology and Agricultural Sciences.

Production and Hosting by Horizon Publisher India [HPI]  
(<http://www.horizonpublisherindia.in/>).  
All rights reserved.

All the articles published by [Journal of Experimental Biology and Agricultural Sciences](#) are licensed under a [Creative Commons Attribution-NonCommercial 4.0 International License](#) Based on a work at [www.jebas.org](http://www.jebas.org).



## 1 Introduction

Rice is the main staple for more than half of the world's population. Asia and Sub-Saharan Africa (SSA) are the largest producers and consumers of rice in the world (FAO 2021). South and Southeast Asia alone produce more than 90% of the world's total rice output. China is the leading producer of rice worldwide, and also the largest consumer while the African continent accounts for only 3% of global rice production in 2019 (FAO 2021). This implies that Africa's contribution to the world rice market, in terms of production volumes, is very low. There is however a huge potential for the continent to increase its production and relative market share. Therefore, there is a need for a concerted effort to attain this goal. Dissemination and adoption of high-performing rice varieties in addition to good agronomic practices among farmers are a potential means of boosting rice productivity in Africa (Lamptey 2021).

The agricultural sector in Ghana has derived numerous benefits from several donor-assisted projects aimed at improving crop yield, reducing poverty, and increasing farmers' incomes (Ragasa et al. 2013). Crop farmers in the northern region of this country have gained much from the introduction of enhanced rice varieties together with other complementary innovations to boost rice production and productivity (Azumah 2019; Damba et al. 2020). The high-yielding rice varieties disseminated by the Ministry of Agriculture (MoFA) and other stakeholders along the rice value chain include Agra, Sakai, Jasmine 85, Afife, GR-18, Nerica, Digang, Tox, Mande, and Faro-15. Rice production in Ghana is dominated by small-scale farmers and most of these farmers use low farm inputs and technologies (Lamptey 2018). Adoption of improved rice varieties are expected to enhance productivity and increase incomes, reduce poverty and consequently ensure equity among beneficiaries (Asante et al. 2004; MoFA 2019). As part of the measures to address the low production and productivity among rice farmers, the government of Ghana with support from development partners, proposed a focused and high-impact approach to transform the rice value chain, with particular emphasis on the northern region of Ghana (MoFA 2016). This approach is aimed at increasing rice production and productivity in the country to facilitate the attainment of the Sustainable Development Goals SDG 1 (no extreme poverty) and SDG 2 (zero hunger). The Northern region of Ghana is chosen for this study because it is considered the breadbasket of Ghana and the hub of rice production in the country. Despite these accolades and the huge potential that exist in the region, the rice productivity is still low (MoFA 2016; MoFA 2019).

Among the reasons for the low productivity in the region, low adoption rates of improved rice varieties are the most common ones (Azumah and Zakaria 2019; Lamptey 2021). Adoption of innovations has been studied extensively, but to the best of our knowledge, not much has been done on the dis-adoption of

innovations, which is equally an important area of study. Though a few dis-adoption studies (Kijima et al. 2011; Kasirye 2013; Odeniyi et al. 2018), have been conducted recently, researchers have not focused much attention on studying dis-adoption as a general subject to formulate a unified "theory" of dis-adoption (Fournier et al. 2012).

Again to the best of our knowledge, there is no single research that combines the adoption and dis-adoption of modern and traditional rice varieties among farmers in the Northern region of Ghana. Odeniyi et al. (2018) also observed that there was no prior research to find out why Nigerian native farmers dis-adopted modern rice varieties.

Looking at adoption and dis-adoption in a single study would add impetus to the strengths of adoption research. This study, therefore, intends to make progress in that direction and look at the adoption and dis-adoption of improved and traditional rice varieties in the Northern region of Ghana.

## 2 Materials and Methods

### 2.1 Studied Location, Sample Size and Data

The study was conducted in the Northern region of Ghana (Figure 1). The Northern region is one of sixteen (16) administrative regions of Ghana. It has fourteen (14) administrative districts.

The natural vegetation of the area mainly consists of grasslands, shrubs, and clusters of trees including the shea tree, baobab, acacia, and other drought-resistant trees. The region experiences mainly two seasons in a year, the dry season which typically starts between November and May while the rainy season lasts between June and October. However, changes in the climatic conditions have led to shifts in the seasonal calendar with the rainy season getting shorter. According to the MoFA (2013), the average annual rainfall ranges between 750mm and 1050mm (30 to 40 inches). The region is the second-largest producer of paddy rice in the country, accounting for 68,407.25 metric tonnes per annum (Azumah 2019). However, the annual paddy rice yield in the region of 1.32Mt/ha is far below the national average yield of 3.65mt/ha (MoFA 2020).

The estimated sample size was 385 farmers, which was appropriate enough to prevent any erroneous conclusions in this study. We adjusted this sample size to 410 to cater to some design effects that might have arisen in the study. However, 404 out of the 410 questionnaires became suitable for the analysis.

A multi-stage sampling technique was employed to select 410 rice farmers from 48 selected communities, 14 zones, and 4 districts. Smith's (2019) sample size formula was used to compute the study sample size. The proportion of the sample assigned to each district was based on the estimated population of rice farmers in each district obtained from a sample frame obtained by Smith (2019).

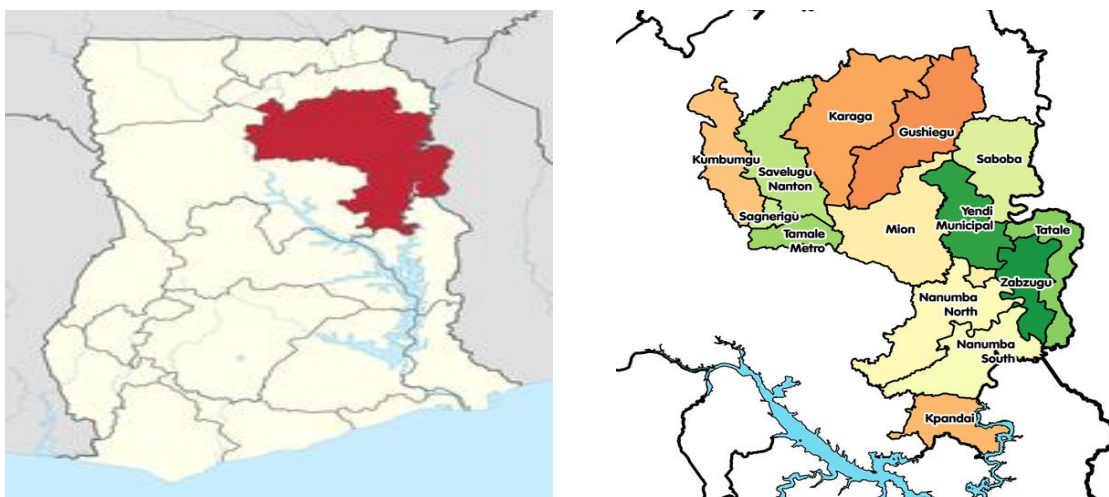


Figure 1 The study area (Source: Google Maps)

Table 1 Estimated sample size per district

District	Sample Size	Percentage	Number of Zones
Tolon	116	28.29	Four Zones
Kumbungu	112	27.32	Four Zones
Savelugu	120	29.27	Four Zones
Nanton	62	15.12	Two Zones
Total	410	100	Fourteen Zones

Source: Authors' construct, 2020

Table 2 Descriptive statistics of respondents' socioeconomic indicators

Variable	Mean	Std. Dev.
Adoption (1/0)	0.46	0.50
Age (Years)	39.69	10.65
Gender (1/0)	0.90	0.30
Education (1/0)	0.29	0.46
Household size (Number)	8.63	4.30
FBOs (1/0)	0.47	0.50
Own phone (1/0)	0.25	0.43
Access to output market (1/0)	0.86	0.34
Access to input market (1/0)	0.85	0.36
Production credit (1/0)	0.35	0.48
Extension service (1/1)	0.80	0.40
Farm plot area (Acres)	3.87	3.81
Government policy (1/0)	0.87	0.34
Road Network (1/0)	0.75	0.44
Mechanization service (1/0)	0.78	0.41
Rainfall (1/0)	0.92	0.28
Harvesting method (1/0)	0.05	0.23

Source: Survey data (2020)



### 3 Results and Discussions

#### 3.1 Profile of the Sampled Farmers

Table 2 shows the descriptive statistics of the sampled rice farmers. The results show that the mean age of the rice farmers was 40 years and about 30% of the farmers had formal education. Martey et al. (2013) revealed that farmers who have attained formal education are more likely to adopt new technology because they are more exposed and have a better understanding of the benefits of the technology being introduced. The average household size was found to be 9 while the mean farm size was 4 acres respectively. MoFA (2017) and Ragasa et al. (2013) reported that about 80% of the rice producers in Ghana are smallholder farmers and mostly have farmland less than one hectare in size. In addition, about 90% of the rice farmers were male. Similarly, about 87% of the farmers were aware of government policies toward rice production. The results also indicate that about 86% of respondents had access to an output market, 85% had access to an input market, 80% had access to extension services, and 35% had access to a production credit. The low level (10%) of women's participation in rice production in the study area corroborates with

Martey et al. (2013) who asserted that women's roles tend to be restricted to domestic activities such that they are unable to find the time and resources required to go into farm activities.

Furthermore, about 92% of the farmers perceived a decrease in the rainfall pattern over the past decade, 75% had access to good roads, 47% were members of FBOs, 25% had personal mobile phones, 78% used tractors for land preparation for rice planting (mechanization). Lastly, about 95% harvested rice manually with the aid of sickles. That is only 5% of the farmers used a combined harvester for rice harvesting.

#### 3.2 Levels of improved rice variety adoption and dis-adoption

The study identified twelve officially recognized and authorized rice varieties in the study area, ten of which were improved and two were traditional. The improved ones were Digang, Mande, Faro-15, GR-18, Nerica, Jasmine 85, Agra, Afife, Tox, and Sakai while the traditional ones were Salma-Saa and Kpokpula. The study also identified two other improved rice varieties (*Moses* and *Iddi*) and seven traditional ones (*Adonga Adongo (Pole)*, *Basolugu*, *Shinkafa Kpana*, *Abugna*, *Alhaji Addae*, *Jakukuo*, and *Anyofula*) in

Table 3 Initial adoption, current adoption, and dis-adoption levels of rice varieties

Main Rice varieties*	Initial Adoption		Current Adoption**		Dis-adoption**	
	Freq.	Percent	Freq.	Percent	Freq.	Percent
Agra <sup>I</sup>	150	37.13	116	77.33	34	22.67
Sakai <sup>I</sup>	2	0.50	1	50.00	1	50.00
Jasmine 85 <sup>I</sup>	166	41.09	67	40.64	99	59.64
Afife <sup>I</sup>	82	20.30	19	23.17	63	76.83
Nerica <sup>I</sup>	68	16.83	2	5.88	64	94.12
Digang <sup>I</sup>	57	14.11	7	12.28	50	87.72
Mandee <sup>I</sup>	55	13.61	10	18.18	45	81.82
GR-18 <sup>I</sup>	52	12.87	3	5.77	49	94.23
Tox <sup>I</sup>	50	12.38	6	12.82	44	87.18
Faro-15 <sup>I</sup>	27	6.68	3	11.10	24	80.90
Salma-Saa <sup>T</sup>	95	23.51	64	67.37	31	32.63
Kpokpula <sup>T</sup>	50	12.38	3	6.00	47	94.00
Others varieties *						
Iddi <sup>I</sup>	52	12.87	3	5.77	49	94.23
Moses <sup>I</sup>	27	6.68	3	11.10	24	80.90
Anyofula <sup>T</sup>	50	12.38	6	12.82	44	87.18
Basolugu <sup>T</sup>	27	6.68	3	11.10	24	80.90
AdongaAdongo <sup>T</sup>	50	12.38	4	8.00	46	92.00
Abugna <sup>T</sup>	50	12.38	3	6.00	47	94.00
AlhajiAddae <sup>T</sup>	50	12.38	3	6.00	47	94.00
ShinkafaKpana <sup>T</sup>	17	4.21	1	5.88	16	94.22
Jakukuo <sup>T</sup>	20	4.95	1	5.00	19	95.00

\*Multiple responses, \*\* Current Adoption + Dis-adoption = Initial Adoption; I = Improved variety; T = Traditional variety (Source: Survey data, 2020)

the area, which were not officially recognized. This sums up to twenty-one; twelve improved and nine traditional rice varieties in the Northern trigon of Ghana. Ragasa et al. (2013) also found several other varieties of rice cultivated by farmers in Ghana besides the officially recognized and authorized ones. The levels of initial adoption, current adoption, and dis-adoption of rice varieties in the study area are shown in Table 3.

The initial levels of adoption for all the rice varieties were generally low (below 40%), except for Jasmine (41%). However, three out of the twenty-one rice varieties in the study area had their current levels of adoption rising above 40%. These were Agra (77.33%), Sakai (50%), and Jasmine (40.64%). Though Sakai had a 50% current level of adoption, it only demanded research purposes (Lamptey 2021), meaning only Agra and Jasmine had high current levels of adoption among the farmers. The dis-adoption levels for all the rice varieties were extremely high (above 50%), except for Agra (22.67%) and Salma-Saa (32.63%). It confirms that the levels of improved rice variety adoption among farmers are indeed low, with correspondingly high levels of dis-adoption across Africa (Kijima et al. 2011; APS 2015; FAO 2021).

### 3.3 Processes of improved rice variety adoption and dis-adoption

This section looks at the processes of improved rice variety adoption and dis-adoption in the study area. Adoption of improved rice varieties in the study area followed the normal process of awareness, trial, acceptance, and usage but the dis-adoption followed an irregular and protracted pattern. The dis-adoption happened either gradually or abruptly, intentionally or unintentionally, corroborating (Rogers 2005). According to the farmers, when they became aware of the improved rice varieties through the various agents and channels of innovation communication, they learned how to cultivate them from either their fellow farmers or agricultural extension officers and researchers. They attended farmer field schools, demonstration farms, group discussions, and community to acquaint themselves with the appropriate ways of cultivating them.

Some of the farmers also said during FGDs that they only saw the performances and output of the improved rice varieties in their fellow farmers' farms and demonstration plots of the extension officers in their communities, and also looked for the seeds in the subsequent cropping seasons to cultivate. Other farmers also said they did not see the performances and output of those varieties but they got the seeds from either traders or their relatives who had brought them from other regions and communities and encouraged them to cultivate. The farmers explained that those of them who did not belong to farmer groups did not have the opportunity to attend the farmer field schools and demonstration farms of the researchers and extension officers, but they either saw the farms or

heard about them. They explained how they adopted the improved rice varieties as follows:

“When we cultivate any new varieties continuously for about four years, we change them and grow different varieties in the same fields. If not, they mix up with wild rice varieties from the soil and neighboring fields. They also become susceptible to pests and diseases infestations as well as a decline in yields, among other reasons. We are normally advised by the extension officers and researchers to buy new certified seeds every four years but those seeds are more expensive. So, we continue to recycle our seeds for subsequent cultivation. Besides, we normally use the same rice fields for all our rice varieties so the only thing we do is a change from one variety to another. However, we normally do not revert to the old varieties because there are other new varieties available for cultivation (adoption). The best thing would have been for us to use different fields for different rice varieties but the land is limited; we have few rice fields. Our lands are also not fertile. So, we spend huge sums of money buying fertilizers and other agrochemicals. It, therefore, becomes difficult for us to keep buying new certified seeds now and then.

Sometimes, we get free improved seeds and fertilizers from MoFA, middlemen, processing companies, and NGOs, so we leave the existing varieties and cultivate those since most of them come with ready markets and other incentive packages. But when they fail us, we stop growing their rice and stick to our varieties. For example, in the case of NERICA, SARI and MoFA used to buy the seeds and grains from us but when they stopped, we had nobody to buy them from us, and we lost woefully. The market women and consumers prefer AGRA and JASMINE 85 to NERICA and other improved rice varieties. We are therefore cultivating AGRA and JASMINE 85 now because they sell”.

Some individual farmers also recounted how they adopted and dis-adopted some improved rice varieties. A contact farmer at Kpachi in the Tolon District said he invested so much money into the cultivation of Jasmine 85 in 2016 because the AVNASH processing company at Nyankpala was buying huge quantities of rice grains from farmers in the district. But he lost his farm to the drought that year and had since not recovered from the shock. So, he stopped cultivating Jasmine 85 in 2016 and started Agra cultivation in 2017. Another farmer at Nabogu in the Savelugu Municipality also said he lost about twenty acres of his Mandee rice farm at Diare to a swam of birds in 2016 at the time of harvest. So, had also stopped growing Mandee since those birds were prevalent in that community, and relocated to Nabogu to cultivate Tox, also known as Nabogu rice. Similarly, a farmer at Jana in the Nanton District recounted:

“In 2017, I harvested over fifty bags of Afife rice on my farm and managed to carry them with the help of laborers to a nearby

roadside. I went to town to look for a vehicle to convey them home but upon my return to the roadside, I realized that bush fire had devoured my entire harvest. I lost both my grains and rice seeds, which I would have used for the sale and subsequent cultivations respectively. I was devastated. So, I had to look for different rice seeds (Salma-Saa) to grow the following year. The Afife was good for my soil and I used to cultivate five acres but now I only cultivate two acres of Salma-Saa”.

In the same way, many farmers in the Kumbungu District said they predicted the weather to sow their rice seeds in the 2017 and 2018 cropping seasons but most of the seeds failed to germinate because the rains did not come down as expected. Those that germinated also got scorched by the sun and weathered. They then looked for different varieties of seeds to sow and those seeds also got rotten and some were washed away, due to flooding.

They said they could not get the same varieties they usually cultivated on their farms (Faro-15, GR-18, Agra, and Jasmine 85) after those horrible incidents, for re-cultivation. So, they resorted to the cultivation of Mandee and Kpokpula, which matured in about four months. However, due to the reduced rainfall pattern in recent years, those two varieties also dried up in the fields before maturity. Hence, they could not break even in 2017 and 2018. They therefore resorted to the cultivation of an improved rice variety called “Moses” and a traditional variety known as “AlhajiIddi”, which were common in the study area. Many farmers at Botanga and Dallon did not experience those devastating effects of droughts and flooding due to the presence of irrigation facilities in their communities. It means adoption of the improved rice varieties occurred after farmers became aware of them, had tried them, and were convinced to accept and grow them for commercial purposes, corroborating (Rogers 2005). The dis-adoption of the improved rice varieties occurred after adoption when farmers faced adverse conditions for their continuous adoption and had lost the needed utility from their adoption decisions, corroborating (Oster and Thornton 2009).

This shows that adoption and dis-adoption are indeed two sides of the same coin. There was relatively little uncertainty in the dis-adoption processes about what farmers were missing, compared with the adoption processes in which uncertainty was inherent. The farmers also adopted the rice varieties by receiving them but dis-adopted them without getting rid of them in their communities. The farmers as well went through several psychological processes such as loss phobia and possession utility in the dis-adoption processes than in the adoption processes, which were more fulfilling and satisfying. The farmers, therefore, showed excitement narrating their adoption experiences but sadness when recounting the processes that led to their dis-adoption decisions. That confirmed the fact that the psychology of choice is markedly different from the psychology of rejection (Oster and Thornton 2009).

The processes of improved rice variety dis-adoption in the study area therefore comprised withdrawal, disengagement, discontinuity, abandonment, desertion and rejection. Each of these process terminologies can be investigated as an entity, over a long period (Taxler and Byerlee 1993). This makes dis-adoption studies a protracted phenomenon compared to adoption studies that are quite dichotomous. The protracted nature of dis-adoption studies discourages many researchers from venturing into that terrain, especially in Ghana.

Thus, the farmers said all of them do not stop cultivating a particular improved rice variety at the same time because every farmer has the reasons for which he or she cultivates rice. However, they said they all cultivate rice for food and income. So, when they realize cultivating a particular improved rice variety does not meet their expectations for food and income, they stop its adoption, one after the other farmer, until the whole community dis-adopts it. They also said they do not re-adopt rice varieties they have once dis-adopted since they keep getting better varieties for adoption. This practice is called “Variety Seeking”, whereby adopters move from adopting one innovation to the other till they get what suits them most (Fournier et al. 2012; Odeniyi et al. 2018). The fact that all the farmers do not dis-adopt improved rice varieties at the same time confirms (Fournier et al. 2012), the view that dis-adoption involves a gradual alienation or a more liminal state of dissociation and separation over time.

### 3.4 Reasons for adoption

Farmers’ reasons for adopting the improved rice varieties are shown in Table 4. The specific reasons farmers gave for adopting improved rice varieties, in order of importance are, ready market for the produce (81.68%), resistance to pests and diseases (76.73%), higher demand for produce (56.93%), advice from extension staff (51.98%) and advice from researchers (50.00%). The ready market for the products existed when the paddy rice was bought at the farm gate by MoFA and SARI staff, middlemen, and processors, who in turn stored, processed, and repackaged it for sale. The farmers were therefore sure of who would buy their produce after harvest and at predetermined prices. Demand for the product, on the other hand, came from consumers or the general public, whose tastes and preferences for the various rice varieties cause farmers to produce those particular varieties, even in the absence of ‘ready markets’. A ready market for the product did not guarantee higher consumer demand for the produce. The farmers, therefore, produced some particular rice varieties like Agra or Jasmine and sold them either directly to consumers or to retailers in the open markets. That way, they did not depend on fixed prices or predetermined bulk buyers such as SARI, MoFA, rice aggregators and processors, or the National Food Buffer Stock Company. However, these produce buying companies purchased paddy rice from the farmers in compliance with government policy

Table 4 Farmers' Reasons for Adopting Improved Rice Varieties

Reasons for Adoption*	Frequency	Percentage
Ready market for the produce	330	81.68
Crops are resistant to diseases/pests	310	76.73
Higher demand for the product	230	56.93
Was advised by extension staff to cultivate	210	51.98
Was advised by researchers to cultivate	202	50.00
Seed more suitable for the soils	120	29.70
Crops very resistant to droughts	145	35.89
Others (nice taste/aroma, easy to cook, easy to mill)	67	16.58
Low input requirements	27	6.68
Got free seeds from promoters	20	4.95

Source: Survey data, 2020 \* Multiple responses N=404

for the rice sector, to help keep the farmers in business, even if a particular rice variety was not in high demand by consumers in the general public. Only 4.95% of the farmers said they adopted the varieties because they got free seeds from promoters such as Non-Governmental Organizations (NGOs), Rice Aggregators, Crop Researchers, and Agricultural Extension Agents (AEAs).

The finding implies that the farmers were mostly motivated by the marketability of the produce after harvest because rice has now become a commercial crop in Ghana (Ragasa et al. 2013; APS 2015). The farmers said during FGDs that most of them farmed rice to sell for money and not only for food. Hence, many of them adopted Agra, Jasmine, and Salma-Saa, which had a ready market and other good qualities such as nice taste and aroma. It means the farmers adopted rice varieties that had a relative advantage over other varieties and these results are in line with Rogers's (2005) hypothesis that innovation would be adopted if it is perceived to have relative advantages over other innovations.

The farmers also emphasized during the FGDs that they normally do not reject any improved rice varieties introduced to them. Rather, they try them for some time before adopting them and they may continue to do so until other newly improved varieties with better qualities are introduced to them for adoption. This also explains why Agra and Jasmine had higher adoption levels than other improved rice varieties, which were promoted earlier in the study area. This means that Agra and Jasmine are also likely to give way to the adoption of other better-improved rice varieties to be promoted in the region, these results are corroborating with Oster and Thornton (2009), who posited that understanding the procedure of innovation adoption, can help to predict adoption patterns.

Similarly, the adoption level of Salma-Saa was higher than that of Kpokpula because Kpokpula is much older in the study area than

Salma-Saa. FGDs with the farmers and KIIs with researchers and extension officers revealed that Kpokpula is an indigenous variety that has been in the region for over half a century now but Salma-Saa is a strain (an incomplete breed) of Jasmine 85 that had been under cultivation in the region before the release of Jasmine 85 about a decade ago. This is in line with Ragasa et al. (2013) who reported that Jasmine 85 (Saa Rice) got accreditation a decade ago, but it was already being cultivated by many farmers in different parts of the country. Salma-Saa has some of the unique characteristics of Jasmine 85, in addition to the fact that it has adapted to the growth and climatic conditions of the area. The farmers explained that the indigenous rice varieties such as Salma-Saa and Kpokpula, have low input requirements and minimal agronomic practices than the improved varieties. They, therefore, continued to cultivate those traditional varieties even when they did not have good markets, milling, and cooking abilities. The farmers added; "we do not buy those seeds", "those seeds are easy to obtain" and "they can still give us some yields even when the rains fail", corroborating Taxler and Byerlee (1993) that grain quality, straw yield, grain yield, and input requirements affect farmers' propensity to adopt farm technologies.

The farmers emphasized that there was no way they would entirely abandon their native varieties to "foreign" ones. According to them "We met our fathers and fore-fathers growing those varieties and we are used to them." They further explained that these varieties have more medicinal, cultural, and religious values than the improved ones: "Some herbalists and traditional authorities prefer the indigenous varieties to the improved ones, as custom demands." They went on to state that the traditional varieties were economical (affordable, easily accessible, easy to cook) for occasions such as marriage, outdoorings, passing out, and funeral ceremonies as well as festivals where a lot of people need to be fed. They reiterated that "Kpokpula" owed its name to the fact that it was more suitable for making "rice balls" than any other rice

variety in the region. Their responses show that some of them were conservatives who exhibited the characteristics of peasant farmers or laggards (Rogers 2005). This is in tandem with Azumah (2019), who found that 35% of the rice farmers in northern Ghana produced solely for a subsistent purpose.

Finally, some of the farmers said they were seed growers in their communities. Therefore, researchers and other farmers from different localities normally contacted them for seeds of various improved rice varieties. So, they produced seeds of various improved rice varieties even when their fellow farmers were no more adopting them. That accounted for the 50% current adoption rate of Sakai even though its initial adoption rate was 0.50%. The reason for seed growers' adoption decision is what is referred to as Future Viability, whereby farmers continue to adopt certain innovations to preserve them for future engagements (Fournier et al. 2012)

### 3.5 Reasons for dis-adoption

This section also discusses farmers' reasons for dis-adopting the main rice varieties, with particular emphasis on the improved ones. The farmers' main reasons for dis-adopting improved rice varieties were high input requirements (95.80%); absence of a ready market for the produce (69.31%), output was no longer demanded by consumers (51.98%), and when seeds made the crops too susceptible to droughts (42.08%). The least reason they gave for their dis-adoption of improved rice varieties was that they were advised by extension staff to stop (26.49%). Other reasons are as shown in Table 5, which are consistent with Doss (2006), who found that farmers willingly adopt high-yielding rice varieties when promoted, but they significantly abandon the varieties in subsequent years, partly due to liquidity constraints. These findings on the dis-adoption of the rice varieties are also consistent with Taxler and Byerlee (1993) who observed that crop characteristics like grain quality, straw yield, grain yield, and input requirements influence farmers' decisions in assessing agricultural innovations.

Other attributes of innovations that determine their levels of dis-adoption include adaptability, reliability, observability, profitability, complexity, and relative advantage (Rogers 2005).

Demand and supply are market forces that determine the market price for products and which also influence their adoption. It implies that the farmers dis-adopted improved rice varieties that had high input requirements and were no longer driven by market forces as well as those that were not compatible with the environment.

Thus, farmers were no longer deriving maximum utility from adopting those innovations and decided on their own to dis-adopt them, without being coerced or intimidated by external forces. Hence, they cited extension officers as having contributed the least (26.49%) to their dis-adoption of improved rice varieties. This is in line with Rogers (2005) who penned that adoption is an individual affair.

KIIs revealed that the advice by extension agents or researchers was not meant for farmers to dis-adopt the varieties but to revert to purchasing certified seeds for their fields after every three or four years and also to desist from cultivating the same improved rice varieties on the same piece of land after four successive years of cultivating those varieties; thus, these results are corroborating with Lamptey (2018). They were likewise advised to avoid "recycling" the same seeds or using hybridized seeds year after year since those seeds do not have the same vigor as the certified seeds. These findings are consistent with Doss (2006), Ragasa et al. (213), APS (2015), and AGRA – SSTP (2016). The idea is to avoid the build-up of pests and diseases associated with those varieties and also to prevent the recessive traits of those varieties from showing up. Martey et al. (2013) and Donkoh and Awuni (2011) also found that rice farmers in the study area discontinued the use of organic manure to fertilize their rice fields due to their poor perception of it.

Table 5 Farmers' reasons for dis-adopting improved rice varieties

Reasons for Dis-adoption*	Frequency	Percentage
High input requirements	387	95.80
No ready market for the produce	280	69.31
Output of seed no longer demanded by consumers	210	51.98
Seeds make crops too susceptible to droughts	170	42.08
Seed are no longer suitable for the soils	150	37.13
Seed too costly	130	32.18
Was advised by researchers to stop	119	29.46
Other Reasons (seed contamination, variety seeking)	113	27.97
Seeds make crops too susceptible to diseases/pests	110	27.23
Was advised by extension staff to stop	107	26.49

Source: Survey data, 2020

\*Multiple responses

N =404

According to the key informants, the farmers sometimes complain of seed contamination due to flooding and cross-pollination with wild varieties (bad rice) in their fields. So, they advise them to replace the impure seeds with pure improved seeds or practice roguing. However, the farmers' perception of the high cost of pure or certified seeds and labor intensiveness of roguing (high input requirements), make them resort to either cultivating local varieties on their fields or not reverting to cultivating the improved varieties they once cultivated. The farmers confirmed during FGDs that they normally do not re-adopt improved rice varieties they dis-adopt because there are several other improved rice varieties to choose from. "We stopped growing them because they were no longer good for us. If they were good for us, we would not have dis-adopted them in the first place. So, why should we go back for them when there are better ones around?" This shifts the reason for dis-adoption to the doorsteps of institutions and agents that promote several improved rice varieties incessantly in the study area. Even though institutions rarely advise farmers to dis-adopt innovations, they do so when the innovations become undesirable or obsolete (Price et al. 2000; Lastovicka and Karen 2005; Martey et al. 2013).

Innovation dis-adoption caused by researchers, extension agents, and market forces are referred to as institutionally induced dis-adoption of undesirable innovations (Lastovicka and Karen 2005; Fournier et al. 2012). Dis-adoption of Nerica, Digang, and Tox was institutionally induced because the farmers abandoned their cultivation due to a lack of ready market for their produce, these results are corroborating with the findings of previous researchers who observed that even though Nerica was also keenly promoted in the study area about a decade ago, the farmers had dis-adopted it alongside the older varieties like Digang and Tox, due to lack of ready market for its output (Kijima et al. 2011; Lamptey 2018; Lamptey 2021). Similarly, Kijima et al. (2011) found that more than 50% of Nerica adopters in Uganda who adopted the Nerica in 2004 abandoned it in 2006, due to the low profitability of Nerica relative to other crops. This finding is contrary to that of Carletto et al. (2007), who opined that pressure to dis-adopt agricultural technologies sets in after 20 years of use. According to the farmers: "sari and MoFA staff normally bring us new improved rice varieties to cultivate, which they claim are better than the existing ones in terms of yield, resistance to pests, diseases and water stress. So, we normally have many varieties at our disposal to choose from. When we produce the newly improved rice varieties, we get high yields but poor markets for them because most consumers and traders are not familiar with them. When we produce them for sale and we do not get good markets for them, we stop and go in for those that the market women like buying. We do that because we need money to pay for our input and tractor services, children's school fees, hospital bills, light bills, and to meet other social and family responsibilities. Besides, we farm to make profit, not losses".

The above extract shows that researchers, extension agents, and market forces served as institutional factors leading to farmer dis-adoption of improved rice varieties. This type of dis-adoption did not occur because the rice varieties had outlived their usefulness in the communities but since they did not meet the tastes and preferences of their target audience. This does not mean that the rice varieties did not have good tastes and nice aroma. Rather, farmers, consumers, and traders were not used to them. They were therefore readily available for adoption but incompatible with the ideals, norms, and values of the social system, corroborating (Rogers 2005). Hence, they were dis-adopted. The best thing should have been to promote their adoption and consumption at the same time. It means rice dissemination projects should factor in promotional campaigns to enhance their demand and consumption by the public.

Rice varieties dis-adopted mainly due to unfavorable environmental factors were Jasmine, Mande, and Afife. These types of improved rice were dis-adopted due to the effects of pests, birds, floods, drought, bushfires, and poor soil fertility on their cultivation. The type of dis-adoption caused by unfavorable environmental factors including, "when seeds make the crops too susceptible to droughts", or pests and diseases infestations are known as nature induced dis-adoption as in termination of human relationships (Duck 1982; Lastovicka and Karen 2005; Fournier et al. 2012). That is because the same principle applies when an adopter dies, migrates, relocates, or stops farming for other occupations that do not need the innovation in question.

However, dis-adoption does not always terminate relationships but it can create brand enemies and former friends (Johnson 2011). Hence, most of the farmers appeared to have abandoned GR-18, Faro-15, Digang, and Nerica, yet those varieties were still in the communities because some farmers were cultivating them. That is perhaps, as the saying goes, "one man's meat is another man's poison". It means the fact that farmers dis-adopt some particular improved rice varieties does not necessarily mean those improved rice varieties are no longer in existence and therefore cannot be adopted by other farmers or be re-adopted by their dis-adopters.

Improved rice varieties, especially Faro-15, GR-18, and Sakai, were dis-adopted by farmers in this study due to "high input requirements". The type of innovation dis-adoption is known as farmer-initiated dis-adoption of unsustainable innovations (Fournier et al. 2012). That is because the farmers complained that the improved rice varieties had high input requirements relative to the traditional varieties. The rationale is that farmers are rational beings, who advise themselves when they realize they can no longer afford an innovation, sustain it with its associated practices, or derive maximum utility from its continuous adoption. This is in tandem with Doss et al. (2003), who found that farmers do not

adopt innovations “wholesale”. Rather, they pick and choose aspects of the innovations that are convenient, applicable, and relevant to them. The farmers said, during FGS that: “We sometimes do not farm certain improved rice varieties because they demand plowing and harrowing, more fertilizers, herbicides, weedicides, and other agro-chemicals. They are also labor-intensive time consuming to plant, transplant and harvest. They do not give good yields when we do not have time for them. The old improved rice and traditional varieties are not like that. They can still give some yields even if we do not have much time and resources for their cultivation”.

The above narrative, therefore, exemplifies what is termed a farmer-initiated type of dis-adoption of unsustainable innovations, this is corroborating with Fournier et al. (2012). It means the farmers dis-adopted some improved rice varieties to adopt other ones. Rogers (2005) described this practice as replacement discontinuance. The farmers’ responses also show that they dis-adopted those varieties due to the negative aspects of the innovations, this is corroborating with Fournier et al. (2012) who posited that technologies dis-adopted are as ineffective as technologies not adopted. That explains why some researchers classify dis-adopters as non-adopters Doss (2006) but Lamptey (2021) classified them as two separate entities with similar characteristics. The reason for the farmers’ behavior above is termed ‘Variety Seeking’, a phenomenon that occurs when the farmers have several alternatives to choose from (Rogers 2005; Fournier et al., 2012).

However, it is not always the case that when farmers dis-adopt some particular improved rice varieties, they would be adopting other improved rice varieties (Lastovicka and Karen 2005). That is why the dis-adoption levels of some improved rice varieties in the study area were high, yet the adoption levels of other improved rice varieties were very low (Asuming-Brempong et al. 2011; Lamptey 2021). Rogers (2005) referred to that practice as disenchantment discontinuance, where a farmer discontinues an innovation with or without replacement as a result of dissatisfaction with the innovation’s performance. Also, the fact that farmers dis-adopt some particular improved rice varieties does not necessarily mean they dislike all improved rice varieties. Hence, though there were higher levels of dis-adoption of many improved rice varieties in this study, the adoption levels of a few improved rice varieties were equally high.

Hence, this study revealed three types of improved rice variety dis-adoption in the study area, with the farmers at the center stage. They were; farmer-initiated type of dis-adoption, institutional initiated farmer dis-adoption, and nature induced dis-adoption as in the termination of human relationships. Since all the three types of innovation dis-adoption occurred in the study area, it means the dis-adoption of improved rice varieties in the region cannot be

blamed solely on the farmers, institutions, or nature because they all served as collaborative actors. This is in tandem with Fournier et al. (2012) that dis-adoption is a process in society that involves many people, besides the dis-adopters. It means many people were implicated in a dis-adoption phenomenon in the study area.

## 4 Conclusions and Future Recommendations

### 4.1 Conclusions

Over the years, rice farmers in Ghana have gained immense benefits from the introduction of enhanced crop varieties that come along with other innovations like tillage, fertilizer, agrochemical application methods, and planting and harvesting methods, among others. However, the levels of adoption of improved rice varieties in the study area have been very low with alarming rates of dis-adoption. While studies on the adoption of improved seed varieties abound in Ghana, there is none on the reasons for the dis-adoption of improved rice varieties, to the best of our knowledge. The objectives of this study were to investigate the levels of adoption and dis-adoption of the main rice varieties in the Northern region of Ghana, for the past ten years and examine the process and reasons for the adoption and dis-adoption.

The findings indicate that the adoption levels were generally low with the most adopted improved rice varieties being Agra (77.33%), Sakai (50%), Jasmine (40.64%), and Afife (23.17%), and the rest falling below 20% each. The dis-adoption levels on the other hand were very high, with the six most dis-adopted improved rice varieties being GR-18 (94.23%), Nerica (94.18%), Digang (87.72%), Tox (87.18%), Mandee (81.82%) and Faro-15 (80.90%). The dis-adoption level of Kpokpula, a traditional variety, was 96.00%, which was higher than that of any of the improved rice varieties. It means the farmers had dis-adopted both improved and traditional rice varieties and were more inclined towards the adoption of the newly improved ones, especially Jasmine and Agra.

Adoption of improved rice varieties in the study area followed a dichotomous process of awareness, trial, acceptance, and usage but the dis-adoption assumed a protracted pattern. The processes of improved rice variety dis-adoption in the study areas comprised withdrawal, disengagement, discontinuity, abandonment, desertion, and rejection. The study revealed three types of innovation dis-adoption in the region, with the farmers at the center stage. Firstly, farmer-initiated dis-adoption of rice varieties such as Faro-15, GR-18, and Sakai which are associated with unsustainable practices. Secondly, institutional initiated dis-adoption of rice varieties like Digang, Nerica, and Tox, having undesirable characteristics. Lastly, nature-induced dis-adoption of rice varieties such as Jasmine, Mandee, and Afife are caused by farmers’ death, relocation, change of occupation, or the effects of climate change.

The five most important reasons for which farmers adopted improved rice varieties in Northern Ghana were a ready market for the produce (81.68%), crop resistance to pests and diseases (76.73%), consumer higher demand for rice (56.93%), advice by extension staff to cultivate (51.98%) and motivation for adoption from researchers (50.00%). Only 4.95% of farmers adopted the varieties because they got free seeds from promoters. It means adopters were mostly motivated by the marketability of the produce after harvest because rice had become a commercial crop in Ghana. The farmers' main reasons for dis-adopting improved rice varieties were high input requirements (95.80%), absence of a ready market for the produce (69.31%), the output being no longer demanded by consumers (51.98%), and when seeds made the crops too susceptible to droughts (42.08%). The least reason for which the farmers dis-adopted improved rice varieties was that they were advised by extension staff to stop cultivation (26.49%). These reasons confirm the fact that farmers readily adopt high-yielding rice varieties when introduced, but they significantly abandon them in subsequent years, partly due to liquidity constraints.

The presence of several improved rice varieties in the study area made the farmers exhibit "replacement discontinuance", by dis-adopting some varieties to adopt other superior varieties. The farmers also exhibited "disenchantment discontinuance", by dis-adopting some varieties with or without replacement, due to dissatisfaction with the performances of those varieties. Thus, the reasons for the dis-adoption of improved rice varieties in the study area were multi-faceted.

#### 4.2 Recommendations

The government could increase the levels of adoption of Agra, Sakai, Jasmine, and Afife, but decrease the levels of dis-adoption of GR-18, Nerica, Digang, Tox, Mande, and Faro-15 by subsidizing their input requirements and providing ready markets to them through the School Feeding Programme. Researchers should also breed improved rice varieties that are adaptable to prevailing climatic conditions in the study area, to be promoted by the AEAs of MoFA and their collaborators. The government, through MoFA, should come out with approved and recommended varieties to be adopted and ensure their compliance. That would help to regulate the proliferation of improved rice varieties in the study area and control the diffusion of existing varieties before new ones are introduced.

Since the government finances the dissemination and adoption of improved rice varieties in the study area, they should also finance disadoption studies to help monitor and evaluate the post-adoption behavior of farmers of improved rice varieties. The monitoring and evaluation officers of MoFA should be adequately resourced to carry out this responsibility for the state and give appropriate feedback to the state research institutions like sari and Csir. Also,

academic researchers in Ghana should be sponsored to study the phenomenon of dis-adoption, to augment the efforts of MoFA staff. Civil society, including NGOs, should likewise collaborate with the government in promoting the adoption and mitigating dis-adoption of improved rice varieties in the region.

The three-fold dis-adoption of rice varieties in the study area has policy implications such that the government and all stakeholders in the rice value chain in this country would have to ensure that farmer-initiated dis-adoption of unsustainable varieties, institutional initiated dis-adoption of undesirable varieties, and nature induced dis-adoption of rice varieties are minimized.

#### References

- AGRA – SSTP. (2016). Ghana Early Generation Seed Study, Final Report for the United State Agency for International Development theory. Retrieved from [https://agrilinks.org/sites/default/files/resource/files/ghana\\_early\\_generation\\_seed\\_report.pdf](https://agrilinks.org/sites/default/files/resource/files/ghana_early_generation_seed_report.pdf).
- Agricultural Production Survey for the Northern Regions of Ghana. (2015). 2013-2014 Results (2015). Final Report, Retrieved from [www.agmanager.info.file](http://www.agmanager.info/file).
- Asante, E. G., Appiah, M. R., Ofori-Frimpong, K., & Afrifa. A. A. (2004). The economics of fertilizer use on some peasant cocoa farms in Ghana. *Ghana Journal of Agricultural Science* 33, 183–190.
- Asuming-Brempong, S., Gyasi, K. O., Marfo, K. A., Diagne, A., et al. (2011). The exposure and adoption of New Rice for Africa (NERICAs) among Ghanaian rice farmers: What is the evidence? *African Journal of Agricultural Research*, 6(27), 5911-5917.
- Azumah, S. B. (2019). Agricultural Technology Transfer, Adoption and Technical Efficiency of Rice Farmers in Northern Ghana. PhD Thesis, *University for Development Studies, Ghana*. Retrieved from [www.udsspace.uds.edu.gh](http://www.udsspace.uds.edu.gh).
- Azumah, S. B., & Zakaria, A. (2019). Fertilizer Subsidy and Rice Productivity in Ghana: A Microeconomic Study. *Journal of Agricultural Studies*, 7(1), 82-102.
- Carletto, C., Kirk, A., & Winters, P. (2007). Non-traditional exports, traditional constraints: The adoption and diffusion of cash crops among smallholders in Guatemala. *World Bank Policy Research Working Paper No.*, 4347.
- Damba, O. T., Ansah, I. G. K., Donkoh, S. A., Alhassan, A., et al. (2020). Effects of technology dissemination approaches on agricultural technology uptake and utilization in Northern Ghana. *Technology in Society*, 62, 101294.
- Donkoh, S.A., & Awuni, J.A. (2011). Adoption of Farm Management Practices in Lowland Rice Production in Northern



- Ghana. *Journal of Agricultural and Biological Science*, 2 (4), 084-093.
- Doss, C. R. (2006). Analyzing technology adoption using microstudies: limitations, challenges, and opportunities for improvement. *Agricultural Economics* 34, 207–219.
- Doss, C. R., Mwangi, W., Verkuijl, H., & de Groot, H. (2003). Adoption of Maize and Wheat Technologies in Eastern Africa: A Synthesis of the Findings of 22 Case Studies, International Maize and Wheat Improvement Center (CIMMYT), Mexico. *E C O N O M I C S Working Paper*, 03-06.
- Duck, S. (1982). *Personal Relationships 4: Dissolving Personal Relationships*. London: Academic Press.
- Food and Agriculture Organization of the United Nations. (2021). World Rice Production and Trade in Brief-Cotecn, FAO; Rome, Italy. Retrieved from <https://www.cotena.com>.
- Fournier, S., Alvarez, C., & Avery, J. (2012). Disadoption Through the Relationship Lens", in NA - Advances in Consumer Research Volume 40, eds. Zeynep Gürhan-Canli, Cele Otnes, and Rui (Juliet) Zhu, Duluth, MN : Association for Consumer Research, Pages: 313-317. Retrieved from <http://www.acrwebsite.org/volumes/1013118/volumes/v40/NA-40>.
- Johnson, A. R., Maggie, M., & Matthew, T. (2011). A Coal in the Heart: Self-Relevance as a Post-Exit Predictor of Anti-Brand Actions, *Journal of Consumer Research*, 38 (1), 108-125.
- Kasirye, I. (2013). Constraints to Agricultural Technology Adoption in Uganda: Evidence from the 2005/06-2009/10 Uganda National Panel Survey, Economic Policy Research Centre, Makerere University, Kampala, Uganda.
- Kijima, Y., Otsuka, K., & Sserunkuuma, D. (2011). Assessing the impact of NERICA on income and poverty in central and western Uganda. *Agricultural Economics*, 38, 327–337.
- Lamprey, C. Y. (2018). Adoption of NERICA among Rice Farmers in the Tolon and Kumbungu Districts in the Northern Region of Ghana. MPhil Thesis, *University for Development Studies*, Ghana. Retrieved from [www.udspace.uds.edu.gh](http://www.udspace.uds.edu.gh).
- Lamprey, C. Y. (2021). Adoption and Disadoption of Improved Rice Varieties among Farmers in the Northern Region, Ghana. PhD. Thesis, *University for Development Studies*, Ghana. Retrieved from [www.udspace.uds.edu.gh](http://www.udspace.uds.edu.gh).
- Lastovicka, J. L., & Karen V. F. (2005) Three Paths to Disposition: The Movement of Meaningful Possessions to Strangers. *Journal of Consumer Research*, 31 (4), 813-823.
- Martey, E., Wiredu, A. N., Asante, B. O., Anim, K., et al. (2013) Factors Influencing Participation in Rice Development Projects: The Case of Smallholder Rice Farmers in Northern Ghana. *International Journal of Development and Economic Sustainability*, 1 (2), 13-27.
- Ministry of Food and Agriculture (2016). Agriculture in Ghana, Facts and Figures 2015, Statistics, Research and Information Directorate (SRID), October 2016, Accra, Ghana.
- Ministry of Food and Agriculture (2019). 2019 Annual Report on Rice Farmers in Kumbungu District, December, 2019, Northern Region, Ghana.
- Ministry of Food and Agriculture. (2013). Agriculture in Ghana: Facts and Figures (2012), Statistics, Research and Information Directorate (SRID), 1–45. August, 2013, Accra, Ghana.
- Ministry of Food and Agriculture. (2017). Planting for Food and Jobs, Strategic Plan for Implementation (2017-2020), Republic of Ghana.
- Ministry of Food and Agriculture. (2020). Agriculture in Ghana, Facts and Figures 2015, Statistics, Research and Information Directorate (SRID), September 2020, Accra, Ghana.
- Odeniyi, K. A., Elizabeth J. Z., Robinson, C., & Srinivasan, S. (2018). Agricultural Technology Disadoption: Why Rural Farmers Abandon Improved Rice Varieties, Tropentag, September 17-19, 2018, Ghent, United Kingdom.
- Oster, E., & Thornton, R. (2009). Determinants of technology adoption: Private value and peer effects in menstrual cup take-up, mimeo University of Chicago.
- Price, L., Eric A., & Carolyn, C. (2000). Older Consumers' Disposition of Valued Possessions, *Journal of Consumer Research*, 27, 179-201.
- Ragasa, C., Dankyi, A., Acheampong, P., Wiredu, A. N., et al. (2013). Patterns of Adoption of Improved Rice Technologies in Ghana, *GSSP Working Paper*, IFPRI, Accra, Ghana. DOI: 10.13140/2.1.5093.4727.
- Rogers, E. M. (2005). *Diffusion of Innovations* (6th Ed.). The Free Press. New York.
- Smith, S. M. (2019). Determining Sample Size, How to Ensure You Get the Correct Sample Size. Retrieved from [www.qualdrics.com](http://www.qualdrics.com).
- Taxler, G., & Byerlee, D. (1993) A Joint-Product Analysis of the Adoption of Modern Cereal Varieties in Developing Countries. *American Journal of Agriculture Economics*, 75, 981-989.



## Journal of Experimental Biology and Agricultural Sciences

<http://www.jebas.org>

ISSN No. 2320 – 8694

### Characterization of Mature Cladodes of *Opuntia ficus-indica* L. Using Morphological and Colorimetric Descriptors

Juan Arredondo-Valdez<sup>1</sup>, Alejandro Isabel Luna-Maldonado<sup>1,\*</sup>,  
Ricardo David Valdez-Cepeda<sup>2</sup>, Humberto Rodríguez-Fuentes<sup>1</sup>, Juan Antonio Vidales-Contreras<sup>1</sup>,  
Uziel Francisco Grajeda-González<sup>1</sup>, Héctor Flores-Breceda<sup>1</sup>

<sup>1</sup>Department of Agricultural and Food Engineering, Faculty of Agriculture, Autonomous University of Nuevo Leon, General Escobedo, N.L., México

<sup>2</sup>Centro Regional Universitario Centro Norte, Universidad Autónoma Chapingo, Calle Cruz del Sur 100, Col. Constelación, CP 98085 Zacatecas, Zac., México

Received – January 22, 2022; Revision – April 14, 2022; Accepted – April 26, 2022  
Available Online – April 30, 2022

DOI: [http://dx.doi.org/10.18006/2022.10\(2\).335.343](http://dx.doi.org/10.18006/2022.10(2).335.343)

#### KEYWORDS

*Opuntia* mature cladodes

Image processing

Color parameters

Linear and nonlinear modeling

ImageJ

#### ABSTRACT

Mexico is the world's leading producer of *Opuntia ficus-indica*. This kind of prickly pear is the most widespread and most commercially important cactus in Mexico. Morphological and colorimetric descriptors are among the most important agronomic traits because these parameters affect the yield, in such a way, the objective of the present research was to present a fast and reliable methodology to obtain the functional relationship in shape and color parameters of *O. ficus indica* cladodes, using a smartphone, a color meter, and open-access software. The acquisition and processing of images discovered interesting relationships between the *Opuntia* cladode's morphological characteristics, as well as colorimetric parameters of the cladodes. The non-linear data behaviors were fitted using deterministic models and CurveExpert software. Results of the study revealed that the best morphological descriptors were Circularity vs. Perimeter ( $r= 0.9815$ ) and Aspect ratio vs. Roundness ( $r= 0.9999$ ). In addition, mean values of the L\*, C, and H color parameters were displayed in a window of a computer program online. It was found that the a-C relationship of the color parameters had the highest correlation coefficient (0.999). Therefore, it can be concluded that the morphological descriptors Circularity vs. Perimeter, Aspect Rate vs. Roundness, and a\*-C color parameter can predict quickly and precisely the quality of *O. ficus-indica*.

\* Corresponding author

E-mail: [alejandro.lunaml@uanl.edu.mx](mailto:alejandro.lunaml@uanl.edu.mx) (Alejandro Isabel Luna-Maldonado)

Peer review under responsibility of Journal of Experimental Biology and Agricultural Sciences.

Production and Hosting by Horizon Publisher India [HPI]  
(<http://www.horizonpublisherindia.in/>).  
All rights reserved.

All the articles published by [Journal of Experimental Biology and Agricultural Sciences](#) are licensed under a [Creative Commons Attribution-NonCommercial 4.0 International License](#) Based on a work at [www.jebas.org](http://www.jebas.org).



## 1 Introduction

Mexico is a world leader in the production of *Opuntia ficus-indica* (prickly pear). In 2019, Mexico produced 863,000 tons of fresh *Opuntia* prickly pear in an area of 12,471.09 hectares; 34,000 tons of this prickly pear annually were exported to other countries, mainly to USA and Canada. In Nuevo León state the prickly pear average yield was 38 t ha<sup>-1</sup> (SIAP 2021). However, the production of fresh *O. ficus-indica* prickly pear in Mexico could be affected by the selection of mature cladodes.

The quantitative evaluation of the shapes of the mature cladodes of the nopal is required in phenotyping research. The morphological descriptors describe the specific characteristics concerning the geometry of a particular trait, in such a way that measuring the physical characteristics of plants (the phenotype), allows researchers to relate them to the genetic makeup of the crops as Farina (2020) works on soybean, or Gutiérrez (2020) working on the morphological characterization of white and purple cocoa. The characterization of agricultural varieties has been based on morphological descriptors, including shape, color, and seed size, in addition to quantitative attributes such as mineral content (Morales-Morales et al. 2019).

Although the shape of an *Opuntia* cladode cannot be reconstructed by knowing the morphological descriptors, these can be discriminating variables in the shape of cladodes (Wirth 2004; Bober 2001; Hyun et al. 2015). Morphological descriptors have been successfully applied for the evaluation of various biological shapes in animals and plants (Žunić 2010; D'Silva and Bhuvanewari 2015) such as the study of Laouadi et al. (2020) who provides a working basis on the morphology of local goats in Laghouat region by phenotypic characterization.

According to Iwata et al. (2004), the quantification of shapes is a prerequisite for assessing the inheritance of morphological features in quantitative genetics. Morphological characterization is necessary because it provides information about the features and structure of objects (Cheesa 2010). The identification of highly discriminant descriptors is important to obtain an efficient and reproducible classification of the mature cladodes of *O. ficus indica*. The potential taxonomic importance of plant and fruit morphology has been recognized by biologists, geneticists, and farmers (Visa et al. 2014). Morphological characterization has been advanced with the modern technologies of acquisition, processing, and analysis of the images of the plants and has acquired much importance for selection, and taxonomic studies (Brewer et al. 2006; Newton and Kendrick 1990; Ahmad et al. 2020).

On the other hand, color is an important sensory attribute to provides the basic quality information for human perception and has a close association with freshness, maturity, variety,

convenience, and food safety. Therefore, colorimetric descriptors are important classification parameters for most agricultural and food products (McCaig 2002). In measuring food color, L \* a \* b \* color space is the most widely used due to the uniform distribution of colors and because it is perceptually uniform (McGuire 1992; Leon et al. 2006). The objective of the present research was to present a fast and reliable methodology to obtain the functional relationship in shape and color parameters of *O. ficus indica* cladodes, using a smartphone a color meter, and open-access software.

## 2 Materials and Methods

### 2.1 Plant materials

One-year-old cladodes of *O. ficus indica* of the Villanueva cultivar were visually selected and collected by personnel experience in the management of *Opuntia* plants at the Alejandra ranch in Zuazua, Nuevo León; geographically located at 25 ° 52' 03" North Latitude and 100 ° 05' 18" West Longitude, located 30 km from the experimental site. The mature cladodes were disinfected with a solution of 1 kg of lime plus 1 kg of copper sulfate diluted in 98 L of water (Bordeaux broth) (Canseco-Guzmán and Canseco-Guzmán 2013). Subsequently, they were sown in 19 L pots, with clay loam soil.

### 2.2 Acquisition of images and morphological descriptors

Thirty mature cladodes were photographed individually, and all the obtained images were processed with the ImageJ version 1.51J8 platform to estimate the shape descriptors. ImageJ can display, edit, analyze, process, save, and print 8-bit, 16-bit, and 32-bit, grayscale, and 8-bit and 24-bit color images. As a first step, each jpg extension image was opened from of the corresponding directory in a personal computer and transformed into an 8-byte image. The threshold was set, converted to a mask, and transformed into a binary image. Subsequently, the binary image was inverted and the scale of cm to pixels was established, the desired morphological descriptors were configured, and again the image was inverted and finally, the *Opuntia* mature cladodes were analyzed with ImageJ software (Figures 1 and 2). A total of 12 morphological descriptors (Area, Length, Minor axis length, Perimeter, Feret Diameter, Aspect ratio, Compactness, Roundness, Strength, Centroid, Center of mass, and Kurtosis) were used to construct the data set and statistical analysis to characterize *Opuntia* mature cladodes and determine the potential use of these descriptors for its classification.

The shape descriptors of the mature cladodes with the Image J platform: Image formats including TIFF, GIF, JPEG, BMP, DICOM, FITS, and 'raw' can be imported and read as single images or stacks and incorporates several useful tools for image

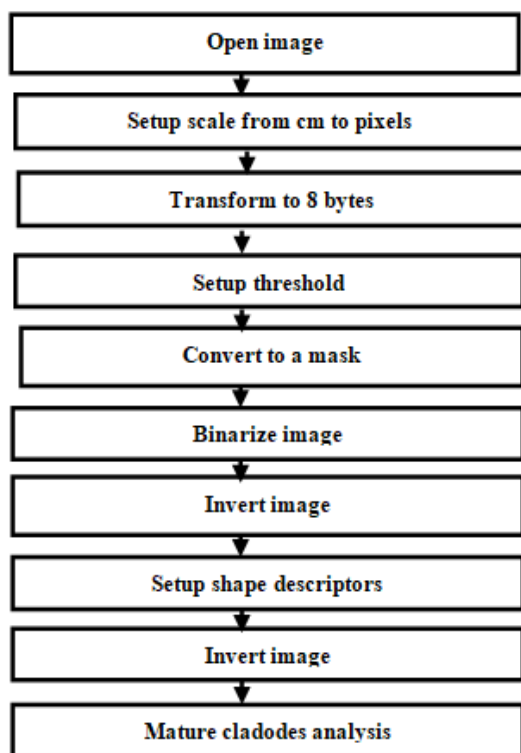


Figure 1 Flow diagram of the image processing operations.

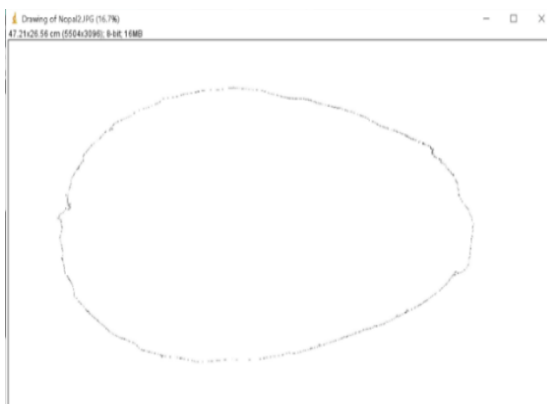


Figure 2 Mature cladodes processed with ImageJ.

processing (Hartig 2013) and incorporate an efficient way of image preprocessing using histogram equalization to properly select the region of interest (Veena Divya et al. 2016). The shape descriptors were:

**Area:** The area of the mature paddle was measured as the number of pixels in its outline silhouette.

- a. **Length of the major axis:** The length of the longest line that can be drawn through the mature paddle was measured as the distance in pixels at the extreme points.

b. **Minor axis length:** The length of the longest line that can be drawn through the mature paddle perpendicular to the major axis, measured as the distance in pixels at the extreme points.

c. **Perimeter:** Length that corresponds to the closed contour of  $n$  vertices in a figure, that is the sum of the sides that form the polygon (polygonalized or vectorized limit).

d. **Feret Diameter:** Diameter of a circle that has the same area as the object, calculated with the formula:  $FD = \text{square root of } [(4 * \text{area}) / \pi]$ .

e. **Aspect ratio (AR):** The relationship between the length of the *Opuntia* mature paddle and its width.

f. **Compactness:** It provides a measure of the roundness of the mature paddle: if it is 1 the mature paddle is approximately circular, when it decreases by 1, the mature paddle is less circular, calculated as  $C = FD / \text{Length of the major axis}$ .

g. **Roundness or circularity:** A measure of roundness or circularity (area-perimeter ratio) that excludes objects from the area of a circle with the same convex perimeter. If the ratio is equal to 1, the object is a perfect circle, when the ratio decreases by 1, the object comes out from a circular shape, calculated as  $R = [(4\pi * \text{area}) / \text{perimeter}^2]$ .

h. **Strength:** Measures the density of an object.

i. **Centroid:** Average of the  $x$  and  $y$  coordinates of all pixels in the image or selection.

j. **Center of mass:** Weighted average of the brightness of the  $x$  and  $y$  coordinates of all pixels in the image or selection. Use the  $XM$  and  $YM$  headers. These coordinates are the first-order spatial moments.

k. **Kurtosis:** The fourth-order time was above the average.

In addition, the mature cladodes' thickness and weight were measured.

### 2.3 Color descriptors

30 *Opuntia* cladodes were sown in 19-liter pots and the color parameters were measured every week, over 16 weeks from October 2019 to February 2020. The parameters  $a^*$ ,  $b^*$ ,  $C$ ,  $L^*$ , and  $H$ , were obtained using a Konica Minolta Chroma Meter CR-410 color meter, with a standard Illuminant C,  $2^\circ$  standard observers, and a field of view with a diameter of 8 mm, aperture 50 mm. The color was taken in the color space  $L^* a^* b^*$ ; where  $L^*$  is the luminosity;  $a^*$  is the chromaticity of green to red, and  $b^*$  is the chromaticity from blue to yellow. The color hue ( $^\circ H$ ) was also measured (Figure 3).



Figure 3 Measuring the color parameters of the mature cladodes.

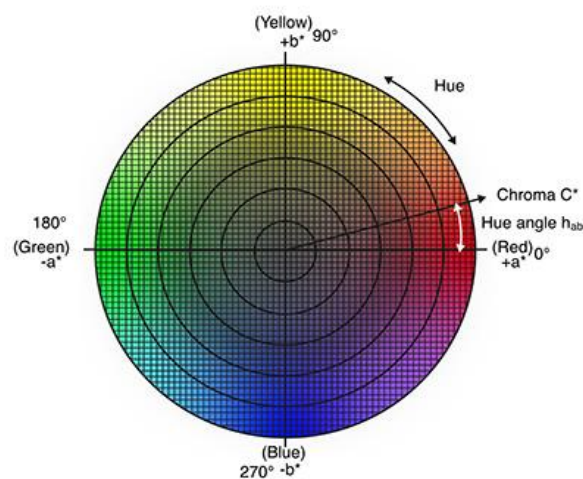


Figure 4 L\*a\*b\* color space (Grajeda-González et al., 2015).

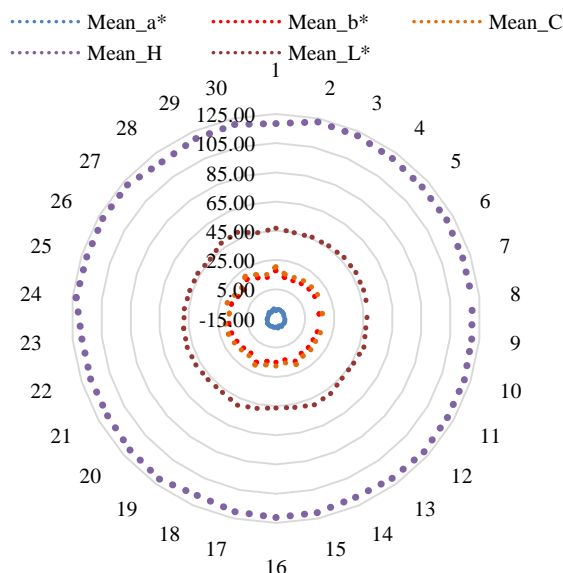


Figure 5 Charts showing mean values of color attributes.

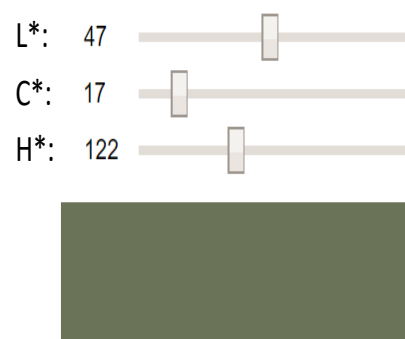


Figure 6 Mean L\*, C, and H color parameters of cladodes.

The relationship between the color parameters,  $a^*$ ,  $b^*$ ,  $C$ , and  $H$ , are shown in the color sphere (Figure 4) where  $C^* = (a^{*2} + b^{*2})^{1/2}$  and  $H = \arctan(b^* / a^*)$  (Grajeda-González 2015). The parameters  $L^*$ ,  $a^*$ , and  $b^*$  were obtained by the average of two measures carried out on two opposite sides of the prickly pear cactus cladodes (figure 5). Johnston online program was used to display the colors corresponding to the measured color parameter mean values of  $L^*a^*b^*$ , (Figure 6) (Johnstone 2019).

**2.4 Statistical analysis**

Descriptive statistics were performed and a total of 12 quantitative variables were analyzed, and parameters such as mean, minimum, maximum, and coefficient of variation were obtained. The analysis

of variance (ANOVA) was applied indicating significant differences with a low probability of error.

Moreover, a correlation analysis between morphological parameters was done to search for a relationship between them. Because of data distribution, heavy-duty nonlinear regression analysis was carried out using CurveExpert Pro: 2.6.5 freeware.

Moreover, the mean values of the color parameters of the 30 cladodes were obtained. An online program was used to visualize the measured  $L^*a^*b^*$  parameters (Figure 6). The ANOVA was carried out (Table 7). The correlation coefficient  $r^2$  and the nonlinear mathematical model were obtained (Table 9).

### 3 Results and Discussion

With the nonlinear regression analysis, we obtained the mathematical models for the combination of seven pairs of the most important morphological parameters, with their corresponding determination coefficient at a 95% confidence level.

The time to analyze images of mature *O. ficus-indica* cladodes to obtain quantitative variables related to their external morphology was reduced up to 9 significant digits' accuracy. The weight of the mature cladodes ranged between 682.95g and 1299.4g, the surface area of the mature cladodes ranged between 337.941 and 618.512 cm<sup>2</sup>, and the width of the cladode ranged between 28.086 cm and 38.511 cm (Table 1). The obtained results of analysis of variance showed a significant difference with a 95% of confidence level in *Opuntia* mature cladodes for all treatments. The mean values, standard deviation, and amplitude of the other variables are also shown in Table 1, as well as the coefficient of variation, which ranged from 0.75% to 70.6%; however, most of the variables

showed a variation coefficient of less than 10%.

The results obtained for the shape parameters from the correlation analysis showed correlation factors of 0.99 for Aspect Ratio and Roundness and 0.96 for Perimeter and Circularity (Table 2). The results of the non-linear regression analysis, using Curve Expert, indicated a strong relationship between the following parameters: Perimeter vs. Area ( $r=0.8975$ ), Circularity vs. Area ( $r=0.9388$ ), Feret Diameter vs. Area ( $r=0.9394$ ), Circularity vs. Perimeter ( $r=0.9815$ ), Feret Diameter vs. Perimeter ( $r=0.9493$ ), Roundness vs. Circularity ( $r=0.8735$ ), Aspect Ratio vs. Circularity ( $r=0.8637$ ), Aspect Ratio vs. Roundness ( $r=0.9999$ ). There were other parameters with a less strong relationship as such as Solidity vs. Area ( $r=0.679$ ), Solidity vs. Perimeter ( $r=0.640$ ), Feret Diameter vs. Circularity ( $r=0.764$ ), Solidity vs. Roundness ( $r=0.763$ ), Solidity vs. Aspect Ratio ( $r=0.753$ ) and the rest of pairs showed a low relationship, with a lower correlation coefficient (Table 3). The parameters of the highest correlation coefficient, as well as the proposed type of mathematical model, are shown in Table 4.

Table 1 Mean, minimum, maximum values, standard deviation, and coefficient of variation of mature cladodes morphological parameters.

	Area	Xm	Ym	Perimeter	Width	Height
Mean	451.891	17.638	14.706	87.807	33.401	18.720
Mín. Value	337.941	15.012	11.747	73.048	28.086	15.848
Máx. Value	634.531	21.91	18.611	144.918	38.511	22.797
Std. Desv.	71.916	1.668	1.723	18.349	3.050	1.779
Variation Coefficient%	15.900	9.457	11.718	20.89	9.130	9.502
	Circularity	Feret Diameter	Kurtosis	Aspect Ratio	Roundness	Solidity
Mean	0.768	33.494	1.977	1.807	0.557	0.986
Mín. Value	0.329	28.372	-0.021	1.510	0.488	0.956
Máx. Value	0.870	38.653	5.624	2.050	0.662	0.993
Std. Desv.	0.132	3.028	1.395	0.149	0.047	0.007
Variation Coefficient %	17.142	9.040	70.600	8.274	8.456	0.751

Table 2 Correlation analysis between mature cladodes morphological parameters.

	Area	Perimeter	Circularity	Feret Diameter	Aspect Ratio	Round	Solidity
Area	1						
Perimeter	0.844	1					
Circularity	-0.688	-0.963	1				
Feret Diam.	0.862	0.679	-0.570	1			
Aspect Ratio.	-0.033	-0.101	0.031	0.453	1		
Round	0.0279	0.087	-0.011	-0.454	-0.996	1	
Solidity	-0.405	-0.378	0.344	-0.476	-0.171	0.160	1

Table 3 Nonlinear regression equation models and coefficient of determination  $r^2$ , with 95% of confidence for shape parameters.

Related variables	Equation model	$r^2$
Perimeter vs. Area	Perimeter = 119.5606 + 43.4425Cos(0.008214Area – 0.01434)	0.805
Circularity vs. Area	Circularity = 0.3824 + $\frac{0.4292Area^{-115.092}}{542.744^{-115.092} + Area^{-115.092}}$	0.881
Feret Diameter vs. Area	Feret Diameter = $\frac{38.1158}{(1 + e^{(19.8949 - 0.0373 Area)})^{\frac{1}{25.5921}}}$	0.882
Aspect Ratio vs. Area	Aspect Ratio = 1.7963 + 0.099 cos(.0984Area – 6.8176)	0.169
Roundness vs. Area	Roundness = 0.5559 + 0.03 cos(0.03875Area + 2.7462)	0.177
Solidity vs. Area	Solidity = 0.983 + 0.00836 cos(0.0235Area + 8.9817)	0.462
Circularity vs. Perimeter	Circularity = 2.152 – 0.01166Perimeter + $\frac{2558}{Perimeter^2}$	0.963
Roundness vs. Perimeter	Roundness = 0.547 + 0.04 cos(0.0871Perimeter + 0.4945)	0.158
Aspect Ratio vs. Perimeter	Aspect Ratio = $e^{11.626 - \frac{195.75}{Perimeter}} - 1.96\ln(Perimeter)$	0.147
Solidity vs. Perimeter	Solidity = 0.977 + $\frac{0.0123Perimeter^{-8.51}}{88.6^{-8.51} + Perimeter^{-8.51}}$	0.410
Feret Diameter vs. Perimeter	Feret Diameter = $\frac{37.83}{(1 + e^{177.83 - 1.94Perimeter})^{1/134}}$	0.901
Roundness vs. Circularity (Circ)	Roundness = 0.949 + (1 – 0.949)[1 – $e^{1.82Circ - 58.7Circ^2 + 82.7Circ^3 - 41.68Circ^4}$ ]	0.763
Aspect Ratio vs. Circularity (Circ)	Aspect Ratio = 1.04 + (1 – 1.04)[1 – $e^{26Circ - 87.8Circ^2 + 128Circ^3 - 66.6Circ^4}$ ]	0.746
Solidity vs. Circularity	Solidity = 0.987 + .0049 cos(189Circularity – 2.629)	0.244
Feret Diameter vs. Circularity	Feret Diameter = 37.885 – 7.374e <sup>-0.0002Circ<sup>-34.287</sup></sup>	0.584
Aspect Ratio vs. Roundness	Roundness = $\frac{151.293}{(1 + \frac{Aspect\ Ratio}{0.0066})}$	0.999
Solidity vs. Roundness	Solidity = 0.987e <sup>-5025.24 – 1030.468Roundness</sup>	0.582
Feret Diameter vs. Roundness	Roundness = 0.538 + $\frac{1 - 0.538}{1 + e^{-66.594 + 20.208\ln(Feret\ Diameter)}}$	0.315
Solidity vs. Aspect Ratio (AR)	Solidity = $\frac{0.969 - 0.473AR}{1 - 0.497AR + 0.0046AR^2}$	0.568
Feret Diameter vs. Aspect Ratio (AR)	Feret Diameter = 278.281 cos(AR + 40.579) + 81.885 cos(2AR + 40.579) + 92.281 cos(3AR + 40.579)	0.347
Feret Diameter vs. Solidity	Feret Diameter = $\frac{(32.599)(5541785617429.7) + 37.474Solidity^{-1803.857}}{5541785617429.7 + Solidity^{-1803.857}}$	0.314

Table 4 Pairs of shape parameters and the model with the highest correlation coefficients and Root Mean Square Error (RMSE).

Related variables	Proposed model	R value	RMSE
Perimeter vs. Area	Sinusoidal Regression	0.897	21.583
Circularity vs. Area	DR. Hill. Regression	0.939	-----
Feret Diameter vs. Area	Richards Regression	0.939	2.869
Circularity vs. Perimeter	Heat capacity Regression	0.981	0.787
Feret Diameter vs. Perimeter	Richards Regression	0.949	33.359
Roundness vs. Circularity	DR multistage-4 Regression	0.873	0.440
Aspect Ratio vs. Circularity	DR multistage-4 Regression	0.864	0.182
Aspect Ratio vs. Roundness	Weibul Model Regression	0.999	0.060
Solidity vs. Area	Sinusoidal Regression	0.679	0.005
Solidity vs. Perimeter	DR Hill Regression	0.640	0.004
Feret Diameter vs. Circularity	Weibul Model Regression	0.764	2.65
Solidity vs. Roundness	Exponential Decline Regression	0.763	0.984
Solidity vs. Aspect Ratio	Gaussian Model Regression	0.753	1.366

Table 5 Color parameter average values.

	Chromaticity a*	Chromaticity b*	Value C	Value H	Luminosity L*
Mean	-9.059	14.592	17.234	121.930	47.084

Table 6 Summary of ANOVA *Opuntia cladodes* color parameters mean values.

Groups	Number	Sum	Means	Variance
Mean_a*	30	-266.94	-8.90	0.25
Mean_b*	30	461.56	15.39	1.96
Mean_C	30	531.15	17.70	2.24
Mean_H	30	3606.40	120.21	1.92
Mean_L*	30	1425.56	47.52	1.66

Table 7 ANOVA of *Opuntia cladodes* color parameters.

Source	SS	df	Ms	F	Probability	F <sub>Critical</sub>
Between	299150	4	74787.415	46541.39487	2.9711E-224	2.434
Within	233	145	1.607			
Total	299383	149				

Moreover, descriptive statistics were performed for the color variables; mean color parameters values in 30 cladodes (Table 5) and parameters such as mean, and variance were obtained (Table 6). The mean values were obtained, showing very little variability over time (Figure 5). An online program was used to visualize the measured L\*a\*b\* parameters, observing a high similarity to human eyesight (Figure 6). An analysis of variance (ANOVA) was also performed for the color parameters L\*, a\*, b\*, C, and H. The ANOVA analysis indicated highly significant

differences in the color variables at 1% confidence levels (Table 7). Subsequently, a correlation analysis was performed between the color parameters of *Opuntia cladodes* (Table 8) and finally, a nonlinear regression analysis was carried out using CurveExpert software (Hyams 2010), obtaining the equations and mathematical models. The correlation coefficient  $r^2$  and the nonlinear mathematical model were obtained, being the highest between a\* vs. C (0.999) as well as between b\* vs. H (0.821) (Table 9).



Table 8 Correlation matrix of *Opuntia* cladodes color parameters.

Correlation matrix					
	Mean_a*	Mean_b*	Mean_C	Mean_H	Mean L*
Mean_a*	1				
Mean_b*	-0.759	1			
Mean_C	-0.819	0.993	1		
Mean_H	0.222	-0.789	-0.723	1	
Mean_L*	-0.244	0.577	0.554	-0.672	1

Table 9 Mathematical models between *Opuntia* cladodes color parameters.

Related Variables	Mathematical Model	R <sup>2</sup>	RSME
a*-C	$a * = \frac{-2.341 * C}{1 + 0.292 * C - 0.00482 * C^2}$	0.999	0.403
b*-H	$b * = 16.59 + 2.356 * \cos(0.489 \cdot H + 87.914)$	0.821	1.176
C-b*	$C = 36.967e^{-e^{(0.963 - 0.0826b*)}}$	0.807	1.461
H-C	$H = 108.375e^{\left(\frac{1.823}{C}\right)}$	0.724	0.987
L*-H		0.682	0.860

Changes in the coloration of *O. ficus indica*, as well as the shapes and sizes of cladodes, are factors of interest to researchers. Here we presented a methodology using the freeware Image J, which it had not been used in *Opuntia* but has been used successfully for microscopy data extraction by Hartig (2013), as well as in cyst delineation for cyst/injury identification in dental studies by Veena Divya et al. (2016). On the other hand, Curve Expert software with good results in prediction models for runoff using rainfall as a single predictor obtaining r<sup>2</sup> of 95%, (Shah et al. 2017). In addition, Aponte (2017) estimated the productivity of *L. laevigatum* (biomass, carbon, and protein production) in the laboratory, establishing a logistic mathematical model with Curve Expert, and obtained an r<sup>2</sup> of 99%. These researchers obtained determination coefficients as to those we obtained using Curve Expert.

### Conclusions

The obtained results of the research show that image processing and linear and nonlinear modeling allowed to characterize the morphology and color of *O. ficus-indica* mature cladodes (Villanueva cultivar cladodes) of a year-old using ImageJ and CurveExpert freeware. Significant correlation coefficient values with a confidence level of 95% for the shape descriptors of the non-linear regression models were obtained between 8 pairs of parameters. From the color features, we obtained very good correlation coefficient values for a\* vs. C and b\* vs. H parameters.

The results of this research will be a helpful protocol for those who wish to carry out similar color and morphology characterization work with mature cladodes of different varieties or other seeds or products.

### Conflicts of Interest

Authors would hereby like to declare that there is no conflict of interests that could arise.

### Acknowledgment

We want to acknowledge the Faculty of Agronomy at the Autonomous University of Nuevo León and PAICYT UANL 2019 (CT696-19) for the financing granted for the development of this project, and to the Saltillo Institute of Technology for their support.

### References

- Ahmad, J., Jan, B., Farman, H., Ahmad, W., & Ullah, A. (2020). Disease detection in plum using convolutional neural network under true field conditions. *Sensors*, 20(19), 5569.
- Aponte, H. (2017). Productividad de *Limnium laevigatum* (Hydrocharitaceae) bajo condiciones de laboratorio. *Polibotánica*, 44, 157-166.
- Bober, M. (2001). MPEG-7 visual shape descriptors. *IEEE Transactions on circuits and systems for video technology*, 11(6), 716-719.

- Brewer, M., Lang, L., Fujimura, K., Dujmovic, N., Gray, S., & van der Knaap, E. (2006). Development of a controlled vocabulary and software application to analyze fruit shape variation in tomato and other plant species. *Plant Physiology*, *141*(1), 15-25.
- Chessa, I. (2010). Cactus pear genetic resources conservation, evaluation and uses. *FAO Cactusnet Newsletter, Special*, *12*, 43-53.
- Canseco-Guzmán, I. V., & Canseco-Guzmán, B. (2013). Manual práctico de cultivo de nopal verdura para los valles centrales y mixteca del Estado de Oaxaca.
- D'Silva, P., & Bhuvaneswari, P. (2015). Various shape descriptors in image processing—a review. *International Journal of Science and Research*, *4*(3), 2338-2342.
- Farina, G. H. (2020). Aplicación de filtros cromáticos en el espacio de color para la detección y medición de formas en plantas de soja. Doctoral dissertation, Universidad Nacional de Mar del Plata, Facultad de Ingeniería; Argentina.
- Grajeda-González, F., Contreras-Salazar, E. A., & Luna-Maldonado, A. I. (2015). Sistema de Procesamiento de Imágenes para Obtener los Parámetros del Color en Frutos de dos Variedades de Tomate.
- Gutiérrez, A. (2020). Caracterización morfológica de tres genotipos criollos promisorios de *Theobroma cacao* L., En Panamá. *Ciencia Agropecuaria*, *30*, 150-169.
- Hartig, S. M. (2013). Basic image analysis and manipulation in ImageJ. *Current Protocols in Molecular Biology*, *102*(1), 14-15.
- Hyams, D. (2010). Curve Expert basic. *Release 1.4*. Retrieved from <https://www.curveexpert.net>.
- Hyun J. II., Kim, H. K., & Oh, W. G. (2015). Study on performance of MPEG-7 visual descriptors for deformable object retrieval. In *2015 21st Korea-Japan Joint Workshop on Frontiers of Computer Vision (FCV)* (pp. 1-5). DOI: 10.1109/FCV.2015.7103701.
- Iwata, H., Niikura, S., Matsuura, S., Takano, Y., & Ukai, Y. (2004). Interaction between genetic effects and soil type in diallel analysis of root shape and size of Japanese radish (*Raphanus sativus* L.). *Breeding Science*, *54*(4), 313-318.
- Johnstone, J. (2019). LCH and Lab colour and gradient picker. Retrieved from <http://davidjohnstone.net/pages/lch-lab-colour-gradient-picker>.
- Laouadi, M., Mennah-Govela, Y. A., Moula, N., Moussiaux, N. A., & Kafidi, N. (2020). Morphological characterization of indigenous goats in the region of Laghouat in Algeria. *Archivos de Zootecnia*, *69*(267), 272-279.
- Leon, K., Mery, D., Pedreschi, F. & Leon, J. (2006). Color measurement in L\* a\* b\* units from RGB digital images. *Food Research International*, *39*(10), 1084-1091.
- McCaig, T. N. (2002). Extending the use of visible/near-infrared reflectance spectrophotometers to measure colour of food and agricultural products. *Food Research International*, *35*(8), 731-736.
- McGuire, R. G. (1992). Reporting of objective color measurements. *HortScience*, *27*(12), 1254-1255.
- Morales-Morales, A. E., Andueza-Noh, R. H., Márquez-Quiroz, C., Benavides-Mendoza, A., et al. (2019). Morphological characterization of cowpea (*Vigna unguiculata* L. Walp) seeds from the Yucatan Peninsula. *Ecosistemas y recursos agropecuarios*, *6*(18), 463-475.
- Newton, G., & Kendrick, B. (1990). Image processing in taxonomy. *Sydowia*, *42*, 246-272.
- Shah, M., Fazil, S. M., Ali, S. R., Pandey, Y., Faisal, S., & Mehraj, I. (2017). Modeling of runoff using curve expert for Dachigam-Telbal catchment of Kashmir valley, India. *Journal of Current Microbiology and Applied Sciences*, *6*(11), 3822-3826.
- SIAP (2021). Servicio de Información Agroalimentaria y Pesquera Producción Agrícola 2018, Ciclo: Ciclicos – Perennes, Modalidad: Riego + Temporal, Cultivo: Nopalitos. Retrieved from <https://nube.siap.gob.mx/cierreagricola/>, accessed on 15 July 2020.
- Veena Divya, K., Jatti, A., Joshi, R., & Meharaj, S. (2016). Image processing and parameter extraction of digital panoramic dental X-rays with ImageJ. In *International Conference on Computation System and Information Technology for Sustainable Solutions (CSITSS) 2016*, Bengaluru, India (pp. 450-454).
- Visa, S., Cao, C., Gardener, B. M., & van der Knaap, E. (2014). Modeling of tomato fruits into nine shape categories using elliptic fourier shape modeling and Bayesian classification of contour morphometric data. *Euphytica*, *200*(3), 429-439.
- Wirth, M. A. (2001). Shape analysis and measurement. University of Guelph. *CIS*, 6320.
- Žunić, J. (2010). Shape descriptors. University of Exeter, College of Engineering, Mathematics and Physical Sciences, Exeter EX4 4QF, U.K. and Mathematical Institute SANU, Knez Mihaila 36, Belgrade, Serbia, 2010.



## Journal of Experimental Biology and Agricultural Sciences

<http://www.jebas.org>

ISSN No. 2320 – 8694

### Relationship of altitude, individual seed weight, and kernel colonization by *Aspergillus flavus* with biochemical parameters of various Ethiopian groundnut (*Arachis hypogaea* L.) accessions

Yonas Syraji, Jeyaramraja P.R.\*

Department of Biology, College of Natural Sciences, Arba Minch University, Arba Minch, Ethiopia

Received – November 09, 2021; Revision – January 17, 2022; Accepted – April 27, 2022

Available Online – April 30, 2022

DOI: [http://dx.doi.org/10.18006/2022.10\(2\).344.358](http://dx.doi.org/10.18006/2022.10(2).344.358)

#### KEYWORDS

Individual seed weight  
Kernel Colonization  
Total carbohydrate  
Protein  
Total free amino acids

#### ABSTRACT

Groundnut is one of the five extensively grown oil crops of Ethiopia. Groundnut kernels contain 40-50% fat, 20-50% protein, and 10-20% carbohydrate and are rich in vitamin E, niacin, riboflavin, thiamine, folic acid, calcium, phosphorus, magnesium, zinc, iron, and potassium. This study aimed to determine individual seed weight, kernel colonization by *Aspergillus flavus*, and biochemical parameters in groundnut seeds collected from different areas of Ethiopia. Groundnut germplasm in the form of seeds was collected from the Ethiopian Biodiversity Institute (EBI), further information about each accession location and altitude was also collected from the institute. Parameters such as individual seed weight (ISW), kernel colonization by *A. flavus*, and biochemical parameters (i.e. total carbohydrate, protein, and total free amino acids) were measured in the groundnut seeds. A negative relationship between ISW and altitude ( $p < 0.01$ ) was observed in this study which indicates that an increase in altitude would result in a decrease in seed weight. A positive relationship between altitude with total carbohydrate ( $p < 0.01$ ) and with total free amino acids ( $p < 0.05$ ) was also observed. Low-ISW accessions exhibited significantly higher total carbohydrates while high-ISW accessions exhibited significantly higher total free amino acids in their seeds. Groundnut seeds of EBI accessions with 0% kernel colonization contained less total carbohydrate, and the accessions with 100% kernel colonization contained the highest total carbohydrates. Besides, total carbohydrates correlated positively with kernel colonization ( $p < 0.01$ ). So, it is postulated that high total carbohydrate makes groundnut seeds susceptible to *A. flavus* colonization.

\* Corresponding author

E-mail: [prjeyaramraja@yahoo.co.in](mailto:prjeyaramraja@yahoo.co.in) (Jeyaramraja P.R.)

Peer review under responsibility of Journal of Experimental Biology and Agricultural Sciences.

Production and Hosting by Horizon Publisher India [HPI]  
(<http://www.horizonpublisherindia.in/>).  
All rights reserved.

All the articles published by [Journal of Experimental Biology and Agricultural Sciences](#) are licensed under a [Creative Commons Attribution-NonCommercial 4.0 International License](#) Based on a work at [www.jebas.org](http://www.jebas.org).



## 1 Introduction

Groundnut (*Arachis hypogaea* L.) is one among the five extensively grown oil crops of Ethiopia (Wijnands et al. 2009). The crop is relatively new to Ethiopia and it was introduced from Eritrea to Hararghe in the early 1920s by the Italian explorers (Ahmed et al. 2016). The major groundnut producer region in Ethiopia is the Oromiya region (41,089 ha), followed by Benishangul-Gumuz (14,759 ha) and Amhara (3,161 ha) regional states (Ahmed et al. 2016). Under rain-fed conditions, it is generally grown and is utilized for extracting cooking oil, and also for confectionary in Ethiopia (Kudama 2013). Besides, this crop helps small-scale producers in getting significant revenue and also helps Ethiopia in getting foreign money earnings through export (Geleta et al. 2007).

Groundnut which is additionally referred to as peanut, earthnut, monkey nut, and goobers is an annual legume. It is one of the world's most important oilseed crops, ranking the 13<sup>th</sup> most important food crop and the 4<sup>th</sup> most important oilseed crop in the world is cultivated in more than 100 countries on six continents (Guchi 2015). Groundnut kernels contain 40-50% fat, 20-50% protein, and 10-20% carbohydrate and are rich in vitamin E, niacin, riboflavin, thiamine, folic acid, calcium, phosphorus, magnesium, zinc, iron, and potassium (Guchi 2015).

Groundnut plays a crucial role in the livelihoods of the poor farmers and the rural economy of many developing countries (Daniel 2009). Poor agricultural exercise and post-harvest treatments of groundnut can lead to an infection by mold fungus *Aspergillus flavus* and *A. parasiticus* releasing the poisonous substance called aflatoxins (Waliyar et al. 2006). The size of groundnut seeds is one important criterion that determines the market value of groundnut. In addition, the size of the seed is one characteristic that is important in selecting parent plants before a hybridization experiment is performed to get improved varieties with heterosis. Therefore, the study deals with an investigation of individual seed weight, kernel colonization by *A. flavus*, and biochemical parameters in groundnut seeds collected from different areas of Ethiopia. The results of the study are expected to form a foundation for further studies in the future on plant breeding/improvement programs.

## 2 Materials and Methods

### 2.1 Sample Collection

Seeds of 50 groundnut accessions were collected from the Ethiopian Biodiversity Institute (EBI), Addis Ababa. The accessions collected from EBI are landraces. Further information about each accession namely, locality of collection and altitude were also collected from EBI. These accessions belong to various

places out of 50 accessions 23 accessions belong to Babile woreda of Misrak Harerge zone in the Oromiya region, 17 accessions belong to Gursum woreda of Misrak Harerge zone in the Oromiya region, 9 accessions belong to Benishangul Gumuz region, Metekel Zone (7 from Guba woreda, 1 from Bulen woreda and 1 from Assosa woreda) and 1 accession belong to Benishangul Gumuz region, Kamash Zone, Blo Jiganifado woreda. Based on the sampling area a total of 50 groundnut accessions from EBI were used for this study.

### 2.2 Individual Seed Weight Determination

Individual seed weight (g) was calculated from 100 seed weight (g) as per the Jayaramraja and Woldeesenbet (2014) procedure.

### 2.3. Kernel Colonization by *Aspergillus flavus*

Kernel colonization was analyzed as per the method described by Arunyanark et al. (2009). Ten seeds from each accession were used for measuring *A. flavus* colonization. Seeds were surface-sterilized for 3 min in a 10% aqueous solution of Clorox (0.525% NaOCl), rinsed three times with sterile water, and placed on a moistened pre-sterilized paper towel in a sterile plastic box. After incubating for 7 days at 25°C, the number of *A. flavus* infected seeds having a greenish mold on the seed coat, was counted and the results were expressed in percent (%).

### 2.4 Analysis of Biochemical Parameters

#### 2.4.1 Estimation of Total Carbohydrates

Total carbohydrates in the seeds of groundnut accessions were measured by following the anthrone method described by Sadasivam and Manickam (2008). 100mg of powdered groundnut seeds were measured and transferred into a boiling tube. Hydrolysis was done by keeping it in a boiling water bath for 3 hours with 5 ml of 2.5 N HCl and then, it was cooled to room temperature. It was then, neutralized with solid sodium carbonate until the effervescence ceased. The volume was made up to 100 ml and then, centrifuged. The supernatant was collected and, 0.5 and 1 ml aliquots were taken for analysis. Standards were prepared by taking 0, 0.2, 0.4, 0.6, 0.8, and 1 ml of the working standard. Here "0" serves as blank. The volume was made up to 1 ml in all the tubes including the sample tubes by adding distilled water. All the tubes were kept on ice and then, 4 ml of ice-cold anthrone reagent was added. All the tubes were heated for 8 minutes in a boiling water bath. Then, the tubes were cooled rapidly and read the green to dark color at 630 nm using a UV-VIS spectrophotometer (RS-295). A standard graph was drawn by plotting the concentration of the standard on the X-axis versus absorbance on the Y-axis. From the graph, the amount of carbohydrate present in the sample tube was calculated.

#### 2.4.1.1 Standard

100mg of glucose was dissolved in 100 ml distilled water in a conical flask. 10ml of this stock standard was taken and diluted to 100 ml of distilled water in another volumetric flask for a working standard solution. A standard curve was drawn using absorbance versus concentration. Total carbohydrate present in the sample was expressed as mg carbohydrate in 100 mg sample (in other words, percent equivalent of glucose).

#### 2.4.2 Estimation of Protein

Soluble proteins in the seeds of groundnut accessions were measured by following Lowry's method described by Sadasivam and Manickam (2008). For this, 500mg of groundnut seeds were peeled and ground with a grinder. To this homogenate, 5ml of buffer was added. This was centrifuged and the supernatant was used for protein estimation. 0, 0.2, 0.4, 0.6, 0.8, and 1ml of the working standard were pipetted out into a series of test tubes. 0.1 ml and 0.2ml of the sample extracts were pipetted out in two other test tubes. The volume was made up to 1ml in all the test tubes. A tube with 1ml of water serves as the blank. 5ml of the alkaline copper solution was added to each tube including the blank, mixed well, and allowed to stand for 10min. Then, 0.5ml of Folin-Ciocalteu reagent was added, rapidly mixed well, and incubated at room temperature in the dark for 30min. The blue color was developed. Readings were taken at 660nm using a UV-VIS spectrophotometer (RS-295). A standard graph was drawn and the amount of protein in the sample was calculated.

#### 2.4.2.1 Standard

50mg of bovine serum albumin was dissolved in 50ml distilled water in a conical flask. 10ml of this stock standard was taken and diluted to 50ml of distilled water in another volumetric flask for a working standard solution. A standard curve was drawn using absorbance versus concentration. The amount of protein was expressed as mg protein/100 mg sample (in other words, percent equivalent of BSA).

#### 2.4.3 Estimation of Total Free Amino Acids

Total free amino acids in the seeds of groundnut accessions were measured by following the method described by Sadasivam and Manickam (2008). For this, 500mg of the powdered groundnut seeds were weighed and ground with a grinder. To this homogenate, 5ml of hot 80% ethanol was added. This was centrifuged and the supernatant was used for amino acids estimation. To 0.1ml of extract, 1ml of ninhydrin solution was added. The volume was made up to 2ml with distilled water. The tube was heated in a boiling water bath for 20min. Then, 5ml of the diluent was added and the contents were mixed. After 15min, the intensity of the purple color was read against a reagent blank in

a colorimeter at 570nm using a UV-VIS spectrophotometer (RS-295). The reagent blank was prepared as above by taking 0.1ml of 80% ethanol instead of the extract.

#### 2.4.3.1 Standard

50 mg leucine was dissolved in 50 ml of distilled water in a volumetric flask. 10 ml of this stock standard was taken and diluted to 100 ml in another volumetric flask for a working standard solution. A standard curve was drawn using absorbance versus concentration. The concentration of the total free amino acids in the sample was found out and expressed as the percent equivalent of leucine (in other words, mg amino acids/100 mg sample).

### 2.5 Statistical Analysis

The data were subjected to statistical analysis using WASP (WEB AGRI STAT PACKAGE Version 2.0), developed by Ashok Kumar Jangam and Pranjali Thali, ICAR Research Complex for Goa, India. Critical difference (CD) values were computed at 0.05 and 0.01 levels to find out whether statistically significant differences existed among the treatments in terms of studied parameters. Correlation coefficient (r) values were computed to find out the relationships among the studied parameters.

## 3 Results and Discussions

### 3.1 Classification of EBI Accessions Based on Altitude of Cultivation

The accessions collected from EBI were classified based on the altitude of cultivation to study the relationship between each studied parameter. To classify the accessions based on altitude, the "Quantiles Classification" method was used in essence. All the accessions were first ranked from lowest to highest altitudes. After ranking, the first 13 accessions (from 554 to 1480 meters) are regarded as "low-altitude" accessions, and the last 13 accessions (from 1699 to 1898 meters) are regarded as "moderate-altitude" accessions. These are presented in Table 1. Of the 13 "low-altitude" accessions, 9 accessions belong to the Benishangul Gumuz region and 4 accessions belong to the Oromiya region. All the "moderate-altitude" accessions belong to the Oromiya region, the Misrak Harerge zone.

### 3.2 Analysis of Individual Seed Weight and Kernel Colonization in EBI Accessions

Since EBI provided only 40 seeds for each accession, individual seed weight (ISW) was calculated from 40 seeds weight (g). Data on ISW and kernel colonization by *A. flavus* in EBI accessions belonging to the Oromiya region, Misrak Harerge zone, and Benishangul Gumuz region are presented in Tables 2 and 3, respectively.

Table 1 Classification of groundnut accessions collected from EBI based on altitude

Low-altitude accessions					
S.N.	Accession no.	Altitude (meter)	Region	Zone	Woreda
1	23523	554	Benishangul Gumuz	Metekel	Guba
2	23522	559			
3	23524	601			
4	23521	614			
5	23529	808			
6	23525	837			
7	23528	850			
8	29488	1227			
9	29572	1288	Oromiya	MisrakHarerge	Babile
10	29573	1350			
11	29574	1350			
12	19755	1459			
13	23531	1480	Benishangul Gumuz	Metekel	Bulen
Moderate-altitude accessions					
S.N.	Accession no.	Altitude (meter)	Region	Zone	Woreda
1	19752	1699	Oromiya	MisrakHarerge	Babile
2	19747	1700			
3	19748	1709			
4	19749	1709			
5	19750	1744			
6	19766	1753			
7	19767	1753			Gursum
8	19764	1762			
9	19765	1765			
10	19763	1805			
11	19762	1839			
12	19760	1898			
13	19761	1898			

The accession no. 29572 which belongs to the Oromiya region, Misrak Harerge Zone, Babile woreda, had very low ISW (0.417 g). The accession no. 23531 and 23521 which belong to the Benishangul Gumuz region, Metekel Zone, Bulen, and Guba woreda respectively registered very high ISW (0.788 g). Groundnut seed size was found to be highly correlated with seed weight and both traits contributed significantly to yield gains (Chiw and Wynne 1983). High ISW is due to the larger seed size.

According to Kabbia et al. (2017) development of groundnut genotypes with a large seed size and seed weight and improved seed, quality attracts consumers' immediate attention. Nautiyal (2002) noted that seed size is another important characteristic that also determines both quality and value. In confectionary type groundnut, there are some important trade attributes. In developing new varieties with quality characteristics for confectionary products seed size is one of the important traits (Amarasinghe et al. 2016).

Table 2 Individual seed weight and Kernel colonization by *A. flavus* in the groundnut accessions from Oromiya region, Misrak Harerge zone

Region, Zone	Woreda	Accession no.	Individual seed weight (g)	Kernel colonization (%)
Oromiya region, Misrak Harerge Zone	Babile	19739	0.519	20
		19740	0.591	10
		19741	0.580	30
		19742	0.525	100
		19743	0.585	90
		19745	0.621	100
		19746	0.580	20
		19747	0.666	30
		19748	0.663	10
		19749	0.584	20
		19750	0.660	0
		19751	0.704	10
		19752	0.555	20
		19753	0.589	20
		19754	0.623	0
		19755	0.626	60
		19756	0.562	10
		19757	0.599	40
	19758	0.516	10	
	19759	0.591	20	
	29572		0.417	10
	29573		0.569	10
	29574		0.522	10
	19760	Gursum	0.553	0
	19761		0.528	10
	19762		0.578	10
	19763		0.550	0
	19764		0.609	10
	19765		0.505	50
	19766		0.571	50
	19767		0.612	30
	19768		0.606	70
	19769		0.472	10
	19770		0.570	50
	19771		0.522	70
	19772		0.478	30
19773	0.540		10	
19774	0.531		10	
19775	0.506		0	
19776	0.563		10	

Table 3 Individual seed weight and Kernel colonization by *A. flavus* in the groundnut accessions from Benishangul Gumuz region

Region, Zone	Woreda	Accession no.	Individual seed weight (g)	Kernel colonization (%)
Benishangul Gumuz region, Metekel Zone	Guba	23521	0.788	0
		23522	0.586	30
		23523	0.594	0
		23524	0.738	0
		23525	0.776	0
		23528	0.644	0
		23529	0.697	0
	Bulen	23531	0.788	0
Benishangul Gumuz region, Kamash Zone	Assosa	23532	0.457	10
	Blo Jiganifado	29488	0.531	0

Table 4 Classification of groundnut accessions collected from EBI based on individual seed weight

Low-individual seed weight accessions						
S.N.	Accession no.	Individual seed weight (g)	Region	Zone	Woreda	
1	29572	0.417	Oromiya	MisrakHarerge	Babile	
2	23532	0.457	Benishangul Gumuz	Metekel	Assosa	
3	19769	0.472	Oromiya	MisrakHarerge	Gursum	
4	19772	0.478				
5	19765	0.505				
6	19775	0.506				
7	19758	0.516				
8	19739	0.519				
9	29574	0.522				
10	19771	0.522	Oromiya	MisrakHarerge	Gursum	
11	19742	0.525			Babile	
12	19761	0.528			Gursum	
13	19774	0.531				
High-individual seed weight accessions						
S. N.	Accession no.	Individual seed weight (g)	Region	Zone	Woreda	
1	19745	0.621	Oromiya	MisrakHarerge	Babile	
2	19754	0.623				
3	19755	0.626				
4	23528	0.644	Benishangul Gumuz	Metekel	Guba	
5	19750	0.66	Oromiya	MisrakHarerge	Babile	
6	19748	0.663				
7	19747	0.666				
8	23529	0.697				
9	19751	0.704	Oromiya	MisrakHarerge	Babile	
10	23524	0.738	Benishangul Gumuz	Metekel	Guba	
11	23525	0.776				
12	23521	0.788				
13	23531	0.788				Bulen



To study the influence of ISW on other studied parameters, the accessions collected from EBI were classified based on ISW by the “Quantiles Classification” method. All the accessions were first ranked from lowest to highest individual seed weight. After ranking, the first 13 accessions (from 0.417 to 0.531g) are regarded as “low-ISW” accessions, and the last 13 accessions (from 0.621 to 0.788g) are regarded as “high-ISW” accessions. These are presented in Table 4. Of the 13 “low-ISW” accessions, 12 accessions belong to the Oromiya region, Misrak Harerge zone while among the 13 “high-ISW” accessions, 7 accessions belong to the Oromiya region, Misrak Harerge zone while the remaining 6 accessions belong to Benishangul Gumuz region, Metekel Zone.

Kernel colonization (%) values ranged from 0 to 100 (Tables 2 and 3). To study the effect of kernel colonization on other studied parameters, the groundnut accessions were classified based on kernel colonization. All the accessions were first ranked from lowest to highest kernel colonization values and then, a few representative accessions are picked up from each kernel colonization value randomly (Figure 1). It is interesting to note that out of the 10 accessions collected from the Benishangul Gumuz

region, 8 accessions showed 0 % kernel colonization (Table 3). On the other hand, out of the 40 accessions collected from the Oromiya region, Misrak Harerge zone, only 5 accessions showed 0 % kernel colonization (Table 2).

### 3.3 Relationship among Altitude, Individual Seed Weight and Kernel Colonization in the EBI Accessions

Table 5 shows statistically significant ( $p < 0.01$ ) negative relationship between ISW and altitude ( $r = -0.415$ ). This indicates that as altitude increases, the seed weight decreases. Thus, groundnut cultivation in low-altitude areas is preferable. Altitude has a negative relationship with temperature. In the studies conducted by Haile and Keith (2017) the optimum temperature for growing groundnut is between 25-30° C. Temperature above 35°C is detrimental to groundnut production. Under lower temperatures the germination is delayed; the delay in germination exposes the seeds to soil pathogen attack for a longer period. Below 17°C, crop growth almost ceases. Cooler temperatures, especially at night, will also delay harvesting. Groundnut should not be grown in areas more than 1,500 meters above sea level as the temperature is likely to be low for groundnut.

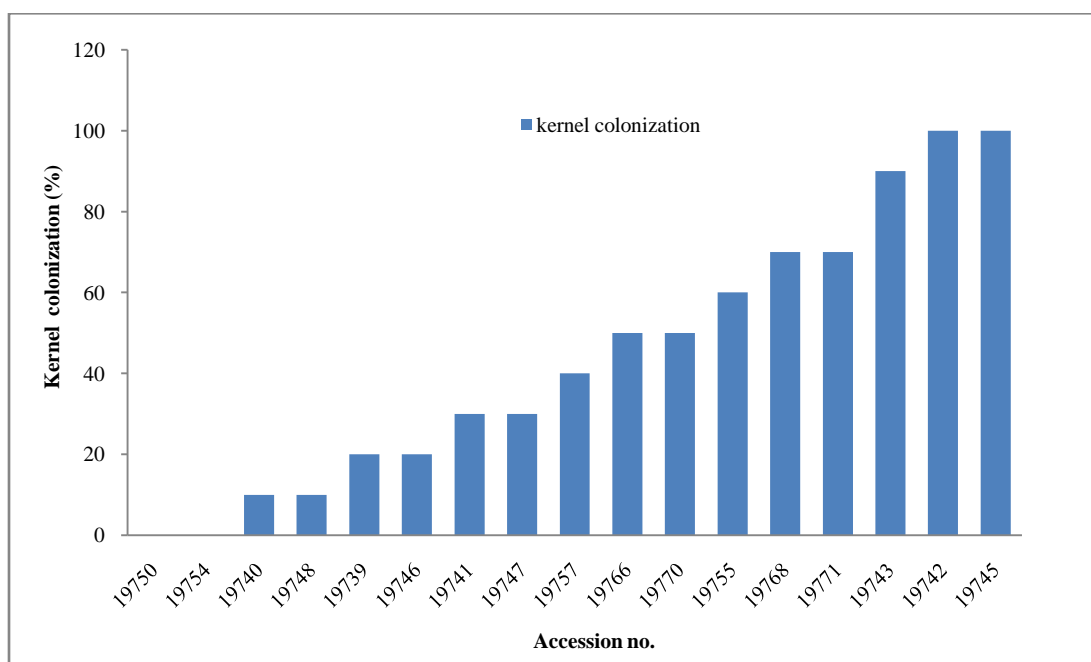


Figure 1 Few representative EBI groundnut accessions with varying levels of kernel colonization values

Table 5 Linear relationship of altitude with individual seed weight and kernel colonization, using data obtained from EBI groundnut accessions

Y	Correlation coefficient (r)	a	b	n
Individual seed weight (g)	-0.415**	0.7254	-0.00009	48
Kernel colonization (%)	0.254*	-0.0607	0.0002	48

\*\* $p < 0.01$ ; \* $p < 0.1$ ; Regression formula  $Y = a + bX$ , where X is altitude, and a and b are regression constants; n is the number of observations

A positive relationship was found between kernel colonization and altitude ( $r = 0.254$ ), which is weakly significant at  $p < 0.1$ . This indicates that with an increase in altitude, there may be an increase in kernel colonization by *A. flavus*.

### 3.4 Analysis of Biochemical Parameters in EBI Groundnut Accessions

Biochemical parameters content namely total carbohydrates, total free amino acids, and protein, were measured in EBI groundnut accessions of different categories *viz.* (a) “low-altitude” accessions vs. “moderate-altitude” accessions, (b) “low-ISW” accessions vs.

“high-ISW” accessions, (c) few representative accessions picked up from each kernel colonization value.

To study the effect of altitude, ISW, and kernel colonization on the biochemical parameter, the biochemical parameter were measured only in the above categories of groundnut accessions. The standard graphs used for the calculation of total carbohydrate, protein, and total free amino acid in the groundnut samples are presented in Figures 2, 3, and 4. Data on total carbohydrate, protein, and total free amino acids in various categories of EBI groundnut accessions are shown in Tables 6, 7, and 8.

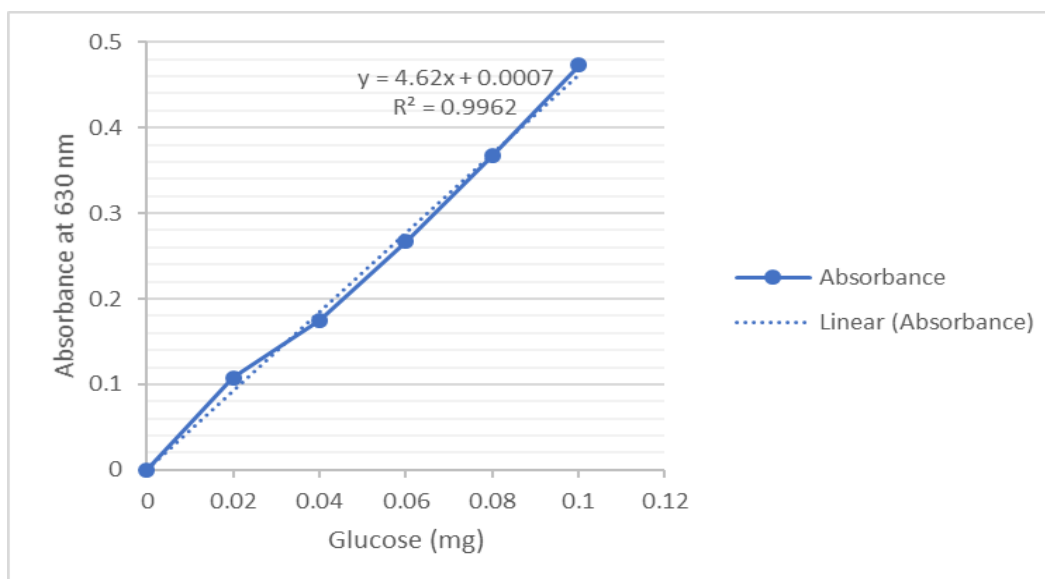


Figure 2 Standard graph used for total carbohydrate estimation

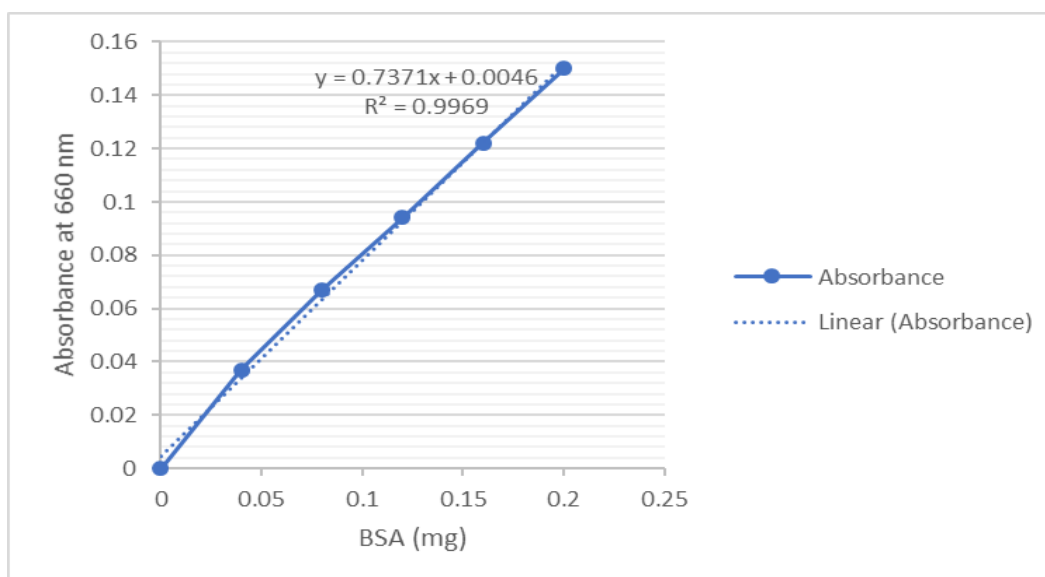


Figure 3 Standard graph used for protein estimation

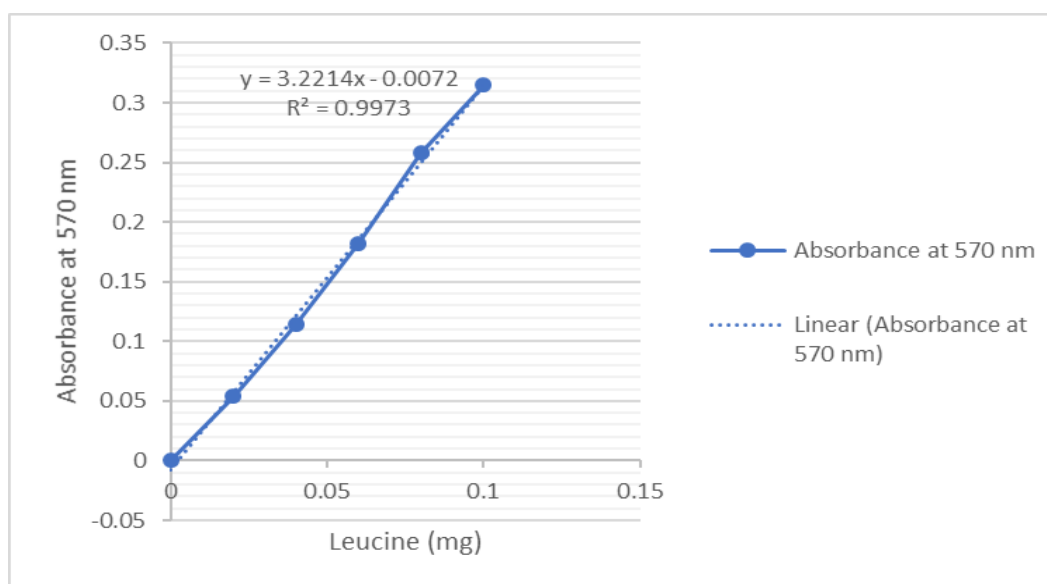


Figure 4 Standard graph used for the estimation of total free amino acids

Total carbohydrate was found to be the highest in the accession 19745 (21.9 %) which belongs to the Oromiya region, Misrak Harerge Zone, Babile woreda, and the lowest in the accession 23521 (7.02 %) that belongs to Benishangul Gumuz region, Metekel Zone, Guba woreda. Groundnut seeds are reported to contain 9.5 to 19.0% total carbohydrates as both soluble and insoluble carbohydrates (Abdel 1982; Woodroof 1983). Carbohydrate content ranging from 6.0 to 24.9% was reported by Duke (1981) in groundnut. Adedeji and Onyema (2019) noticed a total carbohydrate content of 8.2 % in groundnut kernels.

In the two accessions from the Oromiya region, Misrak Harerge Zone, one accession 19768 which belongs to Gursum woreda contained the highest protein (39.5 %), while the other accession 19758 which belongs to Babile woreda contained the lowest protein (16.8 %). Yaw et al. (2008) while studying the chemical composition of groundnut landraces of Ghana observed that the crude protein of the seeds ranged from 18.92 to 30.53%. In the two accessions from the Oromiya region, Misrak Harerge Zone, one accession 19750 belonging to Babile woreda possessed the highest total free amino acids (6.9 %), while the other accession 19771 belonging to Gursum woreda had the lowest total free amino acids (0.37 %).

Table 6 shows the biochemical parameters analyzed in low Vs. moderate altitude groundnut accessions, collected from EBI. Moderate-altitude accessions exhibited significantly ( $p < 0.01$ ) higher total carbohydrate (13.26 %) in their seeds than the low-altitude accessions (10.20 %). Bresson et al. (2009) provided evidence for an altitudinal increase in photosynthetic capacity. Their study showed that the maximum assimilation rate ( $A_{max}$ ) increases significantly with increasing elevation. Hence, it can be

understood that an increase in carbohydrates at high altitudes may be due to an increase in photosynthetic rate.

However, in the case of protein, no significant differences were found to exist between low-altitude accessions and moderate-altitude accessions. According to Suranto et al. (2015), no significant relationship between the contents of protein and the environmental conditions, such as the altitudes, soil pH, temperature, relative humidity, or even soil moisture. On the contrary, Berry and Bjorkman (1980) reported that the plants grown under the low temperature of high altitudes contain a greater amount of proteins including rubisco.

Moderate-altitude accessions exhibited significantly ( $p < 0.05$ ) higher total free amino acids (3.22 %) in their seeds than the low-altitude accessions (1.72 %). Nautiyal (2002) inferred that the increase in the amount of amino acids at higher altitudes could be an adaptational metabolic modification of temperate plant species to high altitudes. Melesse et al. (2012) reported that amino acid concentrations in *Moringa stenopetala* leaves at mid-elevation were higher than those at low elevation, except for aspartic acid, phenylalanine, and serine.

Biochemical parameters analyzed in low Vs. high-ISW groundnut accessions, collected from EBI are shown in Table 7. Low-ISW accessions exhibited significantly ( $p < 0.05$ ) higher total carbohydrate (14.51%) in their seeds than the high ISW accessions (11.22 %). Pattee et al. (1981) reported that carbohydrate concentration was generally highest for the smallest seed size. In addition, immature seeds have higher sugar content than mature seeds (Manda et al. 2004). These observations are in agreement with the results of the present study.

Table 6 Biochemical parameters in low- Vs. moderate-altitude groundnut accessions, collected from EBI

Low-altitude accessions				
S.N.	Accession no.	Carbohydrate (mg/100g)	Protein (mg/100g)	Amino acid (mg/100g)
1	23523	11.61	25.61	1.59
2	23522	11.00	26.82	1.49
3	23524	8.64	24.91	2.04
4	23521	7.02	31.76	1.64
5	23529	10.64	25.45	1.90
6	23525	9.94	26.33	2.29
7	23528	8.32	22.53	2.27
8	29488	11.13	22.17	0.76
9	29572	13.56	28.95	0.47
10	29573	7.75	29.12	2.28
11	29574	12.08	29.98	0.82
12	19755	10.05	23.89	3.78
13	23531	10.84	22.47	1.03
	Mean	10.20	26.15	1.72
Moderate-altitude accessions				
S. N.	Accession no.	Carbohydrate (mg/100g)	Protein (mg/100g)	Amino acid (mg/100g)
1	19752	11.24	20.98	3.33
2	19747	10.78	26.02	3.64
3	19748	12.90	21.78	5.85
4	19749	10.88	23.56	4.19
5	19750	12.18	23.15	6.89
6	19766	17.41	29.90	1.28
7	19767	12.91	25.90	1.17
8	19764	15.99	27.59	4.56
9	19765	11.89	23.57	1.37
10	19763	11.53	24.06	1.28
11	19762	15.34	28.46	3.12
12	19760	17.49	25.76	2.42
13	19761	11.78	20.38	2.75
	Mean	13.26	24.70	3.22
Statistical significance				
Between "low-altitude" & "moderate-altitude" accessions				
	CD (0.01)	2.38	NS	NS
	CD (0.05)	1.76	NS	1.16
	CV (%)	18.5	11.73	57.57

Values are means of triplicates

Table 7 Biochemical parameters in low Vs. high-individual seed weight groundnut accessions, collected from EBI

Low-individual seed weight accessions				
S. N.	Accession no.	Carbohydrate (mg/100g)	Protein (mg/100g)	Amino acid (mg/100g)
1	29572	13.55	28.95	0.47
2	23532	13.30	21.44	0.51
3	19769	14.60	32.52	1.43
4	19772	13.53	26.73	0.61
5	19765	11.89	23.57	1.37
6	19775	18.96	27.22	2.26
7	19758	14.45	16.79	3.70
8	19739	15.47	26.86	3.76
9	29574	12.08	29.98	0.82
10	19771	14.83	23.95	0.37
11	19742	21.05	23.69	4.11
12	19761	11.78	20.38	2.75
13	19774	13.12	31.31	1.75
Mean		14.51	25.64	1.84
High-individual seed weight accessions				
S. N.	Accession no.	Carbohydrate (mg/100g)	Protein (mg/100g)	Amino acid (mg/100g)
1	19745	21.89	21.49	4.20
2	19754	8.44	29.20	1.34
3	19755	10.05	23.89	3.78
4	23528	8.24	22.53	2.27
5	19750	12.12	23.15	6.89
6	19748	12.92	21.78	5.85
7	19747	10.77	26.02	3.64
8	23529	10.56	25.45	1.90
9	19751	14.52	20.19	4.14
10	23524	8.60	24.91	2.04
11	23525	9.90	26.33	2.29
12	23521	7.01	31.76	1.64
13	23531	10.84	22.47	1.03
Mean		11.22	24.55	3.16
Statistical significance				
Between "low-ISW" & "high-ISW" accessions				
	CD (0.01)	NS	NS	NS
	CD (0.05)	2.67	NS	1.284
	CV (%)	25.71	15.769	63.55

Values are means of triplicates

No significant differences existed between low ISW accessions and high ISW accessions, in terms of protein. On the contrary, Prathiba and Reddy (1994) reported that the protein content of small seed varieties of groundnut was high compared to bold seeded varieties. However, it has to be noted that Prathiba and Reddy (1994) worked with only seven groundnut varieties from ICRISAT (International Crops Research Institute for the Semi-Arid Tropics) to arrive at their conclusion while the present investigation dealt with 26 EBI accessions (Table 7).

High ISW accessions exhibited significantly ( $p < 0.05$ ) higher total free amino acids (3.16 %) in their seeds than the low ISW accessions (1.84 %). These results are contradictory to the findings of Prathiba and Reddy (1994) who reported that amino acid composition has no relationship with seed size in groundnut. Again here, it has to be noted that Prathiba and Reddy (1994) worked with only seven groundnut varieties while the present study examined 26 groundnut accessions.

Table 8 illustrates biochemical parameters in EBI groundnut accessions with varying levels of kernel colonization. Statistically significant differences were found to exist among the mean values of biochemical parameters namely, total carbohydrate ( $p < 0.05$ ), protein ( $p < 0.01$ ), and total free amino acids ( $p < 0.01$ ) analyzed in EBI accessions with varying levels of kernel colonization. It was observed that seeds of EBI accessions with zero kernel colonization contained less total carbohydrate, and the accessions with 100 % kernel colonization contained the highest total carbohydrate. Hence, it can be inferred that the high carbohydrate content in groundnut kernels makes them susceptible to *A. flavus* colonization. Sugars are found in soil and glucose is used by most fungi as a source of carbon and energy. Several authors have reported that the genera *Fusarium*, *Aspergillus*, and *Penicillium* use glucose in different metabolic processes (Beyer et al. 2004; Daynes et al. 2008; Olsson et al. 1994; Panagiotou et al. 2008). In most fungi, glucose plays a central role in metabolism (Carlile et al. 2001).

Table 8 Biochemical parameters in EBI groundnut accessions with varying levels of kernel colonization

S. N.	Accession no.	Kernel colonization (%)	Carbohydrate (mg/100g)	Mean Carbohydrate	Protein (mg/100g)	Mean Protein	Amino Acid (mg/100g)	Mean Amino acid
1	19750	0	12.12	10.28	23.15	26.18	6.89	4.11
2	19754		8.44		29.20		1.34	
3	19740	10	13.31	13.12	24.88	23.33	4.96	5.41
4	19748		12.92		21.78		5.85	
5	19739	20	15.47	15.01	26.86	24.79	3.76	3.86
6	19746		14.56		22.72		3.97	
7	19741	30	15.32	13.05	23.57	24.79	4.24	3.94
8	19747		10.78		26.02		3.64	
9	19757	40	14.30	14.3	17.09	17.09	3.48	3.48
10	19766	50	17.41	15.39	29.90	29.15	1.28	1.27
11	19770		13.38		28.40		1.27	
12	19755	60	10.05	10.05	23.89	23.89	3.78	3.78
13	19768	70	17.16	15.99	39.49	31.72	1.20	0.78
14	19771		14.83		23.95		0.37	
15	19743	90	11.33	11.33	21.21	21.21	3.96	3.96
16	19742	100	21.05	21.47	23.69	22.59	4.11	4.15
17	19745		21.89		21.49		4.20	
Statistical significance								
Between the mean values of biochemical parameters in accessions with different kernel colonization values								
			CD (0.01)	NS	7.414	1.951		
			CD (0.05)	5.53	5.547	1.464		
			CV (%)	32.98	18.921	36.63		

Values are means of triplicates

Table 9 Relationships among biochemical parameters in EBI groundnut accessions

Relationship between	r	Significant at	n
Altitude (m) vs. total carbohydrate (%)	0.522	1%	43
Altitude (m) vs. total free amino acids (%)	0.316	5%	43
Individual seed weight (g) vs. total carbohydrate (%)	-0.399	1%	45
Kernel colonization (%) vs. total carbohydrate (%)	0.489	1%	45
Protein (%) vs. total free amino acids (%)	-0.413	1%	45

r = is correlation coefficient and n = is number of observations

### 3.5 Relationships among Biochemical Parameters in EBI Groundnut Accessions

Linear relationships among biochemical parameters in EBI groundnut accessions are shown in Table 9. Altitude had a significantly positive relationship with total carbohydrate ( $p < 0.01$ ), and with total free amino acids ( $p < 0.05$ ). An increase in altitude increases total carbohydrate and total free amino acids in EBI groundnut accessions. These observations are in line with the observation that moderate-altitude accessions had higher total carbohydrate and total free amino acids than the low-altitude accessions (Table 6).

Total carbohydrate was found to correlate positively with kernel colonization ( $p < 0.01$ ). An increase in carbohydrates increases the chances of kernels being colonized by *A. flavus*. That's why, accessions with zero kernel colonization had fewer carbohydrates, and the accessions with 100 % kernel colonization had the highest carbohydrate (Table 8). It has also to be noted that accessions with high ISW showed less total carbohydrate and *vice versa*, as shown in Table 9. This is the reason for the negative relationship ( $p < 0.01$ ) between individual seed weight and total carbohydrates (Table 9). On the contrary, a positive correlation between sugar content and seed size ( $r = 0.56$ ) was observed by Prathiba and Reddy (1994) who worked with only seven groundnut varieties. Nayak et al. (2020) observed a positive relationship between seed size with crude protein content, but not with any other nutritional traits under study in their investigation employing 60 groundnut genotypes.

Significant ( $p < 0.01$ ) negative relationship has been established between protein and total free amino acids. This observation is supported by the findings of Pfarr et al. (2018) who reported that amino acids such as lysine, methionine, cysteine, tryptophan, and threonine are negatively correlated with soybean seed protein concentration.

### Conclusions

A negative relationship between ISW and altitude ( $p < 0.01$ ) observed in this study indicated that an increase in altitude would result in a decrease in seed weight. A positive relationship between

kernel colonization and altitude ( $p < 0.1$ ) observed in this study indicated that an increase in altitude would increase kernel colonization. Since total carbohydrate correlated positively with kernel colonization ( $p < 0.01$ ), it is postulated that high total carbohydrate makes groundnut seeds susceptible to *A. flavus* colonization. Altitude had a significantly positive relationship with total carbohydrate ( $p < 0.01$ ), and with total free amino acids ( $p < 0.05$ ). Total carbohydrate was found to correlate positively with kernel colonization ( $p < 0.01$ ). Total carbohydrate was found to correlate positively with kernel colonization ( $p < 0.01$ ). A negative relationship ( $p < 0.01$ ) between individual seed weight and total carbohydrate was observed. A significant ( $p < 0.01$ ) negative relationship has been established between protein and total free amino acids.

### References

- Abdel, R. (1982). Changes in chemical composition of peanut during development and ripening. *Rivista Italiana Delle Sostanze Grasse*, 59 (6), 285-286.
- Ahmed, M., Mesfin, H., Abady, S., Mesfin, W., & Kebede, A. (2016). Adoption of improved groundnut seed and its impact on rural households' welfare in Eastern Ethiopia. *Cogent Economics & Finance*, 4 (1), 1268747.
- Adedeji, O.J., & Onyema, O.A. (2019). Assessments of lipids contents, carbohydrates contents, protein contents and mineral elements compositions of the seeds and seedlings of germinating groundnut (*Arachis hypogaea*. L). *International Journal of Research and Scientific Innovation*, VI (V), 62-68.
- Amarasinghe, Y., Withanawasam, M., Amarasekara, D., Wijesinghe, G., Pushpakumara, R., & Premathilake, K. (2016). Genetic variability and heritability estimates in large seeded groundnut (*Arachis hypogaea* L.) genotypes. *Plant Gene and Trait*, 7 (15), 1-4
- Arunyanark, A., Jogloy, S., Wongkaew, S., Akkasaeng, C., et al. (2009). Association between aflatoxin contamination and drought tolerance traits in peanut. *Field Crops Research*, 114, 14-22.

- Berry, J., & Bjorkman, O. (1980). Photosynthetic response and adaptation to temperature in higher plants. *Annual Review of Plant Physiology*, 31 (1), 491-543.
- Beyer, M., Röding, S., Ludewig, A., & Verreet, J. (2004). Germination and survival of *Fusarium graminearum* macroconidia as affected by environmental factors. *Journal of Phytopathology*, 152, 92-97.
- Bresson, C., Kowalski, A., Kremer, A., & Delzon, S. (2009). Evidence of altitudinal increase in photosynthetic capacity: gas exchange measurements at ambient and constant CO<sub>2</sub> partial pressures. *Annals of Forest Science*, 66, 505.
- Carlile, M., Watkinson, S., & Gooday, G. (2001). *The Fungi*. London: Academic Press. pp. 588.
- Chiow, H., & Wynne, J. (1983). Heritabilities and genetic correlations for yield and quality traits of advanced generations in a cross of peanut. *Peanut Science*, 10, 13-17.
- Daniel, E. (2009). Groundnut research. In *Presentation for Workshop* (pp. 1-3). Werer Agricultural Research Center, Ethiopia.
- Daynes, C., McGee, P., & Midgley, D. (2008). Utilisation of plant cell-wall polysaccharides and organic phosphorus substrates by isolates of *Aspergillus* and *Penicillium* isolated from soil. *Journal of Ecology*, 1, 94-98.
- Duke, J. (1981). *Handbook of legumes of world economic importance*. Plenum Press, New York.
- Geleta, T., Purshotum, K.S., Wijnand, J.S., & Tana, T. (2007). Integrated management of groundnut root rot using seed quality and fungicide seed treatment. *International Journal of Pest Management*, 53 (1), 53-57.
- Guchi, E. (2015). Aflatoxin contamination in groundnut (*Arachis hypogaea* L.) caused by *Aspergillus species* in Ethiopia. *Journal of Applied and Environmental Microbiology*, 3 (1), 11-19.
- Haile, D., & Keith, S. (2017). *Groundnut cropping guide*. Africa Soil Health Consortium, Nairobi.
- Jeyaramraja, P.R., & Woldesenbet, F. (2014). Characterization of yield components in certain groundnut (*Arachis hypogaea* L.) varieties of Ethiopia. *Journal of Experimental Biology and Agricultural Sciences*, 2(6), 592-596.
- Kabbia, M., Akromah, R., Asibuo, J., Conteh, A., & Kamara, E. (2017). Inheritance of seed quality traits in groundnut (*Arachis hypogaea* L.). *International Journal of Development and Sustainability*, 6 (8), 526-544.
- Kudama, G. (2013). Economics of Groundnut Production in East Hararghe Zone of Oromia Regional State, Ethiopia. *Science, Technology & Arts Research Journal*, 2, 135-139.
- Manda, A., Bodapati, P.N., Rachaputi, N.C., Wright, G., & Fukai, S. (2004). *Aflatoxins and their relationship with sugars in peanut (Arachis hypogaea L.)*. 4th International Crop Science Congress, Brisbane, Convention Centre, 26 September - 1 October 2004. Gosford: The Regional Institute Ltd.
- Melesse, A., Steingass, H., Boguhn, J., Schollenberger, M., & Rodehutsord, M. (2012). Effects of elevation and season on nutrient composition of leaves and green pods of *Moringa stenopetala* and *Moringa oleifera*. *Agroforestry Systems*, 86, 505-518.
- Nautiyal, S. (2002). High altitude acclimatization in four *Artemisia* species: Changes in free amino acids and nitrogen contents in leaves. *Biologia Plantarum*, 26 (3), 230-234.
- Nayak, S., Hebbal, V., Bharati, P., Nadaf, H., Naidu, G., & Bhat, R. (2020). Profiling of nutraceuticals and proximates in peanut genotypes differing for seed coat color and seed size. *Frontiers in Nutrition*, 7, 45.
- Olsson, G., Pott, B., Larsson, L., Holst, O., & Karlsson, H. (1994). Microbial desulfurization of coal by *Thiobacillus ferrooxidans* and thermophilic archaea. *Fuel Process Technology*, 40, 277-282.
- Panagiotou, G., Pachidou, F., Petroustos, D., Olsson, L., & Christakopoulos, P. (2008). Fermentation characteristics of *Fusarium oxysporum* grown on acetate. *Bio resource Technology*, 99, 7397-7401.
- Pattee, E., Young, C., & Giesbrecht, F. (1981). Seed size and storage effects on carbohydrates of peanuts. *Journal of Agricultural and Food Chemistry*, 29 (4), 800-802.
- Pfarr, M., Kazula, M., Miller-Garvin, J., & Naeve, S. (2018). Amino acid balance is affected by protein concentration in soybean. *Journal of Crop Science*, 58, 2050.
- Prathiba, K., & Reddy, M. (1994). Nutrient composition of groundnut cultures (*Arachis hypogaea* L.) in relation to their kernel size. *Plant Foods for Human Nutrition*, 45 (4), 365-369.
- Sadasivm, S., & Manickam, A. (2008). *Biochemical methods (3<sup>rd</sup> edition)*. New Age International (P) Ltd, New Delhi.
- Suranto, T., Purwanto, E., Setyono, P., & Mahadjoeno, E. (2015). The relationship between altitudes and the contents of protein, carbohydrates, lipids of pumpkin (*Cucurbita moschata*). *Agrivita*, 37 (1), 59-66.



- Waliyar, F., Craufurd, P., Padmaja, K.V., Reddy, R.K., Reddy, S.V., Nigam, S.N., & Kumar, P.L. (2006). Effect of soil application of lime, crop residue and biocontrol agents on pre-harvest *Aspergillus flavus* infection and aflatoxin contamination in groundnut. In *International Conference on Groundnut Aflatoxin Management and Genomics* (pp. 45). 5-10 November 2006, Gungdon Hotel, Guangzhou, China.
- Wijnands, J., Biersteker, J., & Van Loo, E.N. (2009). *Oil seed business opportunity in Ethiopia*. Oil seed research report, Addis Ababa, Ethiopia.
- Woodroof, J. (1983). *Peanuts production, processing, products*. 3<sup>rd</sup> edition. Avi Publishing Company, Indian national congress. Westport, Connecticut.
- Yaw, A., Richard, A., Osei, S., Kofi, A., Seth, D., & Adelaide, A. (2008). Chemical composition of groundnut, *Arachis hypogaea* (L) landraces. *African Journal of Biotechnology*, 7 (13), 2203-2208.



Identification of Genetic Diversity among Mutant Taro (*Colocasia esculenta* L. cv WANGI) Using Agro-Morphological Trait and Simple Sequence Repeats (SSR) Molecular Markers

Nor Farah Nadirah Ahmad Noruddin<sup>1</sup>, Nor' Aishah Hasan<sup>1,2,\*</sup>, Umikalsom Hj. Bahari<sup>3</sup>, Abdul Rahim Harun<sup>4</sup>, Faiz Ahmad<sup>4</sup>, Shakinah Salleh<sup>4</sup>, Muhammad Noh bin Norngaini<sup>5</sup>

<sup>1</sup>Faculty of Applied Sciences, Universiti Teknologi MARA, Cawangan Negeri Sembilan, Kampus Kuala Pilah, 72000, Kuala Pilah, Malaysia

<sup>2</sup>Biotechnology, Microbiology and Environmental Collaboration Sciences; Universiti Teknologi MARA, Cawangan Negeri Sembilan, Kampus Kuala Pilah, 72000, Kuala Pilah, Malaysia

<sup>3</sup>Agrobiodiversity and Environment Research Centre, Malaysian Agricultural Research and Development Institute, 43400 Serdang, Malaysia

<sup>4</sup>Agrotechnology & Biosciences Division, Agency Nuclear Malaysia, 43000 Kajang, Malaysia;

<sup>5</sup>Fit RS enterprise, Lot 3924, Lorong Siantan, Kampung Sungai Kelambu, 42700 Banting, Malaysia

Received – February 23, 2022; Revision – April 20, 2022; Accepted – April 28, 2022

Available Online – April 30, 2022

DOI: [http://dx.doi.org/10.18006/2022.10\(2\).359.368](http://dx.doi.org/10.18006/2022.10(2).359.368)

KEYWORDS

Agro-morphological analysis

*Colocasia esculenta* L. cv Wangi

M<sub>1</sub>V<sub>4</sub> generation

Mutant lines

Genetic diversity Taro

ABSTRACT

Taro (*Colocasia esculenta*) is one of the traditional crops with enormous sources of dietary fiber, carbohydrates, vitamins, and minerals contents. Mutation breeding using gamma radiation is one of the most preferred approaches used to induce mutation in taro studies. Molecular markers are widely used to detect such induced mutation and genetic diversity in plants. Therefore, the present study was carried out to evaluate genetic diversity among irradiated taro genotypes in comparison with standard taro variety by using simple sequence repeats (SSR). A total of 200 of M<sub>1</sub>V<sub>4</sub> taro genotypes were used in this study derived from segregating population of chronic-gamma irradiated taro cv Wangi with different ranges of gamma dose. The agro-morphological results revealed that genotype exposure in T6 (120.12 Gy) has the highest plant height (54.53 cm), leaf length (32.24 cm), and leaf width (24.87 cm). Corm's weight was decreased significantly with an increased dose of treatment. All mutants recorded a lower number of corm weight as compared with the control genotype. Out of 10 SSR primers tested, 9 primers have successfully amplified 43 amplicons. The polymorphism information content (PIC) values of SSR markers ranged from 0.20 to 0.80. Cluster analysis classified taro into 3 subgroups mutant and parent genotypes. The results clearly showed that SSR markers are important tools to distinguish mutant genotypes

\* Corresponding author

E-mail: [aishahnh@uitm.edu.my](mailto:aishahnh@uitm.edu.my) (Nor' Aishah Hasan)

Peer review under responsibility of Journal of Experimental Biology and Agricultural Sciences.

Production and Hosting by Horizon Publisher India [HPI]  
(<http://www.horizonpublisherindia.in/>).  
All rights reserved.

All the articles published by [Journal of Experimental Biology and Agricultural Sciences](#) are licensed under a [Creative Commons Attribution-NonCommercial 4.0 International License](#) Based on a work at [www.jebas.org](http://www.jebas.org).



and confirmed their usefulness for phylogenetic studies. Finally, the present investigation indicated that genotypes exposed by T6 (120.12 Gy) are promising high-yielding genotypes that can be recommended as new cultivars and possessed an attractive phenotype appropriate for ornamental use.

## 1 Introduction

*Colocasia esculenta* L. Schott locally known as taro is a major source of energy, and minerals including calcium, iron, fiber, and vitamins that are good for human health. According to Zulkhairi et al. (2020), taro ranked fifth worldwide among the tuber crops and starchy roots after cassava, yam, potato, and sweet potato, and is categorized as an underutilized crop. With the rise in consumer population and patterns in search for healthy food, the demand for taro production has been increasing, and there has been a great deal of research aiming to develop new taro varieties (Koffi et al. 2021).

The naturally existing genetic variability in taro is not sufficient to achieve the desired improvement. Genetic variability in this crop has been exhausted due to natural selection and hence, conventional breeding methods are not very fruitful due to labor-intensive and time-consuming (Miyasaka et al. 2019; Legesse and Bekele 2021). Additionally, taro is affected by at least 10 major diseases and pests in different parts of the world including taro leaf blight (TLB) caused by the fungus-like oomycete *Phytophthora colocasiae*, Raciborski which can reduce corm yield by up to 50% (Mishra et al., 2019; Mbi et al. 2021). Therefore, mutation breeding has been an alternative way of achieving new taro cultivars.

Mutations can occur spontaneously or be generated by mutagens, which are divided into two categories: physical and chemical mutagens (Ma et al., 2021; Kazama et al., 2008). The effect of chemical mutagens on plant materials is generally considered milder, however, chemical mutagens are generally carcinogenic and have uncertain penetration of the target plant (Seetohul et al., 2007; Oladosu et al. 2015). On the other hand, physical mutagen such as ionizing radiation takes less time for irradiation and creates more damage to DNA strands, therefore considerably helping to improve plant breeding.

Previous researchers have used mutation breeding programs to enhance the genetic properties of *C. esculenta* var. *esculenta* for resistance against taro leaf blight (TLB) as shown by Sahoo et al. (2015). These findings indicated that  $\gamma$ -rays suppressed the growth of *Phytophthora* spores in the leaf tissues of taro cultivars namely Telia and Satasankha under in vitro conditions. Fadli et al. (2018) used white taro cultivars (*Xanthosoma sagittifolium* L) to study the effect of cobalt-60 gamma-ray irradiation. Findings suggested that among various doses of gamma rays tested (30; 60; 90; and

120 grays), leaf color variation only occurred at irradiation rates of 30 and 90 gray while plant heights occur at all levels of irradiation. In addition, these researchers identified the Lethal dose (LD50) at 60 grays. In addition, Matsumaya et al. (2020) performed mutational breeding by heavy-ion beam irradiation of multiple shoots of the 'Chiba maru' cultivar. These researchers reported that by using 2–10 Gy neon and carbon ion beams, they achieved a plant survival rate of more than 90 % and used 94 surviving plants for genomic screening. Unfortunately, till now, there is no reported research on the taro mutation breeding program in Malaysia. Therefore, this study is an attempt to use the chronic gamma irradiation approach to improve taro cv Wangi in Malaysia.

The identification of crop diversity is important in plant breeding programs. This is because the identification and characterization of crops are the initial steps in every introduction and improvement program where it can provide valuable information for their introduction and genetic improvement. Previously, identification based on morphological characteristics has been used for many cultivars. However, morphological identification is very subjective because some of the morphological structures are susceptible to the effect of environmental factors and significant variations have been observed to vary in different regions. Therefore, the existing DNA marker technology is the utmost way for assessing genetic relatedness and variability among the crops (Cretazzo et al. 2022). The uses of molecular markers have been employed to determine the diversity of various crops (Rasco et al. 2016) where the simple sequence repeats (SSR) tend to be among the most polymorphic genetic marker types and have been used in the plant genetic identification process (Korir et al. 2013) compared to other markers such as amplified fragment length polymorphism (AFLP) and restriction fragment length polymorphism (RFLP). This is because SSRs do not necessitate high concentrations or quality of DNA and show great repeatability across laboratories and are genetically codominant. Thus, it is suitable for gathering information on polymorphisms to differentiate across genotypes and identify the representative materials for the genetic diversity collection (Romero et al. 2019). Recently, SSR markers were extensively used to study phylogenetic relationships and differences among taro cultivars in Malaysia and India, respectively (Khatemenla et al. 2019; Shahril et al. 2020). In the present study, genetic differences of mutant lines derived from chronic gamma irradiation cv Wangi were also determined using SSR markers.

## 2 Materials and Methods

### 2.1 Plant Material and Breeding scheme

The Malaysian Agricultural Research and Development Institute (MARDI) provided a local taro cultivar (*C. esculenta* L. cv Wangi). Constant and healthy suckers of taro Wangi variety (a total of 200) were irradiated using chronic gamma-ray (radiation source: cesium-137) at Nuclear Malaysia Gamma Greenhouse facility for 35 days control group was placed in a shelter house nearby. The shoot growth from the irradiated sucker ( $M_1V_1$ ) was planted on the field on day 35 after irradiation. The irradiated sucker growth from the  $M_1V_1$  plant was planted at the MARDI greenhouse to develop  $M_1V_2$  populations. Growth data were collected in  $M_1V_2$  generations and chimeric structures were observed and eliminated. Selected individuals with  $M_1V_2$  mutated sucker were propagated for further observation and uniformity in  $M_1V_3$  generation. Then, the potential individuals  $M_1V_3$  mutated sucker with good growth traits were further propagated and planted until being harvested in the field to assess the growth, the agronomy, and also phenotypic traits. The selection process was repeated to generate the  $M_1V_4$  mutant generation. For this study, a total of seven advanced mutant taros from the different treatments of chronic gamma irradiation as shown in Table 1 with one control parent (non-mutant cv Wangi) were selected. Monitoring was done in every week with recommended management practice followed by Hasan et al. (2020).

### 2.2 Agro-morphological analysis

The agro-morphological characteristics of taro were observed after 6 to 8 months before planting in the field. According to International Plant Genetic Resources Institute (2000), nine quantitative traits such as plant height, leaf length, leaf width, number of leaves, number of suckers, number of stolons, corm weight, corm diameter, and corm width traits were measured in the  $M_1V_4$  generations.

### 2.3 Extraction of genomic DNA

The healthy young leaves were harvested from each treatment of  $M_1V_4$  generation taro genotypes for extraction of genomic DNA. The DNA extraction was executed following the CTAB protocol given by Khumaida et al. (2017) with slight modification. The young leaf tissue was cut into small pieces and put into 1.5ml centrifugation tubes with 800 $\mu$ L of CTAB and ground by using a tissue lyser. Then, the sample was incubated in a water bath in 65°C for 1 hour. The equal volumes of chloroform:isoamyl alcohol (24:1) was added into the centrifuge tubes before being centrifuged at 14000 rpm for 15 minutes. After that, the supernatant was transferred into fresh tubes and 200 $\mu$ L of cold isopropanol was added. The pelleting of nucleic acids was obtained by centrifuging at 14000 rpm for 5 minutes. The supernatant was removed and the pellet was washed with 70% of ethanol and centrifuged at 13000 rpm for 4 minutes. The ethanol was discarded and dried at room temperature to obtain the pellet. The obtained DNA was suspended into 100 $\mu$ L of TE buffer and stored at 4°C until it is ready to be used. The quantification of extracted DNA was tested by using a NanoDrop Spectrophotometer (Thermo Scientific NanoDrop™ 1000 spectrophotometer) and 2% of high-resolution agarose gel electrophoresis.

### 2.4 Polymerase Chain Reaction (PCR) based SSR Marker

Ten SSR primers previously evaluated by Khatemenla et al. (2019) were used as shown in Table 2. PCR amplification was conducted on a thermal cycler in a final volume of 25.0 $\mu$ L containing 1.0 $\mu$ L template DNA, 5.0 $\mu$ L buffer, 0.5 $\mu$ L dNTPs, 3.0 $\mu$ L MgCl<sub>2</sub>, 1.0 $\mu$ L each of forward and reverse primers, 0.2 $\mu$ L Taq polymerase, and 13.3 $\mu$ L molecular water. The SSR profiles were denaturated for five minutes at 94°C, then went through 35 amplification cycles (denaturation at 94°C for 15 seconds, annealing between 47°C and 51°C for 15 seconds, extension at 72°C for 15 seconds, and final extension step at 72°C for 7 minutes). A total of 5 $\mu$ L of amplified PCR product was separated through gel electrophoresis on 3% agarose gel stained with FloroSafe DNA Stain and 100 bp DNA ladder as a reference before the product was visualized using Molecular Imager® (GelDoc™ XR, Bio-Rad).

Table 1 Taro Mutant and Dosage Rate of Chronic Gamma Irradiation

Treatment	Ring	Chronic gamma doses (Gy)	Accumulated dose (Gy)
T0	-	0	0
T1	10	0.03 Gy/h	12.01
T2	8	0.04 Gy/h	16.02
T3	6	0.07 Gy/h	28.03
T4	5	0.11 Gy/h	44.05
T5	4	0.17 Gy/h	68.07
T6	3	0.30 Gy/h	120.12
T7	2	0.66 Gy/h	268.28

Ring 10, 10 m from the radioactive source to 0.67 Gy/day; Ring 2, 2 m from the radioactive source

Table 2 The nucleotide sequences (5' to 3') of the primers used for SSR analysis

Primer name	Forward primers	Reverse primers	Temperature (°C)
Ce1 A06	5'-GCT TGT CGG ATC TAT TGT-3'	5'-GGA ATC AGT AGC CAC ATC-3'	51
Ce1 B03	5'- TTG CTT GGT GTG AAT G-3'	5'- CTA GCT GTG TAT GCA GTG T-3'	51
Ce1 C03	5'- TGT TGG GAA AGA GGG-3'	5'- GGG GAA TAA CCA GAG AA-3'	51
Ce1 C06	5'- CCA GAA GAG ACG TTA CAG A-3'	5'- ACG ACT TTG GAC GGA-3'	47
Ce1 F04	5'- AGG GAA TAC AAT GGC TC-3'	5'- ACG AGG GAA GAG TGT AAA-3'	47
Ce1 H12	5'- TAG TTA GCG TGC CTT TC-3'	5'- CAA CAA CTT AAT GCT TCA C-3'	51
Uq73-164	5'- ATG CCA ATG GAG GAT GGC AG-3'	5'- CGT CTA GCT TAG GAC AAC ATG-3'	47
Uq84-207	5'- AGG ACA AAA TAG CAT CAG CAC-3'	5'- CCC ATT GGA GAG ATA GAG AGA-3'	51
Uq97-256	5'- GTA ATC TAT TCA ACC CCC CTT-3'	5'- TCA ACC TTC TCC ATC AGT CC-3'	49
Uq201-302	5'- CTA AGG AGA GGA GAT CCG AAC-3'	5'- CAA GAC GAT GCT GAA CCA-3'	49

## 2.5 Data analysis

Data were analyzed with one-way ANOVA using the statistical program (SPSS version 20). Means separation was carried by the least significant difference (LSD) and Tukey's multiple range tests with significance determined at  $P \leq 0.05$ . The bands obtained in DNA samples amplified were scored '0' for absence and '1' for presence to create a binary data matrix. The polymorphism information content (PIC) of each marker was calculated using the following formula:

$$PIC = 1 - \sum x_i^2$$

The  $x_i$  is the frequency of  $i^{\text{th}}$  allele for each SSR locus. The similarity index was calculated by using Jaccard's coefficient to identify the genetic similarity. The genetic similarity (GS) matrix between treatments based on molecular data was computed using Wang et al. (2021) coefficient where the similarity matrix was used to produce an agglomerative hierarchical clustering by employing Unweighted Pair Group Method with Arithmetic Averages (UPGMA) with average linkage then graphically converted into a dendrogram by using NTSYSpc version 2.1 software.

## 3 Results and Discussions

Physical mutagenesis by gamma irradiation can be used to induce mutations and to create genetic variation with a desirable mutant. Similar to other countries, taro is also considered as a neglected crop and cultivated by a small farmer in Malaysia as a carbohydrate source. However, with the increasing demand for a healthy lifestyle, it is a great potential to promote taro as an alternative carbohydrate source (Okpul et al. 2005). With 43 local varieties available in Malaysia, breeders are actively finding an alternative way to improve the production of taro with high yield, early maturity, and ability to tolerate the local climatic environment (Zulkhairi et al. 2020). However, there is limited information on the genetic variability of taro. Taro *cv* Wangi is a

popular Malaysian local genotype for its large central corm. However, it contains high oxalate contents (Abdullah et al. 2021). To the best of our knowledge, this is the first study in Malaysia that has stated the use of the mutation induction approach in taro that can be applied to improve the genetic variation of taro.

### 3.1 Agro-morphological Traits

The morphological traits of each taro genotype were observed in each replicate of each treatment. The average of agronomic data such as plant height, leaf length, leaf width, number of leaves, number of suckers, number of stolons, corm weight, corm length, and corm diameter was recorded as shown in Table 3.

On average, plants exposed by T6 (102.12 Gy) were the tallest among all materials tested, with a mean height of 54.53 cm. On the other hand, the shortest plant was observed in T1 (12.01 Gy) among all mutants with a 34.98 cm mean height. The leaf length and the leaf width displayed a similar trend. Plant height is the popular metric for assessing the biological impacts of physical mutagenesis. Findings in this study demonstrated that the higher gamma irradiation doses resulted in slower height growth. Previous research by Fadli et al. (2018) on Indonesian taro *cv* white suggested that plant stunted or decreased in plant height was due to the impact of high doses in gamma irradiation that triggered its physiological disorder or chromosomal damage.

For leaf traits, the longest length and the widest width leaf were observed in mutants' plants in T4 and T6, while the shortest was recorded in plants exposure to T1 (12.01 Gy) and T2 (16.02 Gy) (Table 3). The plant in T6 (120.12 Gy) was observed to have a greater number of leaves than the plant exposed by T2 (16.02 Gy) which showed a fewer number of leaves. Similarly, Gharib (2021) showed that gamma rays influenced the number of leaves, and had the greatest effect at a 10 Gy dose, but demonstrated no effect on shoots. In addition, a study from Nurilmala and Mardiana, (2018) on the effect of gamma rays in stevia stated that the low dose exposure

Table 3 Morphological traits of taro mutants in M<sub>1</sub>V<sub>4</sub> generations

Mutant plants	Plant height (cm)	Leaf length (cm)	Leaf width (cm)	Number of leaf (n)	Number of sucker (n)	Number of stolon (n)	Corm weight (kg)	Corm length (cm)	Corm diameter (cm)
Control (parent)	43.67	24.76	18.14*	4.64	0.84*	0.36	1.62*	8.60	15.08
T1	34.98*	18.02*	12.38*	4.68	1.00	0.36	0.27	10.12	15.92
T2	37.93*	18.98*	13.37*	3.96*	0.96	0.40*	0.31	8.36	14.72
T3	36.39*	19.21*	12.53*	4.36*	0.72*	0.16	0.19*	6.16	9.44*
T4	46.48	25.83	17.75*	5.08	1.52*	0.40*	0.37	9.88	16.84*
T5	44.66	23.02	16.60*	5.16	0.92	0.32*	0.27*	7.88	15.24
T6	54.63*	32.24*	24.87*	6.36*	1.36*	0.60	0.34	9.80	17.52*
T7	47.48	25.52	17.40*	4.88	1.12	0.36	0.17*	5.88	9.72*
LSD (0.05)	1.24	2.10	3.07	1.26	1.54	1.58	0.99	1.08	1.34

Mean separation within columns by LSD and Turkey's multiple range tests at 5% level

Table 4 Summary statistics of SSR polymorphisms in this study

Primer	No Amplified Products	No of Polymorphic Products	Polymorphic Loci (%)	Polymorphic information content value (PIC)
Cel A06	1	1	100	0.61
Cel B03	2	1	50	0.80
Cel C03	9	2	22	0.65
Cel C06	4	4	100	0.59
Cel F04	7	4	57	0.72
Cel H12	3	3	100	0.44
Uq 73- 164	1	0	0	0
Uq 84- 207	2	2	100	0.44
Uq 97- 256	7	6	85	0.20
Uq 201-302	7	7	100	0.80
Total	43	30	714	5.22
Average	4.3	3.0	71.4%	0.52

of gamma rays can enhance the growth and the development of the leaves. Furthermore, the highest number of suckers were recorded in plant exposure in T4 and T6. In contrast, plants in T3 recorded the lowest number of suckers and stolon. Corm weight varied significantly among the various mutants. The parent genotypes showed the highest corm weight when compared with other mutants. In contrast, plant exposure in T7 (268.28 Gy) and T3 (28.03 Gy) showed a minimum corm weight of 0.17 and 0.19 kg, respectively. Among mutants, plants of T6 (120.12 Gy) and T4 (44.05 Gy) recorded the highest weight of corm. This was aligned with a study by Lee et al. (2020) where he reported the highest corm weight by using 30 Gy of gamma irradiation. The highest corm length was recorded in the plant of T1 (12.01 Gy) and the lowest was recorded in plant exposure by T7 (268.28 Gy). The widest corm was measured in plants exposed by T6 (120.12 Gy) while the narrowest corm was measured in the plant of T3 (28.03 Gy). The mutation technique has been successfully employed in taro to isolate good mutants with desired economic plant characters (Sianipar and Maarisit 2015). Previous studies indicated that

irradiation of mutants can increase carbohydrate and low calcium oxalate contents (Manzila et al. 2020). Morphological characteristics application to evaluate the genetic diversity was reported to have certain disadvantages as the expression of the phenotypes is influenced by the growth stages and various environmental factors (Ahn et al. 2018).

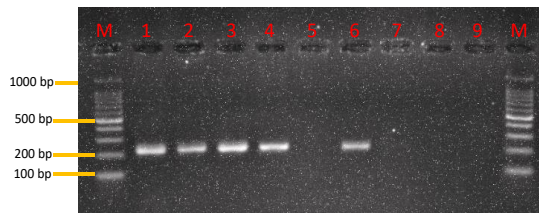
Therefore, the use of DNA markers is encouraged as it is simple, rapid, and reproducible by experiment regardless of environmental conditions, accurate monitoring of seed purity, and determination of cultivars, and it also can be performed at a low cost (Cretazzo et al. 2022).

### 3.2 Microsatellite polymorphism and genetic variability analysis among genotypes

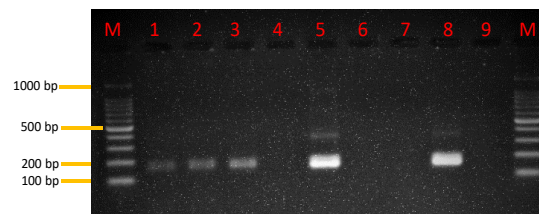
A total of 10 SSR loci were used for the estimation of genetic diversity among 8 mutants and parent taro cv Wangi parental lines. The level of polymorphism among these 8 genotypes of taro was

evaluated by calculating allele number and PIC values for each of the 10 SSR loci. The SSR primer pairs used for genetic diversity

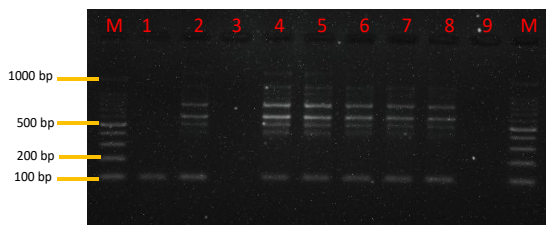
analysis, the number of alleles for each SSR locus, and the PIC values are presented in Table 4.



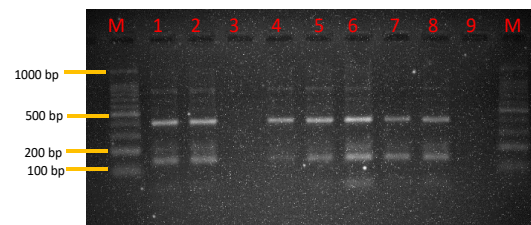
a) SSR primer Cel A06



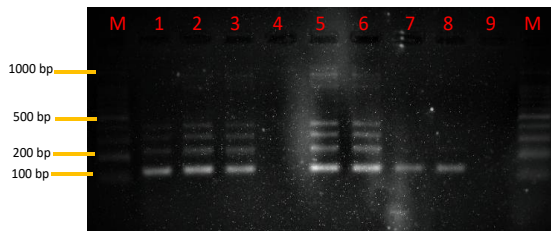
b) SSR primer Cel B03



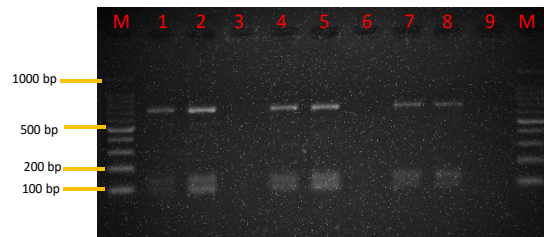
c) SSR primer Cel C03



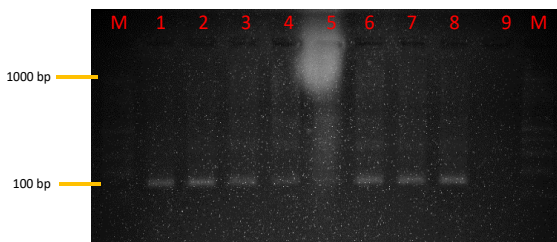
d) SSR primer Cel C06



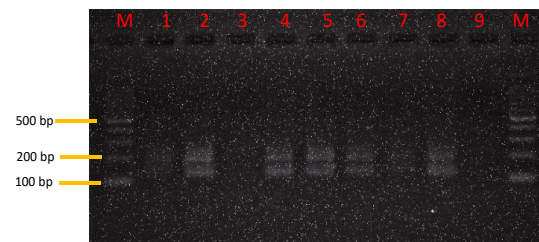
e) SSR primer Cel F04



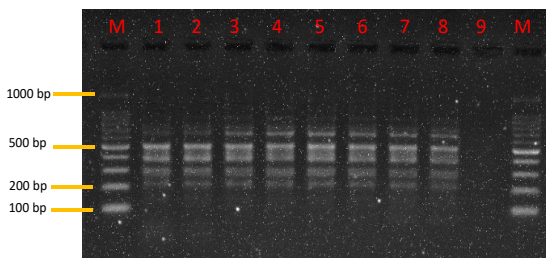
f) SSR primer Cel H12



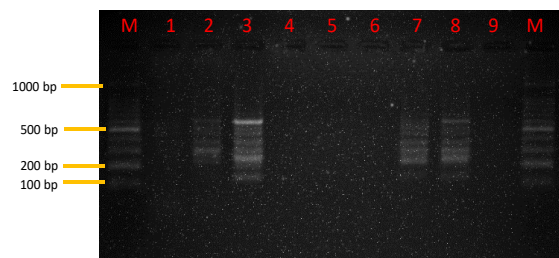
g) SSR primer Uq73-164



h) SSR primer Uq84-207



i) SSR primer Uq97-256



j) SSR primer Uq201-302

Figure 1 Banding pattern of mutant genotype and parent revealed by 10 SSR primers; Lane 1: Parent (taro); Lane 2-8: mutant genotype; Lane 9: Negative control, M: 100bp DNA Ladder

The data from the banding pattern of taro mutant genotypes have been analyzed using 10 polymorphic SSR markers yielding a total of forty-three (43) scorable amplicons were detected with an average of 4.3 alleles per locus. In this study, the total of DNA bands obtained were 30 polymorphic bands out of 43 bands with an overall polymorphism percentage was 71.4 percent. Primer Cel C03 produced the maximum number of amplified fragments with 9 bands meanwhile primer Uq 73- 164 and primer Cel A06 produced the minimum number of amplified fragments (Table 4; Figure 1).

Nine out of ten primers showed polymorphic changes. However, the analysis using primer Uq 73- 164 showed a monomorphic band (Table 4) (Figure 1). Based on the previous study by Oladosu et al. (2015) in mutant rice, monomorphic bands are consistent bands that cannot be used for genetic diversity research but polymorphic bands produce differences that can be used to observe the systematic relationship between the populations that is important to identify genetic changes. In addition, a previous study by Singh et al. (2012) stated that some of the mutants can produce different bands from the control even if the mutants were irradiated by the same dose of gamma rays. Meanwhile, the same size of DNA bands between mutants showed amplified DNA sequence homology while specific bands in one mutant proved the unique genetic variety making the DNA bands profile depend on the degree by which irradiation affects the cells.

Some of the SSR primers were very informative with polymorphic information content (PIC) ranging from 0.20 to 0.80 with an average of 0.52 while one primer which is Uq 73- 164 primer showed no PIC value since it is monomorphic in Table 4. These results were comparable to the PIC values of some mutant crops from previous studies by Manzila et al. (2020) on induced chili pepper mutants (0.53), Shahril et al. (2020) on induced rice mutants (0.51), and gamma-irradiated cowpea mutants (0.51) by Olasupo et al. (2018). The most informative SSR primers were Cel B03 and Uq 201-302 which have the same value (PIC = 0.80). Similarly, Khatemenla et al. (2019) worked on taro in Northeast

India and reported Uq 201-302 with (PIC = 0.82) as the most informative marker. SSR markers with a PIC value of 0.5 or higher were considered effective in selecting the polymorphism rate and have potential in the evaluation of genetic variance (Sianipar et al. 2015). Meanwhile, the least informative primer was Uq 97- 256 with (PIC = 0.20) since the PIC value was closer to one considered to be more informative (Khatemenla et al. 2019).

### 3.3 Genetic relationship between mutants and control cv wangi

The DNA bands of the obtained taro mutants had been converted into a binary number where “1” indicated the presence of a band and “0” indicated the absence of a band. The binary data of the SSR profile can be used to produce a genetic similarity matrix using NTSYSpc software and Jaccard’s coefficient of similarity. The genetic similarity based on SSR markers ranged from 0.22 to 0.83 (Table 5). Genetic similarity analysis has been done previously by Singh et al. (2012) in mung bean mutants which ranged from 0.78 to 1 based on SSR molecular markers. The highest genetic similarity was observed between mutant genotypes exposure in T6 (120.12 Gy) and T7 (268.28 Gy) (0.83) followed by T1 (12.01 Gy) and T7 (268.28 Gy) (0.72). The highest genetic similarity was found between control with mutant genotypes exposure in T1 (12.01 Gy) (0.65) and T4 (44.05 Gy) (0.63) while the lowest similarity was reported in mutant genotypes T2 and T3 (0.22). The genetic similarity between mutant genotype and control was observed between control and plant in T2 (16.02 Gy) (0.38). An earlier study on rodent tuber mutants by Sianipar et al. (2015) reported a significant effect of gamma irradiation on plant mutant genotype, the smaller genetic similarity with more differences were observed in the mutant genotype. This can be observed between control and mutant genotypes exposure of T2 (16.02 Gy), T3 (28.03 Gy), T6 (120.12 Gy), and T7 (268.28 Gy) that have smaller genetic similarities in this study. These results also indicated that the control and taro mutant lines were genetically different.

Table 5 Similarity matrix based on Jaccard’s Coefficient of Similarity of taro mutants

	Control	T1	T2	T3	T4	T5	T6	T7
Control	1.00							
T1	0.65	1.00						
T2	0.38	0.53	1.00					
T3	0.53	0.50	0.22	1.00				
T4	0.63	0.59	0.29	0.61	1.00			
T5	0.60	0.56	0.38	0.58	0.68	1.00		
T6	0.40	0.58	0.41	0.56	0.53	0.48	1.00	
T7	0.46	0.72	0.47	0.57	0.57	0.50	0.83	1.00

Note: “T= treatment”, “1 to 7= number of treatments”



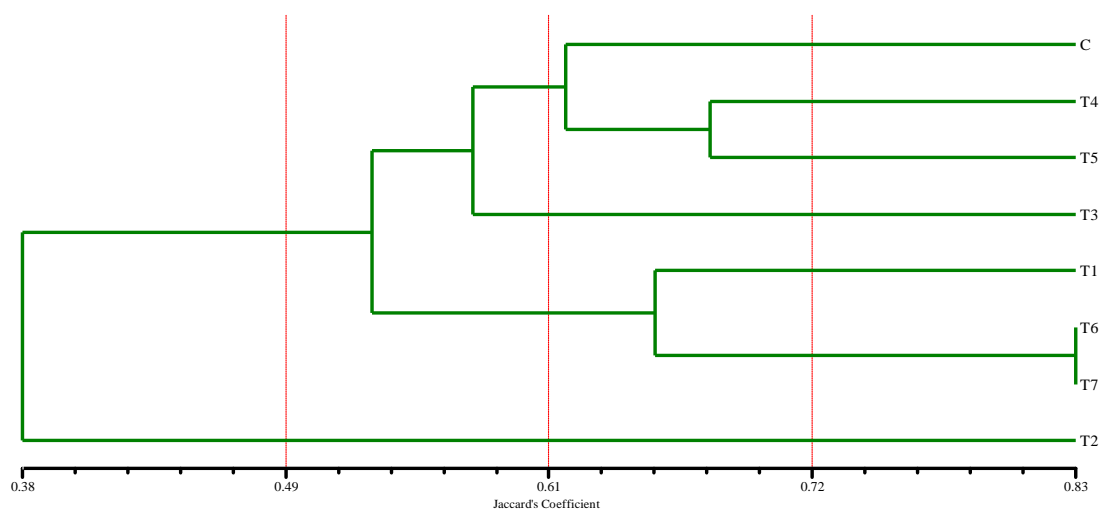


Figure 2 Dendrogram of taro mutant lines and the control based on SSR marker analysis constructed with the UPGMA method

The analysis was carried out by using quantitative similarity with Jaccard's similarity coefficient while clustering using Sequential Agglomerative Hierarchical Nested (SAHN) analysis to generate a dendrogram of mutant taro and control based on SSR markers analysis by using UPGMA cluster (Figure 2). The analysis method revealed that the dendrogram with a similarity coefficient of 0.38 to 0.83. At a similarity coefficient of 0.49, three clusters were formed cluster I consisted of 3 mutant genotypes and control (parent) samples while cluster II consisted of 3 mutant samples, and cluster III consisted of only one mutant sample. Cluster I was divided into two sub-clusters at the coefficient of similarity of 0.61 consisted sub-cluster A with 3 samples which were 2 mutants that have been irradiated by T4 (44.05 Gy) and T5 (68.07 Gy) together with a control sample. Sub-cluster B consisted of only one sample that was irradiated with T3 (28.03 Gy) gamma-ray. Whereas, cluster II consisted 3 mutant samples which were exposed to T1 (12.01 Gy), T6 (120.12 Gy), and T7 (268.28 Gy), while cluster III consisted of only one sample which was in T2 (16.02 Gy) that showed to be divergent and clustered on its own main cluster.

### Conclusion

In the present study, taro mutant genotypes showed a wide range of agronomic characteristics as the effect of chronic gamma irradiation. The present study elucidated morphological and genetic characteristics of parent genotype and seven selected mutants to determine the best genotype. Plant exposure by T7 (268.28 Gy) showed as the promising mutant with the highest plant height (54.53 cm), leaf length (32.24 cm), and leaf width (24.87 cm). The markers generated by SSR primers allowed detection of genetic polymorphism and genetic fingerprinting among the mutants of taro tested. In doing so, they have shown to be useful for the construction of a germplasm collection and providing additional information that could form the basis for the rational

design of breeding programs. The present characterization strategies will help to exploit different mutant lines for developing new taro genotypes with desired traits.

### Acknowledgments

The authors are thankful to Universiti Teknologi MARA, Universiti Putra Malaysia, Agrobiodiversity and Environment Research Centre, Malaysian Agricultural Research and Development Institute (MARDI), and Malaysian Nuclear Agency for guidance and assistance. The authors also would like to extend appreciation to the Ministry of Higher Education (MOHE) for providing financial aids during this research.

### References

- Abdullah, S., Fauzi, N.Y.M., Khalid, A.K., Osman, M., & Mohamad, A. (2021). Effect of Gamma Rays on Seed Germination, Survival Rate and Morphology of *Stevia rebaudiana* Hybrid. *Malaysian Journal Fundamental Applied Science*, 17(5), 543-549.
- Anh, V.L., Inoue, Y., Asuke, S., Vy, T.T.P., Anh, N.T., & Wang, S. (2018). Rmg8 and Rmg7, wheat genes for resistance to the wheat blast fungus, recognize the same avirulence gene AVR-Rmg8. *Molecular Plant Pathology*, 19, 1252-1256.
- Cretazzo, E., Moreno Sanz, P., Lorenzi, S., Benítez, M.L., Velasco, L., & Emanuelli, F. (2022). Genetic Characterization by SSR Markers of a Comprehensive Wine Grape Collection Conserved at Rancho de la Merced (Andalusia, Spain). *Plants*, 11, 1088.
- Fadli, N., Syarif, Z., Satria, B., & Akhir, N. (2018). The effect of gamma cobalt-60 ray irradiation on cultivar growth in taro white

- (*Xanthosoma sagittifolium* L.). *International Journal Environmental Biotechnology Agricultural*, 3(6), 268284.
- Gharib, A.H. (2021). Inducing Genetic Variation in Taro Using Gamma Irradiation. *Egyptian Journal Basic Applied Science*, 36(3), 73-86.
- Hasan, N.A., Suhaimi, L., Ahmad, F., Mohamed Bahari, U., Harun, A.R., & Rafii, M.Y. (2020). Effects of Chronic Gamma Irradiation on the Growth of Local Taro Variety (*Colocasia esculenta* L. WANGI). *Jurnal Sains Nuklear Malaysia*, 32(2), 23 – 30.
- International Plant Genetic Resources Institute (IPGRI) (2000). IPGRI Annual Report (1999). Rome, Italy: IPGRI (pp. 40)
- Kazama, Y., Saito, H., Yamamoto, Y.Y., Hayashi, Y., et al. (2008). LET-dependent effects of heavy-ion beam irradiation in *Arabidopsis thaliana*. *Plant Biotechnology*, 25, 113– 117.
- Khatemenla, Alam, S., Barooah, M., Phookan, D.B., et al. (2019) SSR Marker-Based Molecular Characterization of Some Upland Taro (*Colocasia esculenta* L. Schott) Cultivars of North-East India. *International Journal of Current Microbiology and Applied Sciences*, 8(06), 2310-2320.
- Khumaida, N., Ardie, S.W., & Astuti, M.S. (2017). Characterization of Irradiation Induced Mutants of Cassava (*Manihot esculenta* Crantz) Generated from Jame-jame and Adira-4 Genotypes at M<sub>1</sub>V<sub>2</sub> Generation. *KnE life science*, 22-28. DOI <https://doi.org/10.18502/cls.v2i6.1016>.
- Koffi, J., Koffi, K., Bonny, S., & Bi, A. (2021) Genetic Diversity of Taro Landraces from Côte d'Ivoire Based on Qualitative Traits of Leaves. *Agricultural Sciences*, 12, 1433-1446.
- Korir, N.K., Han, J., Shangquan, L., Wang, C., et al. (2013). Plant variety and cultivar identification: advances and prospects. *Critical Review Biotechnology*, 33(2), 111-125.
- Lee, H.Y., Moon, S., Ro, H.S., Chung, J.W., & Ryu, H. (2020). Analysis of Genetic Diversity and Population Structure of Wild Strains and Cultivars Using Genomic SSR Markers in *Lentinula edodes*. *Mycobiology*, 48(2), 115–121.
- Legesse, T., & Bekele, T. (2021). Evaluation of improved taro (*Colocasia esculenta* (L.) Schott) genotypes on growth and yield performance in North-Bench woreda of Bench-Sheko zone, South-Western Ethiopia. *Heliyon*, 7(12), e08630.
- Ma, L., Kong, F., Sun, K., Wang, T., & Guo, T. (2021) From Classical Radiation to Modern Radiation: Past, Present, and Future of Radiation Mutation Breeding. *Frontier Public Health*, 9,768071.
- Manzila, I., Priyatno, T.P., Nugroho, K., Terryana, R.T., & Hidayat, S.H. (2020). Molecular and morphological characterization of EMS-induced chili pepper mutants resistant to Chili veinal mottle virus. *Biodiversity Journal*, 21(4), 1448-1457.
- Matsuyama, T., Watanabe, M., Murota, Y., Nakata, N., et al. (2020). Efficient mutation induction using heavy-ion beam irradiation and simple genomic screening with random primers in taro (*Colocasia esculenta* L. Schott). *Scientia Horticulturae*, 272,109568.
- Mbi, T.K., Godswill, N.F., Brice, T.L., & Emmanuel, Y. (2021). Field management of Taro (*Colocasia esculenta* (L.) Schott) leaf blight via fungicidal spray of foliage. *Journal Cameroon Academy Science*, 16(3), 197-208.
- Mishra, D., Bhoi, L., Dash, M., Tripathy, S.K., et al. (2019). Mutagenic effectiveness and efficiency of EMS and gamma rays on rice bean (*Vigna umbellata* (Thunb) Ohwi and Ohashi): An underutilized legume crop. *International Journal of Conservation Science*, 7(3),2060-2064.
- Miyasaka, S.C., Renee, M.B., Michael, B., Kantar, M.H., Thomas, W.R., & Paudel, M.S. (2019). Genetic Diversity in Taro (*Colocasia esculenta*). In: Nandwani, D. (eds) *Genetic Diversity in Horticultural Plants, Environmental Development Sustainability*, vol 22, (pp 191–215), Springer, Cham.
- Nurilmala, F., & Mardiana, D. (2018). Nutrients and Anti-nutrients Content Analysis of Bogor Taro Mutant Clone (*Colocasia esculenta*). *IOP Conference Series: Earth and Environmental Science*, 334,012070.
- Okpul, T., Mace, E.S., Godwin, I.D., Singh, D., & Wagih, M.E. (2005). Evaluation of variability among breeding lines and cultivars of taro (*Colocasia esculenta*) in Papua New Guinea using ISSR fingerprinting and agro-morphological characterization. *Plant Genetic Resources Newsletter*, 143, 8-16.
- Oladosu, Y., Rafii, M.Y., Abdullah, N., Malek, M.A., et al. (2015). Genetic variability and diversity of mutant rice revealed by quantitative traits and molecular markers. *Agrociencia Uruguay*, 49(3), 249-266.
- Olasupo, F.O., Ilori, C.O., Stanley, E.A., Owoeye, T.E., & Igwe, D.O. (2018). Genetic Analysis of Selected Mutants of Cowpea (*Vigna unguiculata* [L.] Walp) Using Simple Sequence Repeat and rcbL Markers. *American Journal Plant Science*, 9(13), 2728.
- Rasco, J.L.S., Mendoza, M.R.R., & Abustan, M.A.M. (2016). Molecular Characterization of Taro [*Colocasia esculenta* (L.) Schott] Using SSR Markers. *Philippine Journal Crops Sciences*, 41(3),65-73.

- Romero, M., Mujica, A., Pineda, E., Ccamapaza, Y., & Zavalla, N. (2019). Genetic identity based on simple sequence repeat (SSR) markers for Quinoa (*Chenopodium quinoa* Willd.). *Ciencias Investigacion Agraria*, 46(2), 166-168.
- Sahoo, B.B., Kole, P.C., & Sahoo, M.R. (2015). Effects of  $\gamma$  Irradiation on Leaf Blight Disease of Some Taro (*Colocasia esculenta* (L.) Schott) Genotypes. *International Journal Biology Resources*, 6(1),007-014.
- Seetohul, S., Puchooa, D., & Ranghoo-Sanmukhiya, V.M. (2007). Genetic Improvement of Taro (*Colocasia esculenta* var *esculenta*) through in-vitro mutagenesis. *University Mauritius Research Journal*, 13A, 79-89.
- Shahril, A.R., Azman, N., Kamaruzaman, R., Amri, S.Y., et al. (2020). Genetic diversity of released Malaysian rice varieties based on single nucleotide polymorphism markers. *Czech Journal Genetics Plant Breeding*, 56, 62-70.
- Sianipar, N.F., Laurent, D., Purnamaningsih, R., & Darwati, I. (2015). Genetic variation of the first generation of rodent tuber (*Typhonium flagelliforme* Lodd.) mutants based on RAPD molecular markers. *HAYATI Journal Bioscience*, 22(2), 98-104.
- Sianipara, N.F., Maarisit, W.A. (2015). Detection of Gamma-Irradiated Mutant of Rodent Tuber (*TyphoniumflagelliformeLodd.*) *In Vitro* Culture by RAPD Molecular Marker. *Procedia Chemistry*, 14, 285 – 294
- Singh, S.K., Lavanya, G.R., Bhat, K.V., Babu, G.S., et al. (2012). Microsatellite markers revealed genetic diversity in mungbean mutant lines. *Indian Journal Hill Farming*, 25(1), 38-43
- Wang, S., Ge, S., Colijn, C., Biller, P., Wang, L., & Elliott, L. T. (2021). Estimating Genetic Similarity Matrices Using Phylogenies. *Journal of computational biology: a journal of computational molecular cell biology*, 28(6), 587–600.
- Zulkhairi, A.M., Razali, M., Umikalsum, M.B., Norfaizal, G.M., Athirah, A.A., & Aisyah, M.S. (2020). Determination of Oxalates in Corms of Selected Taro (*Colocasia esculenta*) Varieties in Malaysia Using Ultra High-Performance Liquid Chromatography. *Asian Journal Chemistry Sciences*, 7(3), 28-37.



## Journal of Experimental Biology and Agricultural Sciences

<http://www.jebas.org>

ISSN No. 2320 – 8694

### Dynamics of land-use Change using Geospatial Techniques From 1986 to 2019: A Case Study of High Oum Er-Rbia Watershed (Middle Atlas Region)

Younes OULARBI<sup>1,\*</sup> , Jamila DAHMANI<sup>1</sup>, Fouad MOUNIR<sup>2</sup>

<sup>1</sup>Department of Biology, Laboratory of Plant, Animal and Agro-Industry Productions, Faculty of Sciences, Ibn Tofail University, Kénitra, Morocco.

<sup>2</sup>National Forestry School of Engineers, 511 Salé, Morocco.

Received – January 22, 2022; Revision – March 17, 2022; Accepted – April 29, 2022

Available Online – April 30, 2022

DOI: [http://dx.doi.org/10.18006/2022.10\(2\).369.378](http://dx.doi.org/10.18006/2022.10(2).369.378)

#### KEYWORDS

Google Earth Engine (GEE)

Random Forest (RF)

Environmental changes

Spatio-temporal changes

Remote sensing

Landsat

Land use map

#### ABSTRACT

This work aims to expose the contribution of the use of the cloud google earth Engine (GEE) platform, in particular the capacity of optical monitoring by remote sensing to assess the impact of environmental changes on the evolution of natural resources in the Middle Atlas region. To achieve this goal, the dense time stacking of multi-temporal Landsat images and random forest algorithm based on the Google Earth Engine (GEE) platform was used. The spatial resolution of the images used is 30 meters for the TM 5 sensor (Thematic Mapper) and the OLI 8 sensor (Operational Land Imager). Further, the google earth engine platform is used primarily to download and prepare the images for the dates 1986, 2000, and 2019, then a supervised classification with the Random Forest (RF) algorithm to produce land use maps of selected dates with an overall accuracy exceeding 80%. This was followed by the production of maps and change matrices for the periods 1986-2000 and 2000-2019. The results obtained have shown a decline in grassland, forest land, and water body in parallel with an increase in the following classes: buildings, farmland, and arboriculture during the last 30 years. In addition, elevation was the most important characteristic variable for land-use classification in the study area. Obtained results provide theoretical support for adjusting and optimizing land use in the High Oum Er-Rbia watershed.

\* Corresponding author

E-mail: [younes.oularbi@uit.ac.ma](mailto:younes.oularbi@uit.ac.ma) (Younes OULARBI)

Peer review under responsibility of Journal of Experimental Biology and Agricultural Sciences.

Production and Hosting by Horizon Publisher India [HPI]  
(<http://www.horizonpublisherindia.in/>).  
All rights reserved.

All the articles published by [Journal of Experimental Biology and Agricultural Sciences](#) are licensed under a [Creative Commons Attribution-NonCommercial 4.0 International License](#) Based on a work at [www.jebas.org](http://www.jebas.org).



## 1 Introduction

The Middle Atlas is one of the three great mountain ranges which constitute the framework of the Moroccan geographical space, and these are (i) the Rif in the North, (ii) the Middle and High Atlas in the center, and (iii) the Anti-Atlas in the South (De Waele and Melis 2009). This chain is also characterized by its varied natural resources and its situation as a transit zone. In this mountainous region, the altitudes vary between 600 and 2400 m; and it contains the most beautiful cedar groves in Morocco and the Mediterranean basin. Over the past few decades, human population and activity have seriously threatened biodiversity, ecosystem services, and wildlife habitat. This World's ecological heritage is of major economic, social, cultural, and tourist interest, hence there is a strong need for its conservation and development.

Land use and land cover changes are one of the most important planner issues in recent years because most of these changes are not expected and appear as environmental degradation, water scarcity, and worsening food security (Rasool et al. 2021). In addition, these changes describe the impact of anthropogenic disturbance on the surface of the Earth and play an important role in the studies of regional and global environmental changes (Ran et al. 2019). Land use is the result of the interaction between land's natural vocation and cultural backgrounds (Tsai et al. 2019).

Land cover change is directly linked with land use and gives rise to the degradation of multiple ecosystems (Schürmann et al. 2020). Physical and socio-economic factors are the most important drivers of land-use change they are very important for the modeling of land-use change. These changes in land use and land cover can be described as a factor of change inducing environmental change since they are the basis of either the reduction or the amplification

of greenhouse gas emissions and therefore (MEA 2005).

To prevent and control the effects of land cover and land use changes we need a relevant knowledge of the stat of land cover and land use and the changes associated with these (Anderson 1976). Currently, thanks to the development of earth observation science that makes available the remote sensing data of different dates and locations of the world, detection, and monitoring of land-use change effects can be done at the local and global level (Rogan and Chen 2004).

The combined exploitation of GIS and remote sensing techniques allows the mapping and land use perdition as well as the identification of the different spatial and temporal transitions of these changes (Lillesand et al. 2015), the research using high-resolution images from different dates and GIS techniques under a geospatial modeling environment can provide relevant information for planning environmental and economic development programs to combat the negative effects of environmental changes (MEA 2005).

The Google Earth Engine (GEE) provides a JavaScript and Python coding environment to facilitate multi-source satellite data processing for the user can without downloading and pre-processing the data (Tamiminia et al. 2020).

This study applied dense time stacking of Landsat images to monitor land cover changes in the High Oum Er-Rbia watershed. This study aimed to obtain the land cover and land cover changes information of the High Oum Er-Rbia watershed from 1986 to 2019 based on the GEE platform. The results are expected to provide theoretical support for adjusting and optimizing land use in the High Oum Er-Rbia watershed.

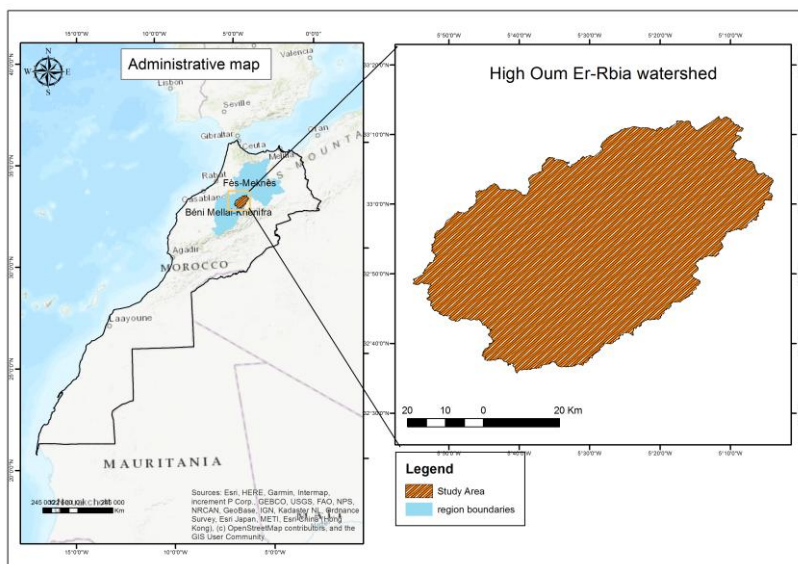


Figure 1 Location of the study area.

## 2 Materials and Methods

### 2.1 Study area

The study area is located in the southwest of the central Middle Atlas Mountain in the Beni mellal-Khenifra region, between 32°35'N to 33°12' N latitude and 5°03'W to 5°55'W longitude. It covers more than 3600 km<sup>2</sup> (El Jazouli et al. 2019). The geographical landscape presents attitudes that can go from 700 m up to 2400m from the high mountains. According to the geological maps the geological formations of the studied, range from Paleozoic to Quaternary, consisting of sub tabular limestone rocks and Liassic dolomitic limestones. The study area is characterized by a Mediterranean climate known for warm/hot and dry summers and mild/cool and wet winters. The annual average precipitation is between 400 and 700 mm, and the minimum and maximum temperature's usual values are respectively 5 and 50°C. The forest vegetation consists mainly of holm oaks and cedars which are mainly located in the upper and middle part of the watershed. The average population density of the study area is 42.32 ha/km<sup>2</sup> according to the 2014 General Population and Housing Census. The Oum Er Rbia River and its tributaries of Srou and Chbouka, crossing the Atlas Mountain chain, drain the studied watershed.

### 2.2 Data preparing

Google Earth Engine is a platform for worldwide geospatial analysis on diverse matters of which we can cite deforestation, climate change monitoring, environmental issues, and water management (Gorelick et al. 2017). The GEE provides Landsat datasets by the United States Geological Survey (USGS,

<https://www.usgs.gov/>) and all acquired Landsat images, are pre-processed, mosaicked, and processed through the JavaScript application programming interface (API) (Bootsma 2021).

In this work, all processing of Landsat TM and OLI data was conducted on the GEE platform (<https://earthengine.google.com>) and in a free GIS environment, the available Landsat TM and OLI Collection 1 Tier 1 top of atmosphere (TOA) reflectance products in the High Oum Er-Rbia watershed were analyzed.

The image processing includes the following steps (i) filter and selects all satellites images (TOA reflectance product) of the period (May–September), (ii) The clouds were removed from the Landsat images of the study area, (iii) then a single image was generate from the image collection by using a reducer function (Pu et al. 2020), (iv) The normalized difference vegetation index (NDVI), the normalized difference-built index (NDBI), and the Modified Normalized Difference Water Index (MNDWI) (MNDWI) were calculated for each image and (v) The slope and aspect from DEM data were added to perform the classification. Therefore, the best image is obtained by a combination of images, cloud-free, combining NDVI, NDBI, MNDWI, slope, and aspect.

### 2.3 Training and Validation Sample Selection

The classification system was determined based on current land use in the High Oum Er-Rbia watershed. In compliance with previous research in the Hight Oum Ee Rbia watershed (El-Bouqdaoui 2007), we adopted seven major land-use types: forest, arboriculture, rangeland, farmland, and buildings, water bodies, and unused land (other lands).

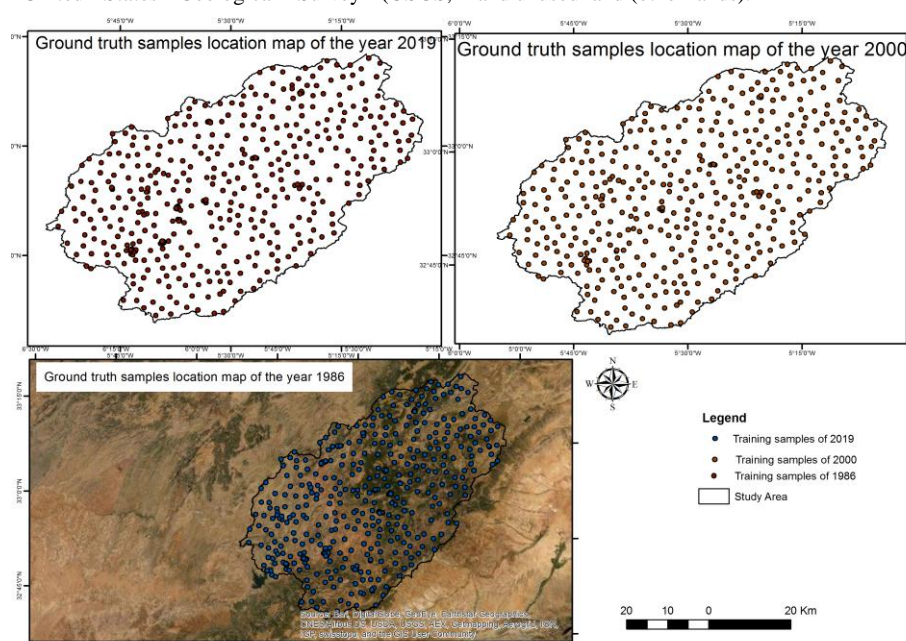


Figure 2 Plot distribution in the High Oum Er-Rbia watershed

Training samples used to create the classification model were collected through (i) visual interpretation of the very high-resolution image on different year's satellites images and (ii) field observations from the area study. In total, more than 1300 plots (440 plots for each year) were collected with more than 40 samples for each land-use type, 70% of which were randomly selected as participants in classification as training samples, and 30% used to verify the classification results as validation samples (Figure 2).

## 2.4 Method

The methodology is based on using Landsat images on the GEE platform. Whose images were pre-processed by date filtering, cloud masking, mosaicking, and clipping to obtain a Landsat TOA composite image and to calculate the characteristic parameters to implement the later classification. Then the training and validation sample datasets already uploaded to the GEE were implemented in the classification. In this study, the random forest (RF) machine learning algorithm was used. The results were validated using a confusion matrix. Finally, the land use transfer matrix was used to analyze the change in each land-use type for each year type in the High Oum Er-Rbia watershed (figure 3).

In the current study, the random forest (RF) algorithm was selected because it can deal with complex data of large dimensions and can usually provide higher accuracy than other traditional algorithms, such as maximum likelihood and single

decision tree (Belgiu and Dragut 2016; Na et al. 2010). The classifier can be presented as an ensemble learning method that creates random features and uses them to generate multiple decision trees and classifies a dataset by using the prediction modes of all decision trees (Tamiminia et al. 2020).

RF has even proven to give good results when used in various applications such as land cover classification on multi-temporal and multi-frequency SAR data (Waske and Braun 2009). The relative importance of each target variable class could be measured with the RF classifier (Rodriguez-Galiano et al. 2012).

In this study GEE platform and RF algorithm was applied based on the field's samples to obtain the Land use classification maps for each separate year, the number of trees was set to 500 and the number of classes is fixed to 7 classes. To evaluate the accuracy of remote sensing image classification, the confusion matrix was produced. The matrix provides the correspondence between the land-use classification results and verification data. In this work, the verification of classification accuracy is reflected by overall accuracy, kappa coefficient, producer's accuracy, and user's accuracy.

## 3 Results and discussions

In this work, a total of 176 satellites images were used (Table 1). All images are free from cloud cover and are part of the Landsat 5 TM and Landsat 8 OLI collection. Favorite

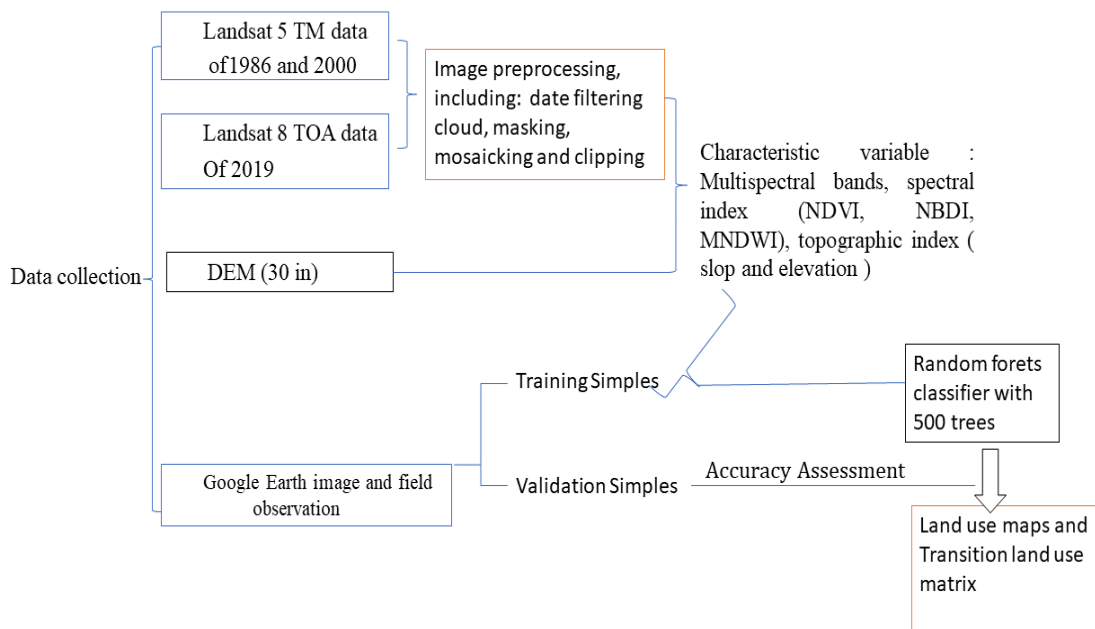


Figure 3 Methodology used for the characterization of spatial and temporal changes in land cover in the study area

Table 1 Characteristics of taken Images

Satellite	Years	Paths	Rows	Number of images	Cloud cover
Landsat 5 TM	1985-1987	200-199	37-38	27	0%
Landsat 5 TM	1999-2001	200-200	37-38	67	0%
Landsat 8 OLI	2018-2020	200-201	37-38	82	0%

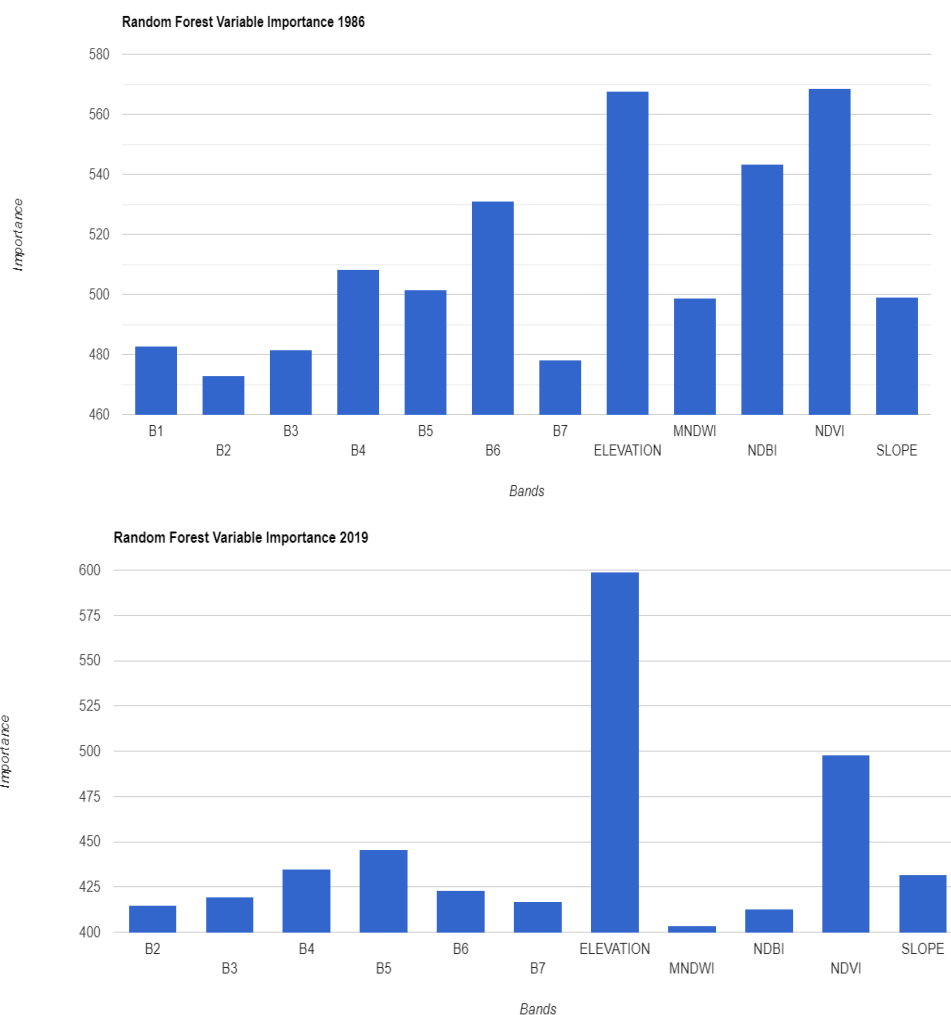


Figure 4 Importance distribution of characteristic variables in Land use classification

### 3.1 Variable Importance Analysis and Accuracy Assessment of Land-use classification

The RF model can analyze the importance of characteristic variables, which improves classification accuracy. The importance of characteristic parameters analyzed on the GEE platform can indicate the greater impact and contribution of the variable to the classification results. Results of the current study showed that elevation and the NDVI were the highest importance score among all the characteristic variables (Figure 4) and the

slope, MNDWI, and NDBI were as followed. These results are in agreement with the findings of Hoshikawa and Umezaki (2014) those who found that terrain has a significant impact on land use classification.

The accuracy of the classification result is an important prerequisite for analyzing land-use changes. The classification results of the study showed that the overall accuracy was 85%, 87%, and 86% for 1986, 2000, and 2019, respectively, and the kappa coefficient was 79%, 82%, and 90 % for 1986, 2000, and



Table 2 Confusion matrix of the classification shown (unit: %).

Land use type	1986		2000		2019	
	User's Accuracy	Producer's Accuracy	User's Accuracy	Producer's Accuracy	User's Accuracy	Producer's Accuracy
Forest	0.92	0.96	0.91	0.93	0.92	0.95
Arboriculture	1	0.65	1	0.42	0.92	0.88
Rangeland	0.8	0.72	0.84	0.83	0.82	0.77
Farmmland	0.76	0.87	0.82	0.88	0.88	0.9
Buildings	1	1	1	0.5	0.9	0.9
Water	0.69	1	1	0.86	1	0.8
Other	1	0.41	0.8	0.67	1	1
Overall accuracy	0.85		0.87		0.86	
Kappa Coefficient	0.79		0.82		0.9	

2019, respectively (Table 2). The overall accuracy of the classification reached the acceptable threshold, indicating that the classification accuracy could meet the requirements of the land-use classification. The confusion matrix showed detailed classification accuracy for each land-use type (Table 2).

### 3.2 Spatiotemporal Characteristics of land use Changes

The GEE platform classification results are shown after applying the model (figure 5), and the Land-use maps of the study area in 1986, 2000, and 2019 are shown in (figure 6). Forest land was the main land use type, occupying more than 45% of the total land

area while the farmland land was the second main land use type with an area ratio of approximately 40% and the Rangeland covers approximately 15 % of the total land area. The construction land, arboriculture, water body areas were the smallest, less than 5% of each one. These results are confirmed by the study of EL-Bouqdaoui (2007).

From 1986 to 2019, the area of forest land, arboriculture land, and construction expanded, especially the percentage of arboriculture land area, which increased from 0.71% to 4%. However, during the study period, the Rangeland and wetland gradually decreased (Figure 6).

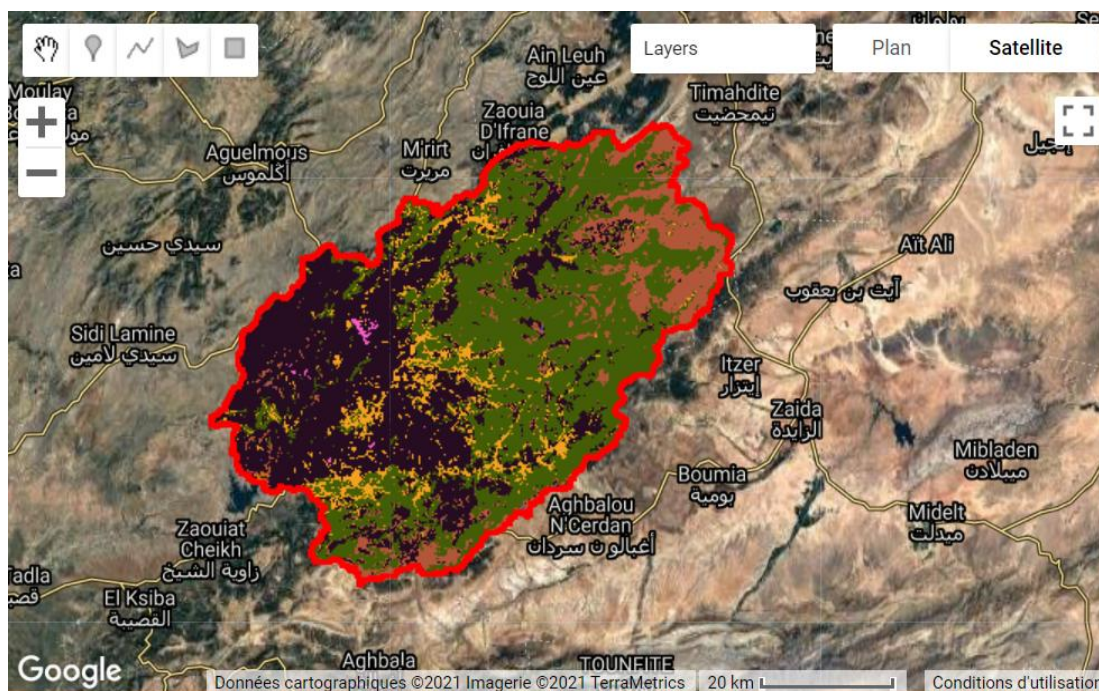


Figure 5 GEE classification result on 2019

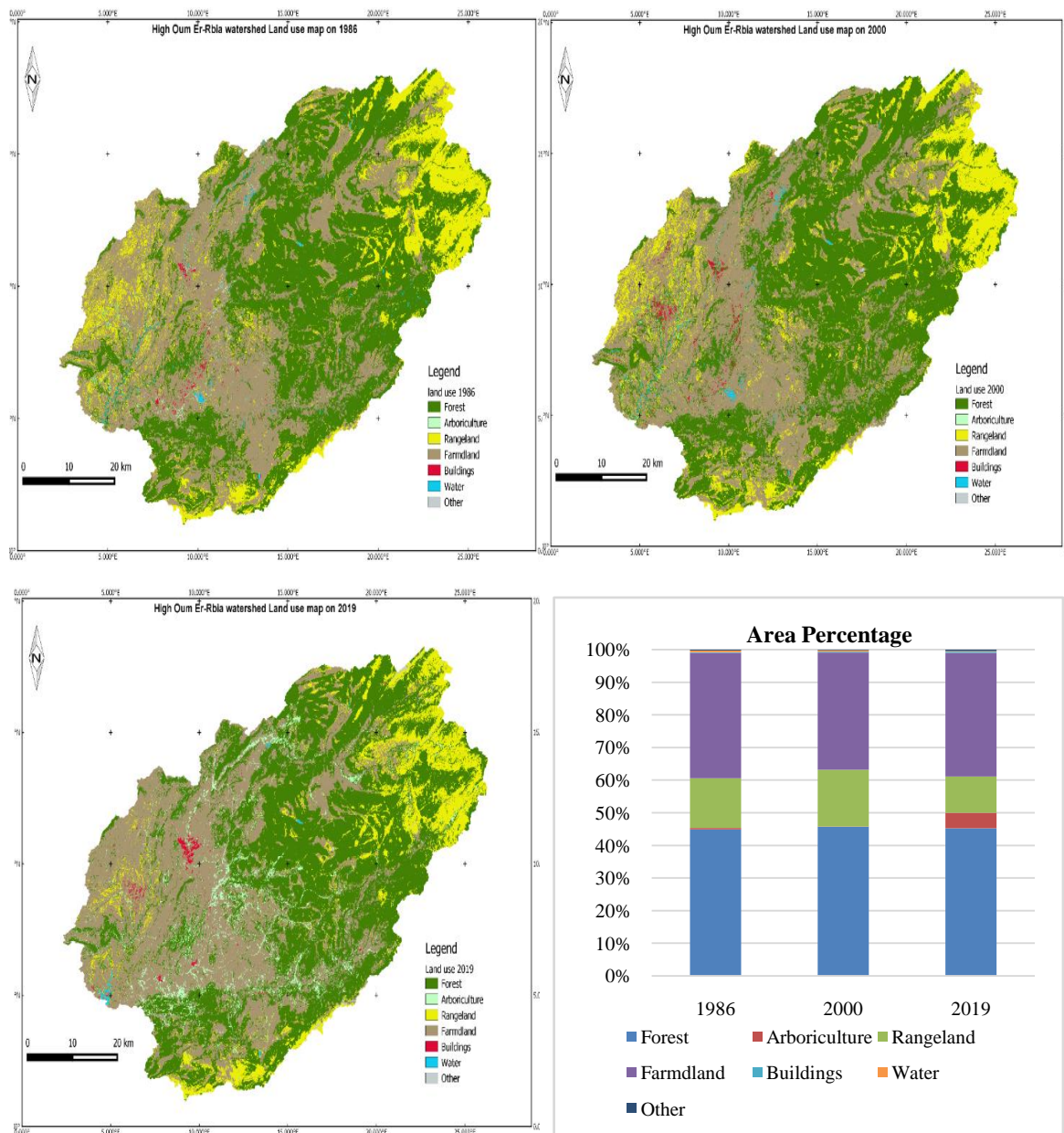


Figure 6 Hight Oum Er- Rbia watershed land use maps on 1986, 2000, and 2019 and area percentage of land use type in the study area

### 3.3 Land use transformation from 1986 to 2019

To observe the changes in various land-use types, we used the spatial analysis method to study the land-use changes transition matrix from 1986 to 2019 and mapped them. From 1986 to 2000, in general, forest land, Rangeland, and buildings were expanded, while the area covered by Arboriculture, farmland, and water body decreased (Tables 3 and 4).

Among the study areas, 12234 hectares of farmland and 4282 hectares of rangeland were transformed into forest land

respectively. The expansion of construction land came essentially from farmland, while the forest land was mainly converted into farmland and rangeland (Table 3). In addition, approximately 712 hectares of water body was converted to Forest land and farmland.

Similarly, from 2000 to 2019, the areas of forest land and rangeland continued to decrease, while arboriculture, farmland, and water bodies expanded. The arboriculture was mainly increased from forest land (6250 hectares), farmland (5742 hectares), and rangeland (364 hectares) (Table 4).

Table 3 Matrix of land use change between 1986 and 2000 (unit: hectares)

		2000							Total 1986
		Forest	Arboriculture	Rangeland	Farmdland	Buildings	Water	Other	
1986	Forest	127190	46	4300	9488	5	15	24	141067
	Arboriculture	886	79	80	1154	8	2	1	2210
	Rangeland	4282	1	26100	11594	29	20	62	42087
	Farmdland	12234	28	15182	94607	978	141	123	123292
	Buildings	44	0	10	469	158	0	0	681
	Water	494	3	33	185	7	313	47	1083
	Other	64	1	56	169	0	7	87	385
	Total 2000	145194	157	45760	117667	1185	498	344	310805

Table 4 Matrix of land use change between 2000 and 2019 (unit: hectares)

		2019							Total 2000
		Forest	Arboriculture	Rangeland	Farmdland	Buildings	Water	Other	
2000	Forest	125567	6250	2037	10902	165	163	109	145194
	Arboriculture	3	136	0	16	0		1	157
	Rangeland	5522	364	22379	17383	41	50	14	45760
	Farmdland	12383	5742	4623	93793	642	397	88	117667
	Buildings	2	12	1	831	330	6	3	1185
	Water	46	28	73	254	1	1	94	498
	Other	4	6	199	59	2	73	1	344
	Total 2019	143528	12538	29312	123239	1182	689	310	310805

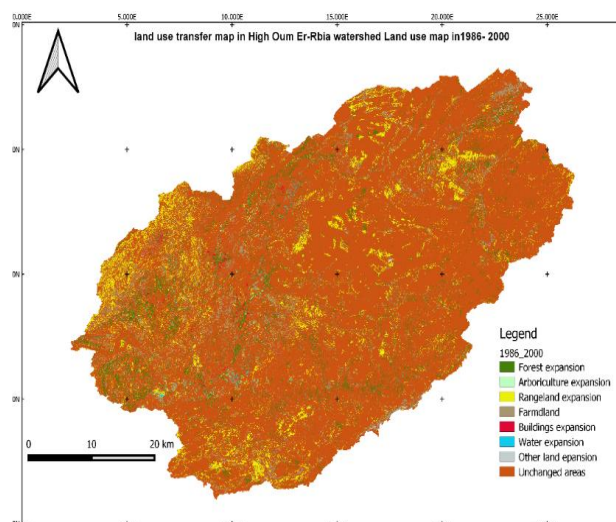


Figure 7 land use transfer map in 1986-2000

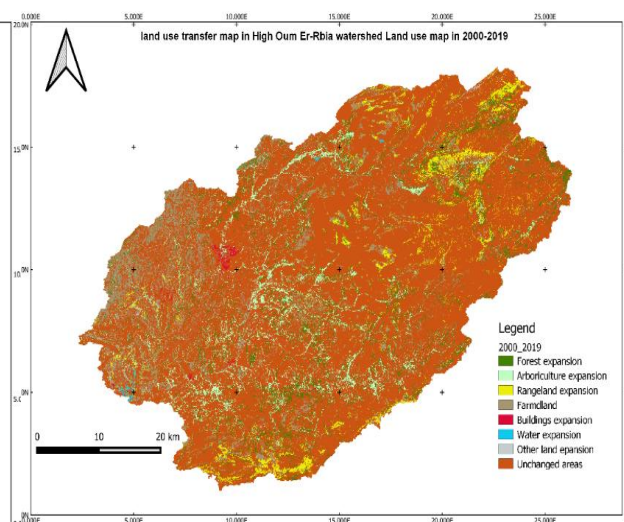


Figure 8 Land use transfer map in 2000-2019

Comparing the spatial-temporal changes in land use between 2000–2009 and 2009–2018 (figures 7 and 8), it was found that the arboriculture area decreased first and then increased, but the forest land area followed the opposite trend. In general, between 1986 and 2019, the rangeland and water were continuously degraded, and the areas of forest land, construction land, and arboriculture gradually increased.

### 3.4 Analysis of land use Classification Variable Importance and Result Verification

This study extracted 12 characteristic variables from satellite imagery and used the RF classifier on the GEE platform to classify land use in the High Oum Er-Rbia watershed. The RF method allows multiple data sources to be used in the modeling process

and classifies land-use heterogeneity properly (Breiman 2001). The variable importance analysis shows that elevation is the main important factor that contributes to the land use classification (Figure 4) in addition to the MNDWI and NDVI which are used to extract vegetation and water present in the study area.

The overall accuracy and kappa coefficient for this study is higher than 80% which is a good result (Gashaw et al. 2018), Accurate training samples and validation samples are the basis of the classification accuracy. Arboriculture and forestland land-use type show the highest user accuracy and producer's accuracy of land use classification results from 1986 to 2019 (Table 2).

### 3.5 Temporal-Spatial Variation of land use Changes

Land-use changes are influenced by the interaction between humans and the environment at different spatial and temporal scales. Monitoring Land use changes can help us understand the causes of their dynamic changes, and it supports land management and decision-making (Ren et al. 2017; Ren et al. 2018). The land-use classification results indicated that forest land was the main land-use type in the high Oum Er- Rbia watershed, followed by farmland land and grassland.

Comparing land-use changes in the Oum Er- Rbia watershed in the periods of 1986–2000 and 2000–2019. The change trajectories of the main land-use types in the periods of 1986–2000 and 2000–2019 were the same. The forest land has continued to decline, but the arboriculture and farmland land show the opposite trend. The buildings area expanded but the water body broadly decreased from 1986.

The difference can probably be attributed to the implementation of the Project of Green Morocco plan. The expansion of construction land was faster after 2000. Moreover, the wetland area decreased from 1986 to 2019, which was mainly due to the drought: a decrease in annual mean precipitation and dry lakes even with the establishment of the Ahmed El Hansalidam commissioned in 2002 there was still a decrease.

### Conclusions

The study used the dense time stacking of multi-temporal Landsat images and the RF machine learning algorithm to map the land use in the high Oum Er- Rbia watershed. Our results demonstrated that from 1986 to 2019, the study area was dominated by forestland, followed by farmland land and grassland. Grasslands and wetlands gradually degraded from 2000 to 2018, while farmland land, arboriculture, construction land, and unused land expanded. Grassland was mainly converted to Farmland and arboriculture land. In addition, the importance analysis of all variables using the RF model found that elevation and NDVI were the most important

characteristic variable for land-use classification in the high Oum Er- Rbia watershed.

### References

- Anderson, J. R. (1976). *A land use and land cover classification system for use with remote sensor data* (Vol. 964). US Government Printing Office.
- Belgiu, M., & Dragut, L. (2016). Random forest in remote sensing: A review of applications and future directions. *ISPRS Journal of Photogrammetry and Remote Sensing*, 114, 24–31.
- Bootsma, E. J. (2021). Mapping time-series evapotranspiration for agricultural applications (Unpublished Dissertation).
- Breiman, L. (2001). Random forests. *Machine Learning*, 45 (1), 5–32.
- De Waele, J., & Melis, M. T. (2009). Geomorphology and geomorphological heritage of the Ifrane–Azrou region (Middle Atlas, Morocco). *Environmentalgeology*, 58(3), 587–599.
- El-Bouqdaoui, K. (2007). Approche méthodologique de l'évaluation du risque potentiel d'érosion des sols du bassin versant du Srou (Moyen Atlas, Maroc) à l' aide de la télédétection et du SIG.
- El Jazouli, A., Barakat, A., Khellouk, R., Rais, J., & El Baghdadi, M. (2019). Remote sensing and GIS techniques for prediction of land use land cover change effects on soil erosion in the high basin of the Oum Er Rbia River (Morocco). *Remote Sensing Applications: Society and Environment*, 13, 361–374.
- Gashaw, T., Tulu, T., Argaw, M., Worqlul, A.W., Tolessa, T., & Kindu, M. (2018). Estimating the impacts of land use/land cover changes on ecosystem service values: The case of the Andassa watershed in the Upper Blue Nile basin of Ethiopia. *Ecosystem Services*, 31, 219–228.
- Gorelick, N., Hancher, M., Dixon, M., Ilyushchenko, S., Thau, D., & Moore, R. (2017) Google earth engine: planetary-scale geospatial analysis for everyone. *Remote Sensing Environment*, 202(1), 18–27.
- Hoshikawa, K., & Umezaki, M. (2014). Effects of terrain-induced shade removal using global DEM data sets on land-cover classification. *International Journal of Remote Sensing*, 35(4), 1331–1355.
- Lillesand, T., Kiefer, R. W., & Chipman, J. (2015). *Remote sensing and image interpretation*. John Wiley & Sons.

- Millennium Ecosystem Assessment. (2005). Ecosystems and Human Well-being. Opportunities and challenges for Business and Industry. Retrieved from <https://www.millenniumassessment.org/documents/document.353.aspx.pdf>.
- Na, X.D., Zhang, S.Q., Li, X.F., Yu, H.A., & Liu, C.Y. (2010). Improved land cover mapping using random forests combined with landsat thematic mapper imagery and ancillary geographic data. *Photogrammetric Engineering & Remote Sensing*, 76, 833–840.
- Ran, Q., Hao, Y., Xia, A., Liu, W., et al. (2019). Quantitative assessment of the impact of physical and anthropogenic factors on vegetation spatial-temporal variation in Northern Tibet. *Remote Sensing*, 11(10), 1183.
- Rasool, R., Fayaz, A., ul Shafiq, M., Singh, H., & Ahmed, P. (2021). Land use land cover change in Kashmir Himalaya: Linking remote sensing with an indicator based DPSIR approach. *Ecological Indicators*, 125, 107447.
- Ren, M., Zeng, W., Yang, B., & Urtasun, R. (2018). Learning to reweight examples for robust deep learning. In *International conference on machine learning* (pp. 4334-4343). PMLR. Retrieved from <http://proceedings.mlr.press/v80/ren18a/ren18a.pdf>
- Ren, Y., Lü, Y., Fu, B., & Zhang, K. (2017). Biodiversity and ecosystem functional enhancement by forest restoration: A meta-analysis in China. *Land Degradation & Development*, 28(7), 2062-2073.
- Rodriguez-Galiano, V. F., Ghimire, B., Rogan, J., Chica-Olmo, M., & Rigol-Sanchez, J. P. (2012). An assessment of the effectiveness of a random forest classifier for land-cover classification. *ISPRS journal of photogrammetry and remote sensing*, 67, 93-104.
- Rogan, J., & Chen, D. (2004). Remote sensing technology for mapping and monitoring land-cover and land-use change. *Progress in planning*, 61(4), 301-325.
- Pu, D. C., Sun, J. Y., Ding, Q., Zheng, Q., Li, T. T., & Niu, X. F. (2020). Mapping urban areas using dense time series of landsat images and google earth engine. *The International Archives of Photogrammetry, Remote Sensing and Spatial Information Sciences*, 42, 403-409.
- Schürmann, A., Kleemann, J., Fürst, C., & Teucher, M. (2020). Assessing the relationship between land tenure issues and land cover changes around the Arabuko Sokoke Forest in Kenya. *Land Use Policy*, 95, 104625.
- Tamiminia, H., Salehi, B., Mahdianpari, M., Quackenbush, L., Adeli, S., & Brisco, B. (2020). Google Earth Engine for geo-big data applications: A meta-analysis and systematic review. *ISPRS Journal of Photogrammetry and Remote Sensing*, 164, 152-170.
- Tsai, Y. H., Stow, D., An, L., Chen, H. L., Lewison, R., & Shi, L. (2019). Monitoring land-cover and land-use dynamics in Fanjingshan National Nature Reserve. *Applied Geography*, 111, 102077.
- Waske, B., & Braun, M. (2009). Classifier ensembles for land cover mapping using multitemporal SAR imagery. *ISPRS journal of photogrammetry and remote sensing*, 64(5), 450-457.



## Journal of Experimental Biology and Agricultural Sciences

<http://www.jebas.org>

ISSN No. 2320 – 8694

### Estimation of nitrogen use efficiency by mango seedlings under nano and convention calcium fertilization using the enriched stable isotope (N-15)

Rawia El-Motaïum<sup>1</sup>, Ayman Shaban<sup>2</sup>, El Sayed Badawy<sup>3</sup>, Ahmad Ibrahim<sup>1\*</sup>

<sup>1</sup>Plant Researches Department, Nuclear Research Center, Egyptian Atomic Energy Authority, P.O. box 13759- Atomic Energy Post office, Inshas, Egypt

<sup>2</sup>Department of Pomology, Faculty of Agriculture, Cairo University, Cairo, Egypt

<sup>3</sup>Soil Science Department, Faculty of Agriculture, Cairo University, Cairo- Egypt.

Received – February 22, 2022; Revision – April 17, 2022; Accepted – April 29, 2022

Available Online – April 30, 2022

DOI: [http://dx.doi.org/10.18006/2022.10\(2\).379.386](http://dx.doi.org/10.18006/2022.10(2).379.386)

#### KEYWORDS

C/N analyzer

Electron Microscope

<sup>15</sup>N Analyzer

Nano-CaO

(<sup>15</sup>NH<sub>4</sub>)<sub>2</sub>SO<sub>4</sub>

Nitrogen use efficiency

<sup>15</sup>N uptake

#### ABSTRACT

This study aimed to investigate the effect of nano-Ca fertilizer on nitrogen uptake, nitrogen use efficiency and determine the best calcium form and dose for mango. A pot experiment was conducted using two year old mango seedlings (cv. Zebda). The pots were filled with sandy soil (8 kg per pot) and one seedling was transplanted into each pot. Four treatments including nano-Ca, convention Ca, soil application and foliar application have been formulated. Calcium was applied as CaO for both the convention and nanoforms. The enriched (<sup>15</sup>NH<sub>4</sub>)<sub>2</sub>SO<sub>4</sub> was applied at a rate of (5g per pot). Plants were harvested at the end of the fall, spring, and summer growth cycles and dried at 70 °C. The dried plant is used for making fine powder and to determine total nitrogen, calcium, and % <sup>15</sup>N atom excess. Results of the study revealed that in all growth cycles, the <sup>15</sup>N translocation was higher under foliar nano-Ca treatment than under convention Ca at a 100% rate. The highest uptake, translocation, and nitrogen use efficiency were observed at 50% (250 mg. L<sup>-1</sup>) foliar nano-Ca treatment in all cycles. In the Fall growth cycle, the values for nitrogen fertilizer use efficiency at 50% nano-Ca rate was 81.8%, while it recorded 64.9% for 25% rate and 51.2% for 100% rate. Calcium concentration, in shoot and roots, was also higher under nano-calcium (for fall cycle = 3.0 for the shoot and 2.8 for root) than the convention calcium (for fall cycle = 2.7% for the shoot and 2.2 for root) for all cycles. The summer growth cycle recorded the highest total biomass under all treatments compared with the fall or spring growth cycles. Allocation of biomass to the shoot was also reported higher under nano-Ca foliar application than that of soil application in all cycles. The best treatment is 50% (250 mg.L<sup>-1</sup>) foliar nano-Ca as it resulted in the highest N-15 uptake, translocation, and nitrogen use efficiency. Nano calcium proves to be more efficient as fertilizer than conventional calcium.

\* Corresponding author

E-mail: [ahmed\\_salem79@yahoo.com](mailto:ahmed_salem79@yahoo.com) (Ahmed Salem Ali Ibrahim)

Peer review under responsibility of Journal of Experimental Biology and Agricultural Sciences.

Production and Hosting by Horizon Publisher India [HPI]  
(<http://www.horizonpublisherindia.in/>).  
All rights reserved.

All the articles published by [Journal of Experimental Biology and Agricultural Sciences](#) are licensed under a [Creative Commons Attribution-NonCommercial 4.0 International License](#) Based on a work at [www.jebas.org](http://www.jebas.org).



## 1 Introduction

The current practices of fertilizer usage have caused serious environmental pollution, soil degradation, groundwater contamination, and economic loss. Fertilizers are not used efficiently and most of it is lost to the environment. Most conventional fertilizers have low nutrient supply efficiency (Elemike et al. 2019). Around 40-70% of the nitrogen and 80-90% of the phosphorus fertilizers applied to the soil are lost to the environment or become unavailable to plants (Rajonee et al. 2017). To overcome the fertilizer loss, the nutrient deficiency of most soils, and the high cost of conventional fertilizer, the reduction in the use of chemical fertilizers is the recent approach to solve these problems. Instead, an increase in fertilizer use efficiency to obtain more yield per unit of fertilizer applied is needed.

Nanotechnology, serve as the latest technology which can provide less harmful and more efficient nano-fertilizer. Several researchers have reported that plant nutrients could be enriched by applying nano-nutrients that can be easily absorbed by plants. The use of nano-fertilizer is expected to help in reducing the fertilizer dose and increase plant productivity. Due to the small particle size (< 100 nm) and high surface area of nano-fertilizer it can easily penetrate the plant and improve uptake and nutrient use efficiency (Singh et al. 2017). Nanoscale (< 100nm) fertilizer has several distinguishing properties like a high surface area to volume ratio, acting as a slow-release fertilizer to provide nutrients throughout the crop growth period, reducing pollution of the environment (Corradini et al. 2010; Wilson and Rowe 2008). The beneficial effect of nanoparticles such as nano-TiO<sub>2</sub> increase photosynthetic rate, dry weight, chlorophyll a (Zheng et al. 2005; Khot et al. 2012); multi-walled carbon nanotubes (MWCNTs) increase the germination rate of tomato seeds by increasing the seed water uptake (Khodakovskaya et al. 2009) and nano-fertilizer prevent the plant from different biotic and abiotic stress (Singh et al. 2017). In addition, nano-scale particles with a higher surface area have a greater number of reaction sites than a particle with a low surface area, which results in enhanced chemical reactivity (Kale and Gawade 2016).

Mango (*Mangifera indica* Linn.) is one of the most important fruit crops in tropical and subtropical areas. It is considered to be the most popular fruit crop in Egypt. Growth of mango occurs in flushes of shoots from apical or lateral buds (Shaban 2009). Vegetative growth of mango trees occurs in both spring and summer cycles. The summer growth cycle recorded the highest significant vegetative growth, highest flowering percentage, the highest number of fruits per panicle, and fruit weight followed by the spring than the fall cycle (Shaban 2009).

Calcium is an essential component of cells, maintaining the structure of cell walls and stabilizing cell membranes (Abd El-Razek et al. 2017). Calcium levels exert a profound effect on the protein and soluble nitrogen content in different parts of Peanut

and Linseed plants (Pal and Laloraya 1973). These researchers suggested that the level of soluble-nitrogen content is generally less in high calcium plants compared to the control.

The <sup>15</sup>N tracer technique is an isotope of broad application for the understanding of biological and/or chemical processes affecting nitrogen movement in the agriculture system (Axmann and Zapata 1990). A common form of fertilizer use efficiency expression is plant recovery or percent utilization of the added fertilizer (Zapata, 1990). Studying the uptake, translocation, and utilization of labeled nitrogen (N-15) can help optimize the dose of nano-calcium fertilizer for mango. The objective of this study was to investigate the effect of nano and convention Ca fertilizer, applied to the soil or as a foliar spray, on nitrogen uptake, translocation, and N recovery (nitrogen use efficiency) in the three growth cycles (Fall, Spring, and Summer) of mango seedlings. This will help to determine the best calcium form, dose, and method of Ca application for mango.

## 2 Materials and Methods

A pot experiment was conducted using two year old mango seedlings (cv. Zebda). The pots were filled with 8 kg per pot of sandy soil (*Typic torripsamments*) as per the recommendation of the Soil Survey Staff (1975). Plants were transplanted into the pots, one plant per pot. Each growth cycle contained 18 plants (6 treatments x 3 replicates).

### 2.1 N-15 labeled fertilizer

Nitrogen-15 fertilizer was applied as (<sup>15</sup>NH<sub>4</sub>)<sub>2</sub>SO<sub>4</sub>, enriched at 10.35% a.e. at a rate of 5g per pot after seedling transplanting. The labeled ammonium sulfate was manufactured at the Shanghai Research Institute of Chemical Industry, Shanghai, China.

### 2.2 Preparation of nano-calcium fertilizer

Nano fertilizers were prepared at the Soil Science Department, Faculty of Agriculture, Cairo University by ball-milling machine (Photon Company, Egypt). Portions of 100g of Ca fertilizer were placed in a stainless steel canister with metal balls of different sizes. The canister was placed on the ball-milling machine and stirred for 26 hours at speed of 1000 rpm/minute. A sample from the milled fertilizer was collected and submitted to the Transmission Electron Microscope (JEM-1400 TEM, Japan) at the Central Laboratories, Faculty of Agriculture, Cairo University for examination of the particle morphology and measuring the size of the Ca-nano particles. A drop of well-dispersed nanoparticles was placed onto the amorphous carbon-coated 200 mesh carbon grid, followed by drying the sample at ambient temperature, before loading it into the microscope (Wang et al. 2014). The size and morphology of the nanoparticles were measured and found to be less than 100 nm (Figure 1).

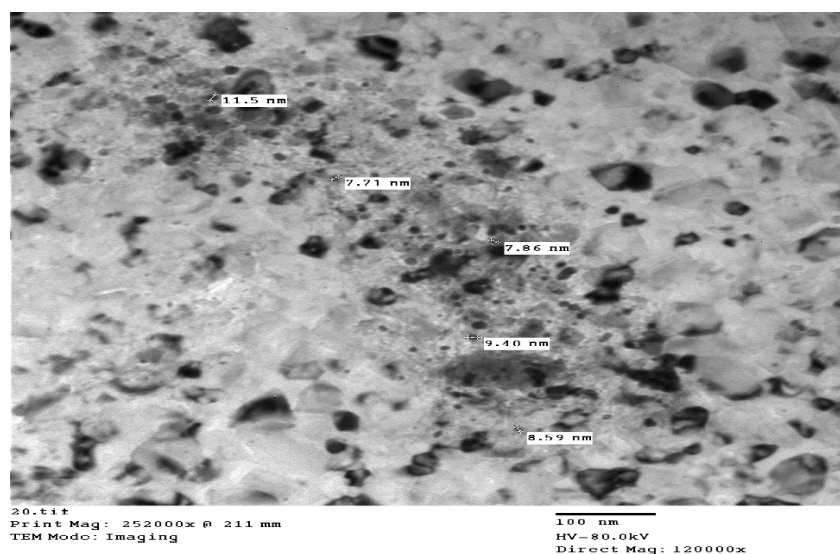


Figure 1 Transmission Electron Microscope Image of Nano-Calcium Particles

### 2.3 Treatments

Calcium fertilizer was applied as calcium oxide (CaO) for both the nano and convention forms, the following treatment were imposed for the recommended dose (i) Ca convention application in soil (100%=6g /pot), (ii) Ca convention application at foliar (100%= 500 mg.L<sup>-1</sup>), (iii) Ca Nano application in soil (100%= 6g /pot), (iv) Ca Nano application at foliar (100% = 500 mg.L<sup>-1</sup>), (v) Ca Nano application at foliar (50% = 250 mg.L<sup>-1</sup>), and (vi) Ca Nano application at foliar (25% = 125 mg.L<sup>-1</sup>).

### 2.4 Nutrient solution

Half strength modified Hoagland solution was prepared according to Stout et al. (1957). Half a liter of the prepared nutrient solution was added to each pot once a week. Plant watering was conducted to keep the soil moisture content at field capacity.

### 2.5 Plant harvest

The labeled ammonium sulfate fertilizer was applied at the beginning of the fall cycle in September. Plants of each growth cycle were harvested at different times. Plants of the fall growth cycle were harvested in December (after 3 months from the application of N-15), in May of the next year for spring, and in September for the summer growth cycle. Plants were washed with deionized water and separated into shoots and roots. All samples were dried at 70 °C and then ground up to very fine powder.

### 2.6 Nutrients analysis

Following plants harvest, they were analyzed for total nitrogen using a C/N analyzer (Elementar, Germany) and for % N-15 atom excess using the Emission Spectrometry N-15 Analyzer (FAN

Fisher No.1-6PC Spectrometer). Calcium was measured using the Atomic Absorption Spectrometry (Shimadzu6800, Japan).

### 2.6.1 Calculation

The following equations were used for the calculation of the following parameters (Zapata, 1990):

Percent nitrogen derived from fertilizer (%Ndff) in plant organs

$$\%N - 15 \text{ dff} = \frac{\%N \text{ a. e. in plant sample}}{\%N \text{ a. e. in the labeled fertilizer}} \times 100$$

Percent % <sup>15</sup>N recovery by plant

$$\%N - 15 \text{ recovery (Utilization)} = \frac{\text{amount of } N - 15 \text{ in plant derived from fertilizer}}{\text{amount of } N - 15 \text{ applied to the soil}} \times 100$$

### 2.7 Experiment Design and Statistical Analysis

Eighteen pots for each cycle were arranged in a Completely Randomized Design with three replicates for each treatment. Data were subjected to analysis of variance (Steel and Torrie 1960) using the MSTAT statistical microcomputer program. The significant means were compared using LSD at 5% probability (Snedecor and Cochran 1980). The results are an average of two seasons.

## 3 Results and Discussion

### 3.1 Nitrogen (<sup>15</sup>N) uptake and translocation under Ca- application

Results in Tables (1, 2, 3) demonstrate that N-15 uptake under convention and nano-calcium applied to the soil at a 100% rate, differs in the different growth cycles. In the fall growth cycle, N-



15 uptake was significantly higher under convention Ca (%<sup>15</sup>Ndff = 35.9) as compared to the nano- Ca (%<sup>15</sup>Ndff =30.0). The opposite trend was observed in the spring growth cycle. The N-15 uptake was significantly higher under nano-Ca (%<sup>15</sup>Ndff =20.4) than under convention Ca (%<sup>15</sup>Ndff = 15.2). While in the summer growth cycle, the uptake was similar under convention Ca (%<sup>15</sup>Ndff = 14.9) and nano-Ca ((%<sup>15</sup>Ndff =14.8). Regarding N-15 translocation to the shoot, results show that the N-15 translocation to the shoot is significantly higher under nano-Ca than under convention-Ca fertilization in all cycles.

Comparing the N-15 uptake under foliar application of nano and convention Ca, at a 100% rate, it was higher under convention Ca (%<sup>15</sup>Ndff = 34.8) than nano-Ca (%<sup>15</sup>Ndff = 17.7) for the fall growth cycle. While in the spring cycle, the opposite trend was observed and the N-15 uptake was higher under nano-Ca by 1.9 fold than the convention-Ca. In the summer growth cycle, the N-15 uptake was higher under nano-Ca by (1.5 fold) than the convention-Ca fertilization. The N-15 translocation in the fall and summer growth cycles was significantly higher under nano-Ca than convention-Ca by 1.6 and 1.5 fold, respectively. While the translocation in the spring was higher under nano-Ca as compared to the convention Ca but this difference was significantly not different. These findings agree with Swietlik (2006) who found that calcium enhanced the translocation of nitrogen.

### 3.2 Effect of foliar nano-Ca fertilization

The N-15 uptake and translocation, during the three growth cycles, at the different foliar nano-Ca application rates (100%, 50%, 25%) were compared. Results of the study revealed that N-15 uptake and translocation were highest at 50% nano-Ca foliar spray relative to 100% or 25% rates, in all three cycles. The trends of the N-15

translocation to the shoot are 50% > 100% >25%. Quantitative results of N-15 uptake and translocation showed that N-15 uptake for the summer growth cycle was 23.5 at 50%, while this was reported 22.7 and 19.6 for the 100% and 25% Ndff respectively. Results of the study also suggest that as Ca concentration increased N-15 uptake and translocation also increased. These results are in agreement with Swietlik (2006) who found that calcium enhanced the translocation of nitrogen.

### 3.3 Total nitrogen percent

Foliar application of nano-Ca in the fall and summer growth cycles at a 100% rate, showed significantly higher nitrogen content than soil application. Fall foliar application results are 1.20% for root and 1.42% for the shoot, while soil application results are 1.16% for root and 1.26 for the shoot. The highest total nitrogen percent was observed in the shoot and received a 50% foliar nano-Ca rate relative to 100% or 25% rates. Quantitative results showed that total nitrogen content in the shoot is 1.35% for the fall, while it was reported as 1.43% for the spring and 1.59% for the summer growth cycles. The percent N was significantly higher in the shoot than the root under both nano and convention Ca fertilization for both soil and foliar application in all cycles. The results agree with Swietlik (2006) who found that the application of calcium increased concentrations of N in the stem and roots of apple seedlings (*Malus x Domestica borkh.*).

### 3.4 <sup>15</sup>N recovery (nitrogen fertilizer use efficiency)

Results presented in Table 1 showed that percent N recovery in the fall growth cycle was significantly higher under nano-Ca (46.3%) than under convention Ca (30.7%) applied to the soil at 100% dose. Whereas, foliar application of Ca at 100% rate

Table 1 <sup>15</sup>N uptake, translocation, and recovery in the Fall growth cycle

Treatments	Method of application	Organ	%Ndff	%N	% <sup>15</sup> N recovery	Amount of <sup>15</sup> N recovered
Convention 100%	Soil	Root	35.9	1.29	30.7	1.54
		Shoot	15.8	1.21		
Convention 100%	Foliar	Root	34.8	1.30	49.3	2.56
		Shoot	28.0	1.22		
Nano-Ca 100%	Soil	Root	30.0	1.16	46.3	2.32
		Shoot	38.3	1.26		
Nano-Ca 100%	Foliar	Root	17.7	1.20	51.2	2.47
		Shoot	44.8	1.42		
Nano-Ca 50%	Foliar	Root	33.9	1.23	81.8	4.09
		Shoot	45.5	1.35		
Nano-Ca 25%	Foliar	Root	20.0	1.11	64.9	3.25
		Shoot	39.9	1.30		
LSD (0.05)			1.91	0.02	2.10	0.08

showed higher %N recovery under nano-Ca (51.2%) than under convention Ca (49.3%), however, this difference is non-significant. The different concentrations of foliar nano-Ca showed that the highest % <sup>15</sup>N recovery was observed at nano-Ca concentration of 50% (81.8%) followed by 25% (64.9%), then 100% (51.2%). Nano-Ca at 50% treatment showed the highest <sup>15</sup>N-recovery and also the highest amount of <sup>15</sup>N recovered (4.09 g) among all treatments.

Results presented in Table 2 showed that %N recovery in the spring growth cycle was significantly higher under nano-Ca (75.4%) than under convention Ca (43.5%) applied to the soil at 100%. Foliar application of Ca at a 100% rate showed significantly higher %N recovery under nano-Ca (68.0%) than under convention Ca (49.3%). The different concentrations of foliar nano-Ca showed that the highest % <sup>15</sup>N recovery was observed at nano-Ca

concentration of 50% (80.1%) followed by 25% (75.9%), then 100% (68.0%). Nano-Ca at 50% treatment showed the highest <sup>15</sup>N-recovery and the highest amount of <sup>15</sup>N recovered (4.01 g) among all treatments.

Results presented in Table 3 showed that %N recovery in the summer growth cycle was significantly higher under nano-Ca (63.6%) than under convention Ca (39.9%) applied to the soil at 100%. Foliar application of Ca at a 100% rate showed significantly higher %N recovery under nano-Ca (61.0%) than under convention Ca (49.3%). The different concentrations of foliar nano-Ca showed that the highest percent <sup>15</sup>N recovery was observed at nano-Ca concentration of 50% (90.4%) followed by 25% (70.4%), then 100% (61.0%). Nano-Ca at 50% treatment showed the highest <sup>15</sup>N-recovery and the highest amount of <sup>15</sup>N recovered (4.52 g) among all treatments.

Table 2 <sup>15</sup>N uptake, translocation and recovery in the Spring growth cycle

Treatments	Method of application	Organ	%Ndff	%N	% <sup>15</sup> N recovery/plant	Amount of <sup>15</sup> N recovered
Convention 100%	Soil	Root	15.2	1.26	43.5	2.18
		Shoot	33.8	1.37		
Convention 100%	Foliar	Root	11.7	1.24	59.2	2.96
		Shoot	36.0	1.46		
Nano-Ca 100%	Soil	Root	20.4	1.29	75.4	3.77
		Shoot	36.0	1.49		
Nano-Ca 100%	Foliar	Root	22.2	1.24	68.0	3.40
		Shoot	38.0	1.43		
Nano-Ca 50%	Foliar	Root	25.8	1.21	80.1	4.01
		Shoot	38.8	1.43		
Nano-Ca 25%	Foliar	Root	19.5	1.19	75.9	3.80
		Shoot	37.3	1.42		
LSD (0.05)			2.46	0.02	1.09	0.09

Table 3 <sup>15</sup>N uptake, translocation, and recovery in the summer growth cycle

Treatments	Method of application	Organ	%Ndff	%N	% <sup>15</sup> N recovery	Amount of <sup>15</sup> N recovered
Convention 100%	Soil	Root	14.9	1.16	39.9	2.00
		Shoot	22.0	1.31		
Convention 100%	Foliar	Root	15.3	1.34	49.3	2.47
		Shoot	20.8	1.50		
Nano-Ca 100%	Soil	Root	14.8	1.22	63.6	3.18
		Shoot	25.7	1.52		
Nano-Ca 100%	Foliar	Root	22.7	1.37	61.0	3.05
		Shoot	30.4	1.48		
Nano-Ca 50%	Foliar	Root	23.5	1.35	90.4	4.52
		Shoot	32.7	1.59		
Nano-Ca 25%	Foliar	Root	19.6	1.20	70.4	3.52
		Shoot	27.7	1.44		
LSD (0.05)			1.20	0.03	1.27	0.11

Results presented in tables (1, 2, 3 & 4) showed that nitrogen fertilizer use efficiency ( $^{15}\text{N}$  recovery), and N-15 translocation to the shoot were higher under nano-Ca than convention Ca for both application methods (soil and foliar) in all cycles. This is evidence of a synergistic relationship between nano-Ca and nitrogen which suggest that nano-Ca facilitate nitrogen translocation. Various previous researchers like Kale and Gawade, (2016) and Singh et al., (2017) have stated that nano fertilizer improves uptake and nutrient use efficiency due to its small size and high surface area.

### 3.5 Calcium concentration

Under soil calcium application, the root exhibited higher Ca concentration than shoot for both nano and convention calcium fertilization. On the contrary, shoot exhibited higher calcium concentrations than root under foliar calcium application for both nano and convention calcium. In general, nano calcium fertilization showed higher Ca concentration in the shoot and root tissues of mango plants than convention calcium for both application methods (soil and foliar) in all cycles. This could be due to the higher uptake and penetration of nano-Ca into the plant tissue. Our results agree with Singh et al. (2017) who stated that due to the small particle size (< 100 nm) and high surface area of nano-fertilizer it can easily penetrate the plant and improve uptake and nutrient use efficiency. Results in Table 4 show that calcium concentration in the leaf is in the sufficient range (2.0-3.4%) according to Jones et al. (1991). They mention that the sufficient range for Ca in mango leaf is (2.0-5.0%). The highest calcium concentration was observed at a nano-Ca concentration of 50% in all cycles.

### 3.6 Calcium-nitrogen interaction

Nano-calcium concentrations exert a profound effect on nitrogen content in the mango plant's shoot and root. Results show that nano-calcium foliar spray has increased nitrogen uptake, translocation, and nitrogen tissue concentration. In the fall growth cycle, the high level of foliar nano-Ca (100%) resulted in significantly higher root nitrogen content (%N=1.20%) than the low level (25%) (%N=1.11%). A similar trend was observed in the spring and the summer growth cycles. This is evidence of a synergistic relationship (positive interaction) between nano-calcium and nitrogen.

The calcium-nitrogen interaction suggested that our results agree with Gunes et al. (1998) who found that applied Ca increased the concentration of Ca and N in tomato plants. These results are also supported by Swietlik (2006) findings related to the calcium stimulation of nitrogen (in the ammonium form) uptake in apple and sour orange.

### 3.7 Total Biomass

Results in Table 5 showed that the plant total biomass is higher in the summer growth cycle followed by the spring growth cycle than the fall cycle. The average biomass of all treatments is 86.2g for the summer growth cycle, 71.8 g for the spring growth cycle, and 61.6 g for the fall growth cycle. In general, nano-calcium fertilizer resulted in significantly higher plant biomass than convention calcium fertilizer. This is could be due to higher  $^{15}\text{N}$  uptake, translocation and nitrogen use efficiency under nano-calcium than convention calcium fertilization. The results are in the same line

Table 4 Calcium concentration in root and shoot of the three cycles

Treatments	Method of application	Organ	% Ca		
			Fall	Spring	Summer
Convention 100%	Soil	Root	2.9	2.7	2.1
		Shoot	2.2	2.0	1.8
Convention 100%	Foliar	Root	2.2	2.0	1.7
		Shoot	2.7	2.5	2.0
Nano-Ca 100%	Soil	Root	3.3	3.4	3.0
		Shoot	2.6	2.3	2.3
Nano-Ca 100%	Foliar	Root	2.8	2.6	2.5
		Shoot	3.0	3.0	2.8
Nano-Ca 50%	Foliar	Root	3.2	2.9	2.8
		Shoot	3.4	3.3	3.1
Nano-Ca 25%	Foliar	Root	2.6	2.5	2.3
		Shoot	2.9	2.9	2.4
LSD (0.05)			0.23	0.15	0.17

Table 5 Plant total biomass and percent shoot biomass relative to the total

Treatments	Method of application	Fall cycle		Spring cycle		Summer cycle	
		Total biomass (g)	% shoot biomass	Total biomass (g)	% shoot biomass	Total biomass (g)	% shoot biomass
Convention 100%	Soil	59.4	75.4	52.5	81.9	76.0	77.6
Convention 100%	Foliar	70.5	80.9	68.6	75.2	85.8	76.7
Nano-Ca 100%	Soil	51.6	75.0	81.1	73.7	90.1	81.9
Nano-Ca 100%	Foliar	44.7	80.1	68.0	83.8	71.2	84.6
Nano-Ca 50%	Foliar	72.0	76.7	80.0	77.5	94.5	79.4
Nano-Ca 25%	Foliar	71.5	78.0	80.6	80.1	99.7	71.9
LSD (0.05)		1.50	1.80	2.00	1.37	2.10	1.80

with Mahmood et al. (2009) who observed a significant highly positive correlation between dry matter yield and Ca concentration in wheat plant tissue.

Allocation of biomass to the shoot was higher under foliar application (80.9%) than the soil (75.4%) application method for convention calcium fertilization (100% rate) for the fall growth cycle, but lower for the spring growth cycle and almost similar for the summer growth cycle. Allocation of biomass to the shoot was higher under Ca foliar application than the soil application method for nano-calcium fertilization at a 100% rate for all growth cycles. Comparing the values of percent shoot biomass under nano and convention Ca-fertilizer, results revealed similar values (75.4%, 75.0%) for the fall cycle, while it recorded a higher value for the convention (81.9%) than nano-Ca (73.7%) for the spring cycle and higher value for nano-Ca (81.9%) than convention Ca (77.6%) for the summer growth cycle. Comparing the 3 levels of foliar nano-calcium, allocation of biomass to the shoot was significantly highest at 100% followed by 50% then 25% for all cycles. Results of the total biomass revealed that the summer growth cycle has the highest total biomass under all treatments compared with the fall or spring cycles. The summer growth cycle was reported to give the highest flowering percentage, number of fruits per panicle, and fruit weight followed by the spring growth cycle and then the fall growth cycle (Shaban 2009). The higher nitrogen use efficiency under nano than convention calcium fertilizer has resulted in higher plant biomass in the former than the latter. Similar results were obtained by Laware and Raskar (2014) who demonstrated that onion crops treated with ZnO-nano particles at 20 and 30 µg/ml showed better growth and flowered 12-14 days earlier than those treated with convention ZnSO<sub>4</sub>.

The total biomass results presented in Table 5 showed that the summer growth cycle recorded the highest total biomass under all treatments compared with the fall or spring cycles. The summer growth cycle was reported to give the highest flowering percentage, the number of fruits per panicle, and fruit weight followed by the spring cycle then the fall cycles (Shaban 2009).

The higher nitrogen use efficiency under nano than convention calcium fertilizer has resulted in higher plant biomass in the former as compared to the later. Similar results were obtained by Laware and Raskar (2014) who demonstrated that onion crops treated with ZnO-nano particles at 20 and 30 µg/ml showed better growth and flowered 12-14 days earlier than those treated with convention ZnSO<sub>4</sub>.

### Conclusions

In conclusion, nitrogen use efficiency (<sup>15</sup>N recovery) was higher under nano-calcium than convention calcium fertilization in all cycles. This finding proves true under the two application methods (soil and foliar). There is evidence of a positive synergistic relationship between nano-Ca and nitrogen, i.e. nano-Ca enhanced <sup>15</sup>N uptake, translocation to the shoot, N tissue concentration, and <sup>15</sup>N recovery. The highest N-15 uptake and translocation was observed at a nano-Ca foliar concentration of 50% relative to 25%. A significantly higher %N was observed in the shoot than the root under nano-Ca fertilization for both soil and foliar application methods in all cycles. Calcium concentration in mango seedlings was higher under nano-calcium than under convention calcium fertilization in all cycles. The summer growth cycle recorded the highest total biomass compared with the fall or the spring growth cycles. Results of the current study recommend applying calcium in the nano form at 50% of the recommended rate as a foliar spray.

### Conflict of interest

The authors declare no conflict of interest

### References

- Abd El-Razek E., Amin, O.A., El-Nahrawy, A.M., & Abdel-Hamid, N. (2017). Effect of foliar application of biosimulated nanomaterials (calcium/yeast nanocomposite) on yield and fruit quality of "Ewais" mango trees. *Annual Research & Review in Biology*, 18, 1-11.

- Axmann, H., & Zapata, F. (1990). Stable and radioactive isotopes. In Hardarson, G. (ed.) *Uses of Nuclear Techniques in Studies of Soil-Plant Relationships*, (pp. 9-34) Training course Series No. 2, IAEA, Vienna-Austria.
- Corradini E., de Moura, M. R., & Mattoso, L. H. C. (2010). A preliminary study of the incorporation of NPK fertilizer into chitosan nanoparticles. *EXPRESS Polymer Letters*, 4, 509–515.
- Elemike E.E., Uzoh, I.M., Onwudiwe, D.C., & Babalola, O.O. (2019). The role of Nanotechnology in the Fortification of plant nutrients and Improvement of Crop production. *Applied Sciences*, 9, 1-32.
- Gunes, A., Alpaslan, M., & Inal, A. (1998) Critical nutrient concentrations and antagonistic and synergistic relationships among the nutrients of NFT-grown young tomato plants. *Journal of Plant Nutrition*, 21, 2035-2047.
- Jones J.B., Wolf, B., & Mills, H.A. (1991). *Plant Analysis Handbook*. Micro-Macro Publishing, Inc., Athens-GA, USA. pp. 195-203.
- Kale A.P., & Gawade, S.N. (2016). Studies on nanoparticle induced nutrient use efficiency of fertilizer and crop productivity. *Green Chemistry & Technology Letters*, 2, 88-92.
- Khodakovskaya, M., Dervishi, E., Mahmood, M., Xu, Y., Li, Z., Watanabe, F., & Biris, A.S. (2009). Carbon nanotubes are able to penetrate plant seed coat and dramatically affect seed germination and plant growth. *ACS Nano* 3, 3221–3227.
- Khot L.A., Sankaran, S., Maja, J.M., Ehsani, R., Schuster, E.W. (2012). Applications of nanomaterials in agricultural production and crop protection: a review. *Crop Protection*, 35, 64–70.
- Laware, S.L., & Raskar, S. (2014). Influence of zinc oxide nanoparticles on growth, flowering and seed productivity in onion. *International Journal of Current Microbiology Applied Sciences*, 3, 874-881.
- Mahmood, I.A., Salim, M., Ali, A., Arshadullah, M., Zaman B., & Mir, A. (2009). Impact of calcium sulphate and calcium carbide on nitrogen use efficiency of wheat in normal and saline sodic soils. *Soil and Environment*, 28, 29-37.
- Pal, R.N., & Laloraya, M.M. (1973). Calcium in relation to nitrogen metabolism: I- Changes in protein and soluble-nitrogen in Peanut and Linseed plants. *Biochemie und Physiologie der Pflanzen*, 164, 315-326.
- Rajonee, A.A., Zaman, S., & Imam ulHuq, S.M. (2017). Preparation, characterization and evaluation of efficacy of phosphorus and potassium incorporated nano fertilizer. *Advances in Nanoparticles*, 6, 62-74.
- Shaban, A.E.A. (2009). Vegetative growth cycles of some mango cultivars in relation to flowering and fruiting. *World Journal of Agricultural Sciences*, 5, 751-759.
- Singh, M.D., Chirag, G., Prakash, P.O., Mohan, M.H., Prakasha, G., & Vishwajith (2017). Nanofertilizer is a new way to increase nutrients use efficiency in crop production. *International Journal of Agriculture Sciences*, 9, 3831-3833.
- Snedecor, D.W., & Cochran, W.G. (1980). *Statistical methods*. 7<sup>th</sup> Ed. Iow State University Press, Ames-Iowa, USA.
- Soil Survey Staff (1975). *Soil Taxonomy*. Agric Handbook, No. 436, USDA, Washington D.C.
- Steel, R.G.D., & Torrie, J.H. (1960). *Principles and Procedures of Statistics*. McGraw-Hill Book Company Inc., New York, USA.
- Stout P.R., Broyer, T.C., & Carlton, A.B. (1957). Comparative chlorine requirements of different plant species. *Plant and Soil*, 8, 337-353.
- Swietlik, D. (2006). The interaction between calcium chloride and ammonium-nitrogen on growth, nitrogen uptake and translocation in apple and sour orange. *Acta Horticulturae*, 721, 159-164.
- Wang, C., Luo, H., Zhang, Z., Wu, Y., Zhang, J., & Chen, S. (2014). Removal of As (III) and As (V) from aqueous solutions using nano scale zero valent iron-reduced graphite oxide modified composites. *Journal of Hazardous Materials*, 268, 124-131.
- Wilson, P. G., & Rowe, R. (2008). A revision of the Indigofereae (Fabaceae) in Australia. 2: Indigofera species with trifoliolate and alternately pinnate leaves. *Telopea*, 12, 293–307.
- Zapata, F. (1990). Isotope techniques in soil fertility and plant nutrition studies. In: Hardarson, G. (ed.) *Use of Nuclear Techniques in Studies of Soil-Plant Relationships*, (pp. 61-128), Training course Series No. 2, IAEA, Vienna-Austria.
- Zheng, L., Zheng, L., Zhou, M., Chai, Q. et al. (2005). Novel function of the flap endonuclease 1 complex in processing stalled DNA replication forks. *EMBO Reports*, 6, 83-89.



## Journal of Experimental Biology and Agricultural Sciences

<http://www.jebas.org>

ISSN No. 2320 – 8694

### Performance of electrical energy monitoring data acquisition system for plant-based microbial fuel cell

Wilgince Apollon<sup>1</sup>, Alejandro Isabel Luna-Maldonado<sup>1\*</sup>, Juan Antonio Vidales-Contreras<sup>1</sup>, Humberto Rodríguez-Fuentes<sup>1</sup>, Juan Florencio Gómez-Leyva<sup>2</sup>, Sathish-Kumar Kamaraj<sup>3\*</sup>, Víctor Arturo Maldonado-Ruelas<sup>4</sup>, Raúl Arturo Ortiz-Medina<sup>4</sup>

<sup>1</sup>Universidad Autónoma de Nuevo León, Facultad de Agronomía, Departamento de Ingeniería Agrícola y de los Alimentos, Francisco Villa S/N, Ex-Hacienda El Canadá, General Escobedo, Nuevo León, 66050, México

<sup>2</sup>TecNM-Instituto Tecnológico de Tlajomulco (ITTJ), Laboratorio de Biología Molecular, Km 10 Carretera a San Miguel Cuytlán, Tlajomulco de Zúñiga, Jalisco, C.P. 45640, México

<sup>3</sup>TecNM-Instituto Tecnológico El Llano Aguascalientes (ITEL), Laboratorio de Medio Ambiente Sostenible, Km.18 Carretera Aguascalientes-San Luis Potosí, El Llano Ags., C.P. 20330, México

<sup>4</sup>Universidad Politécnica de Aguascalientes (UPA), Departamento de Posgrado e Investigación, Calle Paseo San Gerardo No. 207, Fracc. San Gerardo, Aguascalientes, Ags. C.P. 20342, México.

Received – January 16, 2022; Revision – March 22, 2022; Accepted – April 11, 2022

Available Online – April 30, 2022

DOI: [http://dx.doi.org/10.18006/2022.10\(2\).387.395](http://dx.doi.org/10.18006/2022.10(2).387.395)

#### KEYWORDS

Data acquisition system

Open circuit voltage

Polarization curve

Power density

*Stevia rebaudiana*

#### ABSTRACT

Plant microbial fuel cell (Plant-MFC) is an emerging technology that uses the metabolic activity of electrochemically active bacteria (EABs) to continue the production of bioelectricity. Since its invention and to date, great efforts have been made for its application both in real-time and large-scale. However, the construction of platforms or systems for automatic voltage monitoring has been insufficiently studied. Therefore, this study aimed to develop an automatic real-time voltage data acquisition system, which was coupled with an ATMEGA2560 connected to a personal computer. Before the system operation started it was calibrated to obtain accurate data. During this experiment, the power generation performance of two types of reactors i.e. (i) Plant-MFC and (ii) control microbial fuel cell (C-MFC), was evaluated for 15 days. The Plant-MFC was planted with an herbaceous perennial plant (*Stevia rebaudiana*), electrode system was placed close to the plant roots at the depth of 20 cm. The results of the study have indicated that the Plant-MFC, was more effective and achieved higher bioelectricity generation than C-MFC. The maximum voltage reached with Plant-MFC was 850 mV (0.85 V), whereas C-MFC achieved a maximum voltage of 762 mV (0.772 V). Furthermore, the same reactor demonstrated a

\* Corresponding author

E-mail: [alejandrolunaml@uanl.edu.mx](mailto:alejandrolunaml@uanl.edu.mx) (A. I. Luna-Maldonado);  
[sathish.k@llano.tecnm.mx](mailto:sathish.k@llano.tecnm.mx), [sathish.bot@gmail.com](mailto:sathish.bot@gmail.com) (S. K. Kamaraj)

Peer review under responsibility of Journal of Experimental Biology and Agricultural Sciences.

Production and Hosting by Horizon Publisher India [HPI]  
(<http://www.horizonpublisherindia.in/>).  
All rights reserved.

All the articles published by [Journal of Experimental Biology and Agricultural Sciences](#) are licensed under a [Creative Commons Attribution-NonCommercial 4.0 International License](#) Based on a work at [www.jebas.org](http://www.jebas.org).



maximum power generation of  $66 \text{ mW m}^{-2}$  on 10 min of polarization, while a power density with C-MFC was equal to  $13.64 \text{ mW m}^{-2}$ . *S.rebaudiana* showed a great alternative for power generation. In addition, the monitoring acquisition system was suitable for obtaining data in real-time. However, more studies are recommended to enhance this type of system.

## 1 Introduction

The consumption of fossil fuels and the environmental problems caused by their excessive use has made it possible to find other alternatives for the production of clean energy, such as solar energy, which is a universal and reliable source; to respond to the high demand for electricity of the world population (Prabha et al. 2021; Maddalwara et al. 2021). It has been reported that the earth receives approximately 120,000 TW (traveling wave) of solar energy per year, with a power density of  $170 \text{ W m}^{-2}$  achieving the earth's surface, exceeding the current global demand of  $\sim 16 \text{ TW}$  (Sekar and Ramasamy 2015).

On the other hand, other types of sustainable energy sources such as microbial fuel cells (MFCs) and plant-MFCs have been studied to produce bioelectricity (Rusyn et al. 2021; Apollon et al. 2022a). Since their implementation, these technologies have been studied from different angles. For example, MFC technology has been used in diverse fields of application such as (waste) water treatment (Choudhury et al. 2021; Saeed et al. 2022), nutrient recovery (Sharma et al. 2021; Sabin et al. 2022), and remediation of heavy metal (Wang et al. 2022; Lam et al. 2022) as reviewed by Apollon et al. (2022b). MFC uses both the metabolism of microorganisms adhering to the anode compartment, as well as the electrochemical process to transform chemical energy into electrical energy (Logan et al. 2006; Rusyn 2021). Unlike MFC, plant-MFC is a technology that uses the plant's photosynthetic activity to continuously generate bioelectricity. The plant-MFC technology has been implemented in 2008 by Strik and co-workers using the *Glyceria maxima* (Reed manageress) plant to generate bioelectricity (Strik et al. 2008). During the experiment, a power density was reached up to  $67 \text{ mW m}^{-2}$ . Later, Wetser et al. (2015) managed to increase the yield of Plant-MFC using another plant species such as *Spartina anglica*. The maximum power density found in 10 min of polarization was  $679 \text{ mW m}^{-2}$ , which dropped to  $240 \text{ mW m}^{-2}$  in long-term operation (two weeks). In a Plant-MFC system embedded with *Caltha palustris*, the maximum voltage of 1454.1 mV and a current of 11.2 mA, were achieved respectively (Rusyn et al. 2019). Therefore, the performance of a bioelectrochemical system such as Plant-MFC is highly dependent on its type, design, and configuration. In addition, it also depends on the types of materials anodes and cathodes; and also plant species used (Rusyn 2021; Maddalwara et al. 2021).

Plant-MFC has been chosen as one of the safe sources of bioelectricity generation. The use of this technology has made it

possible to largely reduce greenhouse gas emissions. The use of plants in MFCs allows for increasing the amount of biomass, as well as the power generation without the need to harvest the plants (Moqsud et al. 2015). Plant-MFCs can produce sustainable energy 18 times greater than the conventional sediment system. The increase in energy generation is due to the increase in the availability of organic matter (OM) in the anode chamber due to microbial oxidation (Ramadan et al. 2017).

Plant-MFC plays an important role in agricultural systems today. The implementation of this technology allows not only to produce clean energy but also to evaluate the plant growth parameters such as plant height, number of shoots, stem diameter, etc., (Apollon et al. 2020). In previous studies, researchers from different countries have developed Plant-MFC prototypes both to produce bioelectricity, as well as to evaluate plant growth through the system (Angelini et al. 2008; Luo 2009; Helder et al. 2010; Sudirjo et al. 2019a). The results of these investigations reported that the Plant-MFC systems influence both plant height, as well as the amount of biomass produced by the plant. In a study conducted by Apollon et al. (2020), it was found that the Plant-MFC had a positive effect on the plant height parameter. The same phenomenon was confirmed when the plants received doses of  $150 \text{ mg L}^{-1}$  of ammonium nitrate ( $\text{NH}_4\text{NO}_3$ ), by using a prototype based Plant-MFC installed vertically in the soil (Apollon et al., 2022a). However, Plant MFCs also face great challenges concerning power generation in the long-term operation and their large-scale application in real-time. In a review done by Apollon et al. (2021), the most recent advances and trends in terms of Plant-MFC configurations were discussed, as well as the types of membrane, anode, and cathode materials used; the factors affecting the performance of Plant-MFC technologies, the challenges faced by bioelectrochemical systems and their possible real-time applications.

Hence, the main objectives of this study were (i) to build a Plant-MFC by choosing suitable and low-cost materials, as well as evaluating their performance; and (ii) to design an acquisition system to monitor the voltage in real-time in the Plant-MFC.

## 2 Materials and Methods

### 2.1 Design and Implementation of the Data Acquisition System

According to Maldonado-Ruelas et al. (2018), the voltage acquisition of BES technologies such as Plant-MFCs is generally very low power with high electrical impedance. To solve this

problem, it is necessary to make schemes capable of coupling the impedances of the Plant-MFC systems. One of the schemes that must be implemented is the automatic data acquisition system (Arulmani et al. 2021; Zhang et al. 2021), which allows monitoring the voltages without problems through a digital platform system (Attia et al. 2022). The voltage acquisition system used in this study was divided into 6 steps or stages (Figure 1A). Figure 1B shows an ATMEGA2560 (Arduino) that was used in this study. Its

main role was to facilitate the capture of the data as accurately as possible. Additionally, the system was linked with the ATMEGA2560 (Figure 2a), which was connected to a personal computer (Figure 2b).

One of the important features of this Arduino is the number of analog ports it has; in addition to being very easy to handle (Maldonado-Ruelas et al. 2018). The system comprised 32

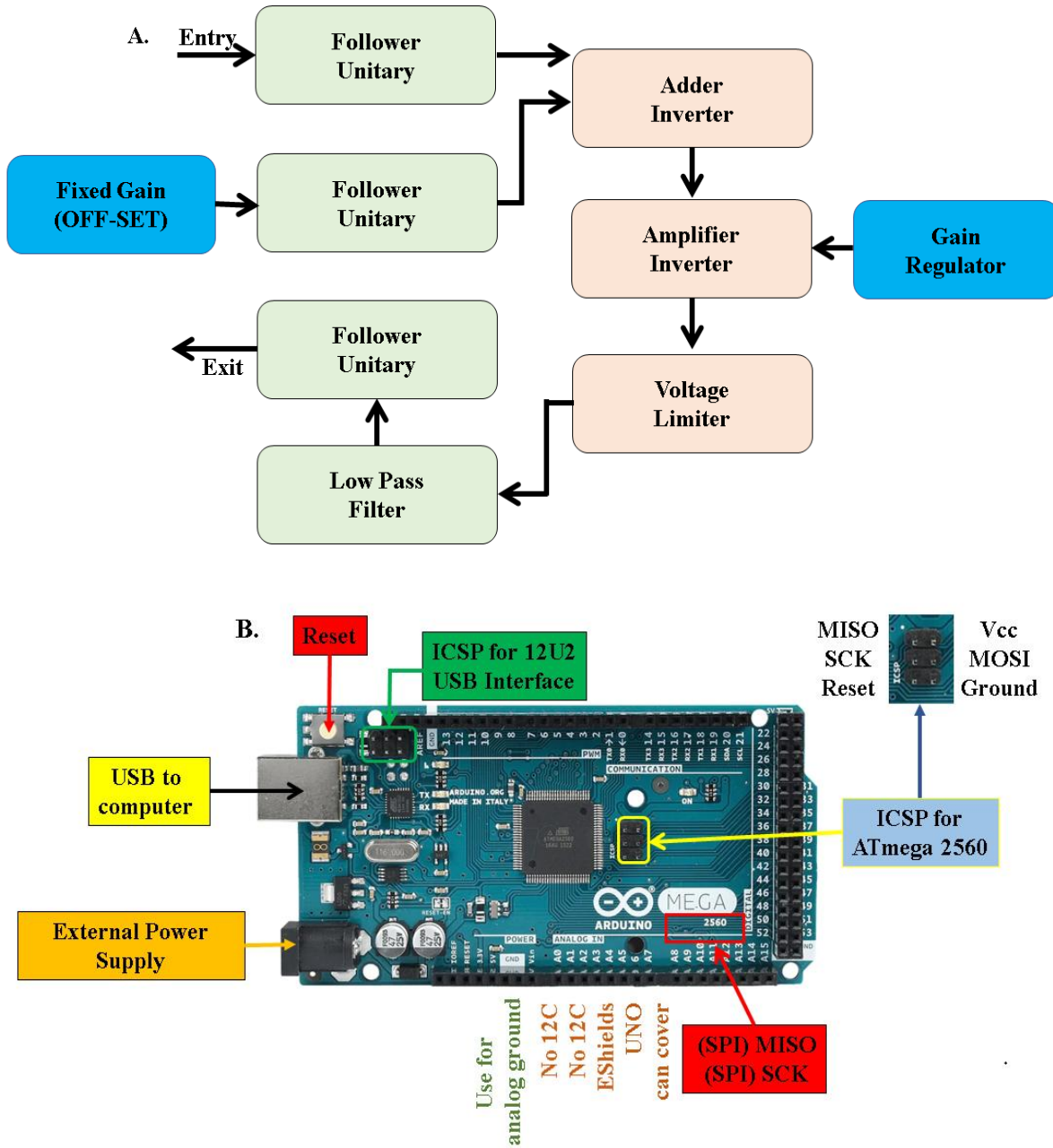


Figure 1 (A) General schematic presentation of the voltage automatic data acquisition system (adapted from Maldonado-Ruelas et al. 2018); and (B) characteristics of the Arduino used in this study.



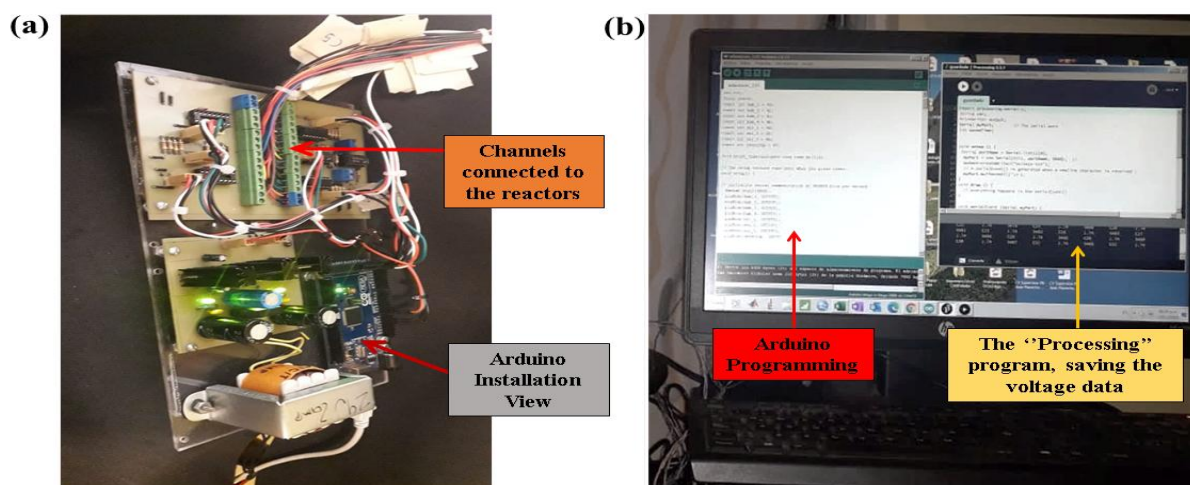


Figure 2 (a) Interface operation phase and (b) monitoring of voltage data by using a personal computer. Two windows are open on the screen. The window on the left shows the Arduino programming code and the window on the right indicates the program that saves the data by generating a .txt file.

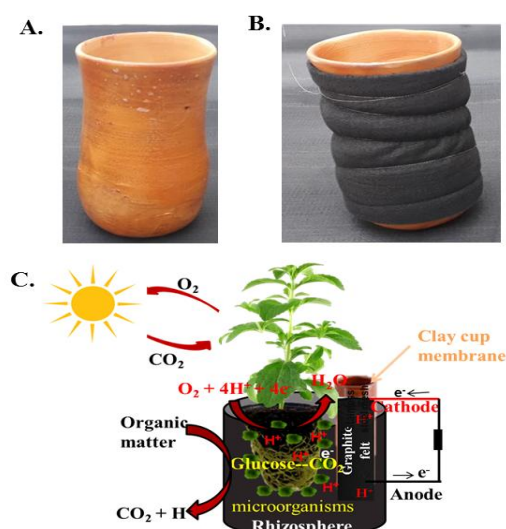


Figure 3 (A) Clay cup membrane, (B) constructed electrode and (C) schematic illustration of the evaluated Plant-MFC.

channels and 16 analog outputs. Before data monitoring, the digital platform was calibrated with the main objective of obtaining accurate data. Finally, the voltage data obtained in real time were automatically saved using the Processing platform (version 3.4) coupled to the interface. The data was updated by generating a ".txt" file with the exact information arranged for later analysis. This allowed avoiding data loss when there was a short circuit or other problems with the system.

## 2.2 Plant-MFC construction and operation

Two individual reactors i.e. (i) Plant-MFC and (ii) C-MFC were manufactured using a clay cup membrane (3 mm thick); the height of 20 cm and diameter of 9 cm (0.0693 m<sup>2</sup>) (Figure 3A).

For the anode electrode (Figure 3B), 648 cm<sup>2</sup> of graphite felt (ESGRAF, S.A de C.V., Mexico) of 6 mm diameter was used, placed around the entire surface of the pitcher. Graphite felt was previously reported as potential anode material (Kuleshova et al. 2021). 270 cm<sup>2</sup> of stainless-steel mesh (NYLOMAQ SL PLATE 9.5 mm 610 X 610 mm) was used as the cathode electrode, which was placed inside the clay cup. Subsequently, the Plant-MFC was embedded with the *S. rebaudiana* plant, as shown in Figure 3C. The electrode system of Plant-MFC was installed manually and placed about 20-30 cm below the soil. The experiment was carried out in the Faculty of Agronomy of the Autonomous University of Nuevo León, for 15 days. During this period, both the Plant-MFC and C-MFC were irrigated every two days with 2L of tap water.

## 2.3 Bioelectricity measurements

The open-circuit voltage (OCV) was recorded (in real time) in a time interval of 15 min/data, by using the constructed data acquisition system, for 15 days. Then, at the final stage of the experiment, 11 external resistances (between the ranges of 100  $\Omega$  to 1000  $\Omega$ ) were manually applied in 10 min of polarization (Rusyn and Hamkalo 2020). Current and power were calculated using Ohm's law as reported by Apollon et al. (2022a). Then, current and power densities were normalized considering the area (0.0693 m<sup>2</sup>) of the anode surface of the Plant-MFC reactor. Eq. (1) indicates ohm's law, and Eqs. (2) – (3) show the bioelectricity calculation process according to the ohm's law (Nasrabadi and Moghimi 2022). Finally, Eq. (4) shows the process of calculation of current density, according to the anode surface projected area (Rusyn et al. 2021; Apollon et al. 2020).

- Voltage (V):  $V = I * R$  (1)
- Current intensity (A):  $I = \frac{V}{R_{ext}}$  (2)
- Power (W):  $P = V * I$  (3)
- Current density:  $I = \frac{V}{A_{anode} R_{ext}}$  (4)

Where:

V: Voltage (Volts).

I: Intensity (A).

R<sub>ext</sub>: External resistance ( $\Omega$ ).

A<sub>anode</sub>: Anode Surface Projected Area.

V<sub>oc</sub>: Open Circuit Voltage (Volts).

## 3 Results and discussion

### 3.1 Performance of the reactors in OCV

Results presented in Figure 4 show that the two evaluated reactors in this study had a different behavior for the OCV parameters. Plant-MFC turned out as a more effective reactor in this study, reaching a higher OCV with a value of 850 mV (0.85 V), whereas, C-MFC indicated an OCV of 762 mV (0.772 V). This behavior is because there was greater bacterial activity in the Plant-MFC than in the MFC (Apollon et al. 2022a); although, the reactors shared the same type of membrane. For instance, when the plant carries out the photosynthesis process, this allows a large number of exudates or organic compounds to be present in the anode compartment (Strik et al. 2008). The aforementioned results were in the ranges reported by Kumar et al. (2018), by using a dual-chambered Plant-MFC (DcPMFC) which was set up with an internal cathode chamber and external terracotta separator air-cathode electrode assembly. However, in another study conducted by Kumar et al. (2020), voltage performances of 292.1 mV (0.2991 V) and 321.7 mV (0.3217 V), were found in two types of reactors: Type-I (horizontal) and Type-II (vertical) of terracotta based ceramic Plant-MFCs (C-PMFC), respectively. These results were inferior to those reached in our study. In addition, a study done by Syed et al. (2021) showed an OCV of 650 mV (0.65 V), by using cattle manure (cow dung and buffalo dung) in MFCs for green energy generation, which was also inferior to that reported in this study. In a study conducted by Apollon et al. (2020), a maximum OCV of 1200 mV (1.2 V) was achieved in a novel vertically integrated plug-in ceramic stick-based Plant-MFCs embedded with two *Opuntia* species (*O. ficus-indica* and *O. joconostle*). During the experiment, the Plant-MFCs were irrigated with 1L /week of water, for 30 days while in the present study 2L of water was used every two days, for 15 days. Previously, the maximum voltage of

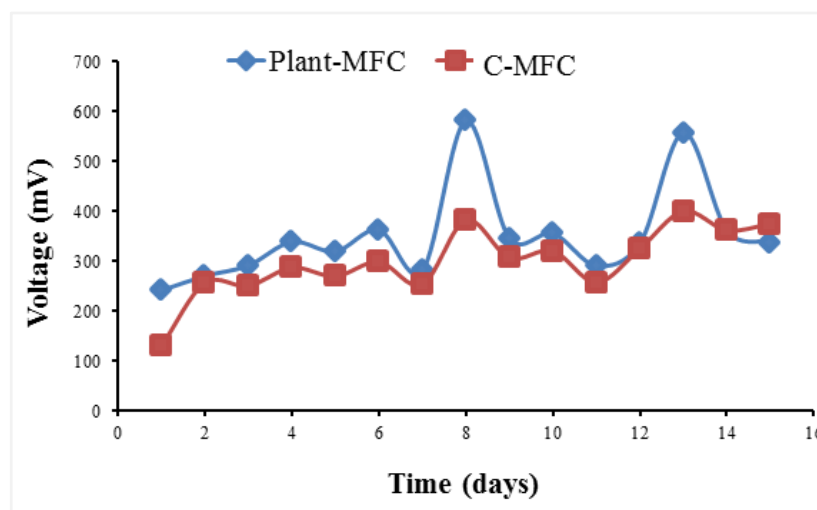


Figure 4 Voltage output performance in the two reactors for 15 days.

1454.1 mV (1.4541 V) was achieved in soil plant-MFC (Rusyn et al. 2019). These results are superior to those found in our study. Therefore, it can be argued that the system used in this study can drive Plant-MFC technology in saturation conditions. In addition, the data acquisition system developed to monitor data in real time was suitable.

### 3.2 Polarization experiment

Polarization was performed at the end of the study. The results have indicated different behavior between both reactors, which shared similar anode compartment (Figure 5a). Maximum voltage of 600 mV (0.6 V) was obtained in Plant-MFC, compared to the C-MFC that indicating a voltage of 448 mV (0.448 V), with a resistance of 1000  $\Omega$ . Plant-MFC showed higher energy efficiency of 186 mA m<sup>-2</sup>, being the best reactor in this study. Subsequently, exhibited a maximum power density of 66 mW m<sup>-2</sup> (Figure 5b), which was higher (86.21% and 74.54%) than that reported by Kumar et al. (2020). Besides, other studies indicated power densities inferior compared to that reached in this study (Sudirjo et al. 2019b; Syed et al. 2021; Apollon et al. 2022a). However, in a

recent study, higher power densities of  $1613.3 \pm 155.5$  (system with five branches) and  $1185.1 \pm 29.1$  mW m<sup>-2</sup> (system with one collector branch), respectively, were reported in microbial electrochemical systems (MES) by optimizing the “anode-collector” (Li et al. 2022). Hence, these researchers found that integrating a metal current collector into the anode electrode was an effective strategy to reduce the power loss of the system and these results were higher than those found in the two evaluated reactors. This difference is due to the types of systems used in both studies, as well as the operation time of the systems.

On the other hand, it is important to look for alternatives to improve Plant-MFC technology. For example, to increase the performance or efficiencies of the systems, it is necessary to apply adequate treatments. Treatment involves adding a catalyst to the electrode to facilitate the transfer of electrons from bacteria to the anode and cathode surfaces to acceptors, as well as structural alteration of the anode and cathode surfaces to accommodate more bacteria for transport electrons. Oxygen (O<sub>2</sub>) is the most commonly used electron acceptor as cathode for the reduction reaction in most studies of Plant-MFCs. It is the most sustainable electron acceptor

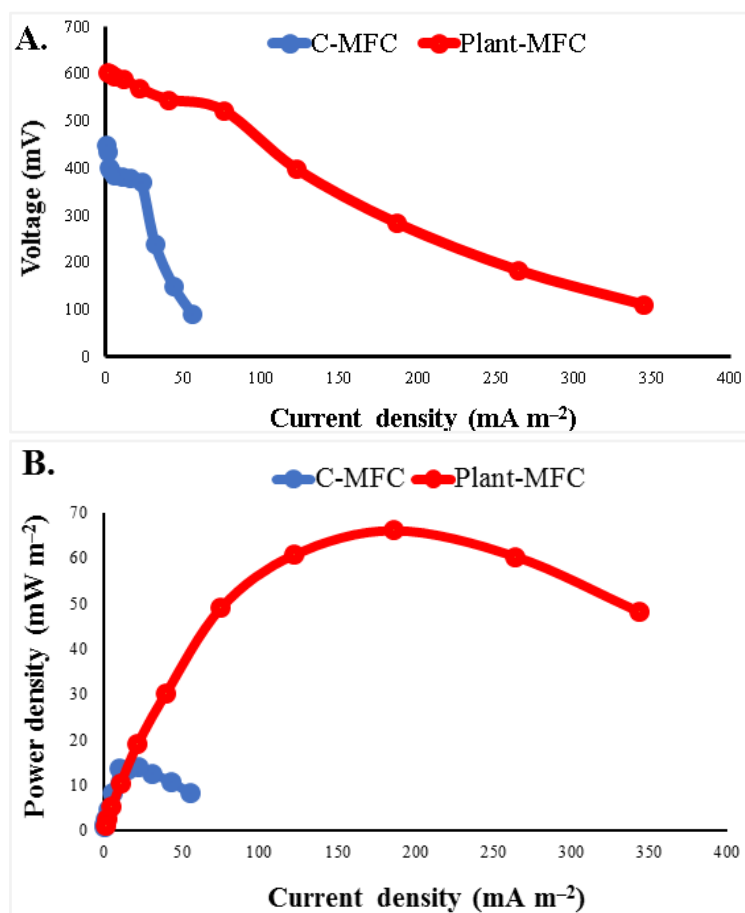


Figure 5 (A) Polarization curve and (B) power density curve of Plant-MFC and C-MFC at the final stage of study.

due to its inexhaustible availability. Biocatalysts, comprising bacteria grown on the cathode surface, lower the critical oxygen concentration from 5.5–6.6 to 0.1 mg L<sup>-1</sup> and improve the oxygen affinity for the cathode (Schröder 2012). Therefore, plants play a crucial role in the production of O<sub>2</sub>, increasing the yield of Plant-MFC. In addition, measuring the voltage of the Plant-MFC in real time allows knowing exactly its efficiency. With this, it can be argued that the implementation of a real-time voltage data acquisition system in BES, allows to save both more time, as well as to obtain real data from the systems. Extending the use of Plant-MFCs on a large scale is inevitable in the future.

#### 4 Conclusions

In this study, the performance of an automatic voltage data acquisition system for Plant-MFC was evaluated. This system allowed to obtain data in real time and prolonged. The use of this system has advantages due to the number of channels, it's cost effective, and its easy handling. In addition, the clay cup membrane used for the reactor design made it possible to produce bioelectricity at a low cost. Finally, alternative electricity production technologies such as Plant-MFCs are needed to satisfy the future electricity demand.

#### Acknowledgment

WA extends his thanks for the Ph.D. grant from the National Council for Science and Technology (CONACYT, for its acronym in Spanish), as well as the Universidad Autónoma de Nuevo León (UANL, for its acronym in Spanish) through the Subdirectorate of Postgraduate Studies of the Faculty of Agronomy (FA-UANL, for its acronym in Spanish) for his acceptance in the Ph.D. Program. WA, also, thanks in a particular way his Doctoral Thesis Committee. In addition, AILM and WA thank PAICYT (Programa de Apoyo a la Investigación Científica y Tecnológica) – (CT1519-21) from Universidad Autónoma de Nuevo León for their support. KSK would like to acknowledge the Technological Development and Innovation projects 2021/Federal Technological Institutes and Centers (TecNM).

#### References

Angelini, L.G., Ceccarini, L., Nassio Di Nasso, N., & Bonari, E. (2008). Comparison of *Arundo donax* L. and *Miscanthus x giganteus* in a long-term field experiment in Central Italy: analysis of productive characteristics and energy balance. *Biomass and Bioenergy*, 33(4), 635–643

Apollon, W., Kamaraj, S. K., Silos-Espino, H., Perales-Segovia, C., et al. (2020). Impact of *Opuntia* species plant bio-battery in a semi-arid environment: Demonstration of their applications. *Applied Energy*, 279, 115788

Apollon, W., Luna-Maldonado, A. I., Kamaraj, S. K., Vidales-Contreras, J.A., et al. (2021). Progress and recent trends in photosynthetic assisted microbial fuel cells: A review. *Biomass and Bioenergy*, 148, 106028

Apollon, W., Valera-Montero, L. L., Perales-Segovia, C., Maldonado-Ruelas, V.A., et al. (2022a). Effect of ammonium nitrate on novel cactus pear genotypes aided by biobattery in a semi-arid ecosystem. *Sustainable Energy Technologies and Assessments*, 49, 101730

Apollon, W., Rusyn, I., González-Gamboa, N., Kuleshova T., et al. (2022b). Improvement of zero waste sustainable recovery using microbial energy generation systems: A comprehensive review. *Science of the Total Environment*, 817, 153055

Arulmani, S. R. B., Gnanamuthu, H. L., Kandasamy, S., Govindarajan, G., et al. (2021). Sustainable bioelectricity production from *Amaranthus viridis* and *Triticum aestivum* mediated plant microbial fuel cells with efficient electrogenic bacteria selections. *Process Biochemistry*, 107, 27–37

Attia, Y.A., Samer, M., Mohamed, M.S.M., Moustafa, E., et al. (2022). Nanocoating of microbial fuel cell electrodes for enhancing bioelectricity generation from wastewater. *Biomass Conversion and Biorefinery*. <https://doi.org/10.1007/s13399-022-02321-7>

Choudhury, P., Ray, R. N., Bandyopadhyay, T. K., Basak, B., et al. (2021). Process engineering for stable power recovery from dairy wastewater using microbial fuel cell. *International Journal of Hydrogen Energy*, 46(4), 3171–3182

Helder, M., Strik, D.P.B.T.B., Hamelers, H.V.M., Kuhn, A.J., et al. (2010). Concurrent bioelectricity and biomass production in three Plant-Microbial Fuel Cells using *Spartina anglica*, *Arundinella anomala* and *Arundo donax*. *Bioresource Technology*, 101, 3541–3547.

Kuleshova, T. E., Gall', N. R., Galushko, A. S., & Panova, G. G. (2021). Electrogenesis in plant–microbial fuel cells in parallel and series Connections. *Technical Physics*, 66, 496–504

Kumar, V.K., Man mohan, K., Manangath, S.P., & Gajalakshmi, S. (2018). Terracotta Separator based Plant Microbial Fuel Cell for Bioelectricity and Catholyte Production. *International Journal of Applied Engineering Research*, 13, 14948-14955

Kumar, V.K., Man mohan, K., Sreelakshmi, P.M., Manju, P., & Gajalakshmi, S. (2020). Resource recovery from paddy field using plant microbial fuel cell. *Process Biochemistry*, 99, 270–281.

- Lam, S. M., Sin, J. C., Zeng, H., Lin, H., et al. (2022). Ameliorating Cu<sup>2+</sup> reduction in microbial fuel cell with Z-scheme BiFeO<sub>3</sub> decorated on flower-like ZnO composite photocathode. *Chemosphere*, 287, 132384.
- Li, J., Liu, G., Chen, D., Li, C., et al., (2022). Enhanced microbial electrochemical systems performance by optimizing the “anode-collector” collection mode: from enhancement mechanism to construction atrategy. *ACS ES & T Engineering*, 2, 263–270.
- Logan, B.E., Hamelers, B., Rozendal, R., Schröder, U., et al. (2006). Microbial Fuel Cells: Methodology and Technology. *Environmental Science & Technology*, 40 (17), 5181–5192.
- Luo, F.L. (2009). Personal Communication. Research Center Jülich, ICG-3, Jülich, Germany.
- Maddalwara, S., Nayaka, K.N., Kumar, M., & Singh, L. (2021). Plant microbial fuel cell: Opportunities, challenges, and prospects. *Bioresource Technology*, 341, 125772.
- Maldonado-Ruelas, V.A., Ortiz–Medina, R.A., Apollon, W., & Silos-Espino, H. (2018). Design and implementation of a voltage acquisition system for nopal-based fuel cells. *Revista de Energias Renovables*, 2(7), 19–25.
- Moqsud, M. A., Yoshitake, J., Bushra, Q. S., Hyodo, M., Omine, K., Strik, D. (2015). Compost in plant microbial fuel cell for bioelectricity generation. *Waste management*, 36, 63–69.
- Nasrabadi, A. M., & Moghimi, M. (2022). Energy analysis and optimization of a biosensor-based microfluidic microbial fuel cell using both genetic algorithm and neural network PSO. *International Journal of Hydrogen Energy*, 47(7), 4854–4867.
- Prabha, J., Kumar, M., & Tripathi, R. (2021). Opportunities and challenges of utilizing energy crops in phytoremediation of environmental pollutants: A review. In Kumar, V., Saxena, G., Shah, M. P. (Eds.), *Bioremediation for Environmental Sustainability* (pp. 383–396). Elsevier.
- Ramadan, B. S., Hidayat, S., & Iqbal, R. (2017). Plant microbial fuel cells (PMFCs): green technolog for achieving sustainable water and energy. In Proceedings book of the 7th basic science international conference basics science for improving survival and quality of life; mar 7-8; malang, Indonesia. p. 82-85.
- Rusyn, I. B., & Hamkalo, K.R. (2020). Electro-biosystems with Mosses on Green Roofs. *Environmental Research, Engineering and Management*, 76(1), 20-31.
- Rusyn, I. B., Vakuliuk, V. V., & Burian, O. V. (2019). Prospects of use of *Caltha palustris* in soil plant-microbial eco-electrical biotechnology. *Regulatory Mechanisms in Biosystems*, 10(2), 233-238.
- Rusyn, R. (2021). Role of microbial community and plant species in performance of plant microbial fuel cells. *Renewable and Sustainable Energy Reviews*, 152, 111697.
- Rusyn, I.B., Medvediev, O.V., & Valko, B.T. (2021). Enhancement of bioelectric parameters of multi-electrode plant–microbial fuel cells by combining of serial and parallel connection. *International Journal of Environmental Science and Technology*, 18, 1323–1334.
- Sabin, J. M., Leverenz, H., & Bischel, H. N. (2022). Microbial fuel cell treatment energy-offset for fertilizer production from human urine. *Chemosphere*, 294, 133594.
- Saeed, T., Majed, N., Kumar Yadav, A., Hasan, A., & Jihad Miah, M. (2022). Constructed wetlands for drained wastewater treatment and sludge stabilization: Role of plants, microbial fuel cell and earthworm assistance. *Chemical Engineering and Technology*, 430, 132907.
- Schröder, U. (2012). Cover Picture: Microbial Fuel Cells and Microbial Electrochemistry: *ChemSusChem*, 5, 957.
- Sekar, N., & Ramasamy, R. P. (2015). Recent advances in photosynthetic energy conversion. *Journal of Photochemistry and Photobiology C: Photochemistry Reviews*, 22, 19–33.
- Sharma, P., Talekar, G. V., & Mutnuri, S. (2021). Demonstration of energy and nutrient recovery from urine by field-scale microbial fuel cell system. *Process Biochemistry*, 101, 89–98.
- Strik, D.P.B.T.B., Hamelers, H.V.M., Snel, J.F.H., & Buisman, C.J.N. (2008). Green electricity production with living plants and bacteria in a fuel cell. *International Journal of Energy Research*, 32, 870–876.
- Sudirjo, E., Buisman, C.J.N., & Strik, D.P.B.T.B. (2019a). Activated Carbon Mixed with Marine Sediment is Suitable as Bioanode Material for *Spartina anglica* Sediment/Plant Microbial Fuel Cell: Plant Growth, Electricity Generation, and Spatial Microbial Community Diversity. *Water*, 11(9), 1810.
- Sudirjo, E., Pim de Jager, Buisman, C. J. N., & Strik, D.P.B.T.B. (2019b). Performance and Long-Distance Data Acquisition via LoRa Technology of a Tubular Plant Microbial Fuel Cell Located in a Paddy Field in West Kalimantan, Indonesia. *Sensor*, 19, 46–47.
- Syed, Z., Sonu, K., & Sogani, M. (2021). Cattle manure management using microbial fuel cells for green energy generation. *Biofuels Bioproduct and Biorefining*, 16(2), 460-470.

- Wang, Xu, D., Zhang, Q., Liu, T., & Tao, Z. (2022). Simultaneous removal of heavy metals and bioelectricity generation in microbial fuel cell coupled with constructed wetland: an optimization study on substrate and plant types. *Environmental Science and Pollution Research*, 29, 768–778.
- Wetser, K., Sudirjo, E., Buisman, C. J. N., & Strik, D. P. B. T. B. (2015). Electricity generation by a plant microbial fuel cell with an integrated oxygen reducing biocathode. *Applied Energy*, 137, 151–157.
- Zhang, K., Wu, X., Wang, W., Luo, H., et al. (2021). Effects of plant location on methane emission, bioelectricity generation, pollutant removal and related biological processes in microbial fuel cell constructed wetland. *Journal of Water Process Engineering*, 43, 102283.



## Journal of Experimental Biology and Agricultural Sciences

<http://www.jebas.org>

ISSN No. 2320 – 8694

### Targeting Omicron (B.1.1.529) SARS CoV-2 spike protein with selected phytochemicals: an in-silico approach for identification of potential drug

Poonam Bansal<sup>1</sup>, Hardeep Singh Tuli<sup>1</sup>, Varruchi Sharma<sup>2</sup>, Ranjan K. Mohapatra<sup>3</sup>,  
Kuldeep Dhama<sup>4</sup>, Priti<sup>5</sup>, Anil K. Sharma<sup>1\*</sup>

<sup>1</sup>Department of Biotechnology, Maharishi Markandeshwar (Deemed to be University), Mullana, Ambala 133207, Haryana, India

<sup>2</sup>Department of Biotechnology & Bioinformatics, Sri Guru Gobind Singh College, Chandigarh

<sup>3</sup>Department of Chemistry, Government College of Engineering, Keonjhar-758002, Odisha, India

<sup>4</sup>Division of Pathology, ICAR-Indian Veterinary Research Institute, Izatnagar, Bareilly-243 122, Uttar Pradesh, India

<sup>5</sup>Department of Biotechnology, K.L. Mehta Dayanand College for Women, Faridabad

Received – March 03, 2022; Revision – April 05, 2022; Accepted – April 17, 2022

Available Online – April 30, 2022

DOI: [http://dx.doi.org/10.18006/2022.10\(2\).396.404](http://dx.doi.org/10.18006/2022.10(2).396.404)

#### KEYWORDS

SARS-CoV-2

Omicron variant

Phytochemicals

Molecular docking

Drugs

#### ABSTRACT

Severe acute respiratory syndrome coronavirus -2 (SARS-CoV-2) emerging variants particularly those of concern contain numerous mutations that influence the behavior and transmissibility of the virus and could adversely affect the efficacies of existing coronavirus disease 2019 (COVID-19) vaccines and immunotherapies. The emerging SARS-CoV-2 variants have resulted in different waves of the pandemic within the ongoing COVID-19 pandemic. On 26 November 2021 World Health Organization designated omicron (B.1.1.529) as the fifth variant of concern which was first reported from South Africa on November 24, 2021, and thereafter rapidly spread across the globe owing to its very high transmission rates along with impeding efficacies of existing vaccines and immunotherapies. Omicron contains more than 50 mutations with many mutations (26-32) in spike protein that might be associated with high transmissibility. Natural compounds particularly phytochemicals have been used since ancient times for the treatment of different diseases, and owing to their potent anti-viral properties have also been explored recently against COVID-19. In the present study, molecular docking of nine phytochemicals (Oleocanthal, Tangeritin, Coumarin, Malvidin, Glycitein, Piceatannol, Pinosyltin, Daidzein, and Naringenin) with omicron spike protein (7QNW (electron microscopy, resolution 2.40 Å)) was done. The docking study revealed that selected ligands interact with the receptor with binding energy

\* Corresponding author

E-mail: [anibiotech18@gmail.com](mailto:anibiotech18@gmail.com) (Dr. Anil K. Sharma)

Peer review under responsibility of Journal of Experimental Biology and Agricultural Sciences.

Production and Hosting by Horizon Publisher India [HPI]  
(<http://www.horizonpublisherindia.in/>).  
All rights reserved.

All the articles published by [Journal of Experimental Biology and Agricultural Sciences](#) are licensed under a [Creative Commons Attribution-NonCommercial 4.0 International License](#) Based on a work at [www.jebas.org](http://www.jebas.org).



in the range of -6.2 to -7.0 kcal/mol. Pinosyltin showed the highest binding energy of -7.0 kcal/mol which may be used as potential ligands against omicron spike protein. Based on the docking studies, it was suggested that these phytochemicals are potential molecules to be tested against omicron SARS-CoV-2 and can be used to develop effective antiviral drugs.

## 1 Introduction

The ongoing coronavirus disease 2019 (COVID-19) pandemic has posed a serious risk to the lives of humans across the world (Dhama et al. 2020; WHO 2022a). COVID-19 was first originated in December 2019 in China (Kim et al. 2020) and later spread globally as a deadly pandemic. The  $\beta$ -coronavirus (novel enveloped RNA) was found responsible for causing an infectious disease named COVID-19, which was phylogenetically similar to the severe acute respiratory syndrome coronavirus (SARS-CoV), and thus this pandemic virus was named SARS-CoV-2 (Coronaviridae Study Group of the International Committee on Taxonomy of Viruses 2020; Owis et al. 2020). Since the SARS-CoV-2 pandemic virus has emerged it has undergone many mutations and evolved into various variants and mutants, and till date of April 2, 2022, five variants of concern (VOC) of SARS-CoV-2 have emerged namely Alpha, Beta, Gamma, Delta, and Omicron (WHO 2022b). On 26 November 2021, World Health Organization (WHO) designated omicron (B.1.1.529) as the fifth variant of concern (VOC) that was reported from South Africa on 24 November 2021. As a most mutated SARS-CoV-2 variant, it is known to have more than 50 mutations in its genome, of which 26-32 mutations are present in spike proteins, which are related to humoral immune escape potential and high transmissibility rate (Shishir et al. 2022; Hanai 2022). Omicron has a doubling time of 2-3 days and has recently caused a very high surge in COVID-19 cases across the globe while posing high public health concerns owing to its adverse impacts on the effectiveness of existing COVID-19 vaccines and antibodies-based therapies resulting in breakthrough infections in vaccinated persons and reinfection in recovered patients, and presently different lineages of Omicron variant are being evolved that might increase the fears amid the pandemic (Khandia et al. 2022; Mohapatra et al. 2022; WHO 2022b). As of April 2, 2022, more than 486 million confirmed cases and over 6.1 million deaths have been reported worldwide due to COVID-19 (WHO 2022b).

Certain drugs having effectiveness against COVID-19 had been reported in the literature including chloroquine, ritonavir, ribavirin, hydroxychloroquine, and oseltamivir, but these were not effective in immunocompromised patients (Narkhede et al. 2020; Ozdemir et al. 2022). Scientists have been working to find potential drugs for COVID-19. Recently, research has been carried out on natural plant-based compounds i.e., phytochemicals which include alkaloids, flavonoids, and other compounds that can be used in COVID-19 treatment (Vardhan and Shood 2020; Pandey et al.

2021; Tuli et al. 2022). Phytochemicals possess various beneficial health-promoting properties including antioxidant and immunomodulatory activities and are gaining interest as they have multiple beneficial effects on the health of human beings including serving as potent anti-viral agents, and have also been reported to act against SARS-CoV-2 (Dhama et al. 2018; Anand et al. 2021; Zrig 2022). Flavonoids are secondary metabolites (produced by plants), which play a wide role in plant physiology such as antiviral, antioxidant, antifungal, anti-inflammatory, antibacterial, and anti-cancer activities (Wang et al. 2018a). Naringenin is a flavanone found in some edible fruits, like *Citrus* species and tomatoes (Zobeir et al. 2018), exhibited cardioprotective, antitumor, antibacterial, antiviral, antiadipogenic, anti-inflammatory, and antioxidant activity (Salehi et al. 2019). Diosmetinis found in *Acacia farnesiana* Wild legume and *Olea europaea* L. leaves are reported to show anti-inflammatory, anticancer, antioxidant, and antimicrobial activities (Wang et al. 2018b). Another phytochemical Pinosalvin possessed antifungal and antibacterial activity (Lee et al. 2005). Piceatannol, a polyphenolic stilbene that is found in various vegetables and fruits has been reported to exhibit anti-inflammatory and anticancer activity (Kershaw and Kim 2017). In-silico studies have revealed that many phytochemicals i.e., fisetin, quercetin, kamferol, curcumin, glycyrrhizic acid, maslinic acid, ursolic acid can act as potential drugs against targeted proteins of COVID-19 (Pandey et al. 2021). Therefore, the present work was planned to find out which natural compounds can inhibit SARS-CoV-2 viral spike protein, and thus docking studies of phytochemicals with the Omicron S-glycoprotein were carried out.

## 2 Materials and Methods

### 2.1 Retrieval of Receptor three-dimensional structure

The three-dimensional crystal structure of the Omicron spike glycoprotein with PDB ID: 7QNW with a resolution of 2.40 Å was downloaded from the online database Research Collaboratory Structural Bioinformatics-Protein Data Bank (RCSB-PDB) (Figure 1) (Dejnirattisai et al. 2021). The protein model was prepared by excluding heteroatoms and water molecules.

### 2.2 Ligand's preparation and analysis of ADME properties

Nine ligands were selected for virtual screening. The ligands library was prepared by downloading the 3-D structures of all the ligands from the PubChem database in sdf format and all structures were



converted into pdb format by OpenBabel (Figure 1). The online software tool was used to determine ADME (Unfavorable absorption, distribution, metabolism, and elimination) profiling of all the ligands (pH 7) (Jayaram et al. 2012). Lipinski's rule of five, including physicochemical properties of ligand viz. molar refractivity, molecular weight (<500 Da), H-bond acceptor (<10), H-bond donor (5), LogP (<5), and drug likeness were considered (Lipinski 2004) (Table 1).

Table 1 Physio-chemical or ADME Properties of ligands

S. N.	Ligands	ADME Properties (Lipinski's Rule of Five)		Drug Likeliness
		Properties	Values	
1.	Oleocanthal	Molecular weight (<500 Da)	304	Yes
		LogP (<5)	2.2	
		H-bond donor (5)	1	
		H-bond acceptor (<10)	5	
		Molar Refractivity	81.3	
2.	Tangeritin	Molecular weight (<500 Da)	372	Yes
		LogP (<5)	3.3	
		H-bond donor (5)	0	
		H-bond acceptor (<10)	7	
3.	Coumarin	Molecular weight (<500 Da)	146	Yes
		LogP (<5)	1.6	
		H-bond donor (5)	0	
		H-bond acceptor (<10)	2	
4.	Malvidin	Molecular weight (<500 Da)	331	Yes
		LogP (<5)	3.03	
		H-bond donor (5)	4	
		H-bond acceptor (<10)	7	
5.	Glycitein	Molecular weight (<500 Da)	284	Yes
		LogP (<5)	2.7	
		H-bond donor (5)	2	
		H-bond acceptor (<10)	5	
6.	Piceatannol	Molecular weight (<500 Da)	244	Yes
		LogP (<5)	2.6	
		H-bond donor (5)	4	
		H-bond acceptor (<10)	4	
7.	Pinosylbin	Molecular weight (<500 Da)	212	Yes
		LogP (<5)	3.2	
		H-bond donor (5)	2	
		H-bond acceptor (<10)	2	
8.	Daidzein	Molecular weight (<500 Da)	254	Yes
		LogP (<5)	2.7	
		H-bond donor (5)	2	
		H-bond acceptor (<10)	4	
9.	Naringenin	Molecular weight (<500 Da)	272	Yes
		LogP (<5)	2.5	
		H-bond donor (5)	3	
		H-bond acceptor (<10)	5	
		Molar Refractivity	70.19	

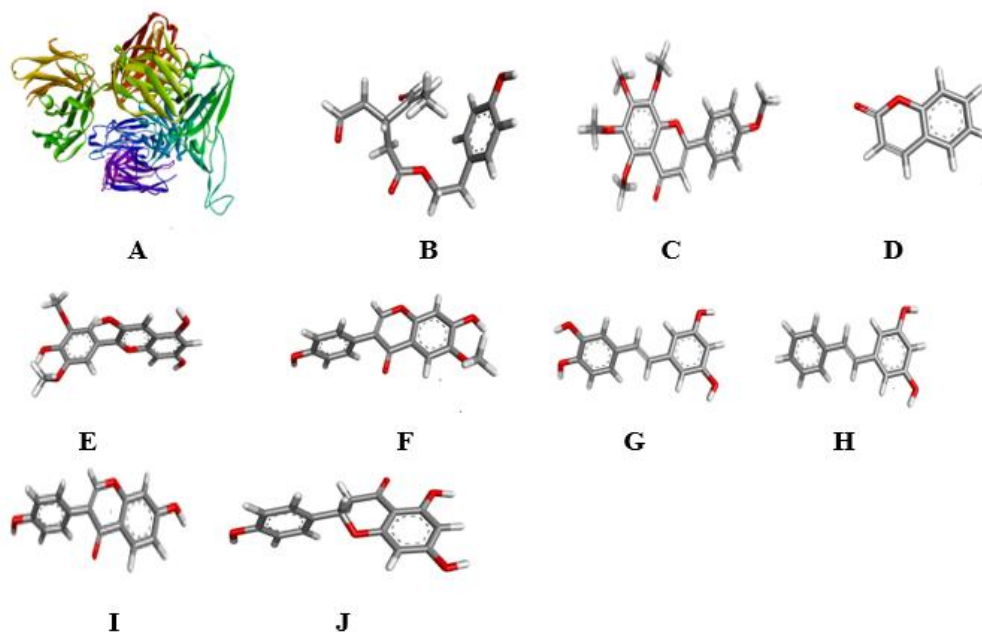


Fig 1 3D view of the receptor (A) Chemical structures of Oleocanthal (B), Tangeritin (C), Coumarin (D), Malvidin (E), Glycitein (F), Piceatannol (G), Pinosyltin (H), Daidzein (I) and Naringenin (J).

### 2.3 Molecular docking of ligands with Omicron Spike-glycoprotein

For virtual screening and binding studies, PyRx v0.8 was used. Universal Force Field (UFF) was applied for energy minimization of ligands and then OpenBabel convert ligands into.pdbqt (O'Boyle et al. 2011). Docked structures with high binding affinity were analyzed using PyMOL and Discovery Studio Visualizer.

### 3 Results and Discussion

A computational method is considered an important approach to search for potential drug candidature. *In-silico* virtual screening offers the advantages of rapid, convenient, and cost-effective testing. Computational studies suggested a mechanism for binding targets proteins to tested molecules (Skariyachan et al. 2020). In computer-aided molecular docking, the highest binding affinity score for the potential ligand in the active site of the receptor is calculated. Molecules binding with the highest binding affinity and least binding energy were the most stable binding with the target protein. Ligands with significant binding affinities were selected. Results revealed that Oleocanthal, Tangeritin, Coumarin, Malvidin, Glycitein, Piceatannol, Pinosyltin, Daidzein, and Naringenin showed the binding affinity in the range of -6.2 to -7.0 kcal/mol with receptor molecule (Table 2).

Docking studies revealed that among nine ligands Pinosyltin showed the best binding with a binding affinity of -7.0 kcal/mol.

The ligands interact with Leu398, Ser446, 32,469, Tyr61,35,508, Pro103, Glu 471, Gln 506, Asn 49,437, Arg 4554, Lys 458 residues of omicron spike glycoprotein. The binding energy of studies ligands were depicted in Table 2. The docked pose of ligand and Glycoprotein (PDB ID: 7QNW) receptor has been shown in Figures 2, 3, 4, 5, 6, 7, 8, 9, and 10.

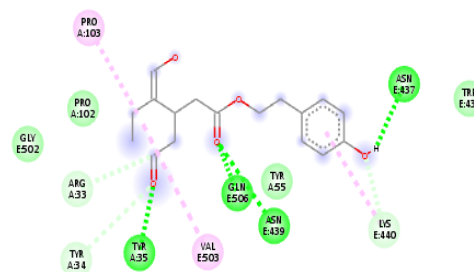
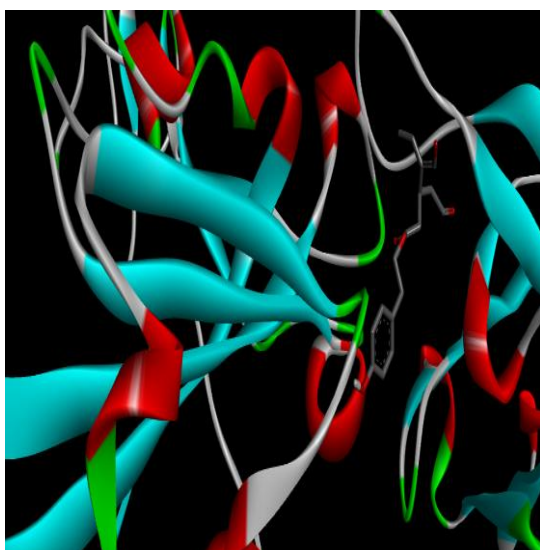
Table 2 Binding affinity of studied ligands with Omicron S-glycoprotein

S. N.	Ligands	Binding Affinity
1	Oleocanthal	-6.2
2	Tangeritin	-6.2
3	Coumarin	-6.3
4	Malvidin	-6.4
5	Glycitein	-6.8
6	Piceatannol	-6.9
7	Pinosyltin	-7.0
8	Daidzein	-6.9
9	Naringenin	-6.9

Docking studies presented in the present study revealed pinosyltin to have the highest binding affinity with the target protein and can be used as potential drugs against the Omicron spike protein. Spike glycoprotein plays a vital role in attachment of host cell surface with coronavirus via ACE-2 receptor. *In silico* binding studies of

natural compounds with Spike glycoprotein may interrupt attachment of ACE-2 receptor and S-glycoprotein and thus attachment of host's ACE-2 receptor and COVID -19 Spike glycoprotein will be lost. These ligands possessed potent effects in different therapeutic clinical conditions. Previous literature had some reports on docking studies of some phytochemicals i.e., quercetin, gingerol, luteolin-7-glucosidase, catechin, allicin, kaempferol, epicatechin-gallate that can be used as anti-COVID-19 agents (Khaerunnisa et al. 2020). Results of the current study are also in agreement with an earlier study by Koulgi et al. (2022) those who reported phytochemicals from AYUSH-64 (a poly

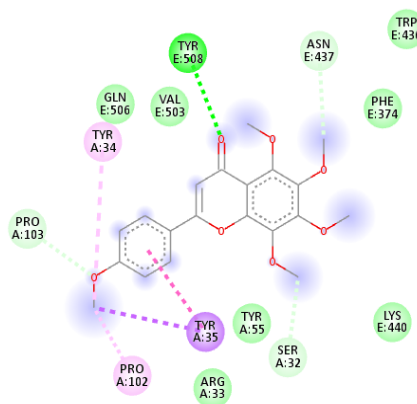
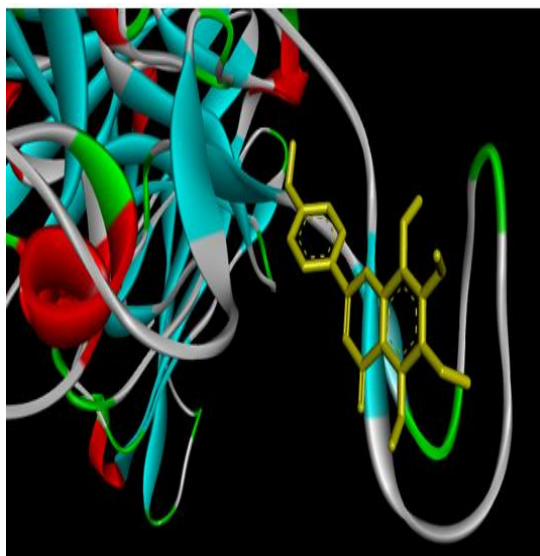
herbal drug) viz. akummicine-N-oxide, akummiginone, echitamine-n-oxide, and echitamic acid may act as a potential drug against Omicron variant of SARS-CoV-2. Further, Nag et al. (2021) study also showed that curcumin and piperine are the most potent to bind with spike protein of omicron SARS-CoV-2 and restrict the viral entry. The computational docking studies of the phytochemicals glycyrrhizic acid and limonin resulted in binding with receptor binding domain of SARS-CoV-2 Omicron and supported traditional medicines can be useful in formulating adjuvant therapies to fight against the pandemic (Vardhan and Sahoo 2022).



#### Interactions

- van der Waals
- Conventional Hydrogen Bond
- Carbon Hydrogen Bond
- Alkyl
- Pi-Alkyl

Figure 2 The molecular docking of Omicron spike protein and Oleocanthal (A) Best binding mode in the pocket of protein (B) The interacting amino acid of target with ligand



#### Interactions

- van der Waals
- Conventional Hydrogen Bond
- Carbon Hydrogen Bond
- Pi-Pi Stacked
- Alkyl
- Pi-Sigma
- Pi-Alkyl

Figure 3 The molecular docking of Omicron spike protein and Tangeritin (A) Best binding mode in the pocket of protein (B) The interacting amino acid of target with ligand

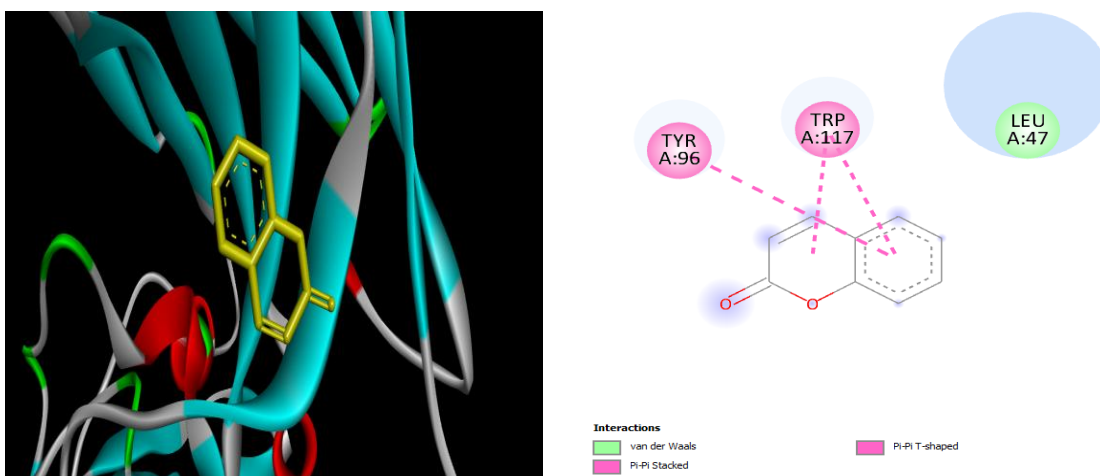


Figure 4 The molecular docking of Omicron spike protein and Coumarin (A) Best binding mode in the pocket of protein (B) The interacting amino acid of target with ligand

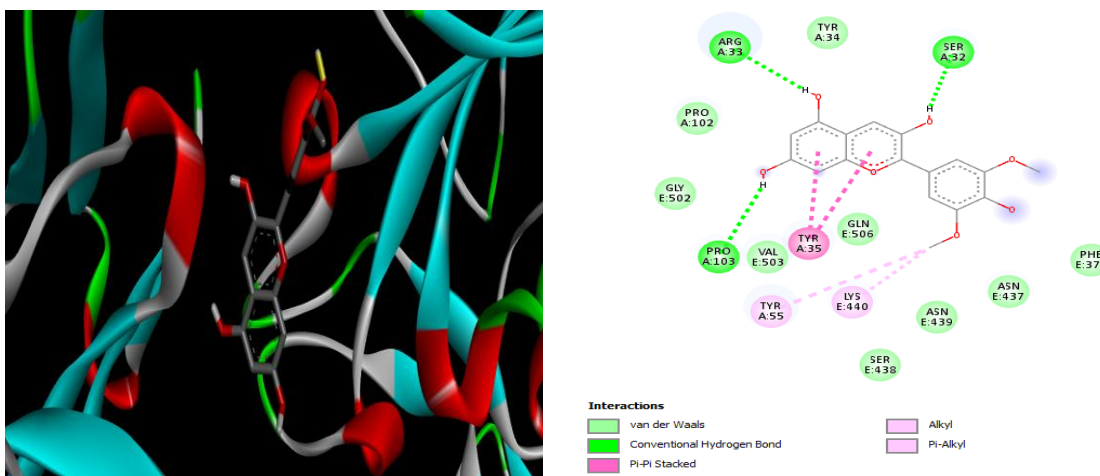


Figure 5 The molecular docking of Omicron spike protein and Malvidin (A) Best binding mode in the pocket of protein (B) The interacting amino acid of target with ligand

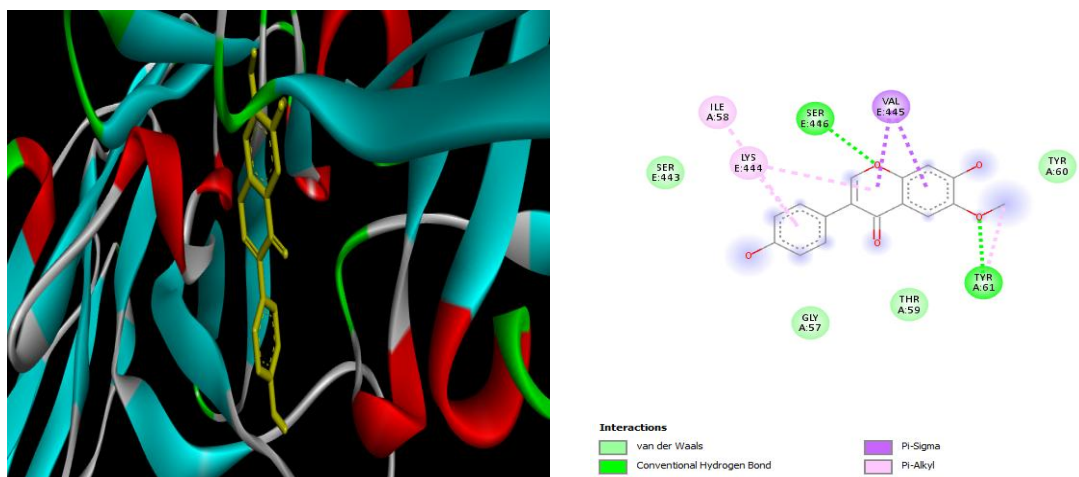


Figure 6 The molecular docking of Omicron spike protein and Glycitein (A) Best binding mode in the pocket of protein (B) The interacting amino acid of target with ligand

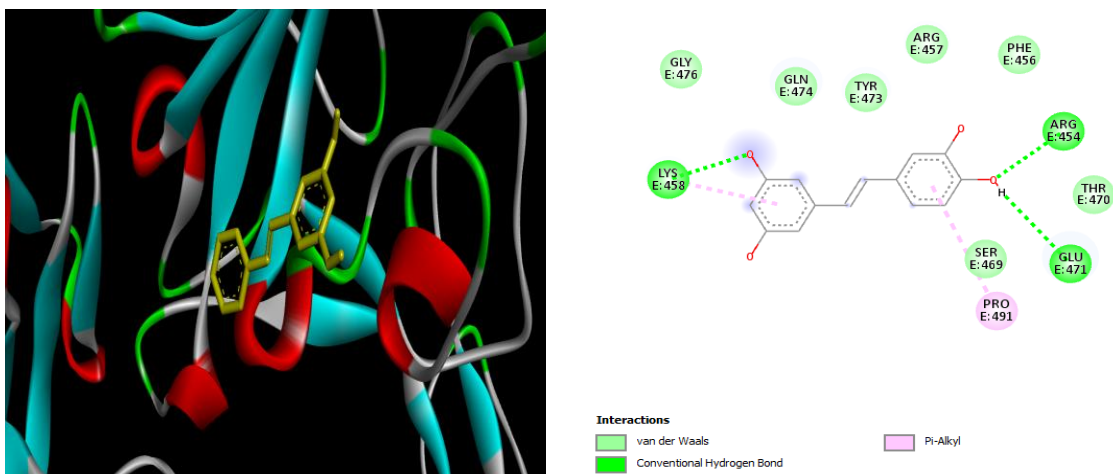


Figure 7 The molecular docking of Omicron spike protein and Piceatannol (A) Best binding mode in the pocket of protein, (B) The interacting amino acid of target with ligand

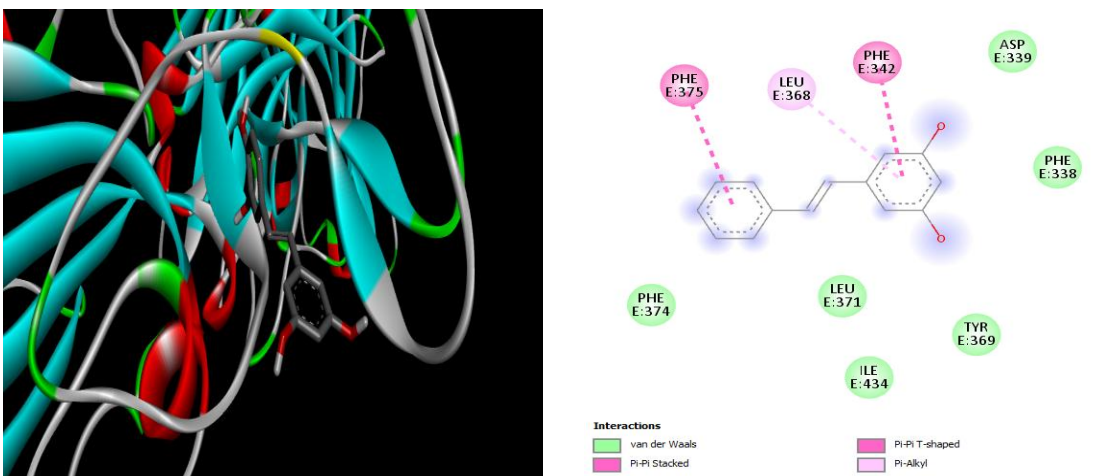


Figure 8 The molecular docking of Omicron spike protein and Pinosyltin (A) Best binding mode in the pocket of protein, (B) The interacting amino acid of target with ligand

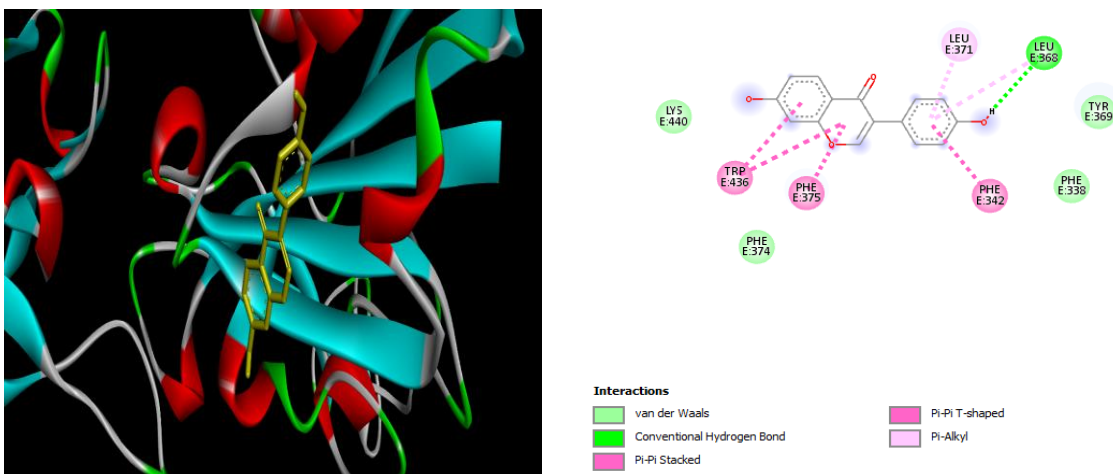


Figure 9 The molecular docking of Omicron spike protein and Daidzein (A) Best binding mode in the pocket of protein, (B) The interacting amino acid of target with ligand

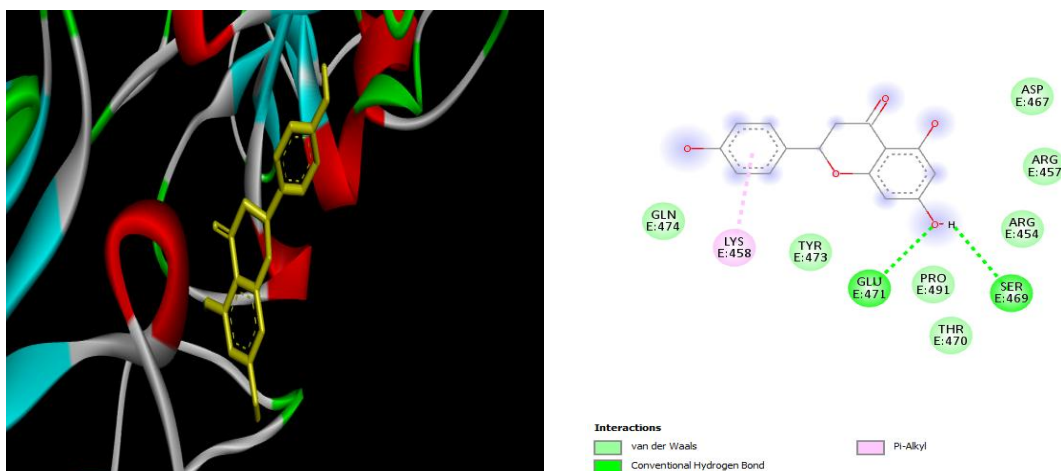


Figure 10 The molecular docking of Omicron spike protein and Naringenin (A) Best binding mode in the pocket of protein, (B) The interacting amino acid of target with ligand

## Conclusion

Scientists are studying a new variant of concern of SARS-CoV-2 named Omicron, the most mutated variant having 26-32 mutations in the spike protein. In the present study, natural products were molecularly docked with Omicron spike protein. Computational-based drug designing is time saving and cost-effective method to select compounds as a potential drugs for further studies. Pinosylinin showed the highest binding energy. Moreover, the compound used in this study satisfies Lipinski's rule of five and can be used as anti-COVID-19 therapeutics. Besides, *in-vivo* and *in-vitro* studies are suggested before using these ligands as a potential drug to combat Omicron infection.

## Conflict of interest

The authors declare no conflict of interest.

## References

Anand, A.V., Balamuralikrishnan, B., Kaviya, M., Bharathi, K., et al. (2021). Medicinal Plants, Phytochemicals, and Herbs to Combat Viral Pathogens Including SARS-CoV-2. *Molecules*, 26(6), 1775

Coronaviridae Study Group of the International Committee on Taxonomy of Viruses (2020) The species Severe acute respiratory syndrome-related coronavirus: classifying 2019-nCoV and naming it SARS-CoV-2. *Nature Microbiology*, 5(4):536-544

Dejnirattisai, W., Huo, J., Zhou, D., et al. (2021). Omicron-B.1.1.529 leads to widespread escape from neutralizing antibody responses. *Preprint. bioRxiv*, doi:10.1101/2021.12.03.471045

Dhama, K., Karthik, K., Khandia, R., Munjal, A., et al. (2018). Medicinal and therapeutic potential of herbs and plant metabolites

/extracts countering viral pathogens - Current knowledge and future prospects. *Current Drug Metabolism*, 19(3):236-263

Dhama, K., Khan, S., Tiwari, R., Sircar, S., et al. (2020) Coronavirus Disease 2019-COVID-19. *Clinical Microbiology Reviews*, 33(4):e00028-20

Hanai, T. (2022). Quantitative in silico analysis of SARS-CoV-2 S-RBD omicron mutant transmissibility. *Talanta*, doi: 10.1016/j.talanta.2022.123206.

Jayaram, B., Singh, T., Mukherjee, G., Mathur, A., Shekhar, S., & Shekhar, V. (2012). Sanjeevini: A freely accessible web-server for target directed lead molecule discovery. *BMC Bioinformatics*, 13 (Suppl 17), S7

Kershaw, J., & Kim, K. H. (2017). The therapeutic potential of piceatannol, a natural stilbene, in metabolic diseases: a review. *Journal of Medicinal Food*, 20(5), 427-438

Khaerunnisa, S., Kurniawan, H., Awaluddin, R., Suhartati, S., Soetjpto, S. (2020). Potential Inhibitor of COVID-19 Main Protease ( $M^{pro}$ ) From Several Medicinal Plant Compounds by Molecular Docking Study. *Preprints*, 2020030226, doi: 10.20944/preprints202003.0226.v1)

Khandia, R., Singhal, S., Alqahtani, T., Kamal, M.A., et al. (2022). Emergence of SARS-CoV-2 Omicron (B.1.1.529) variant, salient features, high global health concerns and strategies to counter it amid ongoing COVID-19 pandemic. *Environmental Research*, 209, 112816. doi: 10.1016/j.envres.2022.112816

Kim, J., Zhang, J., Cha, Y., Koltz, S., et al. (2020). Advanced bioinformatics rapidly identifies existing therapeutics for patients with coronavirus disease-2019 (COVID-19). *Journal of Translational Medicine*, 18, 257

- Koulgi, S., Jani, V., Uppuladinne, V. N. M., Sonavane, U., et al. (2022). Phytochemicals from AYUSH-64 screened against main protease and spike protein of *Omicron* variant of SARS-CoV-2 using ensemble docking approach, <https://doi.org/10.31219/osf.io/67n3g>
- Lee, S. K., Lee, H. J., Min, H. Y., Park, E. J., Lee, K. M., Ahn, Y. H., & Pyee, J. H. (2005). Antibacterial and antifungal activity of pinosylvin, a constituent of pine. *Fitoterapia*, 76(2), 258-260
- Lipinski, C. A. (2004). Lead- and drug-like compounds: The rule-of-five revolution. *Drug Discovery Today Technology*, 1(4), 337-341
- Mohapatra, R.K., Kandi, V., Verma, S., & Dhama, K. (2022) Challenges of the Omicron (B.1.1.529) Variant and Its Lineages: A Global Perspective. *ChemBioChem*, e202200059, doi: 10.1002/cbic.202200059
- Nag, A., Paul, S., Banerjee, R., & Kundu, R. (2021). In silico study of some selective phytochemicals against a hypothetical SARS-CoV-2 spike RBD using molecular docking tools. *Computers in Biology and Medicine*, 137, 104818. <https://doi.org/10.1016/j.combiomed.2021.104818>
- Narkhede, R.R., Cheke, R.S., Ambhore, J.P., & Shinde, S.D. (2020). The molecular docking study of potential drug candidates showing antiCOVID-19 activity by exploring of therapeutic targets of SARSCoV-2. *Eurasian Journal of Medicine and Oncology*, 4, 185-195
- O'Boyle, N.M., Banck, M., James, C.A., Morley, C., Vandermeersch, T., & Hutchison, G.R. (2011) Open babel: an open chemical toolbox. *Journal of Cheminformatics*, 3, 33
- Owis, A.I., El-Hawary, M.S., El Amir, D., Aly, O.M., Abdelmohsen, U.R., & Kamel, M.S. (2020). Molecular docking reveals the potential of *Salvadora persica* favonoids to inhibit COVID-19 virus main protease. *RSC Advances*, 10, 19570-19575
- Ozdemir, E.S., Hillary, H.L., AdemYildirim, A., Srivathsan, V., Ranganathan. (2022). Insilico screening and testing of FDA approved small molecules to block SARS-CoV-2 entry to the host cell by inhibiting Spike protein cleavage. *bioRxiv*, doi: <https://doi.org/10.1101/2022.03.07.483324>
- Pandey, P., Rane, J. S., Chatterjee, A., Kumar, A., et al. (2021). Targeting SARS-CoV-2 spike protein of COVID-19 with naturally occurring phytochemicals: an in silico study for drug development. *Journal of Biomolecular Structure and Dynamics*, 39 (16), 6306-6316
- Salehi, B., Fokou, P.V.T., Sharifi-Rad, M., Zucca, P., et al. (2019). The therapeutic potential of naringenin: a review of clinical trials. *Pharmaceuticals*, 12(1), 11. <https://doi.org/10.3390/ph12010011>
- Shishir, T.A., Jannat, T., & Naser, I.B. (2022). An in-silico study of the mutation-associated effects on the spike protein of SARS-CoV-2, Omicron variant. *bioRxiv* 2022.02.21.481269; doi: <https://doi.org/10.1101/2022.02.21.4881269>
- Skariyachan, S., Gopal, D., Chakrabarti, S., Kempanna, P., et al. (2020). Structural and molecular basis of the interaction mechanism of selected drugs towards multiple targets of SARS-CoV-2 by molecular docking and dynamic simulation studies-deciphering the scope of repurposed drugs. *Computers in Biology and Medicine*, 126, 104054
- Tuli, H., Sood, S., Pundir, A., Choudhary, D., et al. (2022). Molecular Docking studies of Apigenin, Kaempferol, and Quercetin as potential target against spike receptor protein of SARS COV. *Journal of Experimental Biology and Agricultural Sciences*, 10(1), 144-149
- Vardhan, S., & Sahoo, S. K. (2022). Computational studies on the interaction of SARS-CoV-2 Omicron SGp RBD with human receptor ACE2, limonin and glycyrrhizic acid. *Computers in biology and medicine*, 144, 105367, <https://doi.org/10.1016/j.combiomed.2022.105367>
- Vardhan, S., & Sahoo, S.K. (2020). Searching inhibitors for three important proteins of COVID-19 through molecular docking studies. Preprint from arXiv, 1-15 <https://arxiv.org/abs/2004.08095>
- Wang, C., Liao, Y., Wang, S., Wang, D., et al. (2018a). Cytoprotective effects of diosmetin against hydrogen peroxide-induced L02 cell oxidative damage via activation of the Nrf2-ARE signaling pathway. *Molecular Medicine Reports*, 17(5), 7331-7338
- Wang, T. Y., Li, Q., & Bi, K. S. (2018b). Bioactive flavonoids in medicinal plants: Structure, activity and biological fate. *Asian Journal of Pharmaceutical Sciences*, 13(1), 12-23
- World Health Organization (2022a). WHO Coronavirus (COVID-19) Dashboard. <https://covid19.who.int/> Accessed on April 2, 2022.
- World Health Organization. (2022b). Tracking SARS-CoV-2 variants, 2022. Retrieved from <https://www.who.int/en/activities/tracking-SARS-CoV-2-variants>
- Zobeiri, M., Belwal, T., Parvizi, F., Naseri, R., et al. (2018). Naringenin and its nano-formulations for fatty liver: cellular modes of action and clinical perspective. *Current Pharmaceutical Biotechnology*, 19(3), 196-205
- Zrig, A. (2022) The Effect of Phytocompounds of Medicinal Plants on Coronavirus (2019-NCoV) Infection. *Pharmaceutical Chemistry Journal*, 1-5. doi: 10.1007/s11094-021-02540-8



## Journal of Experimental Biology and Agricultural Sciences

<http://www.jebas.org>

ISSN No. 2320 – 8694

### Isolation and determination of *Vibrio* spp. pathogen from *Sciaenops ocellatus* suffering from hemorrhagic disease under cage culture in Vietnam

Pham Thi Hai Yen<sup>1\*</sup> , Nguyen Duy Quynh Tram<sup>1</sup> , Nguyen Quang Linh<sup>2\*</sup> 

<sup>1</sup>University of Agriculture and Forestry, Hue University, Hue 49000, Vietnam

<sup>2</sup>Hue University, 03 Le Loi, Hue 49000, Vietnam

Received – January 05, 2022; Revision – March 03, 2022; Accepted – April 17, 2022

Available Online – April 30, 2022

DOI: [http://dx.doi.org/10.18006/2022.10\(2\).405.415](http://dx.doi.org/10.18006/2022.10(2).405.415)

#### KEYWORDS

Antibiotic

Cage culture

Hemorrhagic disease

Red drum

*Sciaenops ocellatus*

*Vibrio*

#### ABSTRACT

This study was carried out to isolate and determine the *Vibrio* spp. from the Red drum fish (*Sciaenops ocellatus*) suffering from the hemorrhagic disease in Vietnam. In this study, 18 strains of *Vibrio* bacteria were identified from 27 samples of Red drum fish. The isolated bacterial strains were identified with the *16S rRNA* sequencing method and checked for morphological, physiological, and biochemical characteristics by using the API 20E KIT. Results of the study revealed the presence of twelve strains of *V. alginolyticus*, three strains of *V. fluvialis*, and three strains of *V. orientalis*. All *Vibrio* strains have gene similarities with those on the Genbank ranging from 98.05 to 100%. The biochemical characteristics of these 18 isolates were similar and these are susceptible to tetracycline and doxycycline and entirely resistant to ampicillin, amoxicillin, and erythromycin.

\* Corresponding author

E-mail: [nguyenquanglinh@hueuni.edu.vn](mailto:nguyenquanglinh@hueuni.edu.vn) (Nguyen Quang Linh)

Peer review under responsibility of Journal of Experimental Biology and Agricultural Sciences.

Production and Hosting by Horizon Publisher India [HPI]  
(<http://www.horizonpublisherindia.in/>).  
All rights reserved.

All the articles published by [Journal of Experimental Biology and Agricultural Sciences](#) are licensed under a [Creative Commons Attribution-NonCommercial 4.0 International License](#) Based on a work at [www.jebas.org](http://www.jebas.org).





## 1 Introduction

Red drum (*S. ocellatus*) is a marine fish species with high economic value, commonly farmed in Texas and Florida, USA, to provide alternatives to wild-caught fish and stock enhancement efforts (FAO 2009). Red drums have been raising in Vietnam since 1999 and become the most popular species in fish culture due to high productivity (Ministry of Fisheries 2005). In Hue, it has been cultured since 2015 and is more favorable in cage culture in coastal and lagoon areas. Gibson et al. (2021) reported that various *Vibrio* spp. including *V. harveyi* and *V. carchariae* affected the fish cage culture and caused hemorrhagic diseases. Further, *V. vulnificus*, *V. brasiliensis*, *V. cholera*, and *V. parahaemolyticus* are also associated with the Red drums' hemorrhagic disease (Quang et al. 2020). Similarly, Deng et al. (2020) also reported that *Vibrio* is seriously associated with various infectious diseases in marine fish in South China, and these are mainly caused by *V. alginolyticus*, *V. azureus*, *V. fluvialis*, and *V. orientalis* species. In addition, *V. alginolyticus* and *V. parahaemolyticus* strains are also pathogens for the coastal aquaculture systems in Guangdong, China, and Taiwan (Xie et al. 2005). Jeong et al. (2020) indicated the current status and future directions of fish vaccines employing virus-like particles limited and must be integrated intervention to prevent bacterial multiplication. In another study, Cao et al. (2017) also stated that the development of VaBGs (*V. alginolyticus* BGs) like vaccine causes a stronger humoral and cellular immune response and protects mice and fish from *V. alginolyticus*, and found that VaBGs is superior to the conventional FKC vaccine (Formalin-killed whole-cell vaccine). Even *V. alginolyticus*, *S. iniae*, and *Photobacterium damsela* have also been identified as the causative agent of hemorrhagic disease, ulcers, fin erosion, and blindness in Cobia (*Rachycentron canadum*) (Trung and Dung 2018). The aim of this study was to isolate and identify *Vibrio* spp. from the Red drum (*S. ocellatus*) fishes suffering from hemorrhagic disease under cage farming in Thua Thien Hue, Vietnam, and to provide basic data on biochemical characteristics and antibiotic resistance in *Vibrio* bacteria.

## 2 Material and Methods

### 2.1 Sampling and preparation

Thirty-five specimens of Red drums with hemorrhage signs were collected from the four culture cage sites in Hai Duong commune, Huong Tra, Thua Thien Hue, Vietnam. These samples were collected between January to March 2020. The geographic coordinates of sampling sites are: (1) 107°36'39.3984" East and 16°34'0.558012" North; (2) 107°36'51.89544" East and 16°33'57.93696" North; (3) 107°37'3.20988" East and 16°33'58.190796" North; and (4) 107°37'15.12192" East and 16°33'59.01696" North (Figure 1). After collection, the live fish were transported by styrofoam boxes (with manual aerator, temperature from 15 to 18°C) to the laboratory for bacterial isolation and analysis of genes and others.

### 2.2 Physical and chemical characteristics of water

The pH (HANNA HI98107 pH handheld pH meter, Romania), temperature (mercury thermometer), salinity (refractometer), and dissolved oxygen (sera test KIT, Virtue) of the sampling sites water samples were also recorded.

### 2.3 Bacteria isolation and identification

The fish were washed thoroughly under tap water and dried. The outer surface of the fish was disinfected with 70% ethanol, and the fish was opened with a sterilized scalpel. The internal pathological signs were recorded and the damaged tissues from the brain, liver, kidney, and spleen were separated with sterilized culture rods. Extract sticks on the culture rod were inoculated on the thiosulfate citrate bile salts sucrose medium (TCBS, Himedia, India) and cultured at 28°C for 24 hours. The prevalent and loose colonies were further cultured in the TCBS medium under the same conditions for total DNA extraction.

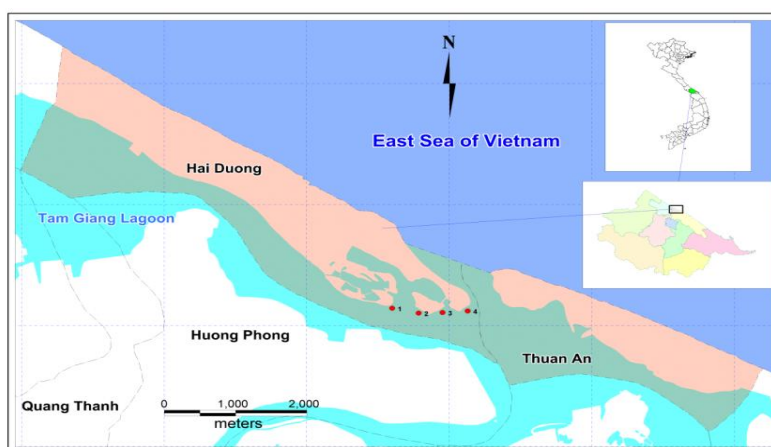


Figure 1 Geographical distribution of the four Sampling sites

## 2.4 Molecular identification of *Vibrio*

### 2.4.1 Total DNA extraction

The *Vibrio* cell lines isolated from Red drum fish with hemorrhagic signs were grown proliferatively on the trypto-casein soy broth (TSB) supplemented with 2% NaCl and shaken at 180 rpm at 30°C for 24 hours. Cell biomass was obtained by centrifugation at 8,000 rpm/min for 2 min at 4 °C. The total DNA of *Vibrio* cell lines was extracted by the modified phenol/chloroform method with some modification and the bacterial cells were directly extracted with phenol SDS/lysozyme or proteinase K (Neumann et al. 1992).

### 2.4.2 *16S rRNA* gene amplification with PCR and nucleotide sequence analysis

The *16S rRNA* gene regions of bacterial strains were amplified by using PCR with specific primer pairs of 27F “AGAGTTGATCMTGGCTCAG” and 1492R “TACGGYTACCTTGTTACGACTT” (Gibson et al. 2021). The PCR was performed on the Applied Biosystems Life Technologies Thermo Fisher Scientific USA systems; the reaction components and thermal cycle used in this study are presented in Table 1.

The PCR product was subject to electrophoresis on 1% agarose gels stained with ethidium bromide, and the electrophoretic images were analyzed with a DyNA Light, Dual-Intensity UV Transilluminator system. This was followed by the purification and sequencing of *16S rRNA* gene region by Sanger method on an ABI PRISM® 3100 Avant Genetic Analyzer (Applied Biosystems) system by Maccrogen Company, Korea. The nucleotide sequence of the genomic region was determined and aligned by using the program Clustal-X (Thompson et al. 1997) and edited by using the BioEdit 7.0.5 software (Hall 1999). The nucleotide sequences of the genomic region were compared with the *16S rRNA* sequences of the microorganisms published on the World GenBank (GenBank) with the BLAST program (<http://www.ncbi.nlm.nih.gov/BLAST/Blast.cgi>).

## 2.5 Physiological and Biochemical characterization

The physiological and biochemical characteristics including Gram staining, oxidase, catalase, oxidase fermentation, bacterial motility was also estimated in the current study. The bacterial motility was determined with the hanging drop method and hemolysis by culturing on agar supplemented with 5% horse blood by Buller's method (Buller, 2004). The bacterial strains were tested by using the API 20E KIT (Bio-Mérieux, France) following the manufacturer's instructions. The reactions were carried out at 28°C, and the results were recorded after 24 hours.

In addition, several biochemical reactions were also carried out to fully understand the characteristics of the isolated *Vibrio* strains. The Voges-Proskauer test and the fermentation of carbohydrates with the purple Broth Base (Difco, UK) supplemented with 5% glucose, fructose, galactose, glucose, glycerol, maltose, mannose was carried out (Phuoc 2014). The viability of *Vibrio* strains at different salt concentrations was conducted on the TSB medium supplemented with 0, 1, 6, 8, and 10% NaCl. The *Vibrio* strains isolated in this study were compared with those isolated by Buller (2004).

## 2.6 Antibiotic susceptibility test

The antibiotic susceptibility of *Vibrio* spp. was tested with the agar plate diffusion method. The *Vibrio* spp. strains were grown proliferatively on the TSB medium supplemented with 2% NaCl and inoculated at 28°C for 24 hrs in a culture cabinet with a shaking speed of 150 rpm. Then, the bacterial cell density was determined by determining the optical density (OD) at 600 nm on a UV-VIS spectrophotometer (U2900, Hitachi, Japan). The preparation was diluted to a concentration corresponding to OD 1 and further reach to 10<sup>6</sup> CFU/mL for the following experiments (Adnan et al. 2013).

One hundred micro-Litre of the 10<sup>6</sup> CFU/mL bacterial solution was evenly spread on the Mueller Hinton Agar medium (MHA, Himedia, India), supplemented with 2% NaCl, and dried at

Table 1 Specific PCR components and thermal cycles for *16S rRNA* gene region amplification

PCR components		Thermal cycle of PCR for <i>16S rRNA</i> gene amplification		
Element	Volume (μL)	Temperature (°C)	Time	Cycle
2× PCR master mix (2.4 mM dNTP each, 0.3 units Taq DNA polymerase)	25	95	5 min	1
10 pmol of 27F primer	1	95	1 min	30
10 pmol/μL of 1492 primer	1	57	50 s	
DNA (50 ng/μL)	1	72	1 min	Lengthen
Sterile distilled water	22	72	10 min	
Total	50	4	Storage temperatures	

ambient temperature for 30 minutes. This was followed by the inoculation of antibiotics discs on the media with the help of sterilized forceps. The antibiotics used in the study are tetracycline 30 ug (Te), amoxicillin 10 ug (Ax), neomycin 30 ug (Ne), ampicillin 10 ug (Am), kanamycin 30 ug (Kn), doxycycline 30 ug (Dx), enrofloxacin 5 ug (Ef), erythromycin 15 ug (Er), and cefotaxime 30 ug (Ct). The plates were incubated in an incubator at 28°C. The diameter of the sterile ring (inhibition zone) was measured after 24 hours.

The bacteria's antibiotic susceptibility or resistance to antibiotics was evaluated from the diameter of the sterile ring followed by the standards of the Clinical and Laboratory Standards Institute, 2018 (Sahu et al. 2018).

## 2.7 Statistical analysis

Database of water environment, infection rate, and physical characteristics were processed by Microsoft Excel version 2016. Further, *16S rRNA* gene region analysis was carried out with the help of MEGA X software.

## 3 Results and Discussion

### 3.1 Physical, chemical water parameters and sample characteristics

Physical and chemical characteristics of water such as pH, temperature, salinity, and dissolved oxygen have been represented in table 2 and the values of the tested parameters are within the acceptable range for nurturing Red drums. Out of 35 collected samples, 27 (77.14%) are showing various infection or disease symptoms. The diseased fish shows various symptoms such as tail amputation, hemorrhaging in gills, body, and skin, and fluid accumulation in the abdominal cavity. In general, environmental factors of the four sampling sites showed small changes and were suitable for Red drum culture, compared with marine water, the water body in the lagoon system a less than salinity.

The collected fish samples have weight ranges from 24.31 to 24.99 g with a length between 11.65 and 15.21 cm (Table 3). The fish body was opened and the internal organs were taken out for testing and checked disease symptoms.

Table 2 Physical and chemical characteristics of the examined sampling sites

Parameter	1		2		3		4	
	Mean ± SD	Min-Max	Mean ± SD	Min-Max	Mean ± SD	Min-Max	Mean ± SD	Min-Max
pH	7.95 ± 0.19	7.8–8.2	7.75 ± 0.31	7.5–8.2	7.83 ± 0.21	7.6–8.1	7.75 ± 0.24	7.5–8.0
T (° C)	26.40 ± 0.64	25.5–27.0	26.85 ± 1.01	26.0–28.0	26.23 ± 1.32	25.0–27.0	26.40 ± 1.14	25–27.6
Salinity (‰)	26.75 ± 4.27	21.0–30.0	25.00 ± 2.16	23.0–28.0	28.00 ± 1.41	27.0–30.0	28.75 ± 0.96	28–30
DO (mg/L)	6.00 ± 0.41	5.5–6.5	6.13 ± 0.25	6.0–6.5	6.38±0.48	6.0–7.0	6.63 ± 0.85	5.5–7.5

Table 3 Fish infection rate and physical characteristics

Point	Samples	Infection rate (%)	Length (cm)	Weight (g)
1	10	80.00	11.65 ± 0.84	24.77 ± 1.13
2	7	71.00	15.21 ± 1.65	26.14 ± 1.57
3	6	66.67	12.13 ± 0.55	24.31 ± 1.16
4	12	83.33	13.89 ± 1.64	24.75 ± 1.43
Total	35	77.14	13.22 ± 1.32	24.99 ± 0.56

Table 4 Ratio of bacterial strains isolated from various organs of hemorrhaged Red drums fish cultured in Thua Thien Hue province

Organ of isolation	Number of colonies	Ratio (%)
Brain	2	11.11
Liver	7	38.89
Kidney	5	27.78
Spleen	4	22.22
Total	18	100

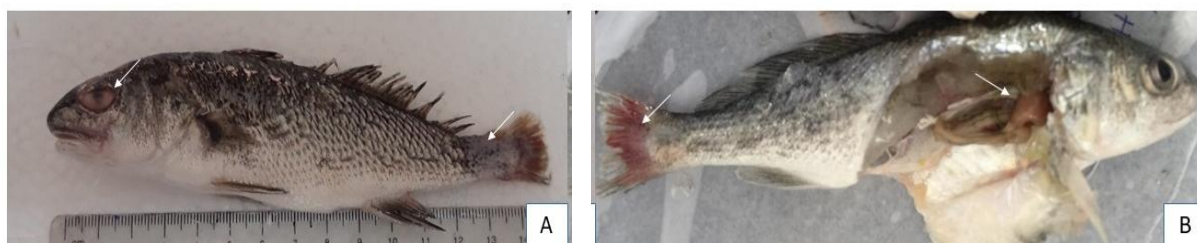


Figure 2 Characteristic signs of hemorrhagic disease are red spots on fins, torn tail, and hemorrhage (arrows, Figures A & B); mucus accumulation in the abdominal cavity (arrow, Figure B)

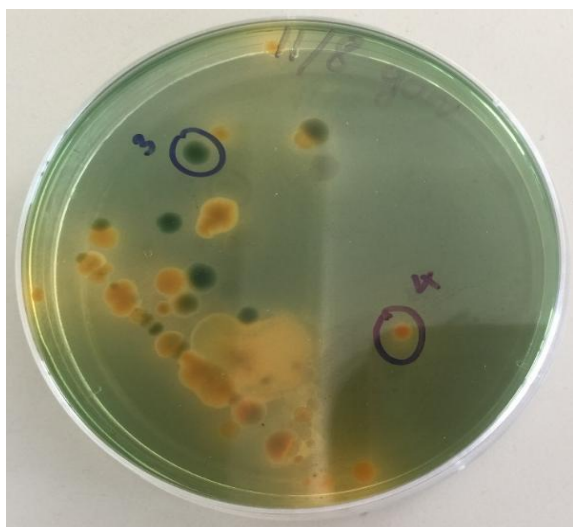


Figure 3 Bacterial colonies isolated on TCBS medium

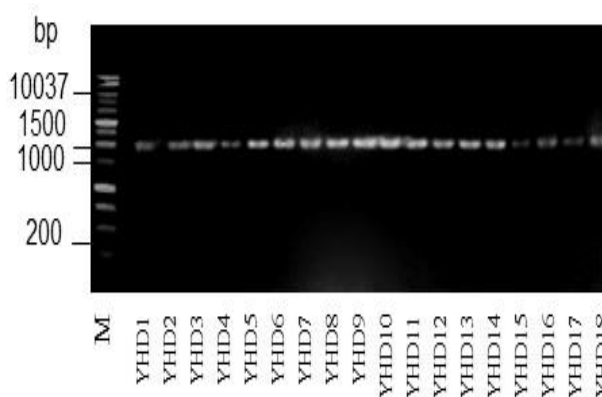


Figure 4 Electrophoresis of PCR product *16S rRNA*  
M: DNA mass scale (Hyper Ladder™ 1 kb (200 bp to 10,037 bp),  
Bioline, Meridian Bioscience)

### 3.2 Isolation and identification of the bacteria

In hemorrhaged Red drums, blue and yellow colonies of *Vibrio* spp. appeared on the TCBS medium after 24 h of culture (Figure 2 & 3). Different parts of the fish body have different levels of infection, and it was reported from 11.11% in the brain to 38.89% in the liver (Table 4), these results suggested higher *Vibrio* infection into the liver as compared to the other organs. However, each organ has a different resistance and needs to be tested separately with nucleotide sequence analysis of the *16S rRNA* gene region (table 4).

### 3.3 Molecular identification and phylogenetic tree generation

#### 3.3.1 PCR product electrophoresis

PCR amplification of *16S rRNA* regions of all 18 bacterial strains isolated from hemorrhaged Red drums collected from all study sites gives a single band with an amplification rate of 100%. All PCR products of bacterial strains are highly concentrated and sharp. The size of the PCR product is approximately 1,500 bp,

consistent with the original expected size (Figure 4). Electrophoresis of *16S rRNA* PCR product and M for DNA mass scale gave 200 bp to 10,037 bp yield (Hyper Ladder™ 1 kb, Bioline, Meridian Bioscience).

#### 3.3.2 Nucleotide sequence of the *16S rRNA* gene region

The nucleotide sequence analysis of the *16S rRNA* gene region of the bacterial strains shows that the PCR amplification rate and the successful nucleotide sequence analysis rate are 100% equal. The sequence edited with the Bioedit software showed the gene regions sized from 1381 to 1448 bp with a mean at 1441 bp. The occurrence rate of each type of nucleotide in the region revealed that the guanine (G) occupies the first position with 31.86% percentages, this was followed by the adenine (25.19%), cytosine (22.31), uracine (20.64), and prevalence (G + C) 54.17% (Table 5).

The *16S rRNA* gene region analysis with the MEGA X software showed that the conserved area for bacterial populations isolated from Red drums has 83/1448 modified nucleotide positions, accounting for 5.73% of the total length of the gene (Table 6).

Table 5 Nucleotide sequence analysis of each *16S rRNA* gene region (%)

No.	Sample code	(U) (%)	C(%)	A(%)	G(%)	G + C(%)	Gene length (bp)
1	YHD1	20.64	22.59	25.34	31.43	54.02	1381
2	YHD2	20.57	22.29	25.28	31.86	54.16	1444
3	YHD3	20.51	22.31	25.35	31.84	54.14	1448
4	YHD4	20.86	22.24	24.93	31.98	54.21	1448
5	YHD5	20.53	22.33	25.10	32.04	54.37	1442
6	YHD6	20.86	22.24	24.93	31.98	54.21	1448
7	YHD7	20.72	22.25	25.16	31.88	54.12	1443
8	YHD8	20.51	22.31	25.35	31.84	54.14	1448
9	YHD9	20.86	22.24	24.93	31.98	54.21	1448
10	YHD10	20.72	22.25	25.16	31.88	54.12	1443
11	YHD11	20.57	22.29	25.28	31.86	54.16	1444
12	YHD12	20.76	22.43	25.35	31.46	53.89	1440
13	YHD13	20.55	22.35	25.19	31.90	54.26	1445
14	YHD14	20.55	22.35	25.19	31.90	54.26	1445
15	YHD15	20.57	22.29	25.28	31.86	54.16	1444
16	YHD16	20.53	22.33	25.10	32.04	54.37	1442
17	YHD17	20.51	22.31	25.35	31.84	54.14	1448
18	YHD18	20.72	22.25	25.16	31.88	54.12	1443
	Mean	20.64	22.31	25.19	31.86	54.17	1441

Table 6 Some characteristics based on *16S rRNA* gene regions of bacterial strains in PCR populations

PCR success rate (%)	Sequencing success rate (%)	Total genomic length (bp)	Percentage of polymorphic nucleotide sites (%)
100	100	1381–1448	5.73

### 3.3.3 Molecular identification

The BLAST results were compared with the world Genbank and reported that 18 bacterial strains belong to the genus *Vibrio*, and among the various *Vibrio* species, *V. alginolyticus* showed the most significant occurrence (67%), this was followed by *V. fluvialis* and *V. orientalis* with the same occurrence rate (17%). The similarities range was reported between 98.05 to 100%. All nucleotide sequences of the bacterial strains are registered on the NCBI Genbank (Genbank Database) with corresponding reference codes (Table 7).

*Vibrio* has been identified as a common pathogen in marine fish species and causing great damage to many marine fish species of economic value (Deng et al. 2020).

This study reported 12 *V. alginolyticus* strains, 3 *V. Fluvialis* strains, and 3 *V. orientalis* strains (Table 7). Among the reported

*Vibrio* spp., *V. alginolyticus* is considered one of the most harmful species for aquatic animals (Deng et al. 2020). Results of the current study are in agreement with the findings of Rameshkumar et al. (2017) those who reported *V. alginolyticus* as the most destructive species for Cobia (*Rachycentron canadum*) under Indian cage cultured aquaculture. Similarly, Dahanayake et al. (2018) isolated a total of 41 *Vibrio* spp., including of 23 *V. alginolyticus*, 11 of *V. fluvialis*, and 7 of *V. antiquarius* from Oyster (*Crassostrea giga*).

### 3.4 Biochemical Characteristics of isolated bacterial strains

The 18 bacterial strains identified in Table 7 were subjected to their morphological, physiological, and biochemical characterization (Figure 5, Table 8).

The physiological and biochemical test with the API 20E KIT (Bio Mérieux, France) indicates that among the 18 strains, 12 strains

Table 7 Percentage similarities of isolates based on *16S rRNA* gene sequencing published in GenBank

No	Isolated	Genbank code	GenBank reference	Similarity (%)
1	<i>V. alginolyticus</i> strain, YHD1	MZ753696	MH298564.1	98.05
2	<i>V. alginolyticus</i> strain, YHD3	MZ753698	CP051109.1	99.59
3	<i>V. alginolyticus</i> strain, YHD5	MZ753700	MN843961.1	99.72
4	<i>V. alginolyticus</i> strain, YHD7	MZ753702	MN938185.1	99.86
5	<i>V. alginolyticus</i> strain, YHD8	MZ753703	CP051109.1	99.59
6	<i>V. alginolyticus</i> strain, YHD10	MZ753705	MN938185.1	99.86
7	<i>V. alginolyticus</i> strain, YHD12	MZ753707	MH298564.1	98.05
8	<i>V. alginolyticus</i> strain, YHD13	MZ753708	MN938360.1	99.65
9	<i>V. alginolyticus</i> strain, YHD14	MZ753709	MN938360.1	99.65
10	<i>V. alginolyticus</i> strain, YHD16	MZ753711	MN843961.1	99.72
11	<i>V. alginolyticus</i> strain, YHD17	MZ753712	CP051109.1	99.59
12	<i>V. alginolyticus</i> strain, YHD18	MZ753713	MN938185.1	99.86
13	<i>V. fluvialis</i> strain, YHD4	MZ753699	CP051126.1	100
14	<i>V. fluvialis</i> strain, YHD6	MZ753701	CP051126.1	100
15	<i>V. fluvialis</i> strain, YHD9	MZ753704	CP051126.1	100
16	<i>V. orientalis</i> strain, YHD11	MZ753706	MN945276.1	100
17	<i>V. orientalis</i> strain, YHD2	MZ753697	MN945276.1	100
18	<i>V. orientalis</i> strain, YHD15	MZ753710	MN945276.1	100

Genbank registration Code No: <https://submit.ncbi.nlm.nih.gov/subs/?search=SUB10184933>

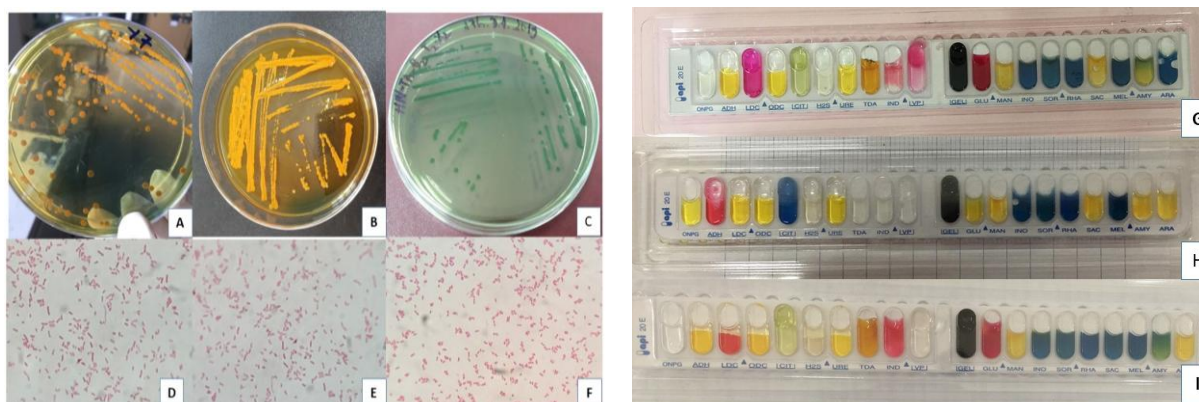


Figure 5 Colony appearance on TCBS: (A) *V. alginolyticus*; (B) *V. fluvialis*; (C) *V. orientalis*; Gram staining (D) *V. alginolyticus*; (E) *V. fluvialis*; (F) *V. orientalis*; identification of bacteria isolated from Red drums with API 20E KIT: (G) *V. alginolyticus*; (H) *V. fluvialis*; (I) *V. orientalis*

showed 414725, 3 strains showed 3246126, and 3 strains showed 4066106 responding to *V. alginolyticus*, *V. fluvialis*, and *V. orientalis* respectively (Buller 2004). Among the reported strains, *V. alginolyticus* strain shows comma-shaped yellow colonies on the TCBS medium and belonging to the Gram-negative bacteria group (Figure 5 A & D). Further, this strain is indole unproductive, capable of degrading nitrate, producing catalase, oxidase, and

positive Voges–Proskauer reaction. *V. alginolyticus* strain can also ferment glucose, sucrose, mannitol, sorbitol, and arabinose. One of these strains is capable of producing H<sub>2</sub>S (11/12). The physiological and biochemical parameters results of *V. alginolyticus* isolated from diseased Red drums are homogenous with *V. alginolyticus* ATCC33787 strains isolated from diseased Oysters (Escalona et al. 2006).

Table 8 Physiological and biochemical parameters of *Vibrio* spp. isolated from diseased Red drums

No.	Indicator	<i>V. alginolyticus</i> (Buller, 2004)	<i>V. alginolyticus</i> <i>n</i> = 12	<i>V. fluvialis</i> (Buller, 2004)	<i>V. fluvialis</i> = 3	<i>V. orientalis</i> = 3 (Buller, 2004)	<i>V. orientalis</i> = 3	
1	Gram staining	–	–	–	–	–	–	
2	Form	Comma	Comma	Curved rod	Curved rod	Curved rod	Curved rod	
3	Colonies on TCBS	Yellow	Yellow	Yellow	Yellow	Green	Green	
4	Colonies on TSA	ND	Milky white	Milky white	Milky white	ND	Milky white	
5	Growth in NaCl solution (%)	0	–	–	–	–	–	
		1	ND	+	+	+	+	
		6	+	+	+	+	+	
		8	+	+(10/12)	–	–	+	+
		10	–/+	–/+	–	–	–	–
6	API 20E	414725	414725	3246126	3246126	4066106	4066106	
7	Oxidase	+	+	+	+	+	+	
8	Catalase	+	+	+	+	+	+	
9	H <sub>2</sub> S synthesis	–	– (11/12)	–	–	–	–	
10	NO <sub>3</sub> decomposition	+	+	+	+	+	+	
11	Indol	–	–	+	+	+	+	
12	Voges–Proskauer	+	+	–	–	–	–	
13	Citrate use	+	+	+	+	–	–	
14	Glucose	+	+	+	+	–	–	
15	Mannitol	+	+	+	+	+	+	
16	Sorbitol	+	+	–	–	–	–	
17	Sucrose	+	+	+	+	–	–	
18	Arabinose	–	–	+	+	+	+	

Among the eighteen bacterial strains three (16.67%) belonging to the Gram-negative *V. fluvialis*, and have curved rod-shaped morphology and yellow colonies on the TCBS medium (Figure 5 B & E). *V. fluvialis* has oxidase-positive nature, capable of producing catalase and indole, fermenting glucose, mannitol, sucrose, and arabinose but not sorbitol. Further, rest three (16.67%) bacterial strains were identified as *V. orientalis* strains and these have blue colonies on the TCBS medium. *V. orientalis* appeared as short curved rods and belong to the group of Gram-negative bacteria (Figure 5 C & F). *V. orientalis* can grow at different NaCl concentrations (1, 6, and 8%) and showed oxidase, catalase, mannitol, and arabinose positive and glucose, sorbitol, sucrose, and H<sub>2</sub>S-negative reaction. *V. fluvialis* and *V. alginolyticus* are well known for carrying out pathogenic factors for aquatic animals (Ramamurthy et al. 2014). Meanwhile, *V. orientalis* belongs to the Orientalis clade in *Vibrio* genus in which *V. tubiashii* and *V. sinoaloensis* have been reported causing diseases for bivalves and

fishes (Hada et al. 1984; Gomes et al. 2018). Moreover, Restrepo et al. (2018) reported a *V. punensis* which is closely related to *V. orientalis*, carrying the toxic genes which cause disease in shrimp. Due to limited information regarding *V. orientalis* strain, this strain is not yet recognized as pathogenic *Vibrio* species for aquatic animals. Thus, further investigations are required to establish the pathogenic characteristics of *V. orientalis*.

### 3.5 Antibiotic susceptibility of *Vibrio* strains

All 18 strains of *Vibrio* are entirely resistant to ampicillin, amoxicillin, and erythromycin (Table 9). Similarly, the Am resistance in *Vibrio* strains isolated from the marine environment was reported by Stabili et al. (2010). Trung and Dung (2018) also reported antibiotic resistance against ampicillin, streptomycin, and erythromycin in *V. alginolyticus* causing disease in the caged Cobia (*R. canadum*) cultured in Kien Giang, Vietnam.

Table 9 Antibiotic susceptibility rate of *Vibrio* strains isolated from diseased Red drums

Antibiotics	Rate (%)								
	<i>V. alginolyticus</i>			<i>V. fluvialis</i>			<i>V. orientalis</i>		
	S	I	R	S	I	R	S	I	R
<b>β-lactams</b>									
Cefotaxime (Ct, 30 ug)	75	25	0	66.7	33.3	0	66.7	33.3	0
Ampicillin (Am, 10 ug)	0	0	100	0	0	100	0	0	100
Amoxicillin (Ax, 10 ug)	0	0	100	0	0	100	0	0	100
<b>Quinolones</b>									
Enrofloxacin (Ef, 5 ug)	66.7	33.3	0	66.7	33.3	0	66.7	33.3	0
<b>Aminoglycosides</b>									
Kanamycin (Kn, 30 ug)	50	33.3	16.7	66.7	33.3	0	66.7	33.3	0
Neomycin (Ne, 30 ug)	41.7	33.3	25	33.3	33.3	33.3	33.3	33.3	33.3
<b>Macroid</b>									
Erythromycin (Er, 15ug)	0	0	100	0	0	100	0	0	100
<b>Tetracyclines</b>									
Tetracycline (Te, 30 ug)	100	0	0	100	0	0	100	0	0
Doxycycline (Dx, 30 ug)	100	0	0	100	0	0	100	0	0

S: Sensitive; I: Intermediate; R: Resistant

All isolates are found sensitive to tetracycline and doxycycline. Tetracycline is an antibiotic allowed in aquaculture, so farmers often use it to prevent and treat the diseases caused by bacteria in fish and shrimp farms. These findings are in agreement with the findings of Trung and Dung (2018). Tetracycline has long been the most commonly used antibiotic in the Korean aquaculture system, especially for the species severely infected by *Vibrio*. According to Hoa et al. (2019), *V. alginolyticus* strains cause disease in sea bass (*Lates calcarifer*) in Vietnam, and these strains are sensitive to doxycycline, erythromycin, nalidixic acid, oxolinic acid, oxytetracycline, streptomycin, sulphonamide, and tetracycline but resistant to ampicillin and neomycin. Table 9 indicated that all 12 strains of *V. alginolyticus* have sensitivity to cefotaxime (75%), enrofloxacin (66.7%), kanamycin (50%), and neomycin (41.7%); but there were 3 strains of *V. fluvialis* and *V. orientalis* are sensitive to cefotaxime (66.7%), enrofloxacin (66.7%), kanamycin (66.7%), and neomycin (33.3%). Kang et al. (2016) reported that 15 strains of *V. alginolyticus* isolated from oysters are completely resistant to ampicillin, highly sensitive to tetracycline (100%); cefotaxime (86.7%), and kanamycin (73.3%), and moderately resistant to erythromycin.

### Conclusions

Results of the current study reported the presence of a total of 18 *Vibrio* strains from the hemorrhaged Red drums cultured in cages. Among the reported 18 strains, 12 strains were of *V. alginolyticus*, 3 of *V. fluvialis*, and 3 of *V. orientalis*. The results from this study

also confirmed that the *Vibrio* spp. are generally homogeneous in biochemical characteristics. Further, isolated *Vibrio* strains have *16S rRNA* gene homology ranging from 98.05 to 100% and correspond to codes 4147125, 3246126, and 4066106 on the GenBank (<https://csdlkhoahoc.hueuni.edu.vn/index.php/certificate/edit/id/16>). These *Vibrio* strains are susceptible to tetracycline and doxycycline and resistant to ampicillin, amoxicillin, and erythromycin.

### Funding statement

This research was supported by Hue University, Vietnam, under Project number DHH2021-02-153

### Conflict of interest

The authors declare that they have no conflict of interest regarding the publication of this article.

### Acknowledgments

We thank all members of the Hue University project who participated in sample collection and isolation of *Vibrio* spp.

### References

Adnan, N., Sultana, M., Ok, I., Nandi, S.P., & Ma, H. (2013). Characterization of ciprofloxacin resistant extended spectrum β-lactamase (ESBL) producing *Escherichia* spp. from clinical waste



- water in Bangladesh. *Advances in Bioscience and Biotechnology*, (4), 15-23.
- Buller, N. B. (2004). *Bacteria from fish and other aquatic animals: a practical identification manual*: CABI publication.
- Cao, J., Zhang, J., Ma, L., Li, L., Zhang, W., & Li, J. (2017). Identification of fish source *Vibrio alginolyticus* and evaluation of its bacterial ghosts vaccine immune effects. *Microbiology Open*, 7(3), e00576.
- Dahanayake, P., De Silva, B., Hossain, S., Shin, G. W., & Heo, G. J. (2018). Occurrence, virulence factors, and antimicrobial susceptibility patterns of *Vibrio* spp. isolated from live oyster (*Crassostrea gigas*) in Korea. *Journal of food safety*, 38(5), e12490.
- Deng, Y., Xu, L., Chen, H., Liu, S., et al. (2020). Prevalence, virulence genes, and antimicrobial resistance of *Vibrio* species isolated from diseased marine fish in South China. *Scientific Reports*, 10(1), 1-8.
- Escalona, G.N., Blackstone, G.M., & A, D. (2006). Characterization of a *Vibrio alginolyticus* strain, isolated from Alaskan oysters, carrying a hemolysin gene similar to the thermostable direct hemolysin-related hemolysin gene (*trh*) of *Vibrio parahaemolyticus*. *Applied and Environmental Microbiology*, 72(12), 7925-7929.
- FAO. (2009). *Sciaenops ocellatus*. In Cultured aquatic species fact sheets. Text by Cynthia K. Faulk, A. Edited and compiled by Valerio Crespi and Michael New. CD-ROM (multilingual). doi: [https://www.fao.org/fishery/docs/CDrom/aquaculture/I1129m/file/en/en\\_reddrum.htm](https://www.fao.org/fishery/docs/CDrom/aquaculture/I1129m/file/en/en_reddrum.htm)
- Gibson Kueh, S., Terence, C., Chew, X. Z., Uichanco, J. A., & Shen, X. (2021). PCR, in-situ hybridization, and phylogenetic analysis suggest that 'big belly' disease in barramundi, *Lates calcarifer* (Bloch), is caused by a novel *Vibrio* species. *Journal of fish diseases*, 44 (12), 1985-1992.
- Gomez-Gil, B., Fajer-Avila, E., Pascual, J., Macián, M.C., et al. (2008) *Vibrio sinaloensis* sp. nov., isolated from the spotted rose snapper, *Lutjanus guttatus* Steindachner, 1869. *International Journal of Systematic and Evolutionary Microbiology*, 58(Pt 7), 1621-1624.
- Hada, H.S., West, P.A., Lee, V.J., Stemmler, J., & Colwell, R.R. (1984). *Vibrio tubiashii* sp. nov., a Pathogen of Bivalve Mollusks. *International Union of Microbiological Societies*, 34(1), 1-4.
- Hall, T. A. (1999). BioEdit: a user-friendly biological sequence alignment editor and analysis program for Windows 95/98/NT. . *Paper presented at the Nucleic acids symposium series*. doi: [https://www.academia.edu/2034992/BioEdit\\_a\\_user-friendly\\_biological\\_sequence\\_alignment\\_editor\\_and\\_analysis\\_program\\_for\\_Windows\\_95\\_98\\_NT](https://www.academia.edu/2034992/BioEdit_a_user-friendly_biological_sequence_alignment_editor_and_analysis_program_for_Windows_95_98_NT)
- Jeong, K.H., Kim, H.J., & Kim, H.J. (2020). Current status and future directions of fish vaccines employing virus-like particles. *Fish & shellfish immunology*, 100, 49-57.
- Kang, C.H., Shin, Y., Jang, S., Jung, Y., & So, J.S. (2016). Antimicrobial susceptibility of *Vibrio alginolyticus* isolated from oyster in Korea. *Environmental Science and Pollution Research*, 23(20), 21106-21112.
- Restrepo, L., Bayot, B., Arciniegas, S., Bajiña, L., et al. (2018). *PirVP* genes causing AHPND identified in a new *Vibrio* species (*Vibrio punensis*) within the commensal Orientalis clade, *Scientific report*, 8,13080:1-14.
- Ministry of Fisheries, N. F. E. C. (2005). *Breeding and rearing techniques of Red drum*. Ha Noi Agriculture.
- Neumann, B. R., Pospiech, A., & Schairer, H. U. (1992 ). Rapid isolation of genomic DNA from gram-negative bacteria. *Trends in Genetics*: 8(10), 332-333.
- Quang, H.T., Lan, T.T., Hai, T.T.H., Yen, P.T.H., et al. (2020). Genetic diversity and toxic genes analysis of *Vibrio* spp. isolated from white leg shrimp and marine fishes cultured in Tam Giang lagoon in Thua Thien Hue province, Vietnam. *Indian journal of Science and Technology* 13(13), 1412-1422.
- Ramamurthy, T., Chowdhury, G., Pazhani, G.P., & Shinoda, S. (2014). *Vibrio fluvialis*: an emerging human pathogen. *Frontiers in Microbiology*, 5(91), 1-8.
- Rameshkumar, P., Nazar, A., Pradeep, M., Kalidas, C., et al. (2017). Isolation and characterization of pathogenic *Vibrio alginolyticus* from sea cage cultured cobia (*Rachycentron canadum* (Linnaeus 1766)) in India. *Letters in applied microbiology*, 65(5), 423-430.
- Sahu, C., Jain, V., Mishra, P., & Prasad, K. N. (2018). Clinical and laboratory standards institute versus European committee for antimicrobial susceptibility testing guidelines for interpretation of carbapenem antimicrobial susceptibility results for *Escherichia coli* in urinary tract infection (UTI). *Journal of Laboratory Physicians*, 10(03), 289-293.
- Stabili, L., Gravili, C., Boero, F., Tredici, S. M., & Alifano, P. (2010). Susceptibility to antibiotics of *Vibrio* sp. AO1 growing in pure culture or in association with its hydroid host *Aglaophenia octodonta* (Cnidaria, Hydrozoa). *Microbial Ecology*, 59(3), 555-562.

- Thompson, J. D., Gibson, T. J., Plewniak, F., Jeanmougin, F., & Higgins, D. G. (1997). The CLUSTAL\_X windows interface: flexible strategies for multiple sequence alignment aided by quality analysis tools. *Nucleic Acids Research*, 25(24), 4876-4882.
- Trung, NB, & Dung, T.T. (2018). Research on bacterial diseases on cobia (*Rachycentron canadum*) cage cultured in Kien Giang province. *Journal of Can Tho University*, 54(2), 60-67.
- Xie Z.Y., Hu C.Q., Chen C., Zhang L.P., & C.H.R. (2005). Investigation of seven *Vibrio virulence* genes among *Vibrio alginolyticus* and *Vibrio parahaemolyticus* strains from the coastal mariculture systems in Guangdong, China. *Letters in Applied Microbiology*, 41(2), 202-207.



## Journal of Experimental Biology and Agricultural Sciences

<http://www.jebas.org>

ISSN No. 2320 – 8694

### Evaluation of Phytochemical and Antibacterial properties of leaf extract of *Cinnamomum tamala* oil

Alok Bharadwaj<sup>1\*</sup>, Arushi Rashi<sup>1</sup>, Gunjan Garg<sup>2</sup>

<sup>1</sup>Department of Biotechnology, GLA University, Mathura (U.P.) - 282406

<sup>2</sup>School of Biotechnology, Gautam Buddha University, Greater Noida (U.P.) – 201312

Received – December 29, 2021; Revision – March 03, 2022; Accepted – April 10, 2022

Available Online – April 30, 2022

DOI: [http://dx.doi.org/10.18006/2022.10\(2\).416.422](http://dx.doi.org/10.18006/2022.10(2).416.422)

#### KEYWORDS

*Cinnamomum tamala*

Leaf concentrate

Phytochemical evaluation

Antibacterial property

#### ABSTRACT

*Cinnamomum tamala*, commonly known as tej patta is widely used as a spice in Indian cuisine for its aroma and flavoring property as the leaves contain essential oil. The essential oil is extracted with the help of the Clevenger apparatus using dry leaves. This oil is mainly used as medicine for releasing gas as well as a carminative agent and diuretic agent. It also improves the digestive system and helps in increasing appetite. This study aimed to determine the phytochemical properties and antibacterial potential of different extracts (aqueous, methanol, and acetone) and oil of *C. tamala* leaves. The phytochemical evaluation shows the presence and absence of alkaloids, flavonoids, phenolic compounds, steroids, tannins, glycosides, terpenoids, saponins, proteins, and carbohydrates in the aqueous, methanol, and acetone extracts. The efficacy of antibacterial properties of prepared extracts was examined against *E. coli* and *Salmonella typhi* (gram-negative bacteria) and *Staphylococcus aureus* and *Bacillus subtilis* (gram-positive bacteria). These bacterial cultures were obtained from IMTech Chandigarh. From the results of the antibacterial study it has become evident that among three extracts, the maximum zone of inhibition was obtained in the aqueous extract which was followed by methanolic and acetone extract. With the help of a Clevenger apparatus, Bay leaf oil was extracted to establish antibacterial properties. Henceforth, to analyze the antibacterial potential of the oil sample, the test was performed against the mentioned bacterial species (*E. coli*, *Salmonella typhi*, *Staphylococcus aureus*, and *Bacillus subtilis*) and reported significant antibacterial activities. From the outcome of this study, it has become clear that Bay leaf oil has potent antibacterial properties against selected bacterial species.

\* Corresponding author

E-mail: [alok.bhardwaj@gla.ac.in](mailto:alok.bhardwaj@gla.ac.in) (Alok Bharadwaj)

Peer review under responsibility of Journal of Experimental Biology and Agricultural Sciences.

Production and Hosting by Horizon Publisher India [HPI]  
(<http://www.horizonpublisherindia.in/>).  
All rights reserved.

All the articles published by [Journal of Experimental Biology and Agricultural Sciences](#) are licensed under a [Creative Commons Attribution-NonCommercial 4.0 International License](#) Based on a work at [www.jebas.org](http://www.jebas.org).



## 1 Introduction

*Cinnamomum tamala* is commonly known as Tejpatta. It is a medium-sized evergreen tree acquiring 8 m in height and a girth of 150 cm. The genus *Cinnamomum* consists of 270 species out of which only 20 species are cultivated commercially in India (Mall et al. 2018). The bay leaf trees are commercially cultivated throughout the country from tropical regions to sub-tropical regions of the Himalayas. Stems are rough, having a brown color. The flowers have a whitish type of color and mostly occur in the last week of March or in the April first week. The fruits are drupe and ripens fruits are dark purple. Seed maturity takes place in approximately one year (Sharma et al. 2009).

The leaves of *C. tamala* are used widely in north India as a spice known as Tejpat. These are used as a replacement for paan (betel leaves) in Kashmir (Kirtikar and Basu 1981). Bay leaf is extensively applied as spices in Indian cuisine for its fragrance and flavoring property as leaves containing essential oil. The leaves' essential oil is extracted by the steam distillation process of dry leaves. The chief element of cinnamon oil includes eugenol, sabinene (4.8%),  $\beta$ -caryophyllene (6.6%), curcumenol (2.3%), and germacrene D (4.6%). Its bark produces cinnamaldehyde which is primarily accountable for its fragrance but other components give the unique flavor and odor. Medicinally the oil is mainly used as an anti-flatulent, diuretic and carminative (Showkat et al. 2004). Traditionally, the leaves are utilized in colic and diarrhoeal preparations (Nadkarni 1976; Duke and Fulton 2002). Further, the essential oil of *C. tamala* revealed fungi toxic activity (Dubey et al. 1998).

Bay leaves or Tejpatta are used daily by the Indians in cooking. Since the ancient era, dry bay leaves are mainly used as a spice and green leaves are used for perfumery purposes. It also shows good medicinal properties. As it stimulates the different digestive

enzymes which enhance digestion. Bay leaf is an important constituent of several kinds of drugs in the pharmaceuticals industries. It is beneficial in the treatment of muscle and joints complications and helps to relieve arthritis, inflamed joints, muscular pains, rheumatism, and sprains. It also improves the digestive system and helps in increasing appetite. It also helps in controlling infections also (Shu 1998). It also showed antibacterial properties against potent gram-positive and gram-negative bacteria. The present study was focused on the phytochemical analysis of bay leaf along with its antibacterial activity. Moreover, its essential oil was extracted and undergoes antibacterial analysis against potentially pathogenic bacteria.

## 2 Materials and Methods

### 2.1 Collection of *C. tamala* leaves

The plant material for the study was purchased from the local markets of Mathura. Cleaning was done two times with running tap water and with distilled water so that all the dust and impurities runoff. At room temperature, leaves were air-dried and then dried in a hot air oven for a few hours. The weight of dry leaves was taken and recorded. It is then crushed by the mixer to get a fine powdered form and the weight of the powder was also taken and recorded (Figure 1). Extraction was carried out using the Soxhlet apparatus. About 30g of leaves powder was taken for each aqueous, acetone, and methanol solvent. Powdered plant material (30g) was uniformly packed in the respective thimbles and covered with cotton wool, the thimble having sample was then placed in the extraction jacket and the continuous extraction was carried out by using respective solvents, i.e., double distilled water (700 ml), acetone (500 ml) and methanol (500 ml). The extraction was carried out till the color of the solvent in the siphon tube become colorless. The temperature of Soxhlet was maintained to approximately 60-70°C for aqueous extraction, 30-40°C for



Figure 1 Preparation of *Cinnamomum tamala* (Bay leaf) (A) Leaf collection (B) Crushed

acetone, and 50°C for methanol extraction. When the extraction is complete, the thimble is removed and again switched on the Soxhlet, and the purified solvent was extracted out from the extract which was used for the further study. Then the extract was poured on a 200mm Petri plate and put overnight in an incubator to incubate it at 50°C till the solvent evaporate, and at last, the extract was collected by scratching it from the plate and then weight the obtained extract and storing it in a sterile vial or sample container.

## 2.2 Preliminary phytochemical screening of *C. tamala*

### 2.2.1 Alkaloids

Hager's test has been used for screening the presence of alkaloids in the extract. A saturated solution of picric acid (TNP) was made and then mixed with 2 ml of the respective extracts. The appearance of yellow ppt. indicates the presence of alkaloids.

### 2.2.2 Cardiac glycosides

For this, 2 ml of glacial acetic acid was collected, and add a drop of FeCl<sub>3</sub> solution into it. In this solution, 2 ml of plant extract and 1 ml of concentrated H<sub>2</sub>SO<sub>4</sub> were also added. The formation of a brown ring at the interface specifies the presence of de-oxy sugar i.e. the characteristics of cardenolide.

### 2.2.3 Saponins

2ml of water was added to the dry extract and shake vigorously. The appearance of foam showed the presence of saponins.

### 2.2.4 Tannins

2 ml of extract was mixed with a few drops of 1% FeCl<sub>3</sub>, and the appearance of blue-black precipitate in the solution confirms the presence of tannins.

### 2.2.5 Steroids

The presence of steroids was screened by Salkowski Test. For this, chloroform was added into the crude extract and this was followed by the addition of a few drops of concentrate H<sub>2</sub>SO<sub>4</sub>, shaking well mix and allowed to stand for some time. The presence of steroids was confirmed by the appearance of red color at the lower layer while the presence of tri-terpenoids was confirmed by yellow color layer formation.

### 2.2.6 Carbohydrates

For carbohydrate screening, Molisch's Test was carried out, in this, 2 ml of sample was taken in a test tube and a small amount of Molisch's reagent ( $\alpha$ -naphthol dissolved in ethanol) was mixed. This was followed by the addition of concentrate H<sub>2</sub>SO<sub>4</sub> slowly through the wall of the test tube, so a ring is formed at the bottom

layer, formation of a bluish-violet ring at the junction confirms its carbohydrates.

### 2.2.7 Proteins

2 ml of extract was taken in a test tube and boiled with Ninhydrin, development of a violet color confirmed the presence of proteins.

### 2.2.8 Phenolic compound

2 ml of extract was mixed with the Bromine water and the presence of yellow precipitate confirms the presence of phenolic compounds.

### 2.2.9 Terpenoids

Take 2 ml of chloroform and carefully add concentrated H<sub>2</sub>SO<sub>4</sub> to form a layer. Add 2 ml of extracts to it. The appearance of reddish-brown color at the interface authenticates the presence of terpenoids.

### 2.2.10 Flavonoids

2 ml of 2% NaOH was added to the extract which produces yellow color which get disappeared when 2-3 drops of dilute acid are added, this is the best test for the screening of the presence of flavonoids.

## 2.3 Antibacterial activity of different bay leaf extracts

### 2.3.1 Test microorganisms

*Escherichia coli* (MTCC 294) and *Salmonella typhi* (MTCC 660) are the two Gram-negative bacterial strains while *Staphylococcus aureus* (MTCC 3160) and *Bacillus subtilis* (MTCC 2057) are the two Gram-positive bacterial strains used for the analysis of antimicrobial activity.

### 2.3.2 Preparation of different concentrations of bay leaf extracts

Prepare different extracts (acetone, methanol, and aqueous) as per the method given in section 2.1. The dried extracts were diluted with appropriate solvents to make different final concentrations (25 mg/ml, 50 mg/ml, 75 mg/ml and 100mg/ml) respectively.

### 2.3.3 Preparation of bacterial inoculum

A loopful culture of each bacterium was inoculated into 4-5 ml peptone water and incubated at 37°C for 24 hours. Now match this bacterial growth with that of 0.5 Mc Farland standards that are formulated by adding 99.5 ml of 1% (v/v) H<sub>2</sub>SO<sub>4</sub> in 0.5 ml of 1.75 % (w/v) BaCl<sub>2</sub>.2H<sub>2</sub>O. If the bacterial growth is dense then dilute it by adding more peptone water to match exactly with the Mc-Farland standard. This concentration is equivalent to 1-2 X 10<sup>8</sup>CFU/ml approximately (Baker et al. 1983).

### 2.3.4 Screening of antibacterial activity of bay leaf extract in different solvents

Disc diffusion method was used to find out the antibacterial activity. Firstly the Nutrient agar media (NAM) was poured into pre-sterilized Petri plates and when it becomes solidified, 0.1 ml of bacterial inoculum (size  $1 \times 10^8$ ) was loaded on the Petri plates and spread using an L-shaped spreader. Now, plates were incubated at  $37^\circ\text{C}$  for one hour. Sterile plain discs were impregnated with different concentrations of extracts (25 mg/ml, 50 mg/ml, 75 mg/ml, and 100 mg/ml) were placed over the Nutrient agar media surface at a specific distance. All the 4 different concentrations of the 3 extracts and 4 discs were impregnated with 15  $\mu\text{L}$  of all respectively and placed on the separate bacterial plates.

Ciprofloxacin, streptomycin, erythromycin, and chloramphenicol antibiotic discs were taken as a positive control for the different bacteria respectively. Disc impregnated with 15  $\mu\text{L}$  of autoclaved distilled water was taken as a negative control for aqueous extract and disc impregnated with 15  $\mu\text{L}$  of a mixture of DMSO and distilled water (20%) was taken as a negative control for acetone and methanol extract. Now plates were incubated at  $37^\circ\text{C}$  for 24 hours for the development of the zone of inhibition. Results were compared with the standard antibiotics discs which serve as positive control and water/DMSO (depending on the solvent used) as a negative control. Each test was carried out three times and the average inhibition zone was documented for all the three extracts and compared it with standard antibiotics i.e. control.

## 2.4 Screening of antibacterial activity of bay leaf oil

### 2.4.1 Extraction of bay leaf oil

About 40 g of the powdered leaves is weighed and 600 ml of double-distilled water was taken. Then the Clevenger apparatus was set up and leaves were subjected to hydro-distillation for about 6-7 hrs at a temperature between  $30\text{-}40^\circ\text{C}$ . After that the apparatus was left undisturbed for some time so that the temperature of the apparatus will decrease, then the essential oil extracted from the leaves was collected and stored at  $4^\circ\text{C}$  until used.

### 2.4.2 Preparation of different concentrations of bay leaf oil

The oil was diluted with ethanol to obtain different concentrations of 50% and 100% (v/v). Furthermore, preparation of bacterial inoculums and screening of antibacterial activity of bay leaf oil was carried out as explained in sections 2.3.3 and 2.3.4.

## 2.5 Statistical analysis

Results (in terms of zone of inhibition) undergo statistical analysis that is performed by one-way analysis (ANOVA) through SPSS ver. 20.0 software and Duncan's multiple tests (DMRT) at  $p < 0.05$

and  $p < 0.01$  by determining the significant variation in mean values between the experimental and control values. These values were defined as mean  $\pm$  S.E.M (standard error mean).

## 3 Results and Discussion

### 3.1 Phytochemical analysis

The results of phytochemical evaluation revealed the difference in the presence and absence of alkaloids, flavonoids, phenolic compounds, steroids, tannins, glycosides, terpenoids, saponins, proteins, and carbohydrates in the Aqueous, Methanol, and Acetone extracts (Table 1). Similar types of results were also obtained by Saluja et al. (2010) and Gill et al. (2015). The presence of these phytochemicals provides a source for various medicinal properties against various pathogenic bacteria and lethal diseases. The important studies conducted on *C. tamala* are for its hypolipidemic effects (Dhulasavant et al. 2010), anti-diabetic and antioxidant (Chakraborty and Das 2009), anti-ulcer (Eswaran et al. 2010), anti-inflammatory (Gambhire et al. 2009), anti-diarrhoeal (Rao et al. 2008), immunosuppressive (Chaurasia et al. 2010) and anti-bacterial (Goyal et al. 2009). Phytochemicals like terpenoids and tannins are credited with anti-inflammatory and analgesic properties. Hence, the presence of all these phytoconstituents enables plants enough potent in the treatment of lethal human infections.

Table 1 Phytochemical screening of different Bay leaf extracts

Tests Name	Results		
	Aqueous	Methanol	Acetone
Alkaloids	-	-	+
Cardiac Glycosides	+	+	-
Saponins	+	-	-
Tannins	+	+	+
Steroids	+	-	+
Carbohydrates	+	+	-
Proteins	-	+	-
Phenolic compounds	-	-	-
Terpenoids	-	-	-
Flavanoids	+	+	+

### 3.2 Antibacterial Activity of bay leaf in different solvents

Antibacterial activities of bay leaf (*C. tamala*) in different solvents (acetone, aqueous, and methanol) were tested against selected pathogenic bacteria and their zones of inhibition were analyzed (Table 2). All the leaf extracts of *C. tamala* showed significant ( $p < 0.01$ ) bactericidal potential against both gram-positive (*B. subtilis*

Table 2A Antibacterial activity of aqueous bay leaf extracts against pathogens

S. N.	Name of Bacteria	Leaf Extract Concentrations				Control +VE	Control -VE
		25 mg/ml	50 mg/ml	75 mg/ml	100 mg/ml	Erythromycin	D.W.
		Zone of inhibition (in cm)					
1.	<i>E. coli</i>	-	0.7±0.2	1.1±0.1	1.6±0.2	3.0±0.1	-
2.	<i>Staphylococcus aureus</i>	-	0.6±0.2	0.9±0.2	1.0±0.1	2.1±0.1	-
3.	<i>Salmonella typhi</i>	-	0.5±0.1	0.6±0.2	0.8±0.2	2.2±0.1	-
4.	<i>Bacillus subtilis</i>	-	0.4±0.1	0.5±0.1	0.9±0.2	2.6±0.2	-

\*Statistical analysis using one way ANOVA/ DMRT revealed results to be significant ( $p < 0.01$ )

Table 2B Antibacterial activity of methanol bay leaf extracts against pathogens

S. N.	Name of Bacteria	Leaf Extract Concentrations				Control +VE	Control -VE
		25 mg/ml	50 mg/ml	75 mg/ml	100 mg/ml	Erythromycin	Methanol
		Zone of inhibition (in cm)					
1.	<i>E. coli</i>	0.5±0.1	0.9±0.2	1.0±0.1	1.1±0.1	1.6±0.2	-
2.	<i>Staphylococcus aureus</i>	0.5±0.1	0.6±0.2	0.6±0.2	0.7±0.2	1.6±0.2	-
3.	<i>Salmonella typhi</i>	-	0.5±0.1	0.7±0.2	1.0±0.1	3.0±0.1	-
4.	<i>Bacillus subtilis</i>	-	0.6±0.2	0.7±0.2	0.9±0.2	2.1±0.1	-

\*Statistical analysis using one way ANOVA/ DMRT revealed results to be significant ( $p < 0.01$ ).

Table 2C Antibacterial activity of acetone bay leaf extracts against pathogens

S. N.	Name of Bacteria	Leaf Extract Concentrations				Control +VE	Control -VE
		25 mg/ml	50 mg/ml	75 mg/ml	100 mg/ml	Erythromycin	Acetone
		Zone of inhibition (in cm)					
1.	<i>E. coli</i>	-	0.4±0.1	0.7±0.2	0.8±0.2	1.0±0.1	-
2.	<i>Staphylococcus aureus</i>	0.5±0.1	0.6±0.2	0.6±0.2	0.9±0.2	1.0±0.1	-
3.	<i>Salmonella typhi</i>	-	0.5±0.1	0.6±0.2	0.8±0.2	2.1±0.1	-
4.	<i>Bacillus subtilis</i>	0.4±0.1	0.5±0.1	0.5±0.1	0.7±0.2	1.9±0.2	-

\*Statistical analysis using one way ANOVA/ DMRT revealed results to be significant ( $p < 0.01$ )

(MTCC 2057), *S. aureus* (MTCC 3160) and gram-negative (*E. coli* (MTCC 294), *S. typhi* (MTCC 660) (Table 2A, 2B and 2C). A dose-dependent bactericidal activity was noticed in all the bay leaf extracts. From the results, it has been clear that the aqueous plant extract shows better inhibition against *E. coli* and *S. aureus*. This result was similar to those of other studies that reported antibacterial activity (Parekh and Chanda 2007; Hassan et al. 2016; Bharadwaj et al. 2020). The methanolic extract shows better inhibition against *E. coli* and *S. typhi*, the similar findings were observed by Parekh and Chanda (2007). Maximum activity was observed against *S. aureus* in acetone extract. These results are in agreement with the findings of Singh et al. (2018) and Dash et al. (2020). The antibacterial activities accessed were compared with that of standard broad-spectrum antibiotics tetracycline as positive control and water and DMSO (according to solvent) as a negative control.

### 3.3 Antibacterial Activity of bay leaf oil in different solvents

Antibacterial activity of bay leaf oil (*C. tamala*) was performed in different concentrations (50% and 100% v/v) against both gram-positive (*B. subtilis* MTCC 2057, *S. aureus* MTCC 3160) and gram-negative (*E. coli* MTCC 294, *S. typhi* MTCC 660) bacterial strains. All the bay leaf oil extracts showed significant ( $p < 0.01$ ) bactericidal potential (Table 3). From the results obtained it has been clear that there is a dose-dependent bactericidal activity. The maximum zone of inhibition was found at 100% (v/v) concentration against *S. aureus* in the volatile oil. These results are in agreement with various previous researchers (Parekh and Chanda 2007; Borkataky and Sood 2014; Hassan et al. 2016; Heer et al. 2017; Manandhar et al. 2019; Dash et al. 2020). The antibacterial activities performed were compared with that of standard broad-spectrum antibiotics as positive control and ethanol as negative control (Table 3).

Table 3 Antibacterial activity of Bay leaf oil against bacterial pathogens

S. N.	Name of Bacteria	Leaf Extract Concentrations		Control +VE	Control -VE
		50 mg/ml	100 mg/ml	Erythromycin	Ethanol
Zone of inhibition (in cm)					
1.	<i>E. coli</i>	0.7±0.2	0.8±0.2	2.0±0.1	-
2.	<i>Staphylococcus aureus</i>	0.6±0.2	0.9±0.2	2.1±0.1	-
3.	<i>Salmonella typhi</i>	0.6±0.2	0.8±0.2	1.5±0.1	-
4.	<i>Bacillus subtilis</i>	0.5±0.1	0.5±0.1	2.0±0.1	-

\*Statistical analysis using one way ANOVA/ DMRT revealed results to be significant ( $p < 0.01$ ).

## Conclusion

The multiple benefits of *C. tamala* made it a true miracle of nature. From this study, it becomes clear that active phytochemicals were present in the various extracts of bay leaf powder and due to the presence of these phytochemicals, all three extracts showed significant antibacterial activity. The aqueous plant extract shows better inhibition against *E. coli* and *S. aureus* while Methanolic extract showed better inhibition against *E. coli* and *S. typhi*. Maximum activity was observed against *S. aureus* in acetone extract and volatile oil.

## Acknowledgment

The authors are thankful to the management of GLA University to carry out this work.

## References

Baker, C.N., Thornsberry, C., & Hawkinson, R.W. (1983). Inoculum standardization in antimicrobial susceptibility testing: evaluation of overnight agar cultures and the rapid inoculum standardization system. *Journal of Clinical Microbiology*, 17(3), 450-457.

Bharadwaj, A., Gupta, A., & Garg, G. (2020). Phytochemical and antibacterial potential of seed extract of *M. fragrance* with reference to its oil activity. *Plant Cell Biotechnology and Molecular Biology*, 21(45&46), 43-51.

Borkataky, M., & Sood, K. (2014). Antibacterial, antioxidant and cytotoxic activities of *Cinnamomum tamala* Nees. leaves. *International Journal of Medicine and Pharmaceutical Sciences*, 4(6):55-62.

Chakraborty, U., & Das, H. (2009). Antidiabetic and antioxidant activities of *Cinnamomum tamala* leaf extracts in stz-treated diabetic rats. *Global Journal of Biotechnology and Biochemistry*, 5, 12-18.

Chaurasia, J.K., Mishra, A., & Tripathi, Y.B. (2010). Immunomodulation property of hexane fraction of leaves of

*Cinnamomum tamala* Linn. in rats. *Cell Biochemistry and Function*, 28(6), 454-460.

Dash, S.S., Samanta, S., Dey, S., Giri, B., & Dash, S.K. (2020). Rapid green synthesis of biogenic silver nanoparticles using *Cinnamomum tamala* leaf extract and its potential antimicrobial application against clinically isolated multidrug-resistant bacterial strains. *Biological Trace Element Research*, 198, 681-696.

Dhulasavnt, V., Shinde, S., Pawar, M., & Naikwade, N.S. (2010). Antihyperlipidemic Activity of *Cinnamomum tamala* Nees. on high cholesterol diet induced hyperlipidemia. *International Journal of PharmTech Research*, 2, 2517-2521.

Dubey, N.K., Yadav, P., & Joshi, V.K. (1998). Screening of some essential oils against dermatophytes. *Philippine Journal of Science*, 127, 139-147.

Duke, J.A., & Fulton, M. (2002). CRC Handbook of Medicinal Herbs, Second ed., CRC Press, Boca Raton, Florida.

Eswaran, M.B., Surendran, S., Vijayakumar, M., Ojha, S.K., Rawat, A.K.S., & Rao, C.V. (2010). Gastroprotective activity of *Cinnamomum tamala* leaves on experimental gastric ulcers in rats. *Journal of Ethnopharmacology*, 128, 537-540.

Gambhire, M.N., Juvekar, A.R., & Wankhede, S.S. (2009). Anti-inflammatory activity of aqueous extract of *Cinnamomum tamala* leaves by in vivo and in vitro methods. *Journal of Pharmaceutical Research*, 2(9), 1521-1524.

Gill, S., Bahuguna, P.P., & Kharkwal, H. (2015). Phytochemical investigation of high altitude medicinal plants *Cinnamomum tamala* (Buch-Ham) Nees and Eberm and *Rhododendron arboretum* Smith. *American Journal of Phytomedicine and Clinical Therapeutics*, 3(6), 512-528.

Goyal, P., Chauhan, A., & Kaushik, P. (2009). Laboratory evaluation of crude extracts of *Cinnamomum tamala* for potential antibacterial activity. *Electronic Journal of Biology*, 5(4), 75-79.



- Hassan, W., Syeda, N.Z., Kazmi, N., Noreen, H., Riaz, A., & Zaman, B. (2016). Antimicrobial activity of *Cinnamomum tamala* leaves. *Journal of Nutritional Therapeutics*, 6(2):1-5.
- Heer, A., Guleria, S., & Razdan, V.K. (2017). Chemical composition, antioxidant and antimicrobial activities and characterization of bioactive compounds from essential oil of *Cinnamomum tamala* grown in north-western Himalaya. *Journal of Plant Biochemistry and Biotechnology*, 26, 191-198.
- Kirtikar, K.R. & Basu, B.D. (1981) Indian Medicinal Plants. Vol. 2, International Book Distribution, Dehradun.
- Mall, D., Gharde, S.K. & Chatterjee, R. (2018). Chemical Constituent of *Cinnamomum tamala*: An Important Tree Spices. *International Journal of Current Microbiology and Applied Sciences*, 7(4), 648-651.
- Manandhar, S., Luitel, S., Dahal, R.K. (2019). In vitro antimicrobial activity of some medicinal plants against human pathogenic bacteria. *Journal of Tropical Medicine*, doi: 10.1155/2019/1895340.
- Nadkarni, K.M. (1976). *Indian Materia Medica*. Popular Prakashan, Bombay.
- Parekh, J., & Chanda, S. (2007). In vitro screening of antibacterial activity of aqueous and alcoholic extracts of various Indian plant species against selected pathogens from *Enterobacteriaceae*. *African Journal of Microbiology Research*, 1(6), 92-99.
- Rao, C.V., Vijayakumar, M., Sairam, K., & Kumar, V. (2008). Antidiarrhoeal activity of the standardised extract of *Cinnamomum tamala* in experimental rats. *Journal of Natural Medicines*, 62, 396-402.
- Saluja, M.S., Sangameswaran, B., Sharma, A., & Dubey, C. (2010). Phytochemical study and in-vitro cytotoxic activity of *Cinnamomum tamala* Linn. against Ehrlich Ascites Carcinoma (EAC) and Dalton's Ascitic Lymphoma (DAL) Cell Lines. *Research Journal of Pharmacognosy and Phytochemistry*, 2(1): 37-40.
- Sharma, G., Nautiyal, B.P., & Nautiyal, A.R. (2009). Seedling emergence and survival in *Cinnamomum tamala* under varying micro-habitat conditions: conservation implications. *Tropical Ecology* 50(1):201-209.
- Showkat, R.M., Sanjrani, M.A., & Kapoor, R. (2004). Chemical composition of essential oil of *Cinnamomum tamala* Nees et Eberm. Leaves. *Flavour and Fragrance Journal*, 19, 112-114.
- Shu, Y.Z. (1998). Recent natural products based drug development: A pharmaceutical industry perspective. *Journal of Natural Products*, 61, 1053-1071
- Singh, V., Bharadwaj, A., Wahi, N., & Tripathi, V.L. (2018). Phytochemical Analysis and In-vitro antimicrobial activities of analysis of *Terminalia arjuna* leaf, bark and fruit extracts in different solvents. *Current Trends in Biotechnology and Pharmacy*, 12(3), 284-292.



# Journal of Experimental Biology and Agricultural Sciences

<http://www.jebas.org>

ISSN No. 2320 – 8694

## In silico targeting of osmoporin protein of *Salmonella* to identify anti-Salmonellosis phyto-compounds

Hardeep Singh Tuli<sup>1,\*</sup>, Vivek Kumar Garg<sup>2</sup>, Deepika Kapoor<sup>2</sup>, Poonam Bansal<sup>1</sup>, Pawan Kumar<sup>3</sup>, Ranjan K. Mohapatra<sup>4</sup>, Kuldeep Dhama<sup>5</sup>, Amit Vashishth<sup>6</sup>, Prachi Seth<sup>7</sup>, Gurpreet Kaur Bhatia<sup>8</sup>

<sup>1</sup>Department of Biotechnology, Maharishi Markandeshwar (Deemed to be University), Mullana, India

<sup>2</sup>Department of Medical Laboratory Technology, University Institute of Applied Health Sciences, Chandigarh University, Gharuan, Mohali 140413, Punjab, India

<sup>3</sup>Institute of Plant Sciences, Agricultural Research Organisations, RishonLeZion, Israel

<sup>4</sup>Department of Chemistry, Government College of Engineering, Keonjhar-758002, Odisha, India

<sup>5</sup>Division of Pathology, ICAR-Indian Veterinary Research Institute, Izatnagar, Bareilly-243 122, Uttar Pradesh, India

<sup>6</sup>Department of Biotechnology & Microbiology, MIET, Meerut, 250005, Uttar Pradesh, India

<sup>7</sup>Department of Applied Science and Humanities, JMIT, Radaur, India

<sup>8</sup>Department of Physics, Maharishi Markandeshwar (Deemed to be University), Mullana, India

Received – March 13, 2022; Revision – April 15, 2022; Accepted – April 27, 2022

Available Online – April 30, 2022

DOI: [http://dx.doi.org/10.18006/2022.10\(2\).423.429](http://dx.doi.org/10.18006/2022.10(2).423.429)

### KEYWORDS

Molecular docking

Receptor

Phyto-compounds

Ellagic acid

Eriodictyol

Naringenin

Osmoporin

*Salmonella*

### ABSTRACT

*Salmonella enterica* serotype *typhi* is a gram-negative, rod-shaped bacterium, and has flagella with the human body as its only reservoir. Typhoid fever was found to cause 21.7 million illnesses and 216,000 fatalities worldwide in 2000, and the International Vaccine Institute estimated 11.9 million cases and 129,000 deaths in low- and middle-income countries in 2010. More than 10 million patients were infected with *S. typhi* each year and the mortality rate is associated with more than 0.1 million patients. Moreover, it is also associated with drug resistance globally which makes the disease more dreadful. Other than antibiotics, various flavonoids showed medicinal effects against many diseases including *S. typhi* infection. Flavonoids are a type of plant bioactive metabolite that have potential medicinal efficacy. The goal of this study was to see if certain flavonoids (ellagic acid, eriodictyol, and naringenin) could interact with the outer membrane of osmoporin (PDB ID: 3uu2) receptor in *Salmonella* and helps in inhibiting its growth. To look for probable ligand-receptor binding relationships, we used Pyrxmolecular docking software. The molecular docking results were analyzed using the Biovia discovery studio visualizer. The current study discovered that selected plant-based compounds interacted with an outer membrane of the osmoporin receptor, resulting in minimization of energy in the range of -6.6 to -7.8 Kcal/mol.

\* Corresponding author

E-mail: [hardeep.biotech@gmail.com](mailto:hardeep.biotech@gmail.com) (Hardeep Singh Tuli)

Peer review under responsibility of Journal of Experimental Biology and Agricultural Sciences.

Production and Hosting by Horizon Publisher India [HPI]  
 (<http://www.horizonpublisherindia.in/>).  
 All rights reserved.

All the articles published by [Journal of Experimental Biology and Agricultural Sciences](#) are licensed under a [Creative Commons Attribution-NonCommercial 4.0 International License](#) Based on a work at [www.jebas.org](http://www.jebas.org).



## 1 Introduction

*Salmonella enterica* serotype typhi is a gram-negative, rod-shaped bacterium, and has flagella with the human body as its only reservoir (Mahmud et al. 2008). Typhoid fever was found to cause 21.7 million illnesses and 216,000 fatalities worldwide in 2000, and the International Vaccine Institute estimated 11.9 million cases and 129,000 deaths in low and middle-income countries in 2010 (Crump et al. 2004). More than 10 million patients were infected with *S. typhi* each year and the mortality rate is associated with more than 0.1 million patients (Stanaway et al. 2019). Moreover, it is also associated with drug resistance globally which makes the disease more dreadful. Typhoid fever is primarily a travel-related disease in developed countries, affecting travelers such as tourists, temporary workers, military personnel, or travelers visiting friends or relatives (VFR) in endemic areas, with risk varying depending on the geographical region visited, period of travel, integration with local cultures, and traveler concurrent diseases or medications (Masuet-Aumatell and Atouguia 2021). In 2018, an outbreak occurred in Pakistan and the patients became resistant to various generation antibiotics like ampicillin, chloramphenicol, fluoroquinolones, trimethoprim-sulfamethoxazole, and even the third-generation antibiotic cephalosporins (Klemm et al. 2018). Serologically, the bacterium is positive for the lipopolysaccharide antigens O9 and O12, and Vi, a polysaccharide capsular antigen. The effectiveness of the parenteral Vi vaccination in young children has lately been proved, as has the protection of Vi vaccines' unprotected neighbors (Crump et al. 2015; Parry et al. 2002). Vi-rEPA, the first Vi conjugate vaccination to reach clinical trials, has been demonstrated to be immunogenic as well as safe in Vietnamese children from 2 to 5 years of age range, with a 91.5 percent protective efficacy and an estimated 89 percent cumulative efficacy after 3.8 years (Lin et al. 2000). Other than humans, *Salmonella* species like *S. typhimurium*, *S. dublino*, *S. newport*, *S. hindmarsh*, *S. derby*, *S. agona*, *S. gallinarum*, etc., also cause many diseases in cattle's, sheep, goats, pigs, horses, and poultry (Lewis et al. 2019). Osmoporin (ompC) is a protein found in *Salmonella* and is responsible for the bacteria's survival and pathogenicity, as well as for diffusing hydrophilic chemicals (Valero-Pacheco et al. 2020).

Phytochemicals have recently emerged as one of the most hopeful holistic alternative methods with few adverse effects (Alsheikh et al. 2020; Tiwari et al. 2018). The antibacterial activity of bioactive phytochemicals and essential oils against *Salmonella* spp. was discovered a very long time before (Osaili et al. 2021). The expense of screening compounds with potential bioactivity is high, and it might take a long period. However, computer-aided drug design (CADD) could save time and money by reducing the cost of molecule synthesis, thereby lowering research costs (Abdullahi and Adeniji 2020). One such CADD technology is *in-silico* molecular

docking, which can essentially predict binding efficacy as well as structure-based drug design (Abdullahi and Adeniji 2020). Furthermore, molecular docking provides valuable insights into structure-activity relationships, mode of activity, and further analysis of protein-ligand interactions. Such research would lead to the creation of innovative therapeutic compounds against pathogenic infections at a faster rate. Furthermore, the molecule's physicochemical properties would provide crucial information during the early stages of therapeutic development (Abdullahi and Adeniji 2020; Abdullahi et al. 2020). Recently a study conducted by Abishad et al. (2021) concluded that *in-silico* molecular docking studies were helpful in understanding the interaction of phytochemical ligands of thymol, carvacrol, and cinnamaldehyde with pathogen protein motifs and inhibit the growth of *S. typhi* bacteria (Abishad et al. 2021) and *E.coli* (Abishad et al. 2021; Osaili et al. 2021). The present study was conducted to propose the possible molecular interactions of selected phytochemicals with microbial osmoporin receptors to tackle salmonellosis.

## 2 Material and Method

### 2.1 Preparation of Receptor structure

Receptor three-dimensional structure with PDB ID: 3UU2 with a resolution of 3.59 Å was downloaded from Research Collaboratory for Structural Bioinformatics, Protein Data Bank (RCSB-PDB), an online database (Figure 1). Heteroatoms and water molecules were excluded from protein structure.

### 2.2 Preparation of ligands and analysis of ADME properties

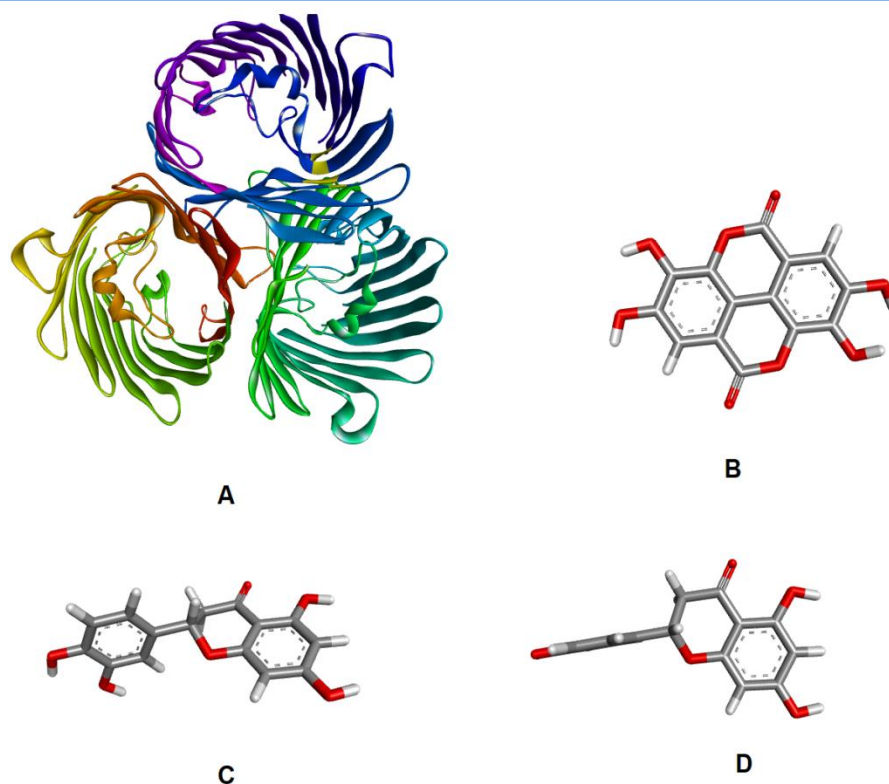
Three ligands were selected for molecular docking. 3-D structures of ligands were downloaded from the PubChem database in sdf format and were converted into pdb format by OpenBabel (Figure 1). ADME (Unfavorable absorption, distribution, metabolism, and elimination), an online software tool was used for profiling all the ligands (pH 7) (Jayaram et al. 2012). Physicochemical properties of ligand include Lipinski's rule of five (molar refractivity, molecular weight (<500 Da), H-bond acceptor (<10), H-bond donar (5), LogP (<5), and drug likeliness) were considered (Lipinski 2004) (Figure 1).

### 2.3 Molecular docking of ligands

PyRx v0.8 was used for molecular docking studies. Docked structures with high binding affinity were analyzed using PyMOL and Discovery Studio Visualizer.

## 3 Results and Discussion

In recent years, emergences of drug-resistant microbial strains are considered to be a serious problem and existing challenge for their treatment. Currently, it has been seen that patients are taking self-



S.No.	Ligands	ADME Properties (Lipinski's Rule of Five)		Drug Likelimes
		Properties	Values	
1.	Naringenin	Molecular weight (<500 Da)	272	Yes
		LogP (<5)	2.5	
		H-bond donar (5)	3	
		H-bond acceptor (<10)	5	
		Molar Refractivity	70.19	
2.	Ellagic acid	Molecular weight (<500 Da)	302	Yes
		LogP (<5)	1.2	
		H-bond donar (5)	4	
		H-bond acceptor (<10)	8	
		Molar Refractivity	68.4	
3.	Eriodictyol	Molecular weight (<500 Da)	288	Yes
		LogP (<5)	2.2	
		H-bond donar (5)	4	
		H-bond acceptor (<10)	6	
		Molar Refractivity	71.8	

## E

Figure 1 3D view of the protein (A), 3-D structure of Naringenin (B), Ellagic acid (C), Eriodictyol (D), and ADME properties of ligands (E).

medication at a higher dose than normally required which results in the development of drug resistance. Literature suggested that *Salmonella* is developing multi-drug resistance against a diverse range of sophisticated medicine including ciprofloxacin and ampicillin (Ge et al. 2022; Chen et al. 2022). Results of previous investigations have shown that medicinal plant's metabolites and their extract possessed potential toxicity against drug-resistant

microbial strains. For instance, Naz et al. (2022) investigated anti-*Salmonella enterica* potential of various plant extracts including *Amaranthus hybridus* leaf > *Aloe barbadensis* leaf > *Adhatoda vasica* leaf, etc (Naz et al. 2022). Similarly, Yang et al. (2022), explored anti *Bacillus subtilis* and anti-*Salmonella typhi* ethyl acetate plant extract with MIC values in the range of 0.78 mg/mL (Yang et al. 2022). Recent data showed that more than 80% of

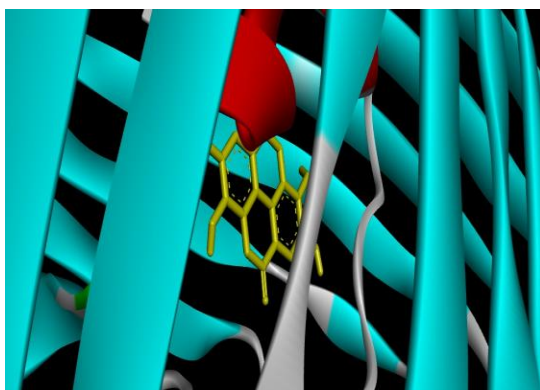


Figure 2 Binding of osmoporin and Ellagic acid. Best binding mode in the pocket of osmoporin and interacting amino acid of the target with a ligand.

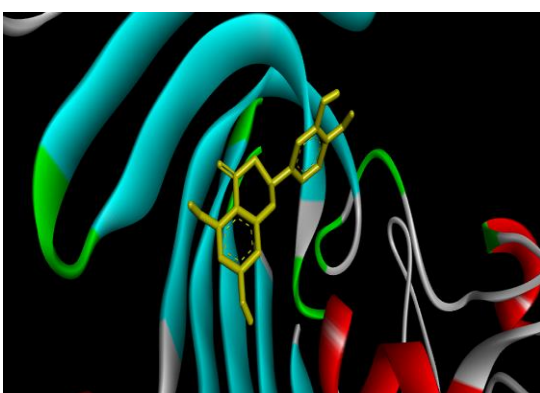
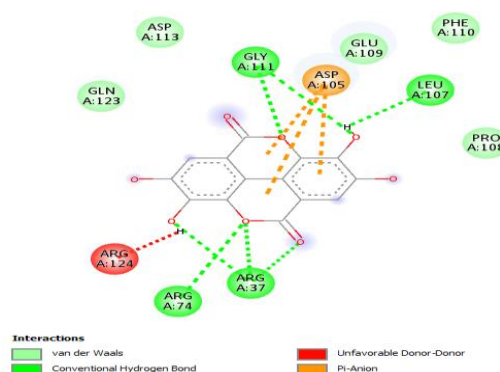


Figure 3 Interactions of osmoporin and Eriodictyol. Best binding mode in the pocket of osmoporin and interacting amino acid of a target with ligand

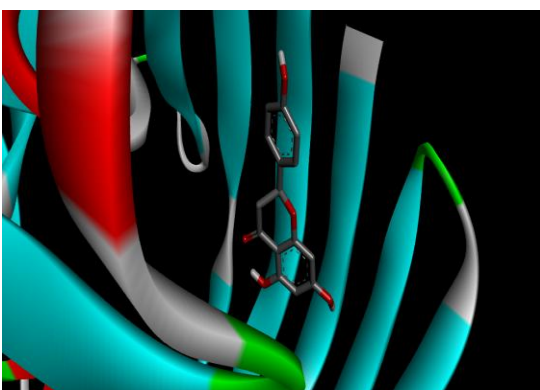
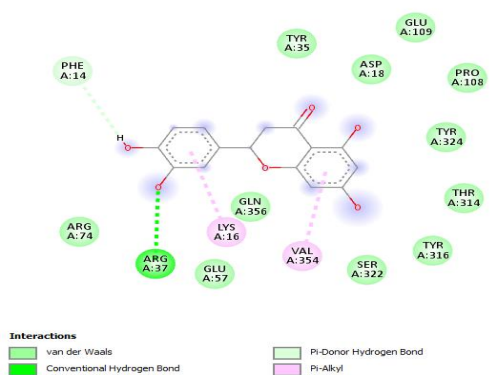
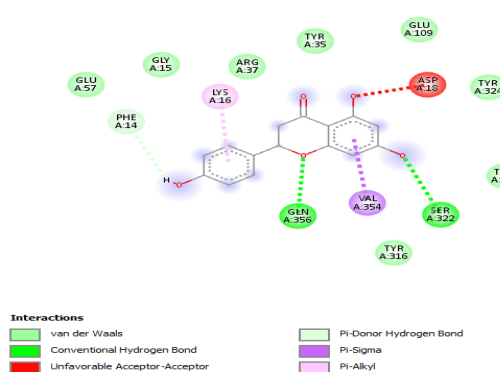


Figure 4 Binding of osmoporin and Naringenin. Best binding mode in the pocket of osmoporin and interacting amino acid of a target with ligand



drugs used globally either have plant-based chemical structures or derivatives (Mahmud et al. 2008). In comparison to previous laborious drug discovery methods, computational-based drug discovery approaches are gaining importance. In this method, best-suited interactions between drugs and receptors are calculated based on their binding efficacy. Minimum binding energies between drugs and receptors are considered to be best for drug discovery (Tuli et al. 2021; Tuli et al. 2022). As per the literature,

minimum energies correspond to the maximum stability of the complex. Therefore, computational studies are considered to be important to screen out active drug moieties from various drug libraries. Results of the present study described that ellagic acid, eriodictyol, and naringenin interact with the osmoporin receptor (PDB ID: 3uu2) protein of *Salmonella* in the range of -6.6 to -7.8 Kcal/mol (Figure 2, 3 & 4). The selected ligands interacted with various amino acids of osmoporin receptor protein including GLY

Table 1 Binding affinity and RMSD value of Ellagic acid

Ligand	Binding Affinity	rmsd/ub	rmsd/lb
ellagic acid	-7.8	0	0
ellagic acid	-7.8	6.183	0.041
ellagic acid	-7.6	12.08	10.001
ellagic acid	-7.5	11.397	9.98
ellagic acid	-7.4	12.16	10.316
ellagic acid	-7.4	16.143	14.334
ellagic acid	-7.4	4.225	2.183
ellagic acid	-7.3	16.176	14.515
ellagic acid	-7.3	4.601	2.812

Table 2 Binding affinity and RMSD value of Eriodictyol

Ligand	Binding Affinity	rmsd/ub	rmsd/lb
eriodictyol	-7.2	0	0
eriodictyol	-7.1	13.608	10.507
eriodictyol	-7.1	6.662	4.21
eriodictyol	-7	18.534	14.143
eriodictyol	-6.9	11.359	8.849
eriodictyol	-6.9	11.008	9.141
eriodictyol	-6.9	12.993	11.341
eriodictyol	-6.9	11.758	9.48
eriodictyol	-6.8	18.456	14.358

111, ASP 105, LEU 107, ARG 124, GLN 356, LYS 16, VAL 354, ASP 18, and SER 122. Further, the interactions with amino acid residue and distance between the amino acid and the ligand pole (Å) of selected ligands i.e., ellagic acid, eriodictyol, and naringenin are provided in Tables 1, 2 & 3 against docked osmoporin receptor protein. The docked pose of ligand and osmoporin receptor protein receptor has been shown in Figure 2, 3 & 4.

Table 3 Binding affinity and RMSD value of Naringenin

Ligand	Binding Affinity	rmsd/ub	rmsd/lb
naringenin	-6.8	0	0
naringenin	-6.8	15.549	11.673
naringenin	-6.7	17.727	14.426
naringenin	-6.7	14.037	12.004
naringenin	-6.7	6.422	4.001
naringenin	-6.7	18.755	14.659
naringenin	-6.6	18.697	14.946
naringenin	-6.6	13.4	11.023
naringenin	-6.6	29.285	27.715

Previous studies have suggested the promising role of phytochemicals to modulate cellular signaling to combat dreadful diseases. It has been observed that several bioactive phytochemicals that are present in our diet possess a diverse range of therapeutic properties (Gupta et al. 2022; Aggarwal et al. 2022). Researchers are in progress to suggest diet associated modifications to fight infectious diseases. In addition, computational drug designing methods can play an important role to screen out the biological efficacy of plant metabolites with recognized cellular targets. As the spanning of dreadful diseases is increasing day by day, and discovery of novel therapeutic agents are not increasing at the same pace. Therefore, the utilities of computational drug discovery methods may not only speed up the

conventional approaches but also enhance the success rate of novel therapeutic findings (Tuli et al. 2022). In the present study, we investigated the binding interactions of plant-based therapeutics with the osmoporin receptor of *Salmonella*. The results of our findings are in good agreement with previous reports. For instance, Abishad et al. (2021) investigated binding free energy for carvacrol, cinnamaldehyde, and thymol in the range of - 5.65 to - 4.97 kcal/mol against osmoporin receptor protein (Abishad et al. 2021). In another study, researchers explored the utility of 20 phytochemicals to interact with pathogenic microbial receptor (Mur B) protein to inhibit the growth of multi-drug resistance *Vibrio cholera* (Ragunathan et al. 2018).

## Conclusion

Salmonellosis is considered to be an emerging microbial infection towards human and animal health. The results of the current study explored molecular docking interactions between ligands (ellagic acid, eriodictyol, and naringenin) and the osmoporin receptor protein of *Salmonella*. In the present investigation, molecular interactions between pathogenic microbial receptors and selected phytochemicals were found in the range of -6.6 to -7.8 Kcal/mol. Therefore, plant-based metabolites can be investigated in near future to design novel anti salmonellosis agents.

## References

- Abdullahi, M. & Adeniji, S.E. (2020). In-silico Molecular Docking and ADME/Pharmacokinetic Prediction Studies of Some Novel Carboxamide Derivatives as Anti-tubercular Agents. *Chemistry Africa*, 3(4), 989–1000.
- Abdullahi, M., Shallangwa, G.A. & Uzairu, A. (2020). In silico QSAR and molecular docking simulation of some novel aryl sulfonamide derivatives as inhibitors of H5N1 influenza A virus subtype. *Beni-Suef University Journal of Basic and Applied Sciences*, 9(1), 1–12.

- Abishad, P., Niveditha, P., Unni, V., Vergis, J., et al. (2021). In silico molecular docking and in vitro antimicrobial efficacy of phytochemicals against multi-drug-resistant enteroaggregative *Escherichia coli* and non-typhoidal *Salmonella* spp. *Gut Pathogens*, 13(1), 46.
- Aggarwal, V., Tuli, H.S., Tania, M., Srivastava, S., et al. (2022). Molecular mechanisms of action of epigallocatechin gallate in cancer: Recent trends and advancement. *Seminars in Cancer Biology*, 80, 256–275.
- Alsheikh, H.M., Al-Sultan, I., Kumar, V., Rather, I.A., et al. (2020). Plant-Based Phytochemicals as Possible Alternative to Antibiotics in Combating Bacterial Drug Resistance. *Antibiotics (Basel, Switzerland)*, 9(8), 1–23.
- Chen, K., Gao, Y., Li, L., Zhang, W., et al. (2022). Increased Drug Resistance and Biofilm Formation Ability in ST34-Type *Salmonella typhimurium* Exhibiting Multicellular Behavior in China. *Frontiers in Microbiology*, 13, 1–8.
- Crump, J.A., Luby, S.P. & Mintz, E.D. (2004). The global burden of typhoid fever. *Bulletin of the World Health Organization*, 82(5), 346–353.
- Crump, J.A., Sjölund-Karlsson, M., Gordon, M.A. & Parry, C.M. (2015). Epidemiology, clinical presentation, laboratory diagnosis, antimicrobial resistance, and antimicrobial management of invasive *Salmonella* infections. *Clinical Microbiology Reviews*, 28(4), 901–937.
- Ge, H., Wang, Y. & Zhao, X. (2022). Research on the drug resistance mechanism of foodborne pathogens. *Microbial pathogenesis*, 162, 105306.
- Gupta, S., Buttar, H.S., Kaur, G. & Tuli, H.S. (2022). Baicalein: promising therapeutic applications with special reference to published patents. *Pharmaceutical Patent Analyst*, 11(1), 23–32.
- Jayaram, B., Singh, T., Mukherjee, G., Mathur, A., Shekhar, S. & Shekhar, V. (2012). Sanjeevini: a freely accessible web-server for target directed lead molecule discovery. *BMC Bioinformatics*, 13 (Suppl 17), S7.
- Klemm, E.J., Shakoor, S., Page, A.J., Qamar, F.N., et al. (2018). Emergence of an extensively drug-resistant *Salmonella enterica* serovar typhi clone harboring a promiscuous plasmid encoding resistance to fluoroquinolones and third-generation cephalosporins. *mBio*, 9(1), e00105-18.
- Lewis, A.M., Melendrez, M.C. & Fink, R.C. (2019). Salmonella', in *Food Microbiology: Fundamentals and Frontiers*, [Online]. StatPearls Publishing, pp. 225–262.
- Lin, F.Y.C., Ho, V.A., Bay, P. V., Thuy, N.T.T., Bryla, D., Thanh, T.C., Khiem, H.B., Trach, D.D. & Robbins, J.B. (2000). The epidemiology of typhoid fever in the Dong Thap Province, Mekong Delta region of Vietnam. *American Journal of Tropical Medicine and Hygiene*, 62(5), 644–648.
- Lipinski, C.A. (2004). Lead- and drug-like compounds: the rule-of-five revolution. *Drug Discovery Today Technologies*, 1(4), 337–341.
- Mahmud, A.K., Chowdhury, A.J., Sarker, Z.M., Miah, R.A., Saleh, A.A., Mandal, R.M. & Dhakal, G.P. (2008a). Typhoid Fever. *Mymensingh Medical Journal*, 17 (2), 236–244.
- Masuet-Aumatell, C. & Atouguia, J. (2021). Typhoid fever infection – Antibiotic resistance and vaccination strategies: A narrative review. *Travel Medicine and Infectious Disease*, 40, 101946.
- Naz, S., Alam, S., Ahmed, W., Masaud Khan, S., et al. (2022). Therapeutic Potential of Selected Medicinal Plant Extracts against Multi-Drug Resistant *Salmonella enterica* serovar Typhi. *Saudi Journal of Biological Sciences*, 29(2), 941–954.
- Osaili, T.M., Hasan, F., Dhanasekaran, D.K., Obaid, R.S., et al. (2021). Effect of active essential oils added to chicken tawook on the behaviour of *Listeria monocytogenes*, *Salmonella* spp. and *Escherichia coli* O157:H7 during storage. *International Journal of Food Microbiology*, 337, 108947.
- Parry, C.M., Hien, T.T., Dougan, G., White, N.J. & Farrar, J.J. (2002). Typhoid fever. *The New England Journal of Medicine*, 347(22), 1770–1782.
- Ragunathan, A., Malathi, K. & Anbarasu, A. (2018). MurB as a target in an alternative approach to tackle the *Vibrio cholerae* resistance using molecular docking and simulation study. *Journal of Cellular Biochemistry*, 119(2), 1726–1732.
- Stanaway, J.D., Reiner, R.C., Blacker, B.F., Goldberg, E.M., et al. (2019). The global burden of typhoid and paratyphoid fevers: a systematic analysis for the Global Burden of Disease Study 2017. *The Lancet Infectious Diseases*, 19(4), 369–381.
- Tiwari, R., Latheef, S.K., Ahmed, I., Iqbal, H.M.N., Bule, M.H., Dhama, K., Samad, H.A., Karthik, K., Alagawany, M., El-Hack, M.E.A., Yattoo, M.I., Farag, M.R. (2018). Herbal Immunomodulators - A Remedial Panacea for Designing and Developing Effective Drugs and Medicines: Current Scenario and Future Prospects. *Current Drug Metabolism*, 19(3), 264-301.
- Tuli, H., Sood, S., Pundir, A., Choudhary, D., et al. (2022). Molecular Docking studies of Apigenin, Kaempferol, and Quercetin as potential target against spike receptor protein of SARS COV. *Journal of Experimental Biology and Agricultural Sciences*, 10(1), 144–149.

- Tuli, H.S., Abbas, Z., Kaur Bhatia, G., Shweta, Sharma, S., et al. (2021). In Silico Evaluation of Selected Flavonoids as Neuraminidase Inhibitors: Hope for the Discovery of Anti-Avian Influenza Virus Compounds. *Indian Veterinary Journal*, 98(5), 19–23.
- Valero-Pacheco, N., Blight, J., Aldapa-Vega, G., Kemlo, P., et al. (2020). Conservation of the OmpC Porin Among Typhoidal and Non-Typhoidal *Salmonella* Serovars. *Frontiers in Immunology*, 10, 2966.
- Yang, Z., Li, L., Chen, C.H., Zhang, Y.Y., et al. (2022). Chemical composition and antibacterial activity of 12 medicinal plant ethyl acetate extracts using LC–MS feature-based molecular networking. *Phytochemical Analysis*, 33(3), 473–489.





## Journal of Experimental Biology and Agricultural Sciences

<http://www.jebas.org>

ISSN No. 2320 – 8694

### Biodegradation of the Azo Dye Airedale Yellow CHD: Understanding using residuals

Vamshi Krishna Mukkera\*, Srivani Katuri

Department of Chemical Engineering, National Institute of Technology, Warangal-506004, Telangana, India

Received – February 01, 2022; Revision – March 20, 2022; Accepted – April 28, 2022

Available Online – April 30, 2022

DOI: [http://dx.doi.org/10.18006/2022.10\(2\).430.439](http://dx.doi.org/10.18006/2022.10(2).430.439)

#### KEYWORDS

Airedale Yellow CHD

Minitab

Biodegradation

Scatter

Residuals

#### ABSTRACT

Textile industries are heavy users of water and also produce lots of contaminated effluents. The main contaminants are azo dyes. Hence, the effluents are to be treated before leaving in the environment. In this study, the azo dye Airedale Yellow CHD was biodegraded using two bacteria *Thalassospira frigidophilosprofundus* (NCIM no 5438) and *Erwinia chrysanthemi Burkholder* (NCIM no 5213) in shaking conical flasks. Effect of Various parameters like pH, temperature, agitation, and concentration of dye solution on its decolorization was investigated. The biodegradation was statistically worked out using MINITAB software for the ANOVA. The residual plots along with the scatter plots for the decolorization of Airedale Yellow CHD using *T. frigidophilosprofundus* and *E. chrysanthemi Burkholder* are also obtained and included in this work. The maximum percent removal of the azo dye was obtained by using *T. frigidophilosprofundus* (77.41%) whereas it was reported at 74.64% by using *E. chrysanthemi Burkholder*. The obtained results formed a good fit according to the obtained normal residual plot which can conclude that the findings of the study are accurate and satisfactory.

\* Corresponding author

E-mail: [kvamshi93@gmail.com](mailto:kvamshi93@gmail.com) (Vamshi KrishnaMukkera)

Peer review under responsibility of Journal of Experimental Biology and Agricultural Sciences.

Production and Hosting by Horizon Publisher India [HPI]  
(<http://www.horizonpublisherindia.in/>).  
All rights reserved.

All the articles published by [Journal of Experimental Biology and Agricultural Sciences](#) are licensed under a [Creative Commons Attribution-NonCommercial 4.0 International License](#) Based on a work at [www.jebas.org](http://www.jebas.org).



## 1 Introduction

Less than one percent of the planet's water is available as clean water and can be used for drinking, but by 2050, its consumption is predicted to increase by more than 35%. Waterways such as lakes, waterways, and ponds, are amassed with rubbish, garbage, and pollutants (Melissa Denchak 2018). Textile industries utilized around  $2.8 \times 10^8$  kg of dyes per year across the world (Jin et al. 2007; Sen et al. 2016). The effluent from textile dyeing and fabric industries accounts for 15–25% of the total textile wastewater (Garg et al. 2020). The textile sector is a significant segment when it comes to the global budget. The textile business accounted for 8.54 percent of the global business and reported an increase in its value every year (World trade statistics 2019; World trade statistics 2020). Meanwhile, in 2020 global exports of textiles grew by 16 percent, driven by an increase in the production of personal protective equipment (PPE). Most types of manufactured goods saw significant gains in the second half of 2020, notably textiles, pharmaceuticals, computers, and telecommunications equipment (World trade statistics 2021). Textile demand is increasing every year, resulting in a huge volume of effluent being dumped into freshwater streams. According to Subramani (2020) from the mid-2000s through the end of 2019, the textiles division got 3.41 million dollars in FDI, whereas India's overall FDI was 456.79 million dollars. The textile division has a high amount of FDI as compared to other divisions. Small textile factories with high manufacturing costs can be found in India. Due to a change in the MSME (Ministry of Micro, Small and Medium Enterprises) scenario, a substantial number of textile exporters will now be classified as MSME and get a 5% interest equalization rebate (Subramani 2020). This will increase the competitiveness of Indian

textile products on the global market, boosting India's textile exports and, in turn, employment creation which results in an increase in textile production. Water is also utilized in industries to make a variety of products, with a significant concentration in the textile industry. These businesses produce a huge volume of polluted (mostly Azo dye-adulterated) water. Azo dyes fall under the category of organic molecules consisting of -N=N- (azo group). Because of the presence of the azo group, they are electron deficient genotoxic substances and are water soluble. Further, these azo dyes are most likely to be absorbed into the bodies of living creatures by inhalation, swallowing, or skin contact. Azo dye polluted wastewater discharge from the textile industries into water bodies without significant treatment or removal, and it harms the aquatic living beings (Hassan and Carr 2018; Bharathiraja et al. 2019).

The azo dye's physical structure has an azo link, which allows various groups such as methyl (-CH<sub>3</sub>), chloro (-Cl), nitro (-NO<sub>2</sub>), hydroxyl (-OH), amino (-NH<sub>2</sub>), and carboxyl (-COOH) to be substituted for the phenyl groups to produce a broad range of azo dyes that are electron acceptors (Saratale et al. 2011). Further, when visible light rays strike the azo dyes, they absorb them (Chang et al. 2000). Moreover, the mixing of these azo dyes in water bodies increases the BOD, COD, and TOC of the water bodies (Saratale et al. 2011). Many researchers have been motivated to create more effective wastewater treatment technologies as a result of the rigorous laws demanding the remediation of effluents before they are discharged into the environment. Many techniques for the treatment of wastewater like physical, chemical, and biological methods are available (Figure 1).

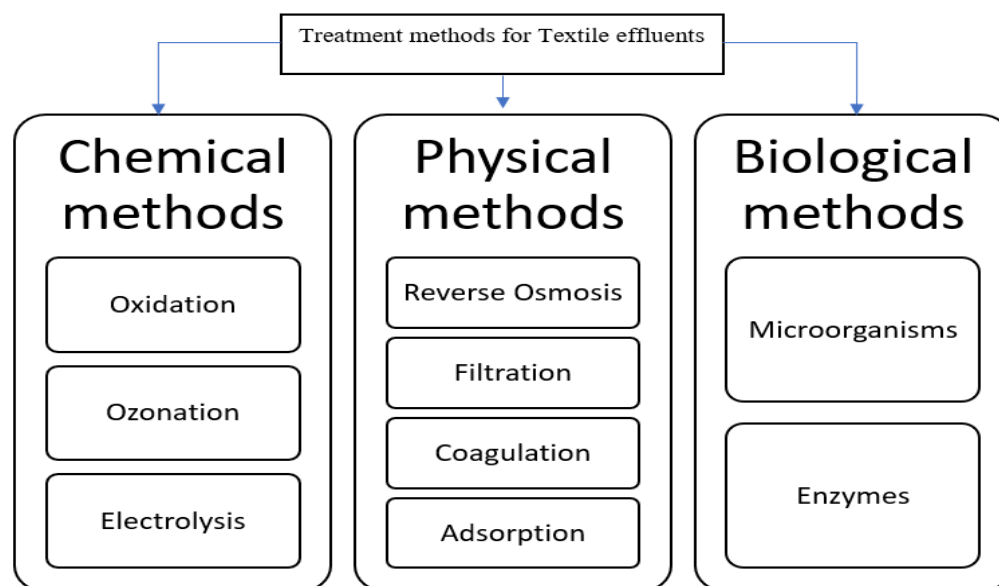


Figure 1 Various methods of treatment of Textile effluents.

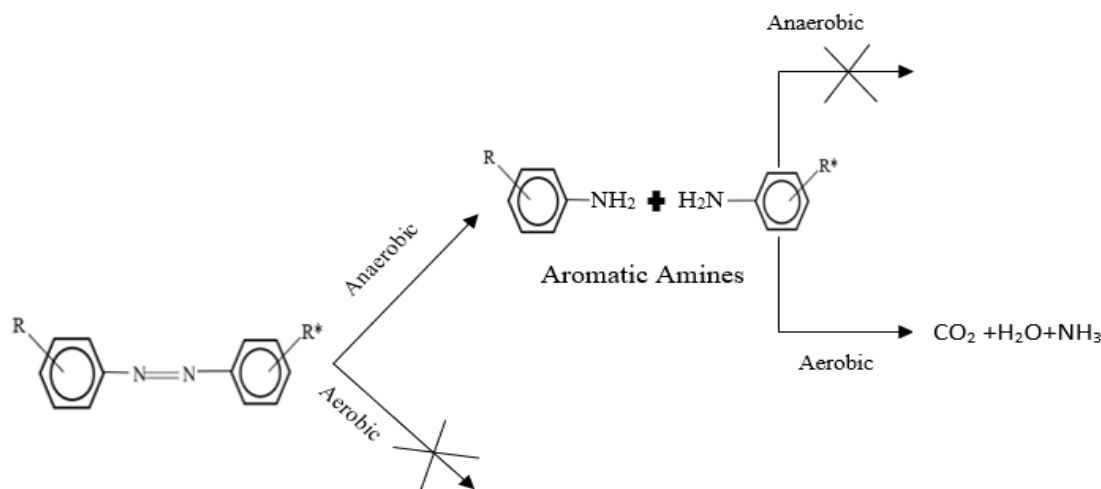


Figure 2 Common outline of the breakage of azo bonds

Various membranes can be used in industry to decolorize and lower the values of parameters like COD, BOD, color, etc (Dos Santos et al. 2007). However, their use has some drawbacks such as expensive investment, membrane fouling, and additional sludge production (Dos Santos et al. 2007). Like this, chemical decolorization techniques have also several drawbacks, including increased operating costs and difficulties scaling up processes to an industrial scale (Atalay and Ersöz 2016). As a result, biological methods for treating azo dyeing effluents can be utilized. The bioremediation process utilizes microorganisms such as fungi and bacteria to remove or modify pollutants (Varjani et al. 2020; Jain et al. 2022). Although dyes are difficult to degrade, but biological methods are used to complete the process and provide other benefits such as ecologically friendly end products, lower costs, reduced sludge, and nontoxic end products (Rai et al. 2005).

There would be no effect on azodye degradation if aerobic conditions were employed for metabolism in biodegradation. Generally, the breakage of azo bonds follows two phases (Figure 2). The initial phase should be anaerobic, which breaks the azo link and produces aromatic amines, which are carcinogenic and harmful to both flora and animals. In the second phase of biodegradation, aerobic conditions are utilized to convert the aromatic amines into carbon dioxide, water, and other by-products (Van der zee and Villaverde 2005). As a result, utilizing microbes to break down azo dyes may require a combination of anaerobic and aerobic conditions.

Bacteria are required since they can break down a wide range of dyes and have a high level of adaptability to changing environmental circumstances (Dos Santos et al. 2007). Because bacteria are ecologically favorable, several researchers employed them for biodegradation (Saratale et al. 2011). These bacteria can break down a wide range of dyes and have a high level of

adaptability to changing environmental circumstances (Dos Santos et al. 2007). This can be the reason why a lot of work involved bacteria but not fungi which may have a long development period and will be a restriction to growing by nitrogen gas (Stolz 2001).

There is very limited information available related to the biodegradation of Airedale yellow CHD (Hema and Suresha 2014). In the current study, an attempt has been taken for the biodegradation of Azo dye Airedale Yellow CHD with the help of two bacterial species i.e. *Thalassospira frigidiphilosophundus* and *Erwinia chrysanthemi Burkholder*. The novelty involved here is the utilization of the selected bacterial strains which were never used anytime for the bio decolorization of dye contaminated wastewater. The goal of this study was to examine the quantity of the dye biodegradation using two distinct microorganisms and to understand the biodegradation of dye using residual plots. The residual plots along with the scatter plots of the decolorization are obtained and included in this work.

## 2 Materials and Methods

### 2.1 Airedale Yellow CHD

The dye Airedale Yellow CHD is also known as Cotton Yellow CH, Chrysophenine, Chrysophenine GX with an empirical formula  $C_{30}H_{26}N_4Na_2O_8S_2$ , and a molecular weight of 680.66 is taken for the study. It's a red-light yellow powder that belongs to the double azo class and is used for dyeing cellulose fiber, cotton, viscose fabric painting, silk, wool, PVA, polyamide fiber, leather, paper, biological shading (World Dye variety 2012). According to the International Union of Pure and Applied Chemistry, it is sodium, 5-[(4-ethoxyphenyl)diazenyl]-2-[(E)-2-[4-[(4-ethoxyphenyl)diazenyl]-2-sulfophenyl]ethenyl]benzenesulfonic acid. It is commonly accepted since it has high purity, high effectiveness, accurate composition, and longer shelf life (Figure 3).

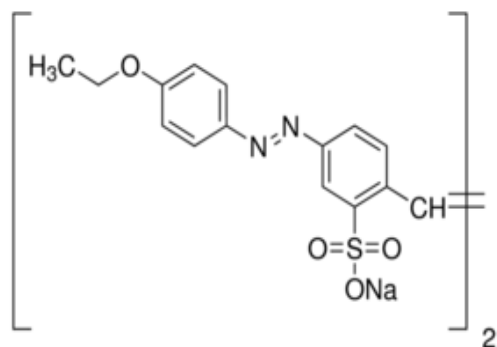


Figure 3 Molecular structure of Airedale Yellow CHD

## 2.2 Microbes (Bacteria) and medium compositions employed in the experiment

The pure bacterial cultures of *T. frigidiphilosprofundus* (NCIM 5438) and *E. chrysanthemi* Burkholder (NCIM no 5213) were obtained from NCL Pune as pure cultures. *T. frigidiphilosprofundus* is an aerobic gram-negative curving rod with a single polar flagellum bacteria that belong to the family rhodospirillaceae proteobacteria and is found in a warm, humid environment (Kaneshiro et al. 2008; Pulicherla et al. 2013; Adapa 2018). The obtained pure culture of bacteria was maintained on the medium supplemented with 5 g<sup>l</sup><sup>-1</sup> bactopectone, 1 g<sup>l</sup><sup>-1</sup> yeast extract, 0.1 g<sup>l</sup><sup>-1</sup> FeCl<sub>3</sub>, 5 g<sup>l</sup><sup>-1</sup> MgCl<sub>2</sub>, 12 g<sup>l</sup><sup>-1</sup> NaCl, 1.8 g<sup>l</sup><sup>-1</sup> CaCl<sub>2</sub>, 0.55 g<sup>l</sup><sup>-1</sup> KCl employed in Nutrient Medium 1 (NM1) having pH 7.6.

*E. chrysanthemi* Burkholder also known as *E. cartovora*, and it's a Gram-negative found either alone or in clusters and can survive under anaerobic environments. Due to its mesophilic nature, it can survive between 27 and 30° C temperature (Kaneshiro et al. 2008). Nutrient agar medium supplemented with 10 g<sup>l</sup><sup>-1</sup> Beef extract, 5 g<sup>l</sup><sup>-1</sup> NaCl, and 10 g<sup>l</sup><sup>-1</sup> Peptone was used for the bacterial multiplication. The pH of the medium was adjusted to 7.5 and the cultures were multiplied at 20°C and 30°C temperatures regularly and after multiplication stored at 4°C in a refrigerator.

## 2.3 Preparation of Azo dye contaminated water to be treated

After making a standard dye solution with a concentration of 1000 mg/l, the samples with the appropriate concentrations were generated by diluting the standard dye solution with deionized water using volumetric proportions. The amount of standard solution to be mixed with deionized water is calculated using the idea of concentration equality, which is described below in equation 1.

$$C_1V_1 = C_2V_2 \quad (1)$$

Where  $C_1=1000$  mg/l,  $V_1$ =volume of standard solution required,  $C_2$ =Concentration of wastewater sample,  $V_2= 100$ ml. All of the tests were done in conical flasks with a capacity of 250 mL.

Experiments were carried out in a temperature-controlled incubator shaker with 100 mL nutrient medium with dyestuff in a 250 mL shake flasks under various circumstances. After 48 hours of incubation, the samples were tested for decolorization. For this, samples were taken and centrifuged for 7.5 minutes at 13,000 rpm. The analysis of supernatants was carried out and the dyestuff and nutrition present in the control flasks and were devoid by microorganisms were tested and the percentage decolorization of the dye is calculated from the below equation 2.

$$y(\%) = \frac{(IA-FA)}{IA} \times 100 \quad (2)$$

Where  $y(\%)$ : % decolorization, IA: Initial Absorbance, FA: Final absorbance

## 2.4 Analytical methods

Analytikjena SPECORD 205 spectrophotometer was used to measure absorbance. For dye, the wavelengths that resulted in the highest absorption were selected. The dye solution is produced in seven different concentrations of 10mg/l, 30 mg/l, 50 mg/l, 90 mg/l, 150 mg/l, 200 mg/l, 250 mg/l. With distilled water as the blank solution, the solutions were evaluated using a UV-Visible spectrophotometer. The wavelength with the highest absorption was 398nm.

## 2.5 Response surface methodology (RSM)

RSM is a statistical technique for modeling and analyzing studies in which multiple input independent factors impact the output response. When running different experiments, the RSM finds the optimum experimental design, which saves a lot of time and work. RSM uses a variety of techniques to design experiments, including Central Composite Design (Said et al. 2015; Olawoye 2016). The decolorization percentage  $y$  is the output variable, which is a dependent selected variable. The independent variables (4) chosen for the studies are the sample concentration (mg/l), pH of the medium, temperature (°C), and agitation (rpm) in the incubator shaker. The number of tests to be performed is specified by the formula  $N=2^n+2*n+n_c$ , where  $N$  is the total number of runs to be performed,  $n$  is the number of independent variables, and  $n_c$  is the number of center points. Based on the applied formula total of 26 tests can be run. Using the software Minitab 14, the data of 26 tests were analyzed to generate residual and scatter plots.

## 3 Results and Discussion

### 3.1 Calibration experiments

The wavelength with the highest absorption was 398nm. The maximum absorbance that is obtained at a wavelength at a particular weight of dye are shown in Table 1.

Table 1 Maximum absorbance obtained at a particular weight of the dye

S. N.	Concentration (mg/l)	Wave Length (nm)	Absorbance
1	10	398	0.3186
2	30	398	0.429
3	50	402	0.611
4	90	398	1.41
5	150	398	2.037
6	200	398	2.35
7	250	398	2.859

The values in table 1 are obtained from the UV Vis spectrophotometer. The dye used here had its standard calibration curve (shown as 'a') and Absorbance vs Concentration (shown as 'b') drawn as shown in figure 4. The standard calibration plot can give us the wavelength at which maximum absorbance is attained and the Absorbance vs Concentration plot gives the concentration of the dye that is treated.

### 3.2 Decolorization of Airedale Yellow CHD with *T. frigidophilosprofundus*

In the work done by Hema and Suresha (2014), the biodegradation of the dye Airedale Yellow CHD required the addition of  $\text{NH}_4\text{Cl}$

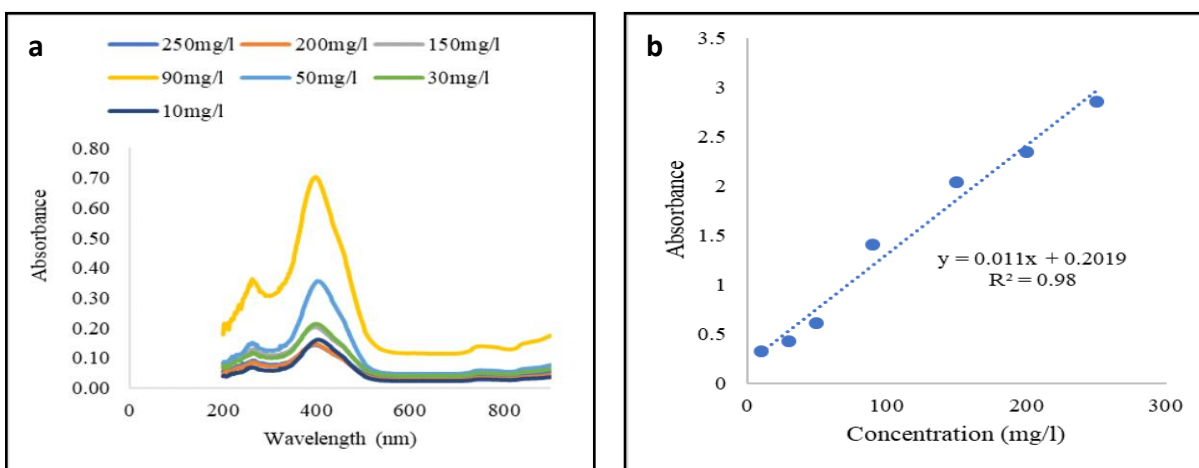


Figure 4 (a) Standard calibrations plot and (b) Plot of absorbance vs concentration of the dye taken

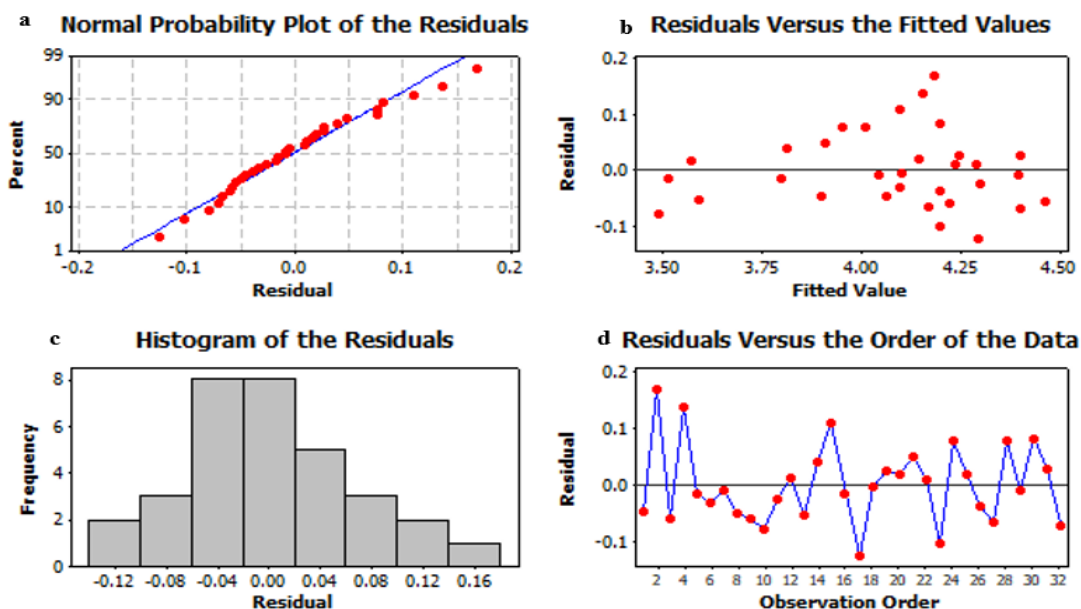


Figure 5 plots showing (a) Normal probability plot of the residuals, (b) Residuals versus the order of the data, (c) Histogram of the residuals, (d) Residuals versus the fitted values of NID

and starch to get a percent decolorization of 63.15%. Whereas, in this current study, while using the bacteria *T. frigidophilosprofundus* the percent decolorization of the dye was 77.41% and there is no need for the external addition of  $\text{NH}_4\text{Cl}$  and starch. The residual plots of degradation of Airedale Yellow CHD using *T. frigidophilosprofundus* are shown in Figure 5.

A residual is a difference between the predicted value and the obtained value. The obtained value is the experimental result and the predicted value is of the software (Olawoye 2016). The normal probability plot was shown if the acquired data follows the normality distribution and whether the gathered data from the trials form a good fit. It depicts the deviation between points and detects deviation. Figure 5a explains that residuals obtained from

experiments form a nearly straight line which implies that the errors were distributed normally. The acceptable limit for the residual value is  $\leq \pm 2$  (Ibrahim et al. 2022) and the obtained residual is very less and are within the limit. Hence it can be stated that the values didn't depart from the approved limitations (Ibrahim et al. 2022). The assumption of constant variance is tested by plotting the residuals against the ascending fitted response values. According to Olawoye (2016), the plot should be random scatter (constant range of residuals across the graph). This has been seen in plot b above. The number of trials that match the residual product is shown in the histogram of the residuals graph, and when the frequency is connected by a straight line, it follows a bell curve, which can describe it as a good fit. There will be a random dispersion on the plot (Olawoye 2016). From c, the residuals don't

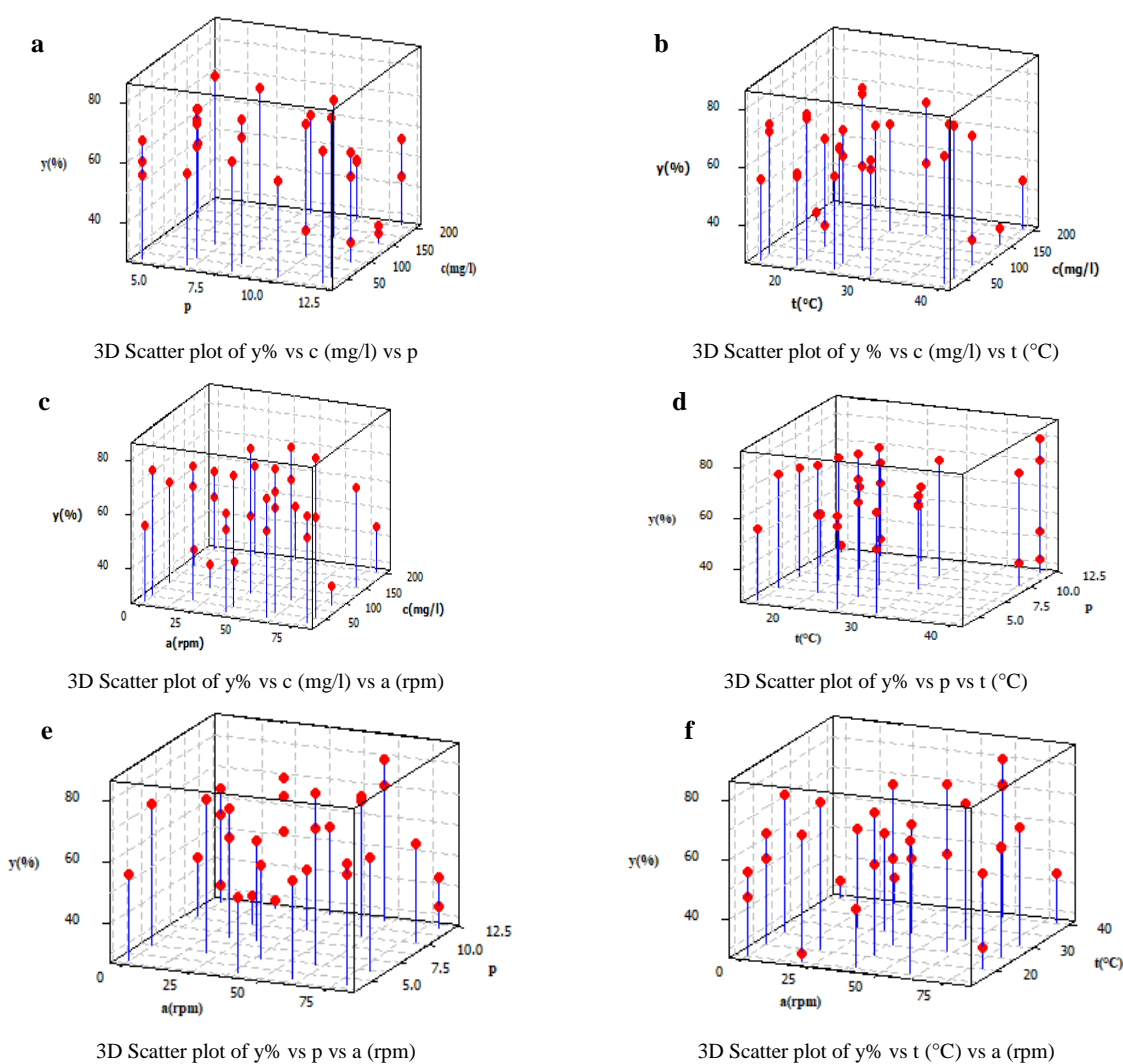


Figure 6 Scatter plots of biodegradation of Airedale Yellow CHD using *T. frigidophilosprofundus*; here, (a) denote the figure of scatter plot of y% vs c (mg/l) vs p, (b) denote the figure of scatter plot of y% vs c(mg/l) vs t(°C), (c) denote the figure of scatter plot of y% vs c(mg/l) vs a(rpm), (d) denotes the figure of scatter plot of y% vs p vs t(°C), (e) denotes the scatter plot of y% vs p vs a(rpm), (f) denote the scatter plot of y% vs t(°C) vs a(rpm); From the above plots, the majority of the data points tend to rise or fall.

show a clear form. It implies that there is very little error in the collection of results of the experiment order (Patidar and Sharma 2021). Since from the above points, the work done in this study complies with the work to be done, to obtain very few errors, this is said to be a valid work to understand the biodegradation of Airedale yellow CHD using *T. frigidophilosprofundus*.

The scatter plots were also obtained as shown in figure 6. They denote the correlation between the result obtained and the input variables (Barker and Westfall 2022). Here 3D plots were obtained, where the points indicate the percentage decolorization obtained at two particular input variables.

### 3.3 Decolorization of Airedale Yellow CHD with *E. chrysanthemi* Burkholder

The maximum amount of decolorization obtained was 74.64 %. The biodegradation of the dye Airedale Yellow CHD required the addition of  $\text{NH}_4\text{Cl}$  and starch in the work of Hema and Suresha (2014) to achieve a percent decolorization of 63.15 percent. The percent decolorization of the dye was 74.64 % that is also without any addition of  $\text{NH}_4\text{Cl}$  or starch from the outside. The residual plots of the runs for degradation of Airedale Yellow CHD using *E. chrysanthemi* Burkholder are shown in figure 7.

The disparity between the predicted and actual value is called a residual. The obtained value is the result of the experiment, whereas the predicted value is the result of the software (Olawoye 2016). The Normal Probability plot illustrates if the acquired data follows a normal distribution and the data from the trials fits together well. It shows the difference between two locations and detects the difference. Our model's residual values did not deviate from approved limitations ( $\leq \pm 2$ ) and fell on a straight line with only a few exceptions, implying that the errors were distributed normally, as the residuals form a nearly straight line (Ibrahim et al. 2022). By displaying the residuals against the ascending fitted response values, the assumption of constant variance is checked and the plot should be random scatter (Olawoye 2016). This can be seen in plot b. The histogram of the residuals graph showed the number of trials that match the residual created, and when the frequency is connected by a straight line, it follows a bell curve, which can be described as a good fit. On the plot, there will be a random dispersion (Olawoye 2016). The residuals shown in plot c don't have a distinct form. It suggests that the experiment order's results are collected with relatively minimal inaccuracy (Patidar and Sharma 2021). Because the work done in this study corresponds with the work that needs to be done to achieve very few errors, it is considered a valid study to investigate the biodegradation of Airedale yellow CHD utilizing *E. chrysanthemi* Burkholder.

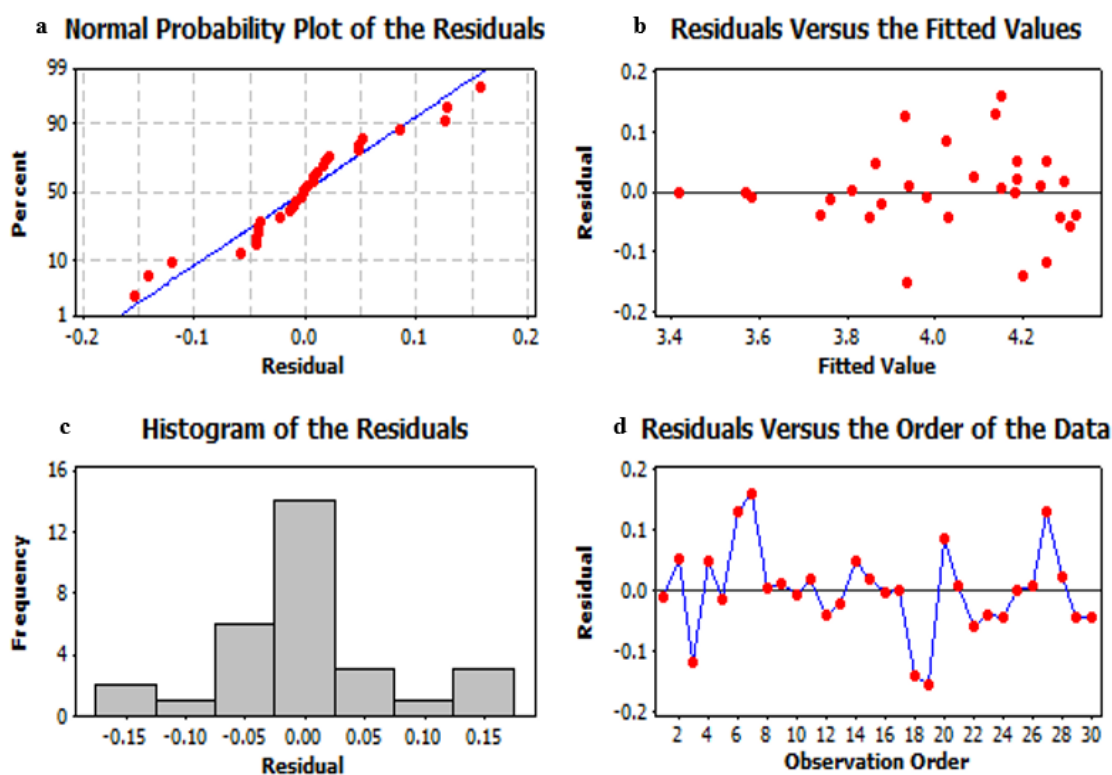


Figure 7 plots showing (a) Normal probability plot of the residuals, (b) Residuals versus the order of the data, (c) Histogram of the residuals, (d) Residuals versus the fitted values of N2D

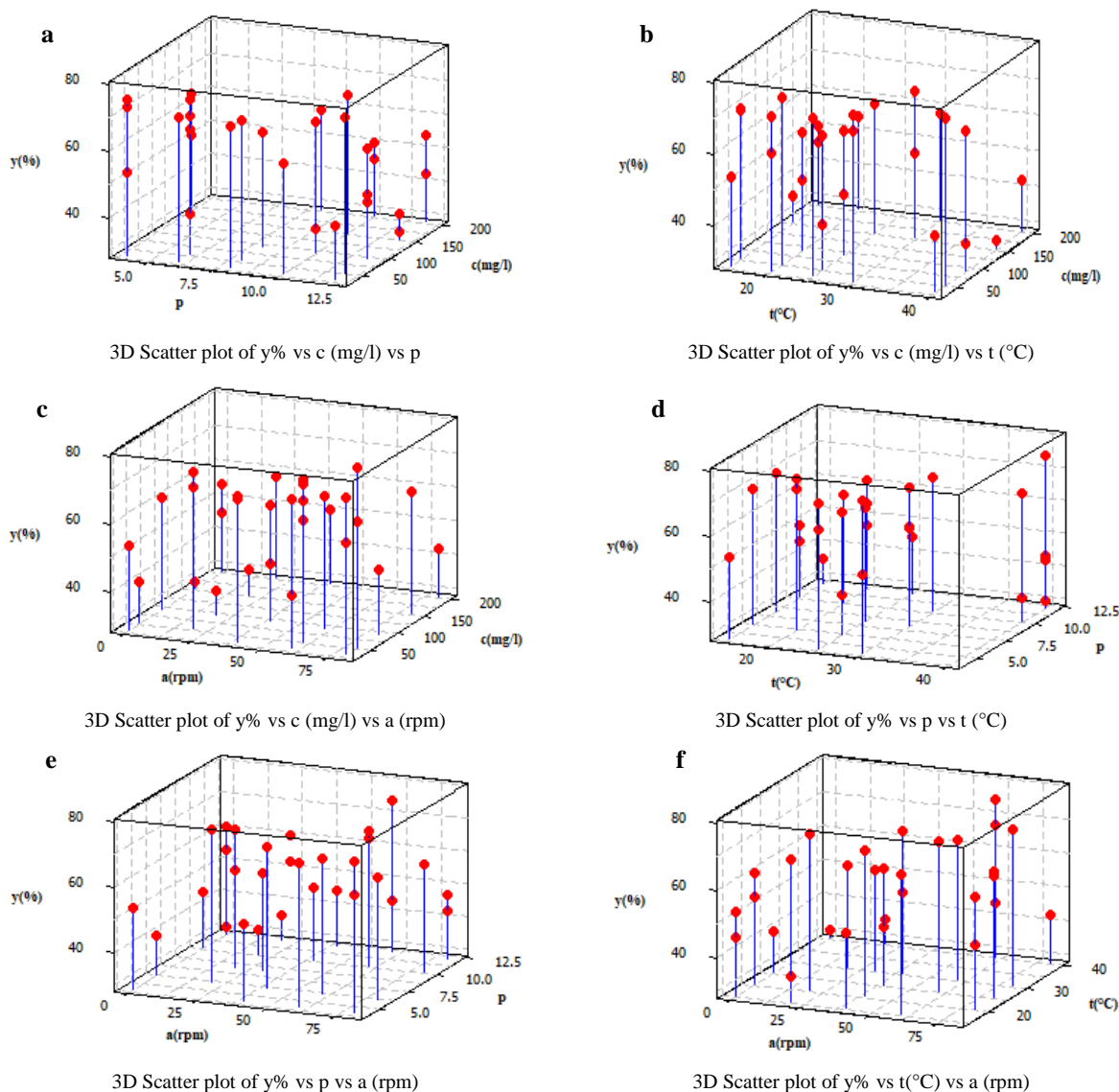


Figure 8 Scatter plots of N2D; here (a) denote the figure of scatter plot of  $y\%$  vs  $c$  (mg/l) vs  $p$ , (b) denote the figure of scatter plot of  $y\%$  vs  $c$  (mg/l) vs  $t$  ( $^{\circ}\text{C}$ ), (c) denote the figure of scatter plot of  $y\%$  vs  $c$  (mg/l) vs  $a$  (rpm), (d) denotes the figure of scatter plot of  $y\%$  vs  $p$  vs  $t$  ( $^{\circ}\text{C}$ ), (e) denote the scatter plot of  $y\%$  vs  $p$  vs  $a$  (rpm), (f) denote the scatter plot of  $y\%$  vs  $t$  ( $^{\circ}\text{C}$ ) vs  $a$  (rpm); From the above plots, majority of the data points tend to rise or fall.

Figure 8 shows the scatter plots that represent the relationship between the acquired result and the input variables (Barker and Westfall 2022). The points reflect the percent percentage decolorization obtained at two specific input variables in these 3D plots.

## Conclusions

The ability of *T. frigidophilosprofundus* and *E. chrysanthemi Burkholder* to decolorize the azo dye Airedale yellow CHD contaminated wastewater is discussed in this work. The maximum

percentage removal of the azo dye was obtained using *T. frigidphilosprofundus* (77.41%), and this was followed by *E. chrysanthemi Burkholder* (74.64%). The use of the bacteria can be considered the novelty of the work. The experimental results are compared with those of the modeled result, represented as residual plots. The obtained normal plots of the Residual plots for decolorization of the dye contaminated wastewater using the bacteria showed the formation of a nearly straight line which can conclude that experimental runs formed a good fit. Moreover, scatter plots showed the interaction between the input variables and the obtained result.



### Acknowledgments

The authors acknowledge the Centre for Automation and Instrumentation, NITW for the characterization facility.

### Conflicts of Interest

The authors report there are no conflicts of interest exist.

### References

- Adapa, V. (2018). *Enhancement of cold active polygalacturonase productivity in a novel marine psychrophile Thalassospira frigidiphilosprofundus s3ba12*. Doctoral thesis, Acharya Nagarjuna University, Guntur, Telangana, India
- Atalay, S., & Ersöz, G. (2016). *Novel Catalysts in Advanced Oxidation of Organic Pollutants*. Springer, New York, pp. 23–34
- Barker, T., & Westfall, J. (2022). *Correlation Analysis with Scatter Plots*. In: Pro Data Visualization Using R and JavaScript. Apress, Berkeley, CA. [https://link.springer.com/chapter/10.1007/978-1-4842-7202-2\\_8](https://link.springer.com/chapter/10.1007/978-1-4842-7202-2_8)
- Bharathiraja, B., Aberna Ebenezer Selvakumari, I., Iyyappan, J., & Varjani, S. (2019). Itaconic acid: an effective sorbent for removal of pollutants from dye industry effluents. *Current Opinion in Environmental Science & Health*, 12, 6-17
- Chang, J. S., Kuo, T. S., Chao, Y. P., Ho, J. Y., & Lin, P. J. (2000). Azo dye decolorization with a mutant *Escherichia coli* strain. *Biotechnology Letters*, 22(9), 807–812
- Dos Santos, A. B., Cervantes, F. J., & van Lier, J. B. (2007). Current technologies for decolorisation of textile wastewaters: Perspectives for anaerobic biotechnology. *Bioresource Technology*, 98(12), 2369–2385
- Garg, N., Garg, A., & Mukherji, S. (2020). Eco-friendly decolorization and degradation of reactive yellow 145 textile dye by *Pseudomonas aeruginosa* and *Thiosphaera pantotropha*. *Journal of Environmental Management*, 110383. 263(March)
- Hassan, M. M., & Carr, C. M. (2018). A critical review on recent advancements of the removal of reactive dyes from dyehouse effluent by ion-exchange adsorbents. *Chemosphere*, 209, 201–219
- Hema, N., & Suresha, S. (2014). Bioremediation of Textile Dye effluent by *Shewanella Putrefaciens*. *International Journal of Pharmacy and Biological Sciences*, 4 (2), 109-116
- Ibrahim, A., El-Fakharany, E.M., Abu-Serie, M.M., ElKady, M.F., Eltarahony, M. (2022). Methyl Orange Biodegradation by Immobilized Consortium Microspheres: Experimental Design Approach, Toxicity Study and Bioaugmentation Potential. *Biology*, 11, 76
- Jain, M., Khan, S.A., Sharma, K., Jadhao, P.R., (2022). Current perspective of innovative strategies for bioremediation of organic pollutants from wastewater. *Bioresource Technology*, 344(Pt B), 126305
- Jin, X. C., Liu, G. Q., Xu, Z. H., & Tao, W. Y. (2007). Decolorization of a dye industry effluent by *Aspergillus fumigatus* XC6. *Applied Microbiology and Biotechnology*, 74(1), 239–243
- Kaneshiro, W. S., Burger, M., Vine, B. G., De Silva, A. S., & Alvarez, A. M. (2008). Characterization of *Erwinia chrysanthemi* from a bacterial heart rot of pineapple outbreak in Hawaii. *Plant Disease*, 92(10), 1444–1450
- Melissa Denchak. (2018, May 14). Water Pollution: Everything You Need to Know. <https://www.nrdc.org/stories/water-pollution-everything-you-need-know>, accessed on 23 January 2022
- Olawoye, B. (2016). *A comprehensive handbook on central composite design (ccd)*. Springer, New York
- Patidar, D. & Sharma, S. (2021). Optimize of Process Parameters of EN31 on WEDM Machine. *International Journal of Research Publication and Reviews*, 2 (3), 174-179
- Pulicherla, K. K., Kumar, P. S., Manideep, K., Rekha, V. P. B., Ghosh, M., & Rao, K. R. S. S. (2013). Statistical approach for the enhanced production of cold-active  $\beta$ -galactosidase from *thalassospira frigidiphilosprofundus*: A novel marine psychrophile from deep waters of bay of bengal. *Preparative Biochemistry and Biotechnology*, 43(8), 766–780
- Rai, H. S., Bhattacharyya, M. S., Singh, J., Bansal, T. K., Vats, P., & Banerjee, U. C. (2005). Removal of dyes from the effluent of textile and dyestuff manufacturing industry: A review of emerging techniques with reference to biological treatment. *Critical Reviews in Environmental Science and Technology*, 35(3), 219–238
- Said, K. A. M., Yakub, I., & Amin, M. A. M. (2015). Overview of Response Surface Methodology (RSM) in Extraction Process. *Journal of Applied Science & Process Engineering*, 2 (1), 279–287
- Saratale, R. G., Saratale, G. D., Chang, J. S., & Govindwar, S. P. (2011). Bacterial decolorization and degradation of azo dyes: A review. *Journal of the Taiwan Institute of Chemical Engineers*, 42(1), 138–157
- Sen, S.K., Raut, S., Bandyopadhyay, P., Raut, S. (2016). Fungal decolouration and degradation of azo dyes: A review. *Fungal Biology Reviews*, 30 (3), 112-133

- Stolz, A. (2001). Basic and applied aspects in the microbial degradation of azo dyes. *Applied Microbiology and Biotechnology*, 56(1–2), 69–80
- Subramani M R. (2020, May 4). Textile Manufacturers Face Three Problems In Cashing In On Global Anti-Chinese Sentiments Post-Covid-19. <https://swarajyamag.com/business/textile-manufacturers-face-three-problems-in-cashing-in-on-global-anti-chinese-sentiments-post-covid-19>, accessed on 23 January 2022
- Van Der Zee F.P., & Villaverde, S. (2005). Combined anaerobic–aerobic treatment of azo dyes-A short review of bioreactor studies. *Water Research*, 39, 1425-1440
- Varjani, S., Rakholiya, P., Ng, H.Y., You, S., Teixeira, J.A. (2020). Microbial degradation of dyes: An overview. *Bioresource Technology*, 314, 123728
- World Dye Variety (2012, June 28). *Dye/World dye variety*. <http://www.worlddyevariety.com/direct-dyes/direct-yellow-12.html>
- World Trade Statistical Review. (2019). *World Trade Statistical Review*. [https://www.wto.org/english/res\\_e/statis\\_e/wts2019\\_e/wts2019\\_e.pdf](https://www.wto.org/english/res_e/statis_e/wts2019_e/wts2019_e.pdf)
- World Trade Statistical Review. (2020). *World Trade Statistical Review*. [https://www.wto.org/english/res\\_e/statis\\_e/wts2020\\_e/wts2020\\_e.pdf](https://www.wto.org/english/res_e/statis_e/wts2020_e/wts2020_e.pdf)
- World Trade Statistical Review. (2021). *World Trade Statistical Review*. [https://www.wto.org/english/res\\_e/statis\\_e/wts2021\\_e/wts2021\\_e.pdf](https://www.wto.org/english/res_e/statis_e/wts2021_e/wts2021_e.pdf)





## Journal of Experimental Biology and Agricultural Sciences

<http://www.jebas.org>

ISSN No. 2320 – 8694

### Machine learning for the classification of breast cancer tumor: a comparative analysis

Madhumita Pal<sup>1</sup>, Smita Parija<sup>1,\*</sup>, Ganapati Panda<sup>1</sup>, Kuldeep Dhama<sup>2</sup> , Ranjan K. Mohapatra<sup>3,\*</sup> 

<sup>1</sup>Electronics and communication Engineering, C. V. Raman Global University, Bidyannagar, Mahura, Janla, Bhubaneswar, Odisha 752054, India

<sup>2</sup>Division of Pathology, ICAR-Indian Veterinary Research Institute, Izatnagar, Bareilly-243122, Uttar Pradesh, India

<sup>3</sup>Department of Chemistry, Government College of Engineering, Keonjhar, Odisha 758002, India

Received – April 01, 2022; Revision – April 20, 2022; Accepted – April 29, 2022

Available Online – April 30, 2022

DOI: [http://dx.doi.org/10.18006/2022.10\(2\).440.450](http://dx.doi.org/10.18006/2022.10(2).440.450)

#### KEYWORDS

Breast cancer

Multilayer perceptron

K-NN

MLP

Random forest

#### ABSTRACT

The detection and diagnosis of Breast cancer at an early stage is a challenging task. With the increase in emerging technologies such as data mining tools, along with machine learning algorithms, new prospects in the medical field for automatic diagnosis have been developed, with which the prediction of a disease at an early stage is possible. Early detection of the disease may increase the survival rate of patients. The main purpose of the study was to predict breast cancer disease as benign or malignant by using supervised machine learning algorithms such as the K-nearest neighbor (K-NN), multilayer perceptron (MLP), and random forest (RF) and to compare their performance in terms of the accuracy, precision, F1 score, support, and AUC. The experimental results demonstrated that the MLP achieved a high prediction accuracy of 99.4%, followed by random forest (96.4%) and K-NN (76.3%). The diagnosis rates of the MLP, random forest and K-NN were 99.9%, 99.6%, and 73%, respectively. The study provides a clear idea of the accomplishments of classification algorithms in terms of their prediction ability, which can aid healthcare professionals in diagnosing chronic breast cancer efficiently.

\* Corresponding author

E-mail: [smita.parija@gmail.com](mailto:smita.parija@gmail.com) (Dr. Smita Parija);

[ranjank\\_mohapatra@yahoo.com](mailto:ranjank_mohapatra@yahoo.com) (Dr. Ranjan K. Mohapatra)

Peer review under responsibility of Journal of Experimental Biology and Agricultural Sciences.

Production and Hosting by Horizon Publisher India [HPI]  
(<http://www.horizonpublisherindia.in/>).  
All rights reserved.

All the articles published by [Journal of Experimental Biology and Agricultural Sciences](#) are licensed under a [Creative Commons Attribution-NonCommercial 4.0 International License](#) Based on a work at [www.jebas.org](http://www.jebas.org).



## 1 Introduction

The World Cancer Research Fund recorded two million new cases of breast cancer in 2018, which resulted in approximately 626,679 deaths. Breast cancer, which is also known as “breast carcinoma,” is the excessive growth of epithelial cells in the lining ducts and lobules of the breast. It is the second leading cause of death in women. As opposed to conducting several tests for the diagnosis of the disease, as recommended by an oncologist, machine learning algorithms can provide a better solution for the automatic prediction of breast cancer. Machine learning is a data mining technique that is used to design an automation system without human interference. The goal of supervised learning is to predict or classify an output based on prior information. Labeled data are required for training the machine learning model. The objective of unsupervised machine learning methods is to detect clusters within a heterogeneous data structure, without a labeled dataset. Thus, it can predict the output without a supervisor (Jiang et al. 2020). Medical applications are another significant area of machine learning. As healthcare applications contain large amounts of data, it is challenging to handle these data. Such data can be managed efficiently by using machine learning techniques. This can aid in the early detection of disease, reduce the cost of medicines, and increase the patient survival rate. Machine learning provides an automatic system approach that helps to diagnose the disease at an early stage and appropriate treatment can subsequently be provided to the patient at the correct time, which will reduce the death rate of patients suffering from this chronic disease (Sun et al. 2017). The proposed method provides an automated machine learning system for the early prediction of breast cancer and recommendations for proper treatment by the oncologist to the patient at the correct time.

Asri et al. (2016) presented a breast cancer analysis model using various machine learning techniques, namely the support vector machine (SVM), naïve Bayes, decision tree (C4.5), and K-nearest neighbor (K-NN). The experiment was performed on the Wisconsin Breast Cancer (original) datasets and simulated using the WEKA data mining tool. The performance analysis demonstrated that the SVM achieved the maximum accuracy (97.13%) with the lowest error rate among all of the algorithms. Muktevi (2020) proposed a breast cancer prediction system with the implementation of a machine learning algorithm. In this study, the author applied an SVM, naïve Bayes, random forest, and logistic regression to the Breast Cancer dataset to predict an accurate model. The experimental results showed that the random forest provided better results on the Breast Cancer dataset compared to other datasets. Moreover, the accuracy, precision, recall, and F1 score were investigated and the components of the confusion matrix were discussed.

Rana et al. (2015) proposed a data mining model for the classification of tumors as malignant or benign. A model with the

implementation of machine learning algorithms such as SVM, logistic regression, and K-NN was presented. In terms of accuracy, the false positive rate, sensitivity, and specificity of all algorithms were compared. In the study, the SVM exhibited the best prediction accuracy of 92.4%. Moreover, Islam et al. (2017) proposed a system using a 10-fold cross-validation method for predicting breast cancer. An SVM and K-NN were used for the detection of breast cancer. The experimental results demonstrated that the accuracies of the SVM and K-NN were 98.57% and 97.14%, respectively. Moreover, the SVM was better at predicting the disease in terms of accuracy.

Singh (2019) determined a biomarker for the prediction of breast cancer by using various machine learning algorithms. The experimental results showed that among nine attributes, glucose, age, and resistance were effective biomarkers for breast cancer prediction. Using these features for classification, the K-NN yielded a maximum classification accuracy of 92.11%, followed by the Gaussian SVM with a classification accuracy of 83.68%. Furthermore, García-Laencina et al. (2015) proposed a prediction model for five-year breast cancer survivability without imputation in 2015. The study showed that K-NN achieved the highest prediction accuracy of more than 81% and receiver operating characteristics of more than 0.78%. Wu et al. (2019) proposed a white-box machine learning model approach to predict the molecular subtypes of breast cancer based on BI-RADS features using MRI and mammography images. A 10-fold cross-validation method was applied to compute the performance (positive predictive value, accuracy, F1 score, and sensitivity) of the decision tree model. Moreover, Islam and coworkers have compared the machine learning techniques for the prediction of breast cancer by using the dataset retrieved from the UCI repository (Islam et al. 2020).

### 1.1 Breast cancer

Breast cancer is the most dangerous chronic disease that commonly occurs in women, normally at the age of above 40 years. Cancer does not cause any pain until it has spread to adjacent tissues. It begins as *in situ* carcinomas such as ductal carcinoma and lobular carcinoma (Sun et al. 2017). These occur on top of the ribs and pectoral muscles, and are divided into three main parts *viz.*, (i) *Glandular tissue* - this tissue creates milk consisting of 15 to 20 lobules. Inside each lobule, grape-like structures known as alveoli are present, (ii) *Stroma* - this consists of adipose/fat tissue and contains the majority of the breast tissue. It contains Cooper's ligaments attached to the skin and pectoralis muscles, and (iii) *Lymphatic vessels* - these consist of drain lymph cells, which contain fluid that drains cellular waste and white blood cells. They mainly drain into the lymph nodes in the axilla/arm-pit. When the menopausal estrogenic hormones discharged by the ovaries stop, the alveolar cells die and the breast

tissue is reinstated. During the menstrual cycle, the production of estrogen and progesterone from the ovaries increases, and after menstruation, the flow is reduced.

Each menstrual cycle causes the alveolar cells to undergo demarcation and apoptosis. Every time a cell bisects, there is a change in the genetic mutation and this mutation causes tumor formation. Therefore, there is an increase in the occurrence of breast cancer with an increase in the number of menstrual cycles during the initial and late stages of menopause. Furthermore, medications containing estrogenic agents may maximize the possibility of breast cancer. Ionizing radiation such as CT scans and MRI may also increase the occurrence of breast cancer. Pregnancy at an early age and breastfeeding for a long period can decrease the risk of breast cancer.

### 1.2 Symptoms

The most common symptoms of breast cancer are (i) hard, painless lump or swelling which is normally found in the upper and outer part of the breast, (ii) swelling under the armpit, (iii) breast immovable, (iv) notching of skin, (v) fibrosis of Lactiferous ducts and suspensory ligaments and (vi) paget diseases

### 1.3 Diagnosis

Early-stage diagnosis of breast cancer is a difficult task, some common methods of breast cancer diagnosis are (i) feeling breast lump, (ii) with MAMMOGRAPHY, (iii) Imaging using ultrasound and MRI, and (iv) biopsy of swelling.

### 1.4 Treatment

Treatment of breast cancer depends on the type and stage of cancer, some commonly available treatment methods are (i) surgery, (ii) radiation therapy, (iii) chemotherapy, and (iv) hormonal therapy.

## 2 Materials and Method

To implement the algorithms of this research, we used the Wisconsin Diagnostic Breast Cancer (WDBC) dataset from the Kaggle site (<https://www.kaggle.com/uciml/breast-cancer-wisconsin-data>). The K-NN, MLP, and RF algorithms were implemented on the dataset to obtain the classification results (Table 1). The code for each algorithm was written in Python and executed in the Jupyter Notebook. Several supervised data prediction techniques were used in the model and their performance was compared to provide a better quality of service for the healthcare system.

Figure 1 presents the architecture of the data mining model for the implementation of machine learning algorithms. It provides an understanding of how to load the dataset and how to extract the features from the dataset by using different stages. The first stage is the selection of a breast cancer dataset online, followed by the pre-processing and transformation of variables in the second stage, and the third stage is the implementation of various ML models. Finally, we have evaluated our model for the prediction of benign or malignant breast cancer using different metrics.

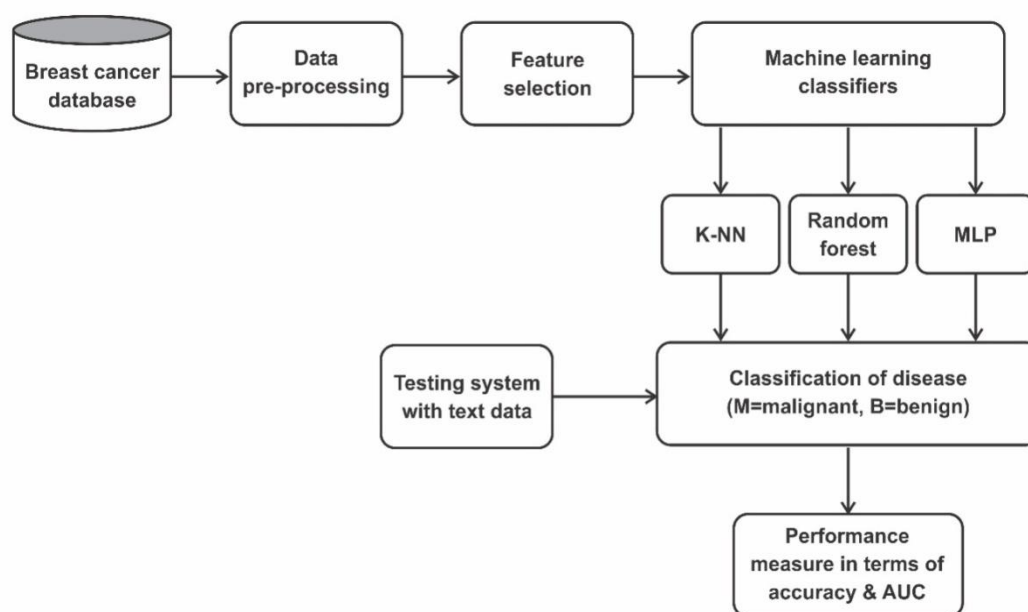


Figure 1 Architecture of data mining model for breast cancer classification

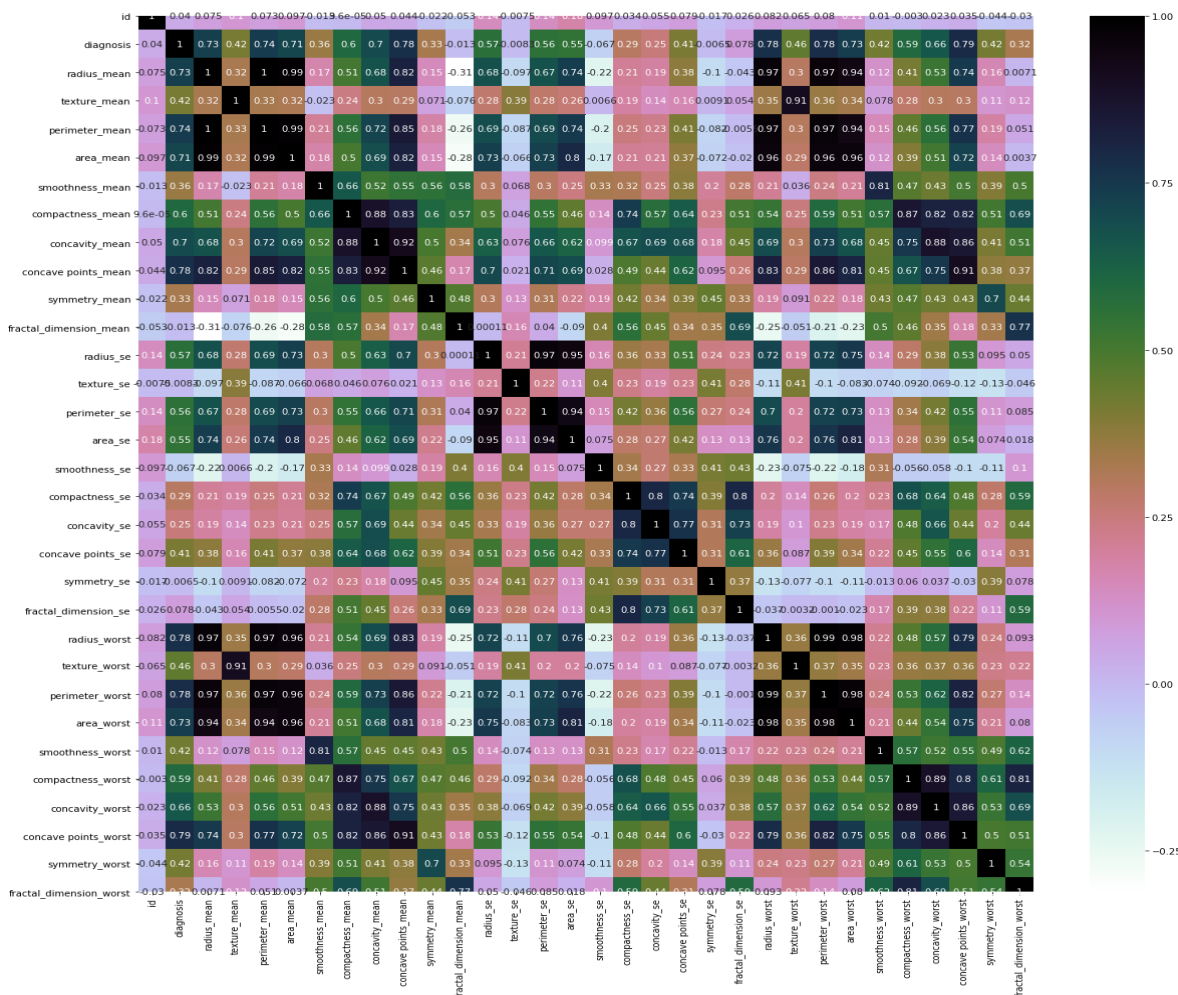


Figure 2 Correlation matrix of the given data set

2.1 Pre-processing and transformation

The breast cancer dataset was converted into the CSV format from the Excel file. Thereafter, by using explorative data analysis, we filtered the data by checking the null values; missing values existed in the dataset. We subsequently correlated the features using a correlation matrix, as illustrated in Figure 2.

2.2 Performance evaluation

To measure the performance of the various machine learning models, we used different metrics, including precision, recall, F1 score, and support. The formulae for calculating the metrics are presented in Table 1. We used confusion matrices for the different algorithms to evaluate the metrics.

2.3 K-nearest neighbor (K-NN)

K-NN is a supervised ML algorithm that is used to classify an unknown object based on the nearest neighbor data point concept.

Table 1 Formulae for calculation of different metrics

Metrics	Formula
Recall	$\frac{TP}{TP + FN}$
Precision	$\frac{TP}{TP + FP}$
Accuracy	$\frac{TP + TN}{TP + TN + FP + FN}$
F1_score	$\frac{2 * precision * recall}{precision + recall}$
Support	TN + FP, TP + FN

By using different distance metric concepts, such as the Euclidean distance and Manhattan distance, the nearest neighbor data point can be determined. The K-NN algorithm is easy to implement, but it is inefficient for a large dimensional dataset. It is a nonparametric model that is used for solving classification

problems (Forsyth et al. 2018). The Euclidean distance for two points in Euclidean space is

$$U(a,b) = \sqrt{\sum_{j=1}^n (b_j - a_j)^2} \quad (1)$$

Where, a, b are two points in n-space, and  $b_j$  and  $a_j$  are Euclidean vectors.

**2.4 Random forest (RF)**

RF is a supervised ML algorithm that is used for classification and regression. However, it is inefficient for regression problems in terms of accuracy (Verikas et al. 2011). It is a type of ensemble classifier that uses a decision tree algorithm in a randomization process. It consists of different decision trees of various sizes and shapes. In this case, random means the random sampling of the training tree while building the decision tree, and a random subset of input features is obtained when splitting at the node (Figure 3). One aspect that restricts decision trees as an optimal tool for predictive analysis is their inaccuracy. Decision trees cannot provide good

classification results. RF combines the integrity of decision trees with docility, which causes a large accuracy rectification.

**2.5 Multilayer perceptron (MLP)**

The MLP is part of the feed-forward ANN technique. The MLP consists of three layers: the input layer, hidden layer, and output layer. Figure 4 depicts an MLP network with three input layers, four hidden layers, and one output layer. In this neural network, the information flows in the forward direction but not in the backward direction. As it is part of the feed-forward neural network, information is passed from input to output through the hidden layer in the forward direction. It uses different nonlinear activation functions at the hidden layer to inject nonlinear mapping from the input to the hidden layer and linear mapping from the hidden layer to the output layer. This method provides better accuracy for a large dimensional dataset. To train the model, a back-propagation learning algorithm is used to minimize the error. The network minimizes the sum of the square error by updating the weight at each layer in the backward pass (Costa et al. 2013).

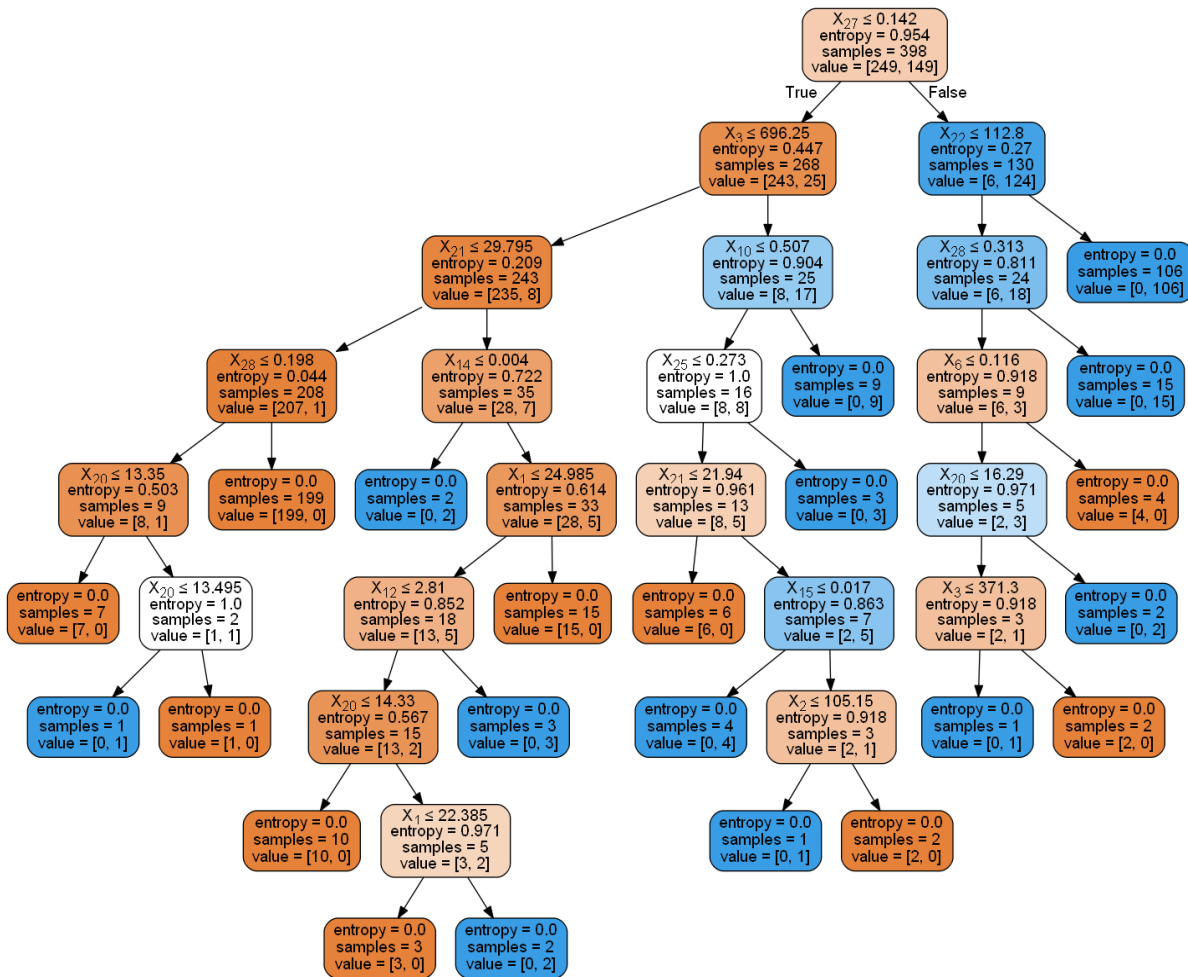


Figure 3 The obtained decision tree

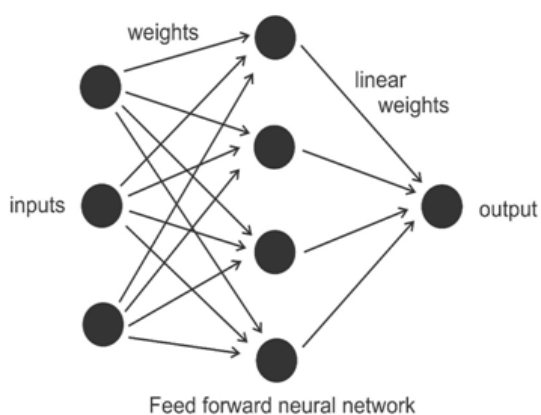


Figure 4 Diagram of feed-forward neural network

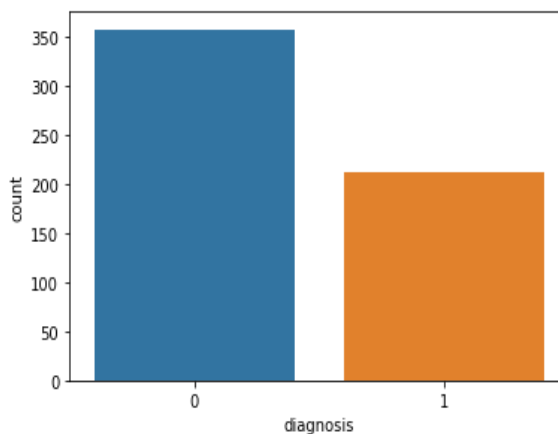


Figure 5 Count plot for classification of breast cancer patients

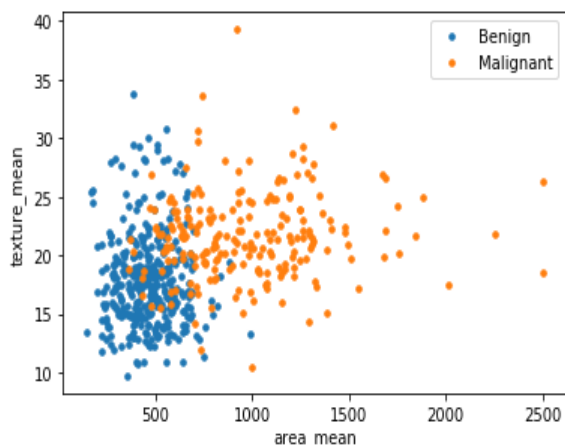


Figure 6 Data visualization plot for breast cancer features

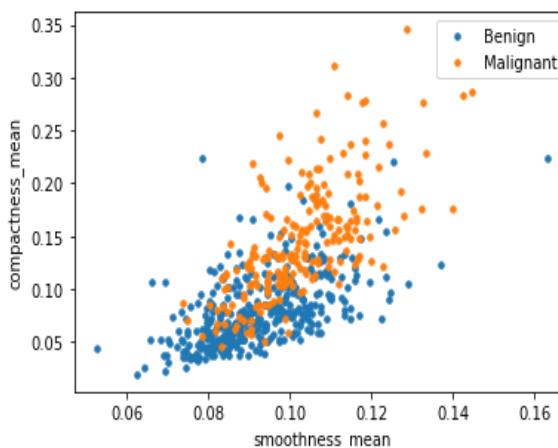


Figure 7 Correlation plot for breast cancer features

### 3 Results and Discussion

The dataset used in this study was the WDBC dataset, accessed from the Kaggle site. It consists of 569 samples and 32 attributes. The dataset was filtered using an explorative data analysis method. The attribute diagnosis indicates whether the breast cancer tumor is benign or malignant (M = malignant (1) and the tumor is cancerous; B = benign (0) and the tumor is noncancerous). Among the 569 samples, the diagnosis feature indicated that 357 samples were benign and 212 were malignant tumors as shown in Figure 5.

Thereafter, the K-NN, MLP, and random forest algorithms were implemented on the dataset using Python code, following which all of the codes were executed in the Jupyter Notebook. The experimental results demonstrated that the prediction accuracy obtained for classification using the K-NN algorithm was 76.3%, that when using the random forest algorithm was 96.4%, and that when using the MLP was 99.4%. In this section, the prediction results of the different machine learning algorithms are discussed. We have employed 10-fold cross-validation for splitting the dataset

into numerous numbers of training and testing datasets for representing the prediction ability of the model more accurately. A total of 80% of the data samples were used for training the model and 20% of the data were used for testing the model. Subsequently, by pre-processing the data, we analyzed the data in terms of accuracy.

A correlation plot gives the correlation between different variables present in the dataset. It is mainly used for feature selection. If two features have a strong correlation value then one feature can be dropped. In this way, the number of input features of the given dataset can be reduced and the performance of the predictive model is increased. The data visualization plots (Figure 6 and Figure 7) show that with the increase in the area mean and compactness means chances of breast cancer tumors being malignant are more. Malignant observations are located in the right left corner and benign observations are located in the left lower corner. The blue color indicates the benign tumor and the orange color indicates the malignant tumor features. The mean of texture and smoothness does not show any impact on overdiagnosis.



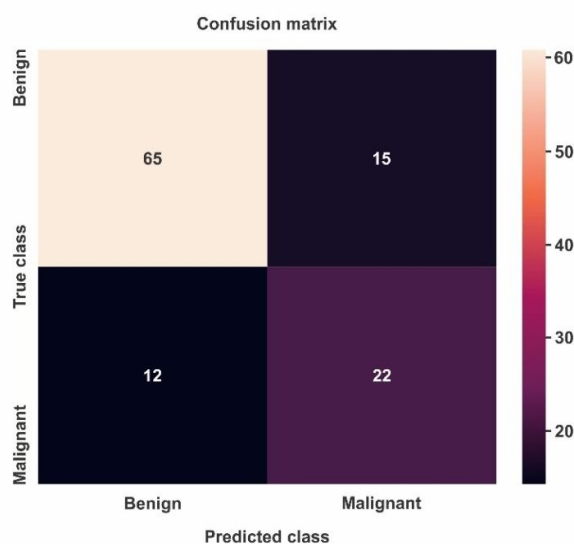


Figure 8 Confusion matrix of K-NN

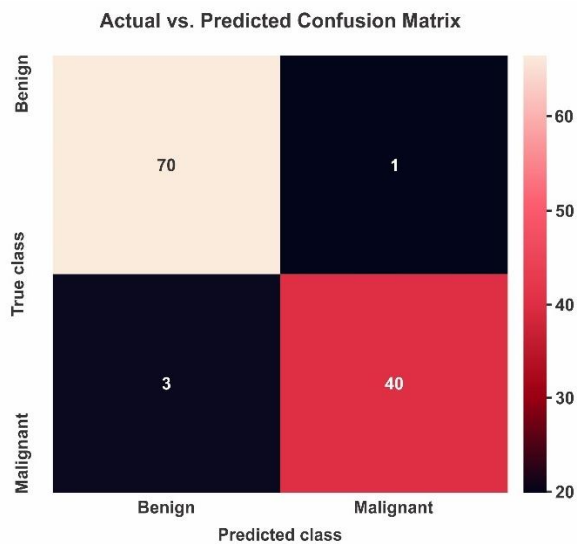


Figure 9 Confusion matrix of RF

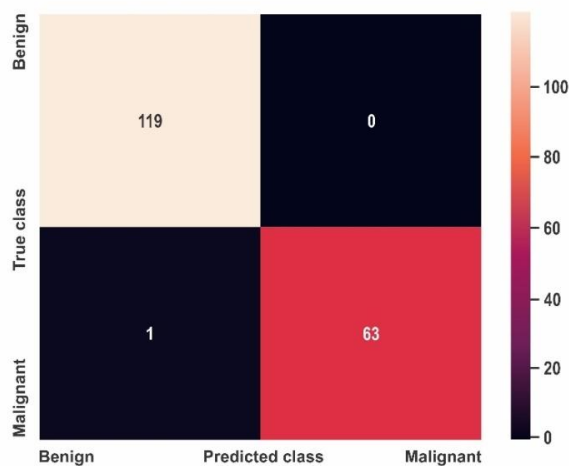


Figure 10 Confusion matrix of MLP

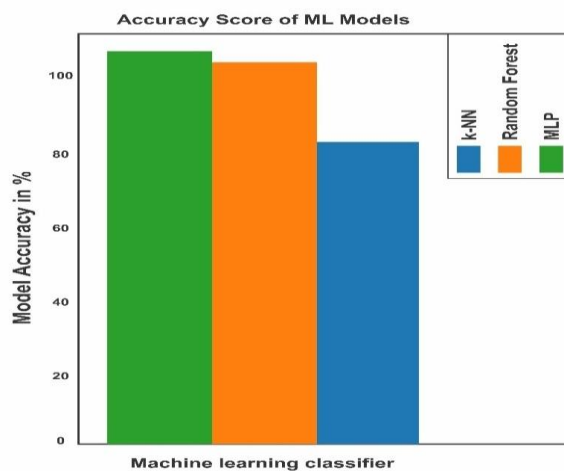


Figure 11 Accuracy comparisons of ML algorithms

### 3.1 Confusion matrix

In this research, different metrics such as accuracy, precision, recall, F1 score, and support were used for the accurate measurement. A confusion matrix is generally used for binary classification problems to measure the accuracy of the model. It consists of four parts viz., TP= true positive, TN= true negative, FP= false positive, and FN= false negative (here FN indicates that the predicted output is zero but the actual output is one; FP indicates that the predicted output is one but the actual output is zero; TP indicates that the predicted and actual outputs are equal; that is, one; and TN indicates that the predicted and actual outputs are equal; that is, zero).

When applying K-NN to the testing data from the confusion matrix (Figure 8), we obtained 65 TPs, namely patients with breast cancer

that were correctly classified, and 22 TN patients without breast cancer that were correctly classified. The algorithm misclassified 12 patients with breast cancer by indicating that they did not (FN), and 15 patients who did not have breast cancer by indicating that they did (FP).

When applying the random forest algorithm to the testing data from the confusion matrix (Figure 9), we obtained 70 TPs, namely patients with breast cancer that were correctly classified, and 40 TN patients without breast cancer that were correctly classified. The algorithm misclassified three patients that did have breast cancer by indicating that they did not (FN) and one patient that did not have breast cancer by indicating that they did (FP). Similarly, when applying the MLP algorithm to the testing data from the confusion matrix (Figure 10), we obtained 119 TPs, namely patients with breast cancer that were correctly classified, and 63

Table 2 Performances measurements of K-NN, RF, and MLP algorithms

K-NN	Precision	Recall	F1 score	Support
0	0.84	0.81	0.83	80
1	0.59	0.65	0.62	34
Accuracy	-	-	0.76	114
Macro avg	0.72	0.73	0.72	114
Weighted avg	0.77	0.76	0.77	114
Random forest				
0	0.99	0.96	0.97	71
1	0.93	0.98	0.95	43
Accuracy	-	-	0.96	114
Macro avg	0.96	0.97	0.96	114
Weighted avg	0.97	0.96	0.96	114
MLP				
0	0.99	1.0	1.0	119
1	1.0	0.98	0.99	64
Accuracy	-	-	0.99	183
Macro avg	1.0	0.99	0.99	183
Weighted avg	0.99	0.99	0.99	183

TN patients without breast cancer disease were correctly classified. The algorithm misclassified one patient that had breast cancer by indicating that FN and the FP rate for the MLP algorithm were zero.

We can compare the RF confusion matrix to that of K-NN. It can be observed that K-NN was worse than RF in predicting patients with breast cancer (22 vs. 40) and worse at predicting patients without breast cancer (65 vs. 70). According to our study, RF should be selected between the two algorithms as it provides outstanding performance compared to K-NN for classifying breast cancer. Finally, we used the MLP on the testing dataset to create a confusion matrix. Moreover, RF was worse than the MLP in predicting patients with breast cancer (40 vs. 63) and worse in predicting patients without breast cancer (70 vs. 119). Therefore, among these three algorithms, the MLP provided an outstanding prediction accuracy of 99.4%. Moreover, our model gives excellent performance with prediction accuracy of 99.4% and AUC of 99.8% respectively using MLP algorithm (Asri et al. 2016).

According to Table 2, the precision, recall, F1 score, and support values obtained when using the K-NN algorithm were 0.84, 0.81, 0.83, and 80, respectively for the benign class and 0.59, 0.65, 0.62, and 34, respectively for the malignant class. The accuracy values in terms of the F1 score and support were 0.76 and 114,

respectively, and the macro average values in terms of the precision, recall, F1 score, and support were 0.72, 0.73, 0.72, and 114, respectively. The weighted average values in terms of the precision, recall, F1 score, and support were 0.77, 0.76, 0.77, and 114, respectively.

When implementing the RF algorithm, the precision, recall, F1 score, and support values obtained were 0.99, 0.96, 0.97, and 71, respectively, for the benign class and 0.93, 0.98, 0.95, and 43, respectively, for the malignant class. The accuracy values for a random forest in terms of the F1 score and support were 0.96 and 114, respectively. The macro average values in terms of the precision, recall, F1 score, and support were 0.96, 0.97, 0.96, and 114, respectively. The weighted average values in terms of the precision, recall, F1 score, and support were 0.97, 0.96, 0.96, and 114, respectively.

With the MLP algorithm, the precision, recall, F1 score, and support values were 0.99, 1.0, 1.0, and 119, respectively, for the benign class and 1.0, 0.98, 0.99, and 64, respectively, for the malignant class. The accuracy values in terms of the F1 score and the support were 0.99 and 183, respectively. The macro average values in terms of the precision, recall, F1 score, and support were 1.0, 0.99, 0.99, and 183, respectively. The weighted averages in terms of precision, recall, F1 score, and support were 0.99, 0.99, 0.99, and 183, respectively.

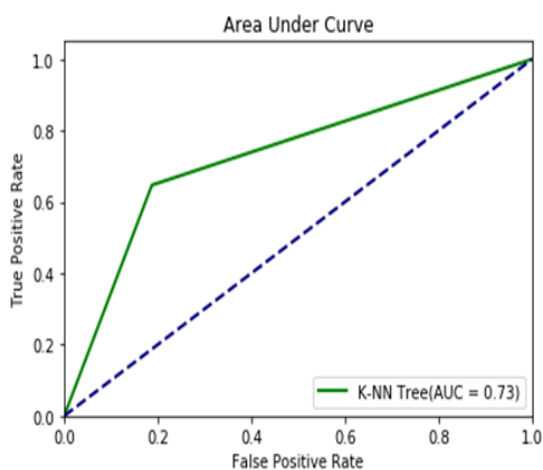


Figure 12 AUC of K-NN algorithm

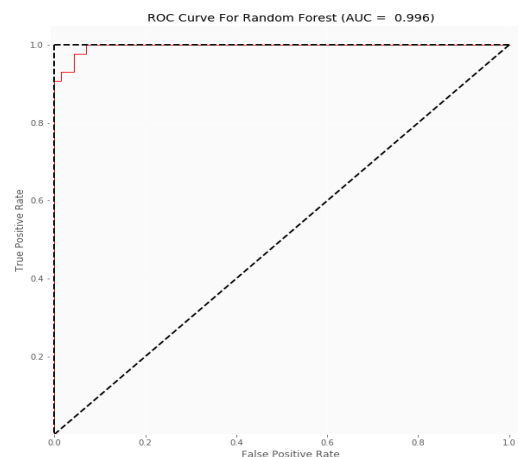


Figure 13 AUC of RF algorithm

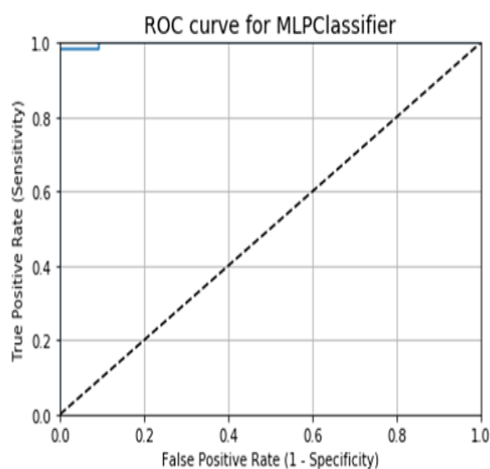


Figure 14 AUC of MLP algorithm

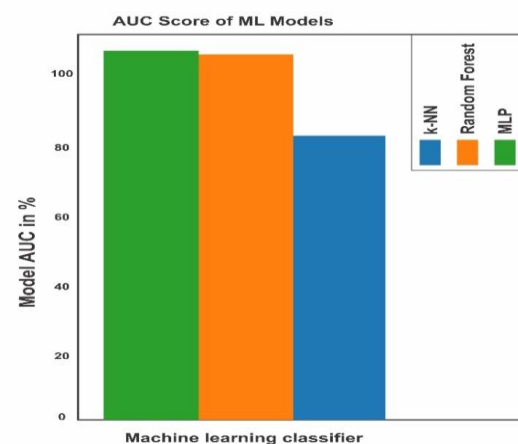


Figure 15 Comparison of AUC scores for different ML algorithms

It can be observed from Figure 11 that K-NN is a lazy learner and is not very active during the training process, unlike the other classifiers used to build the models. According to the graph, the accuracy obtained by the MLP (99.4%) was better than the accuracy obtained by the random forest (96.4%) and K-NN (76.3%) algorithms. Moreover, the MLP yielded the highest value of correctly classified instances and a lower value of incorrectly classified instances than the other classifiers.

The AUC is plotted with the TP rate (y-axis) against the FP rate (x-axis); TP rate =  $TP/TP+FN$ ; FP rate =  $FP/TN+FP$

A model provides excellent classification if the AUC value is nearly 1. In this case, it indicates how accurately the model predicts whether a patient suffers from breast cancer. According to Figure 12, the AUC value for the K-NN algorithm was 0.73, which means that there is a 73% chance that our model can accurately distinguish between the benign and malignant classes. Similarly,

according to figure 13 for the RF algorithm, there is a 99.6% chance that the model can accurately predict breast cancer. It can be observed from Figure 14 that there is a 99.9% chance that the model can accurately classify the benign and malignant classes with the MLP algorithm. The highest diagnosis rate was obtained with the MLP algorithm using the AUC parameter, as illustrated in Figure 15.

The FP rate was the lowest (zero) when using the MLP classifiers. From the results, we may understand why the MLP has outperformed the other classifiers. According to the experimental results, the highest accuracy value (99.4%) was achieved by using the MLP algorithm in extracting the features of tumors (benign or malignant). It is observed that the performance of the MLP algorithm was better than those of the other classifiers in the accuracy, sensitivity, specificity, and precision. Moreover, a comparative analysis for the prediction of breast cancer disease is presented in Table 3.

Table 3 Performance comparison of proposed work with published works

Authors	Technique	Accuracy
Islam et al. (2020)	ANN	98.57
Latchoumi and Parthiban (2017)	WPSO-SSVM	98.42
Chaurasia et al. (2018)	Naïve Bayes	97.36
Sakri et al. (2018)	Naïve Bayes	81.3
	Rep tree	80
	K-NNs	75
Banu and Subramanian (2018)	Bayes belief network	91.7
	Tree augmented naïve bayes	94.11
	Boosted augmented naïve bayes	91.7
Kaur et al. (2019)	RF	95.71
	MLP	96.42
Proposed work	RF	96.4
	MLP	99.4

## Conclusions

This study has provided a clear idea of the accomplishment of classification algorithms in terms of their prediction ability, which can aid healthcare professionals to diagnose chronic disease (breast cancer) efficiently. Our goal was to achieve high accuracy for breast cancer classification by using a supervised machine learning algorithm. Our proposed model yielded the highest accuracy of 99.4% when using the MLP algorithm, followed by the random forest algorithm with 96.4% and the K-NN algorithm with 76.4%. The highest diagnosis rate was 99.8% achieved by the MLP algorithm, followed by random forest (99.6%) and K-NN (73%) when using the AUC parameter. We hope that our work will be very helpful in the determination of reliable biomarkers for the detection of breast cancer tumors with a larger dataset.

## Acknowledgments

All authors acknowledge their respective Institutes and Universities.

## Funding

No funding received.

## Conflicts of interest

There are no conflicts to declare.

## Data Availability

Not applicable

## References

- Asri, H., Mousannif, H., Moatassime, H.A., & Noel, T. (2016). Using Machine Learning Algorithms for Breast Cancer Risk Prediction and Diagnosis. The 6th International Symposium on Frontiers in Ambient and Mobile Systems (FAMS 2016). *Procedia Computer Science*, 83, 1064 – 1069.
- Banu, A.B., & Subramanian, P.T. (2018). Comparison of Bayes classifiers for breast cancer classification. *Asian Pacific Journal of Cancer Prevention*, 19(10), 2917–20.
- Chaurasia, V., Pal, S., & Tiwari, B. (2018). Prediction of benign and malignant breast cancer using data mining techniques. *Journal of Algorithms and Computational Technology*, 12(2), 119–26.
- Costa, K., Ribeiro, P., Carmargo, A., Rossi, V., et al. (2013). Comparison of the techniques decision tree and MLP for data mining in SPAMs detection in computer networks. *Proceedings of the 3rd international conference on innovative computing Technology*, 344–348.
- Forsyth, A.W., Barzilay, R., Hughes, K.S., Lui, D., et al. (2018). Machine Learning Methods to Extract Documentation of Breast Cancer Symptoms from Electronic Health Records. *Journal of Pain and Symptom Management*, 55(6), 1492-1499.
- García-Laencina, P.J., Abreu, P.H., Abreu, M.H., & Afonso, N. (2015). Missing data imputation on the 5-year survival prediction of breast cancer patients with unknown discrete values. *Computers in Biology and Medicine*, 59, 125–133.

- Islam, M., Haque, R., Iqbal, H., Hasan, M., et al. (2020). Breast Cancer Prediction: A Comparative Study Using Machine Learning Techniques. *SN Computer Science*, 1, 290.
- Islam, M.M., Iqbal, H., Haque, M.R., & Hasan, M.K. (2017). Prediction of Breast Cancer Using Support Vector Machine and K-Nearest Neighbours 2017 IEEE Region 10 Humanitarian Technology Conference (R10-HTC), Dhaka, Bangladesh.
- Jiang, T., Gradus, J.L., & Rosellini, A.J. (2020). Supervised machine learning: A brief primer. *Behavior Therapy*, 51(5), 675-687.
- Kaur, P., Kumar, R., & Kumar, M. (2019). A healthcare monitoring system using random forest and internet of things (IoT). *Multimedia Tools and Applications*, 78, 19905-19916.
- Latchoumi, T.P., & Parthiban, L. (2017). Abnormality detection using weighed particle swarm optimization and smooth support vector machine. *Biomedical Research*, 28, 4749-51.
- Muktevi, S. (2020). Prediction of Breast Cancer Disease using Machine Learning Algorithms. *International Journal of Innovative Technology and Exploring Engineering*, 9(4), 2868-2878.
- Rana, M., Chandorkar, P., & Dsouza, A. (2015). Breast cancer diagnosis and recurrence prediction using machine learning techniques. *International Journal of Research in Engineering and Technology*, 4(4), 372-376.
- Sakri, S.B., Rashid, N.B.A., & Zain, Z.M. (2018). Particle swarm optimization feature selection for breast cancer recurrence prediction. *IEEE Access*, 6, 29637-29647.
- Singh, B.K. (2019). Determining relevant biomarkers for breast cancer using anthropometric and clinical features: A comparative investigation in machine learning paradigm. *Biocybernetics and Biomedical Engineering*, 39, 393-409.
- Sun, Y.S., Zhao, Z., Yang, Z.N., Xu, F., et al. (2017). Risk Factors and Preventions of Breast Cancer. *International Journal of Biological Sciences*, 13(11):1387-1397.
- Verikas, A., Gelzinis, A., & Bacauskiene, M. (2011). Mining data with random forest: a survey and results of new tests. *Pattern Recognition*, 44(2), 330-349.
- Wu, M., Zhong, X., Peng, Q., Xu, M., et al. (2019). Prediction of Molecular Subtypes of Breast Cancer using BI-RADS Features Based on a "White Box" Machine Learning Approach in a Multi-modal Imaging Setting. *European Journal of Radiology*, 114, 175-184.



## Journal of Experimental Biology and Agricultural Sciences

<http://www.jebas.org>

ISSN No. 2320 – 8694

### Dielectric properties of the tissues with different histological structure: Ex vivo study

Andrew K. Martusevich<sup>1,2,4,\*</sup> , Elena S. Golygina<sup>2</sup>, Vladimir V. Nazarov<sup>1,2</sup>,  
Ivan V. Bocharin<sup>2</sup>, Inessa A. Minenko<sup>1,4</sup>, Mikhail Yu. Artamonov<sup>1,4</sup>

<sup>1</sup>Sechenov University, Moscow, Russia

<sup>2</sup>Privolzhsky Research Medical University, Nizhny Novgorod, Russia

<sup>3</sup>Institute of Applied Physics of Russian Academy of Sciences, Nizhny Novgorod, Russia

<sup>4</sup>MJA Research and Development, Inc., USA

Received – February 17, 2022; Revision – April 16, 2022; Accepted – April 30, 2022

Available Online – April 30, 2022

DOI: [http://dx.doi.org/10.18006/2022.10\(2\).451.455](http://dx.doi.org/10.18006/2022.10(2).451.455)

#### KEYWORDS

Dielectric properties

Biological tissues

Near-field resonance  
microwave sensing

Dielectric permittivity

Conductivity

#### ABSTRACT

This study aimed to estimate the dielectric properties of tissues with different histological structures. For this, specimens of fibrous (n=9), muscular (n=7), and fatty (n=11) human tissues were studied. The estimation of dielectric permittivity and conductivity of these specimens was tested with a program and apparatus device for near-field resonance microwave sensing, including 5 applicators with different depths of study. Results of the study demonstrated that this technology can visualize the shape, localization, and linear decisions of biological objects. The currently used method allows distinguishing the tissue histological type. It was stated that fibrous tissue has a maximal level of median and highest dielectric permittivity, and the minimal value of this parameter was fixed for fatty specimens (in 4.26 and 4.53 times lower than in fibrous one, respectively). Muscular tissue has an intermediate value of dielectric permittivity, approaching a level close to fibrous tissue.

\* Corresponding author

E-mail: [cryst-mart@yandex.ru](mailto:cryst-mart@yandex.ru) (Andrew K. Martusevich)

Peer review under responsibility of Journal of Experimental Biology and Agricultural Sciences.

Production and Hosting by Horizon Publisher India [HPI]  
(<http://www.horizonpublisherindia.in/>).  
All rights reserved.

All the articles published by [Journal of Experimental Biology and Agricultural Sciences](#) are licensed under a [Creative Commons Attribution-NonCommercial 4.0 International License](#) Based on a work at [www.jebas.org](http://www.jebas.org).



## 1 Introduction

Currently, there is a wide range of medical imaging technologies; among these some most common are ultrasound, computer, and magnetic resonance imaging (Gladkova and Sergeev 2007; Schertlen et al. 2002; Turchin 2016; Bogomolova et al. 2017). On the other hand, not all types of tissues including integumentary tissues, including the skin and the nearest subcutaneous layers can be effectively visualized with a sufficiently high resolution (Arsenyev et al. 2011; Turchin 2016; Bogomolova et al. 2017; Martusevich et al. 2017). These facts necessitate the need for further search for new medical imaging methods based on other physical principles and their experimental and clinical testing (Naito et al. 1997; Raicu et al. 2000; Schertlen et al. 2002; Hayashi et al. 2005; Kostrov et al. 2005; Baloshin et al. 2011; Martusevich et al. 2017; Martusevich et al. 2018).

In this regard, attention is drawn to the possibilities of near-field resonant microwave sensing, which allows an integral assessment of the dielectric properties of biological objects (Raicu et al. 2000; Schertlen et al. 2002; Reznik and Yurasova 2006; Baloshin et al. 2011). This technology characterized both the generalized and deep structure parameters of biological samples without any restrictions on morphological tissues analyzed (Naito et al. 1997; Schertlen et al. 2002; Hayashi et al. 2005; Arsenyev et al. 2011; Baloshin et al. 2011; Bogomolova et al. 2017; Martusevich et al. 2018). Microwave sensing makes it possible to carry out non-invasive and non-destructive diagnostics of any living tissues (Schertlen et al. 2002; Kostrov et al. 2005; Arsenyev et al. 2011; Baloshin et al. 2011). This technique potentially can conduct non-contact research including through physical barriers i.e. bandages or wound coverings (Schertlen et al. 2002; Bogomolova et al. 2017; Martusevich et al. 2018). At the same time, the possibilities and diagnostic prospects of near-field microwave sensing in experimental and clinical medicine

have not been fully studied (Schertlen et al. 2002; Arsenyev et al. 2011; Bogomolova et al. 2017; Martusevich et al. 2018). In this regard, the work aimed to identify the features of the dielectric properties of various types of tissues.

## 2 Material and methods

Samples of fibrous (n=9), muscular (n=7), and adipose (n=11) human tissue has been removed intraoperatively and were used for the study. To assess the dielectric properties of these biological samples, a hardware and software complex for near-field resonant microwave sensing was used, this complex was supplemented by a system of 5 applicators (Kostrov et al. 2005; Martusevich et al. 2017; Martusevich et al. 2018).

To assess the dielectric properties, tissue fragments were placed on a plastic Petri dish, the lid of which was mapped, representing a navigation grid for point-by-point sensing with an area of up to 50X30 points in increments of 5 mm. Using this grid, a matrix of resonant frequencies was obtained, based on which the dielectric permittivity and conductivity were determined, and forming a microwave profile of the object and its environment. The results were processed using the Statistica 6.0 program.

## 3 Results and Discussion

Results of the current study established that the use of near-field resonant microwave sensing unambiguously determined the boundaries of the visualized object, regardless of its shape and histological structure. Thus, the analysis carried out by one-dimensional linear scanning of a biological sample, beginning and ending outside of it, indicated a significant and statistically significant decrease in the perceived frequency in the area strictly corresponding to the localization of a fragment of fibrous tissue (Figure 1).

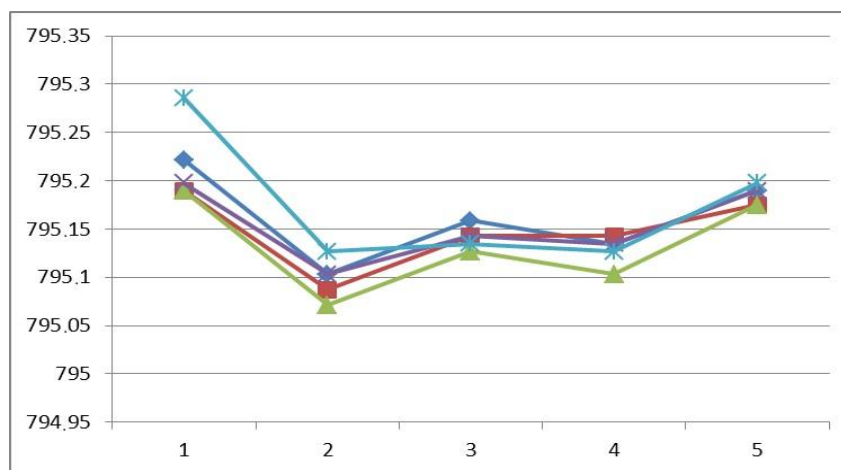


Figure 1 Effect of various microwave fragments on various fibrous tissue using an applicator with a maximum penetration depth of 5 mm (each line corresponds to one tissue fragment; the numbers on the OX axis indicate the measured point: 1 and 5 – points lying outside the biological tissue fragment, 2-4 – points in the projection of the biological tissue fragment)

The data obtained by one-dimensional scanning of a fragment of fibrous tissue are also confirmed by the two-dimensional study of these samples of biological tissue. In addition, the use of a similar, close to tomographic technology makes it possible to demonstrate the deep heterogeneity of a tissue fragment. This particularly justifies the possibility of assessing the structure of the skin changed as a result of thermal exposure (burn). It should be emphasized that specified homogeneity of the tissue sample occurs both in terms of dielectric permittivity ( $\epsilon$ ) and the conductivity of the object ( $\sigma$ ). So, whenever using a sensor that can evaluate the dielectric properties of an object at a depth of 2 mm, the peculiarities of the location of the object in the Petri dish should be taken into account so that the radiation can capture only the surface layers of the sample. This ensures only a minimal displacement of the dielectric constant. With the increase in the depth of sensing to 3.5 mm, sensor No. 3 can be used which leads to a more significant change in the parameter, the clearest visualization of the studied sample is provided at the maximum depth of sensing used (5 mm.). The pattern recorded in this case fully corresponds to the localization, shape, and linear dimensions of the fragment of biological tissue.

Concerning conductivity, the nature of the "response" of the signal depends to a lesser extent on the depth of sounding (Figure 2, right column). According to this indicator, a picture close to the

dimensions of the analyzed object is recorded for all sensors but are slightly different in shape from the real one only according to the readings of sensor No. 3.

In general, the conducted experiment with a sample of intraoperatively removed tissue made it possible to verify the possibility of detecting the localization, shape, and linear dimensions of the biomaterial by the method of near-field resonant microwave sensing on the created software and hardware complex.

In the second part of this experiment, a comparative assessment of the effect of the tissue histotype on the nature of the displacement of the microwave pattern indicating the dielectric properties of the object was carried out (Figure 3).

It has been established that both fat and muscle tissue have satisfied visualization using near-field microwave sensing, and this concerns the assessment of the shape and size of the samples. At the same time even without additional mathematical processing, the differences in the shift of the resonant frequency of radiation that occurs between these histological types of biological objects and consequently the variability of their dielectric properties can be reported. Thus, muscle tissue, which has a significantly higher density compared to fat and increased metabolic activity of cells, also demonstrates a more distinct shift in the resonant frequency.

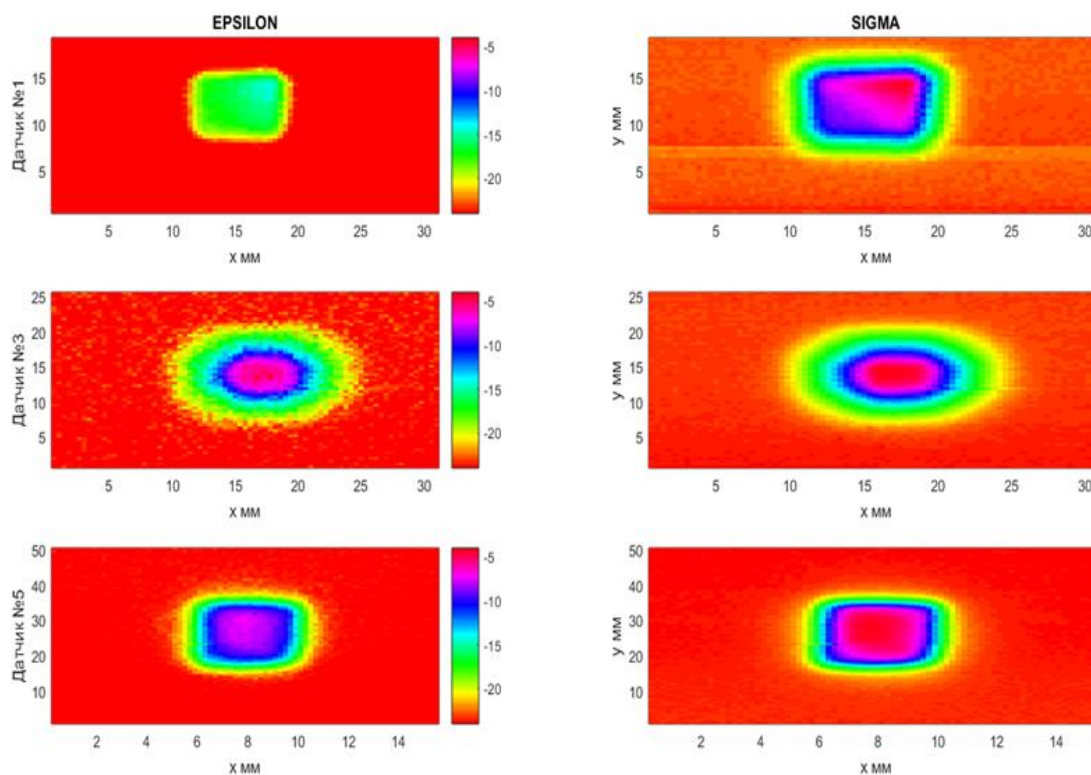


Figure 2 Results of two-dimensional scanning of a fragment of fibrous tissue by various sensors-probes for permittivity ( $\epsilon$ ) and conductivity ( $\sigma$ )



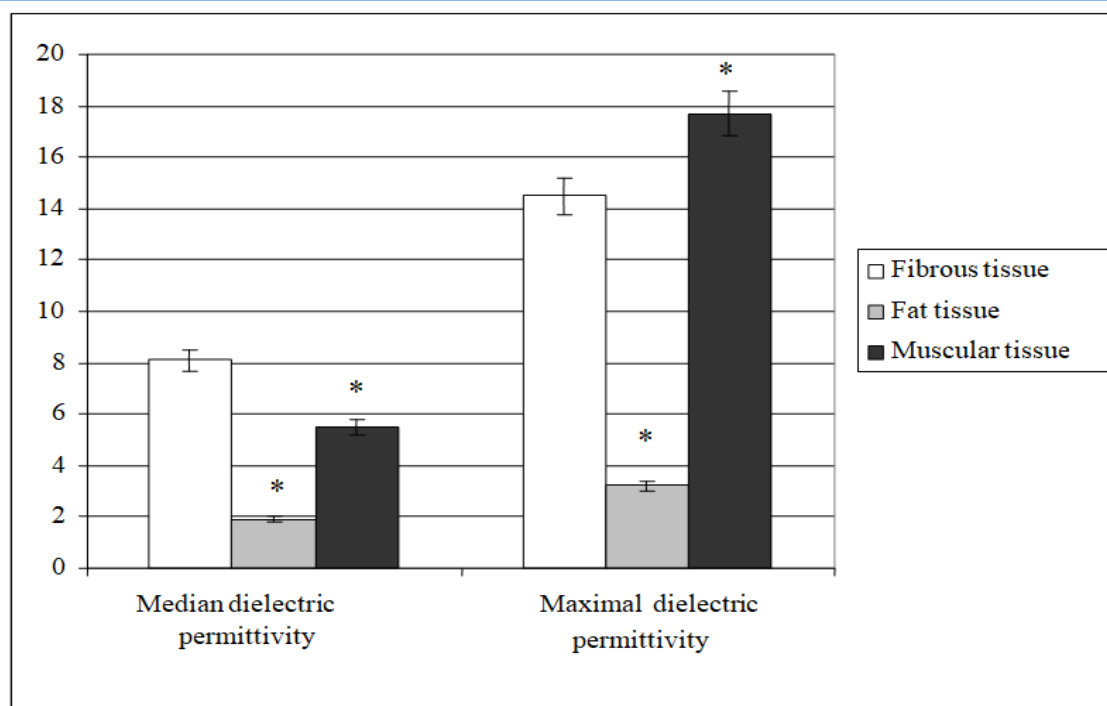


Figure 3 The level of average ( $\Delta\epsilon_{cp}$ ) and maximal ( $\Delta\epsilon_{max}$ ) dielectric permittivity of fragments of various tissues; \* revealed a level of statistical value ( $p < 0.05$ ) of differences in fibrous tissue

Based on the microwave pattern, the adipose tissue is less unambiguously changed with the dielectric permittivity in a small central area of the sample. Such differences in the dielectric properties of tissues of various histological types make it possible to talk about the diagnosis of the condition of the burn wound and the periwound zone, as well as to assess the depth of thermal damage to the skin and underlying tissues, creating a fundamental justification for instrumental diagnostics in combustiology.

To quantify the dielectric characteristics of tissues of various histological structures, the average ( $\Delta\epsilon_{cp}$ ) and maximal ( $\Delta\epsilon_{max}$ ) dielectric permittivity of the samples was calculated (Figure 3). It has been revealed that fibrous tissue has the highest level of both average and maximum permeability, while the lowest value of the indicators turned out to be characteristic of adipose tissue, for which the average permeability was 4.26 times lower than that of fibrous ( $p < 0.05$ ) and the maximum – 4.53 times, respectively ( $p < 0.05$ ). Muscle tissue occupies an intermediate position between them and approaches more to the level of fibrous tissue which is due to the sufficiently high density of muscles and their high metabolic activity.

Results of the study revealed that as a thermo-modification the dielectric characteristics of bio-tissue are significantly transformed. This might be because these are significantly dependent on the content of water in the studied object (Reznik and Yuasova 2004; Kostrov et al. 2005; Hayashi et al. 2005; Martusevich et al. 2018),

and when heated, there is a significant decrease in tissue hydration. Similar dynamics of the parameter were reported in previous studies, which included a comparative assessment of the dielectric properties of the skin and subcutaneous structures in healthy Wistar rats with model thermal trauma (Bogomolova et al. 2017; Martusevich et al. 2018). This confirms the diagnostic informativeness of the analysis of the dielectric permittivity of tissues under the influence of high temperatures, including thermal burns. This indicates a violation in metabolic shifts which cause changes in the ionic composition of the intercellular substance, osmolarity, and other physical and chemical characteristics (Hayashi et al. 2005; Ida et al. 2016; Turchin 2016). These facts can be used as an experimental justification for the possibility of detecting the boundaries of thermal tissue damage that occurs in real burns.

### Conclusion

Thus results of the experiment made it possible to objectify the diagnostic value of the technology of near-field resonant microwave sensing on real biological samples. In addition, the possibility of the hardware and software complex to visualize the shape, localization, and linear dimensions of a biological object has been also confirmed. It is also shown that the studied technology can differentiate tissues of various histotypes. At the same time, it was found that fibrous tissue has the highest level of both average and maximum dielectric permittivity, while the

lowest value of the indicators turned out to be characteristic of adipose tissue, for which the average permeability was 4.26 times lower than that of fibrous tissue, and the maximum was 4.53 times, respectively. Muscle tissue occupies an intermediate position between them, approaching more to the level of fibrous tissue.

### Conflict of interest

None declared.

### References

- Arsenyev, A.V., Volchenko, A.N., Likhacheva, L.V. & Pechersky, V.I. (2011). Application of the RF-near-field sounding method in diagnostics of biological objects. *Scientific and Technical Bulletin of Information Technologies, Mechanics and Optics*, 2, 154.
- Baloshin, Y.A., Sorokin, A.A. & Volchenko, A.N. (2011). Electrodynamic model of HF near-field sensing of physical objects. *Proceedings of Universities. Instrumentation*, 12, 68.
- Bogomolova, E.B., Martusevich, A.K., Klemenova I.A. et al. (2017). Application of modern imaging methods in assessing the condition and predicting the development of pathological scars. *Medicine* 3, 58.
- Gladkova, N.D. & Sergeev, A.M. (2007). *Manual of optical coherence tomography*, M. Fizmatlit.
- Hayashi, Y., Miura, N., Shinyashiki, N. & Yagihara, S. (2005). Free water content and monitoring of healing processes of skin burns studied by microwave dielectric spectroscopy in vivo. *Physics in Medicine & Biology*, 50 (4), 8.
- Ida, T., Iwazaki, H., Kawaguchi, Y. et al. (2016) Burn depth assessments by photoacoustic imaging and laser Doppler imaging. *Wound Repair and Regeneration*, 24(2), 349-355.
- Kostrov, A.V., Smirnov, A.I., Yanin, D.V. et al. (2005). Resonant near-field microwave diagnostics of inhomogeneous media. *Izvestiya RAS Physical series*, 69 (12), 1716.
- Martusevich, A.K., Krasnova, S.Y., Galka, A.G., Peretyagin, P.V. & Kostrov, A.V. (2018). Near-field resonant microwave sounding as a method of studying the deep structure of a burn wound in an experiment. *Modern technologies in medicine* 10 (3), 109.
- Martusevich, A.K., Yanin, D.V., Bogomolova, E.B., Galka, A.G., Klemenova, I.A. & Kostrov, A.V. (2017). Possibilities and prospects of using microwave tomography in skin condition assessment. *Biomedical Radioelectronics* 12, 3.
- Naito, S., Hoshi, M. & Mashimo, S. (1997). In vivo dielectric analysis of free water content of biomaterials by time domain reflectometry. *Analytical Biochemistry*, 251 (2), 163.
- Raicu, V., Kitagawa, N., & Irimajiri, A. (2000). A quantitative approach to the dielectric properties of the skin. *Physics in Medicine & Biology*, 45 (2), 1.
- Reznik, A.N. & Yurasova, N.V. (2004). Near-field microwave tomography of biological media. *Journal of Technical Physics* 74 (4), 108.
- Reznik, A.N. & Yurasova, N.V. (2006). Detection of contrast formations inside biological media using near-field microwave diagnostics. *Journal of Technical Physics* 76 (1), 90.
- Schertlen, R., Pivit, F., & Wiesbeck, W. (2002). Wound diagnostics with microwaves. *Biomedical technology (Berlin)* 47 (1, 2), 672. <https://doi.org/10.1515/bmte.2002.47.s1b.672>.
- Turchin, I.V. (2016) Methods of optical biomedical imaging: from subcellular structures to tissues and organs. *Advances in Physical Sciences* 186 (5), 550.